6-18-2004

Hydraulic, Diffusion, and Retention Characteristics of Inorganic Chemicals in Bentonite

Naim Muhammad
University of South Florida

Hydraulic, Diffusion, and Retention Characteristics of Inorganic Chemicals in Bentonite

By

Naim Muhammad

A dissertation submitted in partial fulfillment
of the requirement for the degree of
Doctor of Philosophy in Civil Engineering
Department of Civil and Environmental Engineering
College of Engineering
University of South Florida

Major Professor: Alaa K. Ashmawy, Ph.D.
Manjriker Gunaratne, Ph.D.
A. Gray Mullins, Ph.D.
Luis Garcia-Rubio, Ph.D.
V.R. Bhethanabotla, Ph.D.

Date of Approval:
June 18, 2004

Keywords: Landfill, Clay Liner, Coefficient of Permeability, Electrical Conductivity, Retardation Factor, Partition Coefficient, Adsorption Capacity.

DEDICATION

To my beloved family

ACKNOWLEDGEMENTS

The author expresses his deep gratitude and sincere appreciation to his major supervisor Associate Professor Dr. Alaa K. Ashmawy for his valued advice, guidance, encouragement and constructive criticism throughout this study. The author wishes to express his sincere appreciation and thanks to all his committee members: Dr. Manjriker Gunaratne, Dr. A. Gray Mullins, Dr. Luis Garcia-Rubio and Dr. Thomas Pichler for their interest, useful suggestions and constant support in this study. The author is also grateful to Dr. Audrey D. Levine and Ms. Barbara Dodge of Environmental Lab, Mr. Jay Bieber of Nanomaterials and Nanomanufacturing Research Center (NNRC), Mr. Robert R Smith and Mr. Tom Gage Machine Shop for their technical support and using their facilities.

The valuable discussions with and constructive suggestions from Mr. Darwish El-Hajji, Ms. Maysson Sallam, and Ms. Jessica A Schenning are gratefully achnowledged. The author is also grateful to all his colleagues for their constant help and support throughout this study.

The author deeply appreciates the funds provided in part by the Florida Center for Solid and Hazardous Waste Management and the financial assistance in the form of Graduate Research Assistantship and Teaching Assistantship and facilities given by the Department of Civil and Environmental Engineering of the University of South Florida.

TABLE OF CONTENTS

LIST OF TABLES

LIST OF FIGUES

LIST OF SYMBOLS

Å = Angstrom unit = 1 x 10^{-10} m

ΔG^o = standard free energy change of the reaction

μ^o = Gibbs free energy at standard pressure and temperature

K_{eq} = thermodynamic equilibrium constant

K_E = revised equilibrium constant

E_{att} = electrostatic attraction energy

E_{tot} = total energy change

ΔE_{tot} = overall change of energy

r_s = effective radius of the charge surface

r_A = radius of displaced ion A

r_B = radius of displaced ion B

E_A = hydration energy of displaced ion A

E_B = hydration energy of displaced ion B

ψ = electrical potential

ρ_{ch} = charge volumetric density (C m^3),

D = relative permittivity of the medium

D = Dielectric Constant

D* = effective diffusion coefficient

D^*_A = apparent diffusion coefficient

ε_o = dielectric constant of the void (C V^{-1} m^{-1})

k = Boltzmann's constant (1.38045 x 10^{-23} J/^{o}K)

k = coefficient of permeability

T = absolute temperature

η_i = ionic concentration of the specie i

e = unit electronic charge (16 x 10^{-20} Coulomb)

e = void ratio

ψ_o = electrical potential at concentration η_{io}

eq = equivalent charge

fw = formula weight

K = Debye-Huckel parameter

ν = ionic valence

m = mass of a particle

v = velocity

k = the Boltzman constant

W_s = weight of the dry sample

W_{fs} = weight of the flask filled with soil and water

W_{fw} = the weight of the flask

G_s = specific gravity of soil solids

HYDRAULIC, DIFFUSION, AND RETENTION CHARACTERISTICS OF INORGANIC CHEMICALS IN BENTONITE

Naim Muhammad

ABSTRACT

Inorganic contaminants, while transported through the bentonite layer, are chemically adsorbed onto the particle surfaces and exhibit a delay in solute breakthrough in hydraulic barriers. Transport of inorganic leachate contaminants through bentonite occurs by advection, diffusion or a combination of these two mechanisms. During the process of chemical solute transport through low permeability bentonite, the amount of cation exchange on the clay particle surface is directly related to the cation exchange capacity (CEC) of montmorillonite and other mineral constituents.

The process of diffusion and advection of various inorganic leachate contaminants through bentonite is thoroughly investigated in this study. Diffusion characteristics are of specific interest as they have a prominent effect on the long term properties of bentonite compared to advection. This is mostly true if the hydraulic conductivity of the material is less than 10^{-8} cm/s and if the thickness of the barrier is small. Chemical reactions in the form of cationic exchange on the clay particle surfaces has been incorporated in the analysis of the diffusion process. Adsorption-desorption (sorption) reactions of chemical compounds that influence the concentrations of inorganic leachates during transport in bentonite clay have been modeled using the Fick's fundamental diffusion theory. Partition coefficients of the solutes in pore space, which affect the retardation factor of various individual ions of chemical solutions, have been investigated during transient diffusion and advection processes.

Several objectives have been accomplished during this research study. An evaluation has been carried out of the hydraulic conductivity of bentonite with respect to single species salts and various combinations of electrolyte solutions. Diffusion properties of inorganic leachates through bentonite have been characterized in terms of apparent and effective diffusion coefficients. Time-dependent behavior of the diffusive ions has been analyzed in order to determine the total retention capacity of bentonite before electrical conductivity breakthrough and steady-state chemical stability are reached. An analytical solution of the attenuation of various inorganic ions concentrations through bentonite has been developed. Finally, recommendations were made for landfill liners exposed to highly concentrated inorganic leachates.

CHAPTER ONE

INTRODUCTION

1.1 Scope and Significance

One of the main problems in the geoenvironmental field is the intrusion of toxic contaminants from waste disposal and other sources into the underlying ground water supply. Clays are commonly used as barriers in landfills, slurry walls, and similar structures to slowdown the movement of contaminants because of their higher water absorption capacity. Bentonite clays are also being used as buffers in nuclear fuel waste disposal sites to control the spread of radioactive materials into the ground (Hancox, 1986; Cheung, 1994).

Bentonite clay, when used in the field as a hydraulic barrier, comes in contact with various inorganic chemicals which eventually cause the performance of bentonite clay to diminish in terms of permeability and chemical outflux (Anderson *et al*., 1985; Cadena *et al*., 1990; Chapuis, 1990; Cheung *et al*., 1980). Earlier research carried out at USF on ash monofill leachate revealed a significant amount of inorganic chemicals such as sodium, calcium, magnesium, and potassium, with initial concentrations well above the accepted drinking water standard (Muhammad and Ashmawy, 2003). Attempts were made to use an alternate liner system with sand-ash-bentonite mixture to arrest the chemical outflux while permeation without much success because of the porous structured formed within the mixture.

Bentonite is a very highly plastic swelling clay of the smectite mineral group, and is mineralogically known as “montmorillonite”. Because of the low permeability of bentonite clay, and the low hydraulic gradients to which it is typically subjected,

molecular diffusion and advection are both equally important transport mechanisms. Molecular diffusion coefficients are therefore important parameters in predicting rates and fluxes of various species of contaminants flowing into the natural soils. Inorganic contaminants, while transported through the bentonite layer, are chemically adsorbed onto the particle surfaces and experience a delay in solute breakthrough in hydraulic barriers. Transport of inorganic leachate contaminants through bentonite could occur either by advection or diffusion or a combination of these two types. During the process of chemical solute transport through a low permeability bentonite layer, cation exchange takes place on the clay particle surfaces due to the high cation exchange capacity (CEC) of montmorillonite minerals.

The process of diffusion and advection using various inorganic leachate contaminants through bentonite is thoroughly investigated in this dissertation. Diffusion study is particularly interesting in bentonite barriers as it is found to be prominent compared to advection, when the hydraulic conductivity of the material is less than 2.0 x 10^{-8} cm/s (Shackelford, 1988). In addition, the diffusion characteristics of bentonite have not been thoroughly studied and have gained little attention in the geoenvironmental literature until recently. Chemical reactions in the form of cation exchange on the clay particle surfaces must be incorporated during the diffusion process study. Adsorption-desorption (sorption) reactions of chemical compounds that influence the concentrations of inorganic leachates during transport in bentonite clay may be modeled using Fick's diffusion theory. "Partition coefficients" of solutes in pore space, which affect the retardation factors of various individual ions of chemical solutions, are investigated during transient diffusion and advection processes.

The time dependent degradation of hydraulic conductivity of the bentonite portion of conventional geosynthetic clay liners (GCL's) is an urgent concern particularly for ash monofills. The increase in hydraulic conductivity of bentonite is caused by aggressive leachates containing high amounts of divalent or higher valence cations, especially in landfills subjected to high percolation. The levels of some soluble metals and chlorides in landfill leachates exceed USEPA drinking water standards, indicating the importance of liners with high retention capacity of chemical elements that can sustain their

characteristics for a long duration. Since bentonite is used to contain and to reduce the flow of liquids in inorganic contaminant environments, further investigation has become necessary to validate its usage in retaining certain ions from the leachate solutions before reaching chemical equilibrium between influent and effluent. In addition, the increase in hydraulic conductivity of bentonite, caused by leachates containing high amounts of divalent or higher valence cations, is investigated in this research study.

It has been reported that Ca^{2+} and Mg^{2+} ions, often present in municipal solid waste (MSW) and incinerator ash, can be detrimental to the bentonite if permeated over extended periods of time (Petrov and Rowe, 1997). Due to high cation (+ion) exchange capacity (CEC) and isomorphic replaceable characteristics of montmorillonite microstructure layers, the increase in hydraulic conductivity of bentonite can even be observed within a very short period (48 hours) with highly concentrated ionic solutions. The low hydraulic conductivity characteristics of bentonite are caused by the hydration of interlayer spacings through a process called "inner-crystalline swelling". Further adsorption of monovalent cations on the negatively charged interlayer and external surfaces (osmotic swelling) causes the formation of the electrical "double layer" in between the mutually repellant surfaces and thus causes separation. As the osmotic swelling is only caused by the hydration of monovalent (namely, Na^{+}) ions, presence of highly concentrated polyvalent cations will inevitably negate the formation of a dispersed clay microstructure and will cause the staggered formation of aggregated clay due to the reduction in the thickness of diffuse double layer (Van Olphen, 1977) as shown in figure 1.1 (Ashmawy, *et al.* 2002).

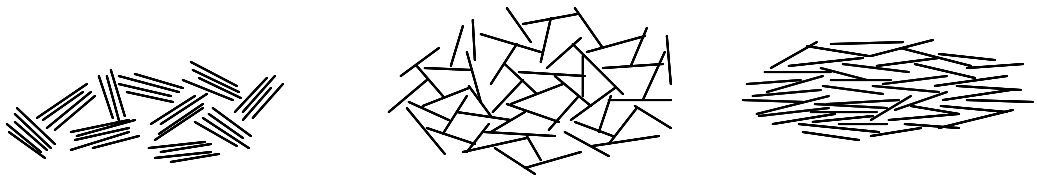

(a) (b) (c)

Figure 1.1 Schematic Representation of Clay Particles Under (a) Initial Saturation with Multivalent Cations; (b) Initial Saturation with Water or Monovalent Caions; and (c) Pre-Hydration Followed by Multivalent Cations

Aggregated formation of bentonite clay layers from a dispersed structure will increase the free pore space, thus resulting in higher hydraulic conductivity and higher free flow of highly concentrated soluble metallic ions into the ground. When the permeant contains monovalent cations, i.e., no ionic exchange occurs, the amount of interlayer bound water and interlayer spacing will vary according to the variation in the concentration of the permeated liquid (Jo *et al*., 2001; Van Olphen 1977). Since the volume of bound water is affected by the size of the hydrated cation, solution pH, and anion concentration, these factors also affect the hydraulic conductivity of the bentonite (Mitchell, 1993; McBride, 1994; Egloffstein, 1995).

The rate of cation exchange in a sodium bentonite is dependent on, among many other factors, hydraulic gradient, solution concentration, temperature, and time (Mitchell 1993; Egloffstein 1995). As the bentonite lining system would be laid underneath the leachate collection system in a landfill, the effects of hydraulic gradient and temperature would be minimal on the degradation of the hydraulic conductivity of bentonite layer. Another potential degradation mechanism involves changes in the mineral microstructure. This is most likely to occur at low pH values due to dissolution of clay particles. Alumina in the octahedral layers of the montmorillonite can be dissolved by hydrolysis, thus causing ionic exchange of Al^{3+} for Na^{+} in the interlayer spacing and a reduction in the amount of bound water (Norrish and Quirk, 1954; Mathers *et al*., 1956; Egloffstein, 1995).

In this study, inorganic contaminant leachates, such as those typically found in ash monofill landfills, were synthesized in the laboratory by combining various chemical compounds in deionized (DI) water. Diffusion and hydraulic conductivity tests were conducted on bentonite materials under various boundary conditions, and the concentration of various ions, namely, sodium, calcium, potassium and magnesium, of influent and effluent solutions were determined at various stages of flow. The chemical composition of the bentonite was determined by Energy dispersive spectroscopy (EDS), while mineral compositions were carried out by the XRD method.

Commercially available Wyo-Ben bentonite was in this study in conjunction with various inorganic ions commonly found leachate in contaminants such as NaCl, $MgCl_2$,

KCl, and $CaCl_2$. As the ionic retention capacity of bentonite clay materials can be beneficially exploited in various flow barriers, the ion absorption capacity of bentonite was determined under various saturation and loading conditions.

1.2 Research Objectives

The specific objectives of this research are itemized as follows:

(a) Evaluation of the hydraulic conductivity of the bentonite clay with respect to single salts and various combinations of electrolyte solutions under a range of hydraulic gradients.

(b) Evaluation of the change of hydraulic conductivity of the bentonite clay for various pre-hydrated conditions, sequencing of inorganic electrolyte solutions, testing method (i.e. flexible wall and rigid wall permeameter), and porosity values of bentonite clay.

(c) Determination of "lag time", breakthrough time, and rate of diffusion of various inorganic dissolved salt solutions through bentonite clay under various chemical gradients.

(d) Characterization of diffusion properties of inorganic leachates through the bentonite layer in terms of apparent and effective diffusion coefficients, and adsorption capacity of the particles under various loading conditions.

(e) Analysis of the time-dependent behavior of the diffusive ions in order to determine the total retention capacity of the bentonite layer before electrical conductivity breakthrough and steady-state chemical stability are reached.

In order to achieve the above objectives, it was also very important to characterize the bentonite clay material in terms of its chemical compositions and physical and hydraulic properties.

1.3 Dissertation Outline

Chapter Two of this dissertation presents the general usage of bentonite, information related clay mineralogy with detailed bentonite clay mineralogy, permeant characteristics, and general background material on water-bentonite interaction. Literature review on diffuse-double layer (DDL) of clay particles is also presented in this chapter, which includes mathematical models of DDL and the factors that affect the size of DDL.

Characterization of the bentonite used in this research is presented in Chapter Three. Mineral and chemical compositions of bentonite as determined by X-Ray Diffraction (XRD) and Energy Dispersive Spectroscopy (EDS) methods, respectively, are presented in this chapter. Physical and geotechnical properties of bentonite clay, such as grain size distribution, Atterberg limits, specific gravity, swell index, and cation exchange capacity with or without synthetic dissolved salts are included.

Chapter Four presents the experimental apparatus, along with the design concept and materials and fabrication of permeability and diffusion equipment. In order to prevent any chemical reaction due to aggressive chemical leachates during permeability, modification to conventional flexible wall permeameters were introduced.

Hydraulic characterization of bentonite clay is discussed in chapter Five of this dissertation. Comparison of hydraulic conductivity test results carried out on flexible wall and rigid wall permeameters is discussed in this chapter. Various factors affecting hydraulic conductivity are also discussed. Results of the chemical analysis of effluent at various stages of permeation are presented.

Chapter Six presents experimental methods of diffusion tests and chemical analysis of the diffusant. IN addition, pH measurements, electrical conductivity (EC), and ionic analysis test results are included in this chapter.

The fundamentals of transport theory and an analysis of diffusion of chemical solutions through bentonite clay are discussed in chapter Seven. Determination and analysis of various diffusion parameters are also discussed. In this chapter, the main

contributions in terms of characterizing the partition coefficient, retention factor, and retention capacity of bentonite are presented.

Chapter Eight summarizes the research findings and provides recommendations for future work.

CHAPTER TWO

MATERIALS AND METHODOLOGY

2.1 Bentonite in Landfills

Bentonite, named after an American geologist who discovered this type of clay in about 1890 in Fort Benton, Wyoming, is a clay mineral with expansive characteristics and low permeability, where montmorillonite is the main mineral. Montmorillonite, named after a deposit located in southern France, swells when contacted with water approximately 900% by volume or 700% by weight. When hydrated under confinement, the bentonite swells to form a low permeability clay layer with the equivalent hydraulic protection of several feet of compacted clay when used in traditional landfill applications (Bruno, 2002).

Because of its low permeability characteristics, bentonite clay, with or without treated materials, is being used in combination with geosynthetics to form a composite commonly known as a geosynthetic clay liner (GCL), which has been in use in the USA in the landfill construction since 1988 (Koerner, 1999). GCLs are rolls of factory-fabricated thin layers of bentonite clay sandwiched between two geotextile layers or glued to a geomembrane which are used in the lining system as well as cover construction. GCLs are used as a hydraulic barrier and/or contaminant layer for leachate, either in place of a composite layer or in addition to other layers in bottom landfill lining system.

Due to surrounding environmental conditions and applied superimposed loads, conventional compacted clay liners (CCLs) develop internal cracks and shrinkage that lead to significant increase in seepage and leakage of contaminant liquid into the ground

soil and water. Bentonite used in GCLs is commonly a sodium bentonite, where sodium ions are located in the interstitial water, between clay platelets, in an adsorptive layer that results in the bentonite swelling characteristics. This swelling allows the bentonite to seal around penetrations, giving the GCL self sealing characteristics. During hydration, a confined layer of dry bentonite changes into a dense monolithic mass with no observable individual particles. A fully hydrated sodium bentonite layer can have a hydraulic conductivity of approximately one hundred times lower than a typical compacted clay liner (CCL). A single GCL of less than 25 mm provides superior hydraulic performance than of a meter of typical compacted clay.

Bentonite, within geosynthetic clay liners, has been used extensively over the past two decades, and is being investigated further to improve quality and performance in many other applications, including lining systems. It is also being used as part of landfill cover systems in landfill construction (Daniel, 1995). Besides GCLs, bentonite clay is also being used in mixed-in-plant (in-situ) systems, where a mixture of one or two different types of soils as a base material is enriched with bentonite to obtain low permeability clay base liners (Koch, 2002). As the mixing of in-situ materials with bentonite is becoming popular, the mixed-in-plant option represents a very flexible, fast and economical way of landfill construction, especially in European countries (Koch, 2002). Bentonite with cement is also used in various construction processes and temporary and permanent sealing barriers, such as slurry walls during construction of diaphragm walls or cut-off walls. The technical properties of these materials are well documented, and their integrity as a sealing barrier has been demonstrated in field applications. Since the bentonite clay is now processed and produced in bulk in factory, its properties and qualities are well documented, which gives the design engineers more confidence in predicting its behavior, characteristics and cost analysis in landfill and other geotechnical applications (Lin and Benson, 2000).

Most of the GCL products manufactured in North America use sodium bentonite clay of mass per unit area of 3.2 to 6.0 kg/m^2 with an average clay thickness of 4.0 to 6.0 mm and of hydraulic conductivity typically in the range of 1 x 10^{-9} to 5 x 10^{-9} cm/s

(Koerner, 1997). Cross-sections of some of the presently available GCLs are shown in figure 2.1.

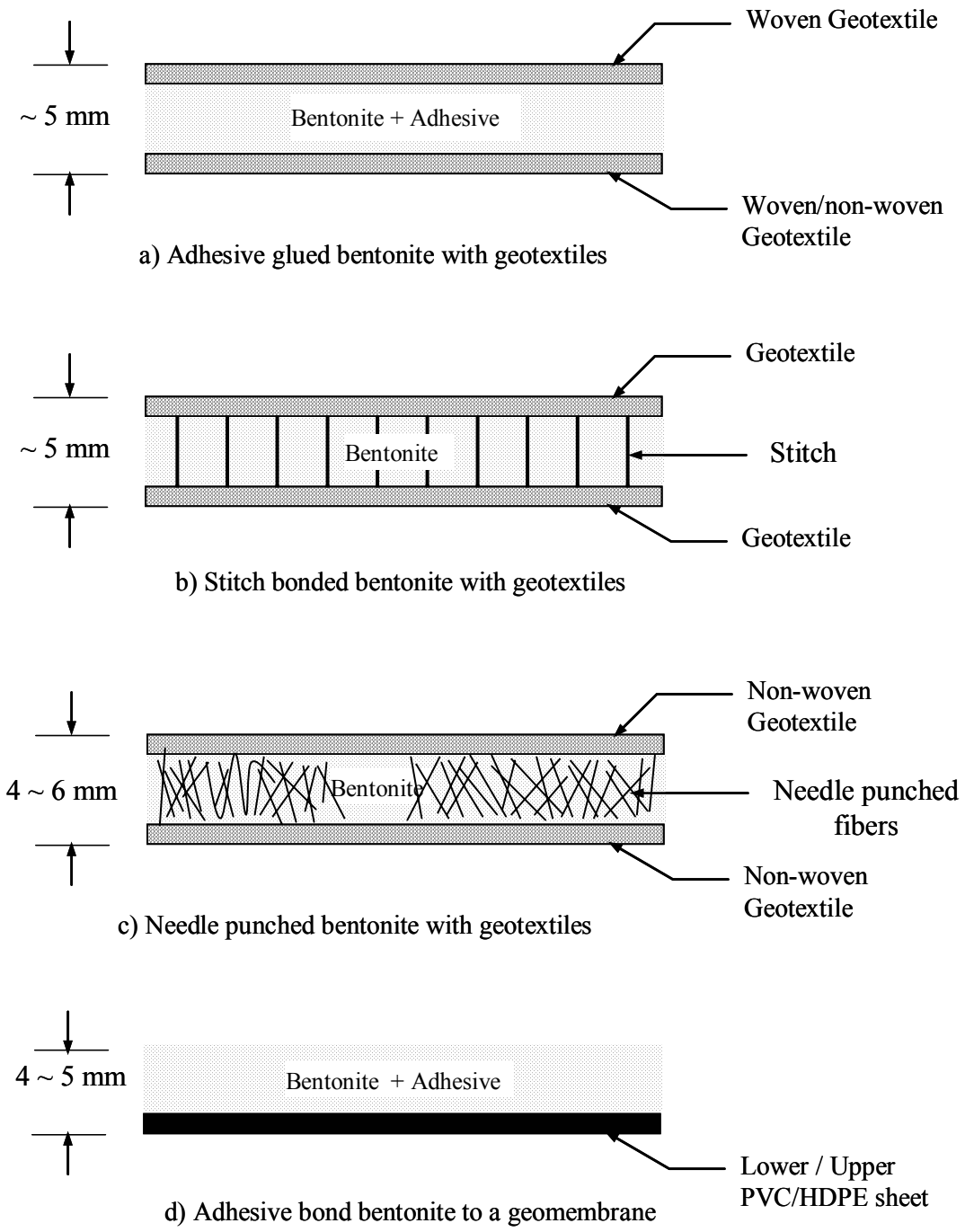

Figure 2.1 Cross-Section Sketches of Various GCLs

2.2 Bentonite Clay

Fundamentals of bentonite in terms of its mineralogy, cation exchange capacity, and interaction with water are discussed in this sub-section.

2.2.1 Basic Clay Mineralogy

Clay minerals are generally classified according to their crystal structure and geometry. Basic elements of clay minerals are two-dimensional arrays of silicon-oxygen (Si-O) tetrahedron called "tetrahedral sheet " and aluminum- or magnesium-oxygen-hydroxyl (Al-, Mg-O-OH) octahedron called "octahedral sheet". The tetrahedron unit in a tetrahedral sheet is composed of four equidistant oxygen atoms arranged in the form of a tetrahedron with a silicon atom at the center as shown in figure 2.2(a) and (b) (after Grim, 1968; Holtz and Kovacs, 1981). All the bases of tetrahedrons are connected to form a single plane in a single sheet, and the tips of oxygen are pointed in the same direction. A top view of the silica sheet, shown in figure 2.2(c), reveals the linkage of the silicon atoms with the oxygen that forms a hexagonal network with "holes" in the middle (after Warshaw and Roy, 1961).

The octahedral sheet in clay minerals is a group of octahedron units, which are composed of six oxygen atoms or hydroxyl groups positioned at equal distance from each other, with an aluminum, magnesium, iron, or other atom at the center as shown in figure 2.3. An octahedron unit is shown in figure 2.3(a), and the linkage of octahedron units to form an octahedral sheet is shown in figure 2.3(b) (after Grim, 1968). Octahedral sheets are represented as a rectangular diagram, while the schematic diagram of a silica tetrahedral sheet or silica is represented by a trapezoid in the clay mineralogy as shown in figure 2.4.

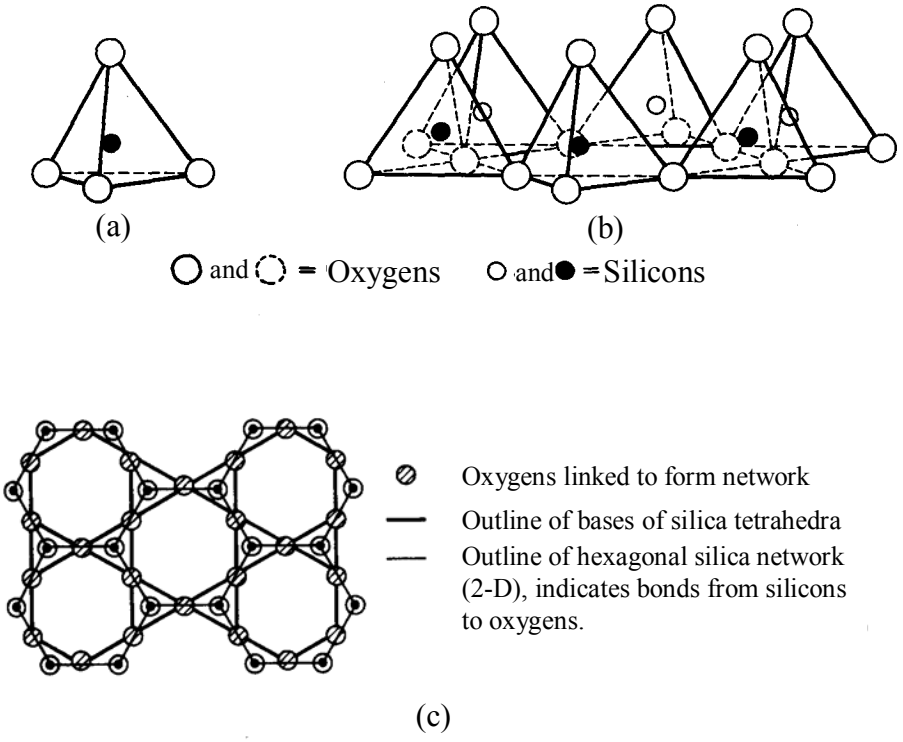

Figure 2.2 Diagrammatic Sketch Showing Clay Tetrahedral (a) a Single Silica Tetrahedron, (b) Isometric View of Silica Sheet, and (c) Top View of Silica Sheet (after Holtz and Kovacs, 1981)

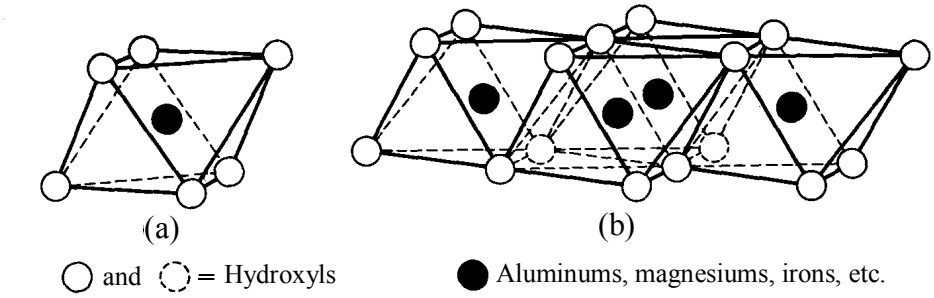

Figure 2.3 Diagrammatic Sketch Showing Octahedral (a) a Single Octahedral Unit and (b) the Sheet Structure of the Octahedral Units (after Grim, 1968).

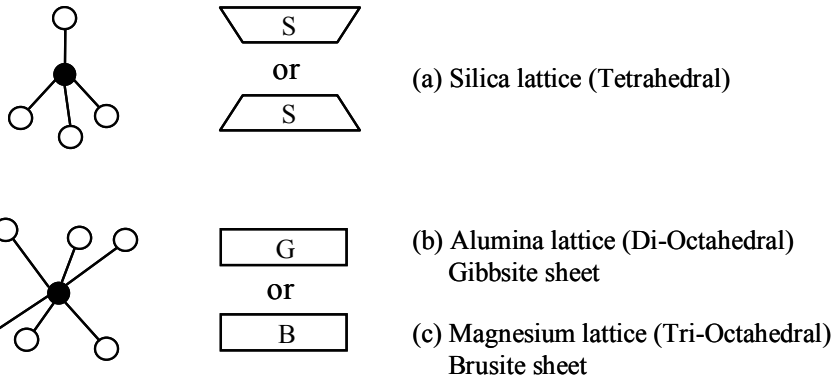

Figure 2.4 Sheet Representation

It can be highlighted that two of every three central spaces of an octahedron are filled with aluminum atoms, keeping the third one vacant. The octahedral sheet where the anions are hydroxyls and two thirds of its available spaces are filled with cations (aluminum) is known as gibbsite as represented by 'G' in the alumina lattice shown in figure 2.4(b). The cations in the octahedral sheet can be substituted with other cations through a geological process called isomorphous substitution. When all the available spaces of cations are filled with magnesium atoms, the mineral is then called brucite shown in figure 2.4(c). Depending on the combinations of various sheets and cations, which in turn form different crystal basic structures, clay minerals have been divided into various groups.

When Al^{3+} cations are located in two of every three available sites in an octahedral sheet, such minerals are known as dioctahedral. In contrast, when divalent cations such as Fe^{2+}, Mg^{2+}, Zn^{2+}, etc., are found to be filled in all the available sites, then such clay minerals are called trioctehedral.

The tetrahedral (T) and octahedral (O) sheets are joined in such a way so as to form two-layer clays (T-O), three-layer clays (T-O-T), or mixed-layer clays that are mixtures of two and three layers clays. The linkage between tetrahedral and octahedral sheets causes the sharing of oxygen atoms and hydroxyls at their interface. Clay minerals show various types of chemical compositions due to the fact that Al^{3+} in octahedral sheets can be replaced by other trivalent cations, such as Fe^{3+}, Cr^{3+}, or divalent cations, such as

Fe^{2+}, Mg^{2+}, Zn^{2+}, or other cations (Faure, 1998). Furthermore, silicon ions (Si^{4+}) in tetrahedral sheets can also be replaced by Al^{3+} ions due to isomorphous substitution, which takes place during the geological formation of various clay minerals. All these substitutions of ions produce excess imbalanced negative charges on the clay particles that, in turn, adsorb positively charged cations to the outer surfaces of tetrahedral sheets of adjacent clay units in order to satisfy electrical neutrality.

2.2.1.1 Classification and Chemical Composition

Clay minerals are classified into groups according to the number of layers and their crystal structure. Each group is divided into subgroups according to their chemical composition in octahedral sheets, and further divided into individual species of clay minerals. Clay minerals are mainly divided into two-layer, three-layer, and mixed-layer clays as follows:

(a) Two-Layer Clays (1 : 1 layer = One Tetrahedral : One Octahedral)

Two-layer clay minerals consist of repeated combinations of one layer of tetrahedral sheet and one layer of octahedral sheet as shown by a representative sheet in figure 2.5. The repeated sheets are bonded by sharing O^{2-} ions between octahedral cations (Al^{3+}) and tetrahedral cations (Si^{4+}) as shown in the structure of a kaolinite layer in figure 2.6 (Grim, 1968). The mineral group of these clays is known as kaolinite with each layer thickness of 0.72 nm as shown in a schematic diagram in figure 2.6. Depending on the isomorphic substitution of cations of octahedral sheets, kaolinite group minerals are further divided into two subgroups, namely, kaolinite (dioctahedral) and serpentine (trioctahedral).

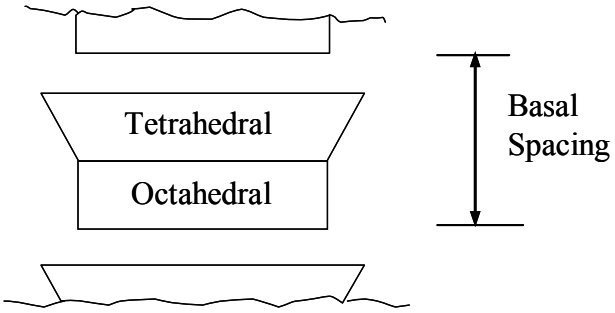

Figure 2.5 Repeated Sheet Representation for
1:1 (Tetrahedral : Octahedral) Layer

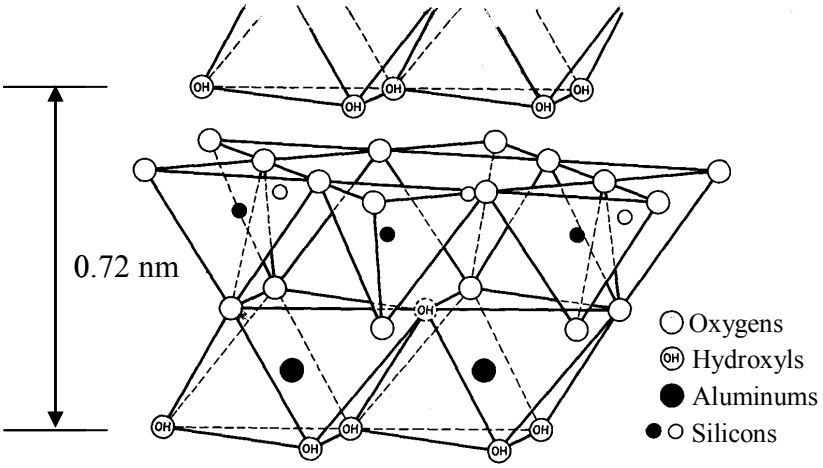

Figure 2.6 Diagrammatic Sketch of the Structure of
the Kaolinite Layer (After Grim, 1968)

The common minerals of the kaolinite subgroup are kaolinite and halloysite which are represented by the same chemical formula $Al_2Si_2O_5(OH)_4 –nH_2O$, where n is the number of water molecules that occupy the interlayer spaces of the clay aggregates. The value of n is zero for kaolinite clay and 4 for halloysite clay. The ideal structure of the kaolinite subgroup minerals produces no ionic charge imbalance, as shown in figure 2.7, and therefore no cations are affected in their interlayer spaces. The individual layers are bonded by strong hydrogen bonds between the OH^- groups of the octahedral sheet and O^{2-} ions of the adjacent tetrahedral sheet. As hydration is not possible within the

interlayer spaces, kaolinite clays do not commonly swell when submerged in water, whereas the halloysite mineral contains a layer of water in its interlayer space which causes an increase in layer thickness of 10.1 Å (McBride, 1994). The interlayer water molecules of halloysite mineral can easily be irreversibly removed by slightly increasing the temperature, after which it behaves like kaolinite clay.

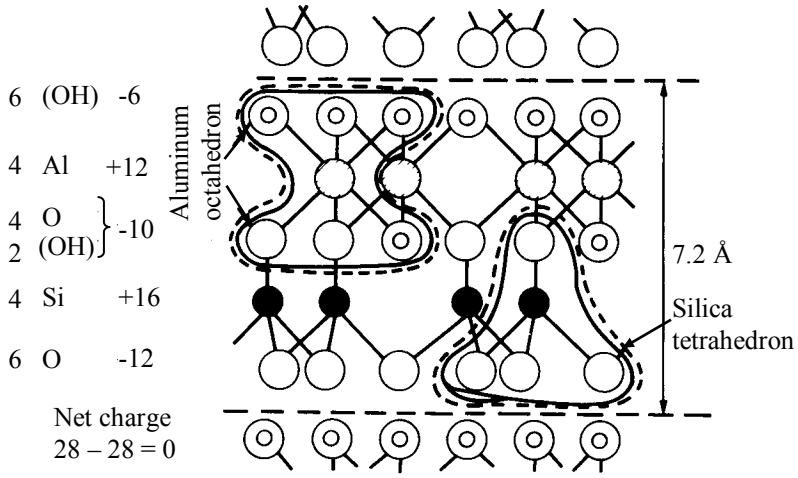

Figure 2.7 Charge Distribution on Kaolinite
(after Mitchell, 1993)

In the serpentine subgroup of kaolinite, the gibbsite dioctahedral sheet is replaced by a brucite trioctahedral sheet, where three magnesium ions replace two aluminum ions and produce ionic balance on its surface. The chemical formula of serpentine is $Mg_3Si_2O_5(OH)_4$ or $Fe_3^{2+}Si_2O_5(OH)_4$ which is known as greenalite, where three Fe^{2+} ions replace two Al^{3+} ions in the octahedral sheet.

(b) Three-Layer Clays (2: 1 layer = two tetrahedral : one octahedral)

These clay minerals consist of an octahedral sheet sandwiched in between two sheets of tetrahedrals with the oxygen tips of the tetrahedrons combining with the hydroxyls of the octahedron to form a single layer as shown in the figure 2.8 (Holtz and Kovacs, 1983; Faure, 1998). Depending on their chemical composition, crystal

structures and physical properties, these minerals have been divided into six groups, namely, pyrophyllite, smectite, vermiculite, mica, brittle mica and chlorite (Faure, 1998).

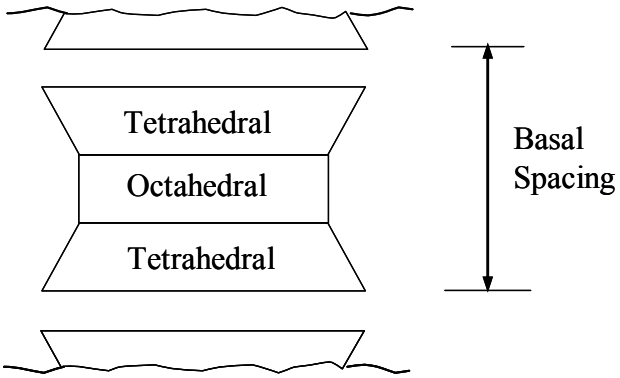

Figure 2.8 Repeated Sheet Representation for 2:1 (Tetrahedral : Octahedral : Tetrahedral) Layer

[Smectite] is the largest group in the three-layer clays, where the minerals are produced due to full or partial replacement of Al^{3+} in the octahedral sheet and partial replacement of Si^{4+} in the tetrahedral sheet (Grim, 1968, Faure, 1998). The smectite group is divided into two subgroups, namely, dioctahedral when isomorphous substitution occurs in alumina (gibbsite) octahedral sheets and silica tetrahedral sheets, and trioctahedral when substitution occurs in magnesium (brucite) octahedral sheets and silica tetrahedral sheets. Substitution of Si^{4+} in the tetrahedral layer is commonly limited to only 15% by mainly Al^{3+} ions, while Al^{3+} in the octahedral sheets are generally replaced by various types of cations such as Mg^{2+}, Fe^{2+}, Zn^{2+}, Ni^{2+}, Li^{+}, etc. (Grim, 1968).

Montmorillonite is the most commonly found mineral in the dioctahedral smectite subgroup, where substitution of one Mg^{2+} occurs in every sixth Al^{3+} in octahedral sheets, as shown in figure 2.10, and no substitution takes place in tetrahedral sheets. This results in a net charge deficiency of about 0.66 – per unit cell as calculated in figure 2.10. This net charge deficiency is balanced by exchangeable cations adsorbed between the unit layers and around their edges as shown in the crystalline structure in figure 2.9. The

stoichiometric formula for a unit cell of Na-montmorillonite where the interlayer cation is sodium is written as $[Si_8(Al_{3.34}Mg_{0.66})O_{20}(OH)_4].Na_{0.66}$. Other commonly found exchangeable cations adsorbed within the interlayer spaces are Ca^{2+}, K^+, and Mg^{2+}.

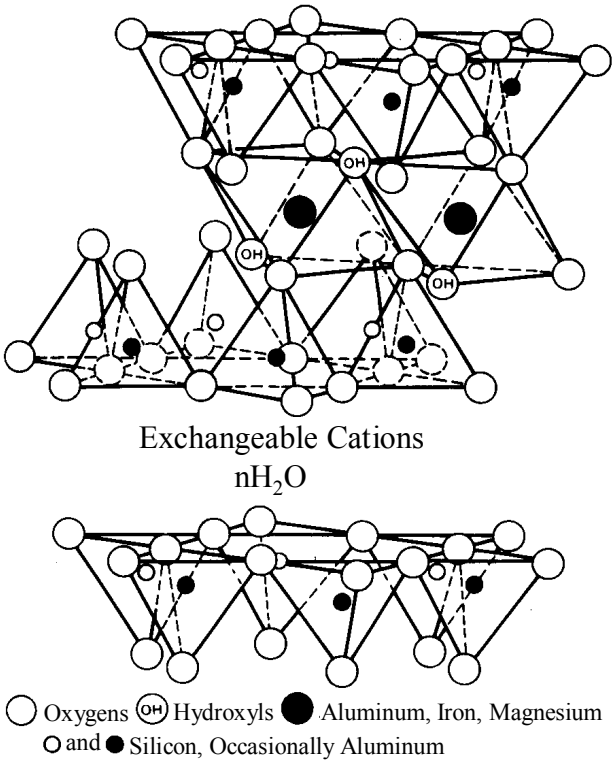

Figure 2.9 Diagrammatic Sketch of the Montmorillonite

The trioctahedral smectites include the mineral species saponite, hectorite, and sauconite (Faure, 1998). In saponite, the octahedral sheet is fully occupied by Mg^{2+} instead of Al^{3+}, and the charge deficiency is due to the isomorphous substitution of Si^{4+} by Al^{3+} in its tetrahedral sheet. The chemical formula of unit cell of saponite is given by Grim (1968) as $[Mg_6(Si_{7.34}Al_{0.66})O_{20}(OH)_4].Na_{0.66}$.

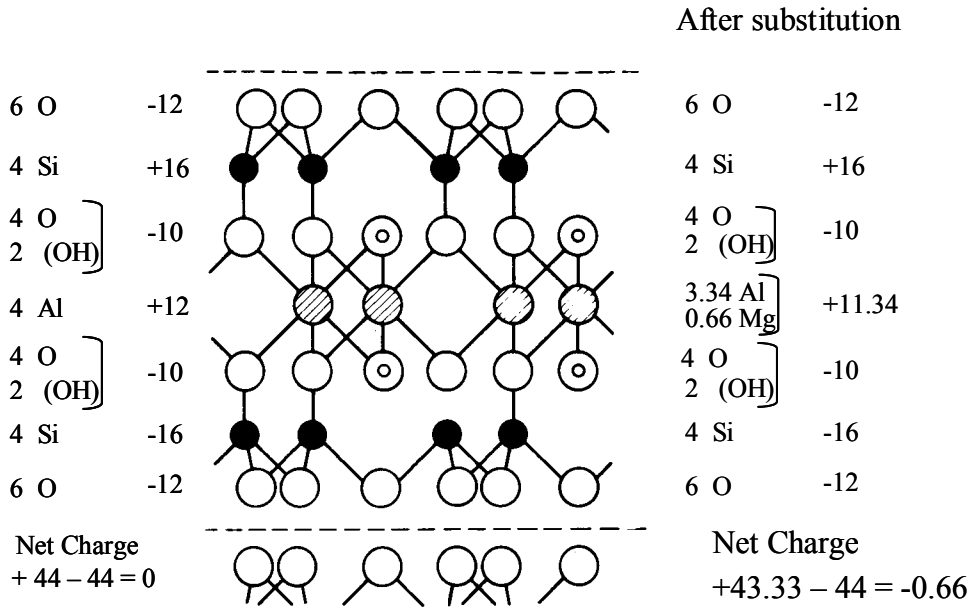

Figure 2.10 Charge Distribution in Montmorillonite (After Mitchell, 1993)

[Vermiculite], like smectite, has 2:1 layer sheet structures with both the dioctahedral and trioctahedral forms of clay mineral. The chemical formula of a typical vermiculite is given by McBride (1994) as $[(Mg, Al, Fe^{3+})_6(Si_{8-x}Al_x)O_{20}(OH)_4]$ $(Mg.Ca)_x$ where, x = 1 to 1.4. The structure is unbalanced mainly due to the substitutions of Al^{3+} for Si^{4+} in tetrahedral sheet and causes a residual net charge deficiency of 1 to 1.4 per unit cell. The higher charge deficiency in the tetrahedral sheet causes exchangeable cations in the interlayer (mainly Mg^{2+} with small amount of Ca^{2+}) to electrostatically pull the layer together and thus reduce the layer thickness. As reported by Grim (1968), many researchers have concluded that vermiculite has only two molecules sheets of water present in the interlayer, creating the characteristic spacing of 14Å, as shown in figure 2.11(b). In trioctahedral vermiculite, the charge deficiency in the tetrahedral sheet is partly compensated by an additional positive charge in the Al or Fe octahedral sheet.

[Illite] is a nonexpandable dioctahedral clay under the mineral group called mica. Its basic unit is a layer composed of two inward-pointing silica tetragonal sheets with a central octahedral sheet, as shown in figure 2.11 (a). In the illites, one-sixth of Si^{4+} ions

are replaced by Al^{3+} in octahedral sheets, which generates the net-unbalanced-charge deficiency of 1.3 per unit cell (Grim, 1968). The resultant charge deficiency is compensated by the potassium ions in the interlayer spaces, which are fitted into the hexagonal holes formed by the silica sheets. Therefore, illite has a low cation exchange capacity with very little or no water adsorption, which prevents it from swelling.

[Chlorites] are the 2:1 layered clay minerals which can be trioctahedral or dioctahedral in nature. In chlorites, the negative charge produced due to replacement of Si^{4+} by Al^{3+} is neutralized by the positive charge of brucite sheets generated due to the replacement of Mg^{2+} by Al^{3+} sandwiched in the interlayer position which bonds two tetrahedral sheets of two adjacent layers.

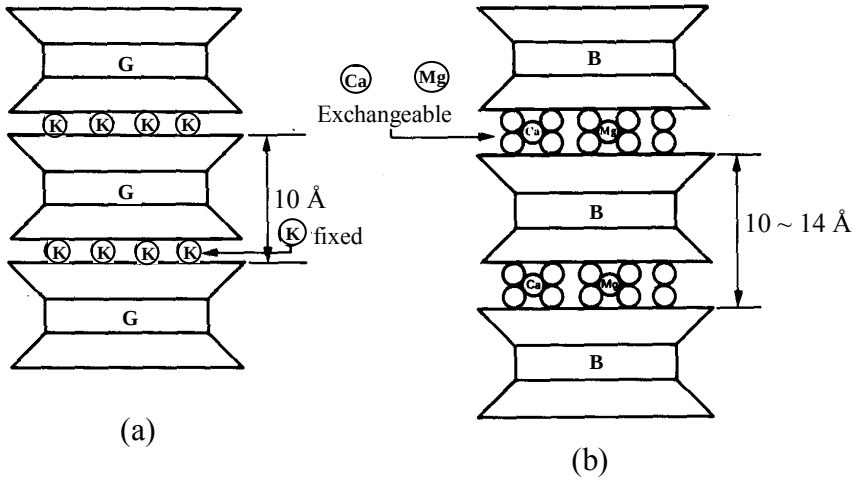

Figure 2.11 Schematic Diagram of the Structures of (a) Illite and (b) Vermiculite

2.2.2 Cation Exchange Capacity

Cations are attracted and held in between the sheets, on the surfaces, and on the edges of particles in order to maintain the electro-neutrality of particle charges. The cations, which are exchangeable and readily available to be replaced by similar or other

types of cations under different environmental and phase conditions, are quantified in terms of the cation exchange capacity of clay.

Cation Exchange Capacity (CEC) is defined as the quantity of cations reversibly adsorbed by clay particles, expressed as milliequivalents (meq) per 100 grams of dry clay mineral. As shown in the table 2.1, the cation exchange capacities of montmorillonite and vermiculite minerals are the highest (in the range of 80~150 meq/100g) among all clay minerals because of their high isomorphous substitution within the octahedral and tetrahedral layers, respectively, which results in a large ionic deficiency.

Table 2.1 Some Clay Minerals Characteristics (after Mitchell, 1993)

Mineral	Interlayer bond	Basal sapcing	Specific surface (m^2/gm)	Cation exchange capacity (mEq/100 g)
Kaolinite	Hydrogen strong	7.2 Å	10-20	3-15
Montmorillonite	Oxygen-Oxygen Very weak	9.6 Å	700-840	80-150
Illite	K ions: strong	10 Å	65-100	10-40
Vermiculite	Weak	10.5-14 Å	870	100-150
Chlorite	Strong	14 Å	-	10-40

When water comes in contact with clay particles, adsorption of positively charged ions with hydrated water molecules occurs at the interface between the solid phase and the aqueous phase. According to Sposito (1989, 1981), adsorption of cations on clay particle surfaces and interlayers can take place by any of the three mechanisms as shown in figure 2.12.

The siloxane surface, the plane of oxygen atoms on the surface of a 2:1 layer silicate, is characterized by a series of hexagonal cavities among its constituent oxygen atoms, which are formed by six corner-sharing tetrahedra. The diameters of these cavities are found to be around 0.26 nm and are surrounded by six sets of electron orbits originating from the nearby oxygen atoms (Sposito, 1989, 1981).

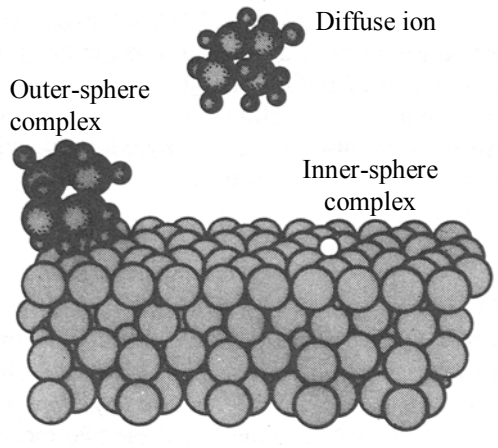

Figure 2.12 The Three Mechanisms of Cation Adsorption on a Silicate Surface; e.g. Montmorillonite (after Sposito, 1989)

The activity of a siloxane surface cavity depends on the charge distribution of the surrounding layer silicate structure. A siloxane cavity can act as a mild electron donor if the near layer charge deficiency is low or zero, and can produce a complex with neutral dipolar molecules such as water. The complexes formed in the cavity on a neutral interlayer silicate structure are very unstable and easily separable from their constituents. On the other hand, if negative charges are present in the octahedral layer, complexes formed in the cavity with interlayer cations and water molecules become strong enough to be immobile and can even get much stronger when formed near the surface of a negatively charged tetrahedral sheet where the layer charges are much closer to the cavity surface oxygen atoms.

Two types of surface complexes are shown in figure 2.12, namely, the inner-sphere complex, which is the result of the entrapment of ions or molecules within the surface cavity without the interference of water molecules, and the outer-sphere complex, which is produced by ions or molecules with at least one molecule of water attached to the surface functional group. Outer-sphere complexes, which are formed due to electrostatic bonding, are generally weaker than inner-sphere complexes involving either ionic or covalent bonding mechanisms.

Besides forming inner-sphere and outer-sphere complexes, the interlayer cations can also be adsorbed and neutralized by the negatively charged clay particles to form a diffuse-ion swarm, as shown in figure 2.12. Such diffuse ions are dissociated from the surface functional groups and are free to move in the interparticle solution.

Readily exchangeable ions in soil are those that can be easily replaced by other ions in an electrolyte solution passing through the soil. Ions located within the diffuse-ion swarm and the outer-sphere complex are the main readily exchangeable ions in the soil.

2.2.3 Cation Replaceability

Exchangeable cations are hydrated when mixed with water or liquid solutions and are readily displaced into solutions by cations of other types of higher replaceability (McBride 1994). The capacity of cationic replaceability depends mainly on the valence, the relative abundance of different ion types in the solution and the silicate exchangeable layer, and the hydrated ion size. As generally reported in the geochemistry and fundamental soil mineralogy literature (Mitchell, J. K, 1993; Schulze, D.G. 1989; Kelly, W.P. 1948; McBride, M.B. 1994), higher valence cations replace lower valence cations and smaller hydrated cations or larger ionic radius cations replace larger hydrated cations or smaller ionic radius cations of the same valence that are present in the exchangeable sites.

Besides the above criteria for cation replaceability, the concentration of cations in the solution plays an important role in the replacement process. In general, the replaceability series, also known as the "lytropic series," is as follows:

$$Li^{+} < Na^{+} < K^{+} < Rb^{+} < Cs^{+} < Mg^{2+} < Ca^{2+} < Ba^{2+} < Cu^{2+} < Al^{3+} < Fe^{3+}$$

An exception to the above replaceability is possible when the cations of lower replacing power exist in very high concentrations in solution relative to high replacing power cations (Mitchell, 1993). Table 2.2 and 2.3 show the radii of ions in dry and hydrated condition respectively.

Table 2.2 Radii of Ions

Ions	Ionic radius (Å)
Li^+	0.68 – 0.82
Na^+	1.07 – 1.40
K^+	1.46 – 1.68
Mg^{2+}	0.66 – 0.97
Ca^{2+}	0.83 – 0.95
Al^{3+}	0.47 – 0.61
Fe^{3+}	0.57 – 0.63

After Faure, G. 1998

Table 2.3 Hydrated Radius of Cations

Ions	Hydrated Ionic radius (Å)
Li^+	7.3 – 10.0
Na^+	5.6 – 7.9
K^+	3.8 – 5.3
Mg^{2+}	10.8
Ca^{2+}	9.6

After Mitchell, 1993

Ion exchange can also be viewed a chemical reaction, but exchange of ions occurs only due to broken bonds and long range electrostatic bonds of low energy (McBride, 1994). As such, ion exchange "reactions" are similar to inorganic chemical reactions and are typically written in the same form as given in equation (2.1), where Na^+ ions from a layer of silicate clay surface are exchanged by Ca^{2+} in a $CaCl_2$ solution.

$$CaCl_2\,(aq) + 2NaX(s) = 2NaCl\,(aq) + CaX_2(s) \qquad (2.1)$$

where (aq) and (s) refer to the aqueous electrolyte solution and solid (exchanger) phases, respectively, and X represents the relatively insoluble aluminosilicate portion of the clay mineral. The aluminosilicate can be assumed to act as a single anion with an equivalent charge of one.

Thermodynamic theories that are applicable to inorganic chemical reactions are also applicable in the same way to those of cation exchange reactions (Sposito, 1981). The thermodynamic potential of a reaction is commonly described by the Gibbs-Duhem equation as expressed in equation (2.2). The standard free energy change of the reaction (ΔG^o) defines the direction of the reaction as follows:

$$\Delta G^o = \sum_{products} \mu^o - \sum_{reactants} \mu^o \qquad (2.2)$$

where the superscript ^{o} refers to the conventional standard state which is at standard temperature (25^{o}C) and standard atmospheric pressure (101.3 kPa). The symbol μ refers to Gibbs free energy of each chemical species. When ΔG^{o} is negative, the forward reaction has excess energy when it occurs in the standard state.

An example of soil thermodynamics theory has been cited by Sposito (1981) in terms of cation exchange reaction that occurs between an aqueous electrolytic solution of Ca^{2+} cations and Na^{+} saturated Camp Berteau montmorillonite. The cation exchange reaction can be expressed as:

$$2NaX\ (s) + Ca^{2+}\ (aq) \longleftrightarrow CaX_2\ (s) + 2Na^{+}\ (aq) \qquad (2.3)$$

where $X \equiv \left[Si_{11.94}\left(Al_{4.358}Fe^{3+}_{0.612}Fe^{2+}_{0.045}Mg_{0.955}\right)O_{29.85}\left(OH\right)_{5.97}\right]$ represents the aluminosilicate part of the montmorillonite normalized to the fractional charge deficiency [obtained by dividing each stoichiometric coefficient in the chemical formula of Camp Berteau montmorillonite by 0.335 eq/fw, the cation exchange capacity due to isomorphous substitutions].

The standard free energy for the above cation exchange reaction, as given in equation (2.3), can be calculated from the individual reactants' and products' free energy (μ^{o}) (Sposito, 1981; Faure 1998).

μ^{o} (Na-mont) = -5,346.1 kJ mol^{-1}

μ^{o} (Ca-mont) = -5,352.3 kJ mol^{-1}

μ^{o} (Na^{+} (aq)) = -261.9 kJ mol^{-1}

μ^{o} (Ca^{2+} (aq)) = -553.5 kJ mol^{-1}

The standard free energy change for the reaction in equation (2.3) can be calculated for the Na- and Ca-montmorillonite by dividing the above corresponding values by 0.335 and multiplying by the valence of the exchangeable cation to place them on an equivalent basis as follows:

μ^{o} (NaX(s)) = (1/0.335) μ^{o} (Na-mont) = -15,958.5 kJ mol^{-1}

μ^{o} (CaX_2(s)) = (2/0.335) μ^{o} (Ca-mont) = -31,954.0 kJ mol^{-1}

Therefore, the net change in free energy, ΔG^o, is:

$\Delta G^o = \{-31,954.0 + 2\ (-261.9)\} - \{2\ (-15,958.5) + (-553.5)\}$

$= -7.3\ \text{kJ mol}^{-1}$

Since the free energy due to the cation exchange reaction according to equation (2.2) is negative, the forward reaction has an excess energy when it occurs in the standard state, which favors the direction as written. Thus, the reaction and formation of Ca-montmorillonite is thermodynamically favorable.

The hydration energy of cations, defined as the amount of energy released when dry cationic substances are mixed or hydrated in water, has also been used in the Eisenman energy model of cation exchange, where the behavior of ions of different radius has been incorporated. As described by McBride (1994), the electrostatic attraction energy, E_{att}, between an adsorbed cation and the surface charge site is inversely proportional to the finite distance between the charge centers, as shown in figure 2.13, and is given by equation (2.4) as follows:

$$E_{att} \alpha \frac{e^2}{(r_s + r_A)} \qquad (2.4)$$

where e is the electronic charge unit. This is the energy that is required to displace the water molecules present between the cations and the charged clay surface.

The presence of water molecules on the clay surface is the result of the hydration of the clay surface and the exchangeable cations. The total energy change, E_{tot}, in excess of the attraction energy due to the movement of a monovalent ion, A^+, from the solution to the surface is given by McBride (1994) as:

$$E_{tot} \infty \left\{ -\left(\frac{e^2}{r_s + r_A} \right) + E_s + E_A \right\} \qquad (2.5)$$

where r_A and E_A are the radius and hydration energy of cation A, respectively. The parameter r_s is the effective radius of the charge surface, as shown in figure 2.13, and E_s is the hydration energy of the surface. For the cation exchange of ion B^+ by ion A^+ on the same clay surface, the overall change of energy would be:

$$\Delta E_{tot} \propto \left\{ \left(\frac{e^2}{r_s + r_B} - \frac{e^2}{r_s + r_A} \right) - (E_B - E_A) \right\} \qquad (2.6)$$

where r_B and E_B are the radius and hydration energy of displaced ion B.

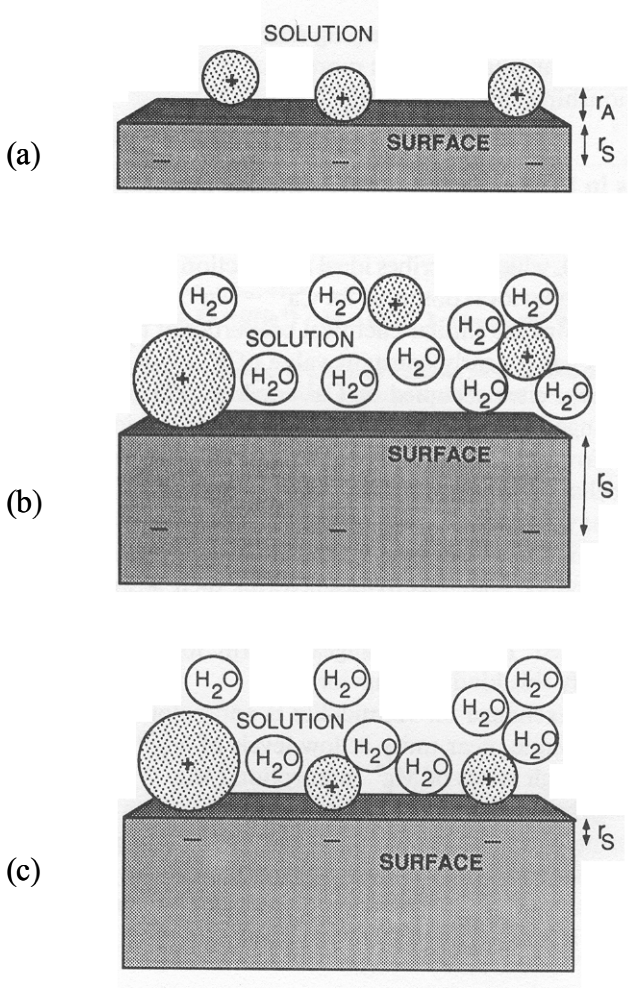

Figure 2.13 Schematic Diagram of the Clay Surface-Exchange Cation Interaction in (a) Dry Condition, (b) Water on a "Weak Field", (c) Water on a "Strong Field" Exchanger (after McBride, 1994)

When the distance between the cation charge center and the location of negative structural charge in the clay ($r_s + r_A$ or $r_s + r_B$) is large, as is the case for montmorillonite minerals where isomorphous substitution occurs in the octahedral layer, the electrostatic term of equation (2.6) is negligible. Therefore, in the weak field condition, as depicted in figure 2.13, the total change of energy due to cation exchange would be equivalent to the

difference in ionic hydration energies. From Table 2.4, it is clear that the cations of higher hydration energies can be easily replaced by cations of lower hydration energies to come into contact with the surface and release energy during the process. It can be noted that the Eisenman model is not considered to be a complete solution as it does not cover the changes of entropy (disorder) of various cations during exchanges.

Table 2.4 Hydration Energy of Metal Cations (after McBride, 1994)

Ion	Hydration energy (kcal/mol)	Ion	Hydration energy (kcal/mol)
Li^+	124	Mg^{2+}	460
Na^+	97	Ca^{2+}	381
K^+	77	Ba^{2+}	312
Rb^+	71	Al^{3+}	1114
Cs^+	63	Fe^{3+}	1046

2.3 Permeant Characteristics

Bentonite clay is being used in various applications of solution containment as well as a water barrier, in which a number of chemicals are dissolved. These chemicals may be generated from many different industrial, commercial, and household application processes. This section is mainly focused on sources of various chemical solutions that are blended in water which are required to be contained by clay liners and similar barrier materials.

2.3.1 MSW Leachate

Bentonite clay, as an active component of Geosynthetic Clay Liners (GCL) is being widely used in Municipal Solid Waste (MSW) landfill construction where the

proper functioning of the lining system is critical in terms of containment effectiveness of generated leachates. Leachate is formed when water infiltrates the waste in the landfill cell. The water within the landfill could be generated either from a combination of precipitation from rain and melted snow, or from the waste itself. As the liquid moves through the landfill, many organic and inorganic compounds, such as heavy metals, are transported through the leachate.

The amount of leachate produced is directly linked to the amount of precipitation around the landfill. The amount of liquid waste in the landfill also affects the quantity of leachate produced. Leachates are potentially hazardous wastes in landfill sites. It is of the utmost importance that leachates are treated and contained within the landfill to prevent any contamination and mixing with fresh ground water.

Leachate generated from municipal solid waste (MSW) and hazardous waste (HW) landfills is a mixture of organic and inorganic compounds, as well as dissolved and colloidal solids. In order to design a collection and treatment system for leachate, it is important to have an understanding of the wastes placed in the landfill, as well as the physical, chemical, and biological processes that are occurring within the landfill.

The quality and chemical composition of leachates vary tremendously depending of a number of factors which include mainly:

(a) Waste Composition

The waste composition of MSW, especially household refuse (eg. food, garden wastes, animal residues, etc), contributes and determines the range and extent of biological activity within the landfill (Chen and Bowerman, 1974). Inorganic constituents in leachates are mainly derived from construction and demolition debris, industrial wastes, household furniture and electrical appliances, vehicle parts and tires, etc.

(b) Depth of Waste

Higher depth of waste is found to contribute to higher concentrations of leachate at the base of the waste layer before entering into the lining

systems. Deeper waste also requires a longer time to decompose as the water takes longer to reach larger depths. As the water percolates through the deeper waste, it travels a long distance and reacts with larger quantities of waste material, which eventually yields a highly concentrated chemical solution at the base lining system (Qasim and Chiang, 1994).

(c) Moisture Availability

The quantity of water or the degree of saturation of waste materials within the landfill is the most important controlling factor of leachate quality. High quantities of moisture within loose or less compacted waste landfills increase the rate of flushing, which removes the majority of the contaminants during the early stages of filling, whereas in more compacted or low permeability landfills, high moisture causes an increase in the rate of anaerobic microbial activity which generates high strength of organic leachates (McBean *et al*., 1995; Chen and Bowerman, 1974). Low amounts of moisture take longer to fully react with all the available inorganic and organic agents of waste materials and therefore develop a slow stabilization rate of the landfill chemistry (McBean *et al*., 1995; Miller *et al*., 1994)

(d) Oxygen Availability

The amount of available oxygen controls the type of decomposition (i.e. anaerobic or aerobic) of organic components in landfill wastes. Aerobic decomposition happens when the oxygen is available within the landfill, i.e., during the operation stage, at the top layer of the waste, and within loosely compacted waste fills where air voids are available. Carbon dioxide, water, lightly concentrated organic compounds, and heat are generated during aerobic decomposition while highly concentrated organic acids, ammonia, hydrogen, carbon dioxide, methane, and water are produced during anaerobic degradation (McBean *et al*., 1995).

(e) Temperature

Temperature within the landfill is responsible for bacterial growth, which controls organic and chemical reactions of the waste materials. The solubility of many inorganic salts [e.g. NaCl, KCl, $MgCl_2$, $Ca_3(PO_4)_2$] increases with temperature. However, the solubility of a number of other chemical compounds that are present in leachates, such as $CaCO_3$ and $CaSO_4$, deceases with increasing temperature as investigated by Lu *et al*. (1985).

(f) Age of Landfill

The age of a landfill directly controls the quality of leachate. Leachates with maximum contaminants are found within 2-3 years of the final placement of wastes in the landfill, after which the amount of contaminants decline steadily over the next 10-15 years (McBean *et al*., 1995; Lu *et al*., 1985). Depletion of inorganic compounds is much faster than that of organic compounds which continue for a long period of time due to bacterial and other microorganism reactions (Lu *et al*., 1985).

Table 2.5 shows the wide variation in leachate quality as investigated by various researchers (after Reinhart and Grosh, 1998). A more detailed breakdown of organic and inorganic compounds of two MSW landfill leachates is given in Table 2.6, which was published in a report by the Ontario Ministry of Environment, Canada, in 1996.

2.3.2 Ash Leachate

Ash from Waste-To-Energy (WTE) facilities is being generated in abundance in the United States of America as the volume of solid waste increases with the increasing growth of population. The incinerated residues, composed of bottom ash and fly ash, are commonly disposed in landfills under Subtitle D ash monofills, provided that the

materials are non-hazardous according to USEPA's recommended Toxicity Characteristics Leaching Procedure (TCLP) test.

The main factors, among many others, which affect the variation in chemical composition of ash are believed to be the source of burning materials (type of solid waste), methods of incineration, and additives used in the process of neutralizing hazardous materials (Muhammad and Ashmawy, 2003).

Table 2.5 Chemicals in Leachates as Found by Different Researchers (after Reinhart and Grosh, 1998)

Parameter	Ehrig, 1989	Qasim and Chiang, 1994	South Florida* Landfills, 1987	Pohland and Harper, 1985
BOD (ppm)	20 – 40,000	80 – 28,000	-	4 – 57,700
COD (ppm)	500 – 60,000	400 – 40,000	530 – 3,000	31 – 71,700
Iron (ppm)	3 – 2,100	0.6 – 325	1.8 – 22	4 – 2,200
Ammonia (ppm)	30 – 3,000	56 – 482	9.4 – 1340	2 – 1,030
Chloride (ppm)	100 – 5,000	70 – 1330	112 – 2360	30 – 5,000
Zinc (ppm)	0.03 – 120	0.1 – 30	-	0.06 – 220
P (ppm)	0.1 – 30	8 – 35	1.5 – 130	0.2 – 120
pH	4.5 – 9	5.2 – 6.4	6.1 – 7.5	4.7 – 8.8
Lead (ppm)	0.008 – 1.020	0.5 – 1.0	BDL – 0.105	0.001 – 1.44
Cadmium (ppm)	<0.05 – 0.140	<0.05	BDL – 0.005	70 – 3,900

BDL – below detection limit

* - South Florida Water Management District, 1987.

Chemical analysis of various types of fly ash conducted by many researchers revealed that the major four minerals present in the fly ash are silica (SiO_2), alumina (Al_2O_3), calcium oxide (CaO), and iron oxide (Fe_2O_3). Other minor minerals, which are normally less than 5% in total weight, are magnesium oxide (MgO), sodium oxide (Na_2O), titanium oxide (TiO_2), potassium oxide (K_2O), phosphorus oxide (P_2O_3), sulfur trioxide (SO_3), and trace metals oxide (Edil *et al*., 1992; Joshi *et al*., 1994;

Wentz *et al.*,1988; Porbaha *et al.*, 2000; Hettiaratchi *et al.*, 1999). The four major minerals found in combined MSW ash are the same as those in fly ash but the amount of calcium oxide (CaO) is predominant compared to other minerals because of the presence of free-lime used in the process of incineration (Keith and Goodwin, 1990).

Table 2.6 Chemical Composition of Two MSW Landfill Leachates

Parameter	Muskoka	Guelph
Benzene (ppb)	18	19
Toluene (ppm)	263	201
Ethylbenzene (ppm)	35	80
m + p-xylene (ppm)	66	148
O-xylene (ppm)	37	85
NH^{4+} (ppm)	103,000	865,000
K (ppm)	114	1301
Ca (ppm)	203	883
Mg (ppm)	29	525
Fe (ppm)	38	1
B (ppm)	1	8
Cl^- (ppm)	98	2464
EC (mS/cm)	1.4	9.9
pH	5.4	7.0

The electrical conductivity (EC) of the effluent solution is found to be reduced to around 1000 microsiemens/cm from their initial high values of 100,000 microsiemens/cm within less than 5 pore volumes of flow though the specimens of compacted ash materials Therefore it is concluded that the majority of the salts (chlorides and sulfides) are "flushed" out of the sample within a maximum of 5 pore volumes (Muhammad and Ashmawy, 2003).

The research conducted by Muhammad and Ashmawy (2003) on ash leachates also reveals the pattern of attenuation of sodium, calcium and potassium in the effluent

permeant with pore volumes of permeation. It was observed that the initial high calcium concentration of 15,000 to 35,000 ppm was reduced to below 3,000 ppm within 5 pore volumes of permeation, with further reduction to less than 500 ppm after around 12 pore volumes. The same trend was also observed for sodium and potassium ion concentrations. The concentration of sodium ions was reduced from an initial high concentration of around 10,000 -12,000 ppm to less than 500 ppm within 8 pore volumes. Similarly, potassium ions decreased in concentration from around 6,000-9,000 ppm to less than 500 ppm within 5 pore volumes of permeation. The trend of attenuation of all the main elements replicates the attenuation of EC values of effluent.

2.3.3 Other Sources of Inorganic Leachates

Bentonite waterproofing has proven reliable for a wide range of applications, including underslab, back-filled walls, plaza deck, and property line construction such as soldier piles and lagging. Underslabs typically are installed directly on a properly compacted substrate, eliminating the requirement for a mud slab. The swelling properties of bentonite are effective in sealing small concrete cracks caused by settlement, seismic action or other similar conditions. For installations where groundwater is contaminated or has a high level of salt concentration, contaminant-resistant bentonite characteristics are required.

Bentonite waterproofing systems are employed on fresh concrete as soon as the concrete forms are removed in order to preserve concrete water / cement ratio and to prevent any external ingress into the concrete. Limitations of bentonite waterproofing include proper confinement for maximum performance. Bentonite waterproofing should not be installed when properly compacted back-fill or concrete cover is absent, as proper confinement is required.

Bentonite can be used to form a cut-off wall by injection or pressure grouting and/or slurry trenching. It is also being used in repairing cracks of earth dams or

embankments used in storing industrial byproducts containing organic or inorganic contaminants, as shown in figure 2.14.

Bentonite is also used in pipe connections such as at the joints between concrete or synthetic pipes and manholes in sewer construction, where a large amount of contaminated slug flows constantly, as shown in figure 2.15. Other uses include earthen ponds and lagoons, where bentonite is exposed to the contained water, which affects its performance if highly concentrated dissolved salts are present. The swelling property when hydrated allows bentonite to fill voids or unexpected opening in sandy soils, where it acts as a "self-healing" material.

Drilling fluids have been used for years to stabilize boreholes during drilling operations. In the 1950's, civil and geotechnical engineers discovered that deep, narrow trenches excavated in granular soils could also be stabilized using the same technology to prevent collapse of the sidewalls. The excavated materials could then be mixed with bentonite slurry and backfilled, providing an economical barrier to lateral flow of water and many fluid pollutants since fluid loss of the pure bentonite plays can affect long term performance. The amount of fluid loss is also affected by the quality of the water that is expected to be in contact with the bentonite.

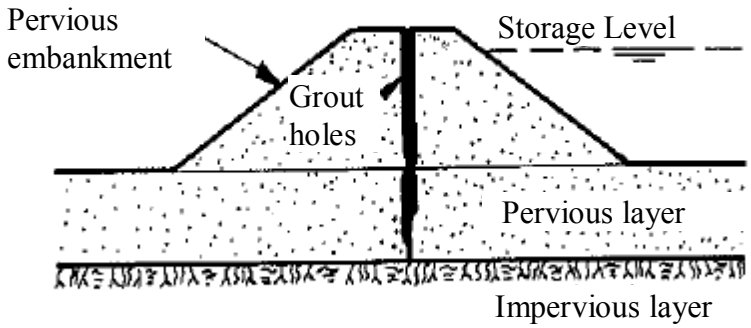

Figure 2.14 Application of Bentonite in Embankment or Earthen Dam

In all of the above applications, bentonite is expected to encounter water-borne contaminants or highly concentrated organic or inorganic salt solutions where Ca, Mg, K,

and Na dissolved cations are present. The existence of these cations in salt solutions is responsible for the deteriorating performance of the bentonite component of the structure.

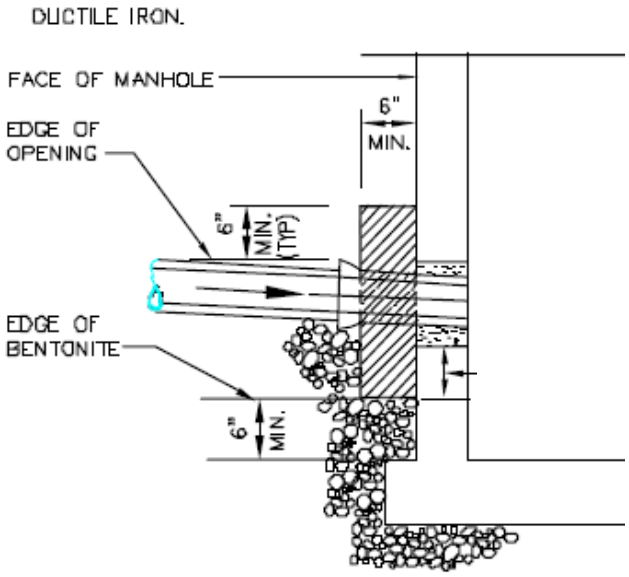

Figure 2.15 Application of Bentonite in Manhole-Pipe Connection

2.4 Water-Bentonite Interaction

Adsorbed cations needed to neutralize the negatively charged particles are tightly held on the clay surface in the dry phase of the clay. Dried clays adsorb water from the atmosphere at low relative humidities. Clays in the smectite group swell when they adsorb water, and need temperatures above 100^{o}C to remove most of the water within the pore spaces. Much higher temperatures in the range of 500 ~ 1000^{o}C are needed to remove all the water within clay interlayer spaces, which is held tightly on the clay particles due to the negative charge on the surface.

In the clay chemistry literature, clays are considered to be lyophobic (liquid hating) or hydrophobic (water hating) colloids rather than lyophilic or hydrophilic colloids, even though water is adsorbed by the clay particles. Hydrophilic colloids are

those that adsorb water so as to form a colloidal solution instantaneously (van Olphen, 1977). Clays are considered hydrophobic because:

(a) it has a two-phase system with a large interfacial surface area,

(b) clay-water behavior is dominated by clay surface forces, and

(c) it can flocculate in the presence of small amount of salts.

2.4.1 Mechanisms of Interaction

The following mechanisms for clay-water interaction are possible:

(a) Hydrogen Bonding

Because the clay mineral's exposed surfaces are either composed of oxygens or hydroxyls ions, hydrogen bonding develops with oxygen attracting the positive corner (H^+) of water molecules and hydroxyl attracting the negative portion (O^-), as shown in figure 2.16(a). This bond will redistribute and reorient the charges in normal water, and the bonded water molecules will progressively alter the direction of adjacent molecules. The bonding will become less rigid with distance from the surface of the clay due to the surface force fields as well as the increase in the force fields of the water structure (Mitchell 1993).

(b) Exchangeable Cations

Exchangeable cations that are attracted on the negatively charged surfaces get hydrated when mixed with water and are attracted to the clay surface in the form of hydrated molecules, as shown in figure 2.16(b). Positively charged cations are surrounded by the negative corner of the water molecules.

(c) Attraction by Osmosis

The concentration of hydrated cations near to the charged surface is higher due to the electrostatic attraction. Due to this electrostatic attraction, cations are prevented to diffuse away from the surface so the concentration of water molecules is lower at near the surface of clay particles. This variation in water concentration causes water molecules to

diffuse toward the vicinity of the charged surface due to osmotic pressure, as shown in figure 2.16(c) (Mitchell, 1993).

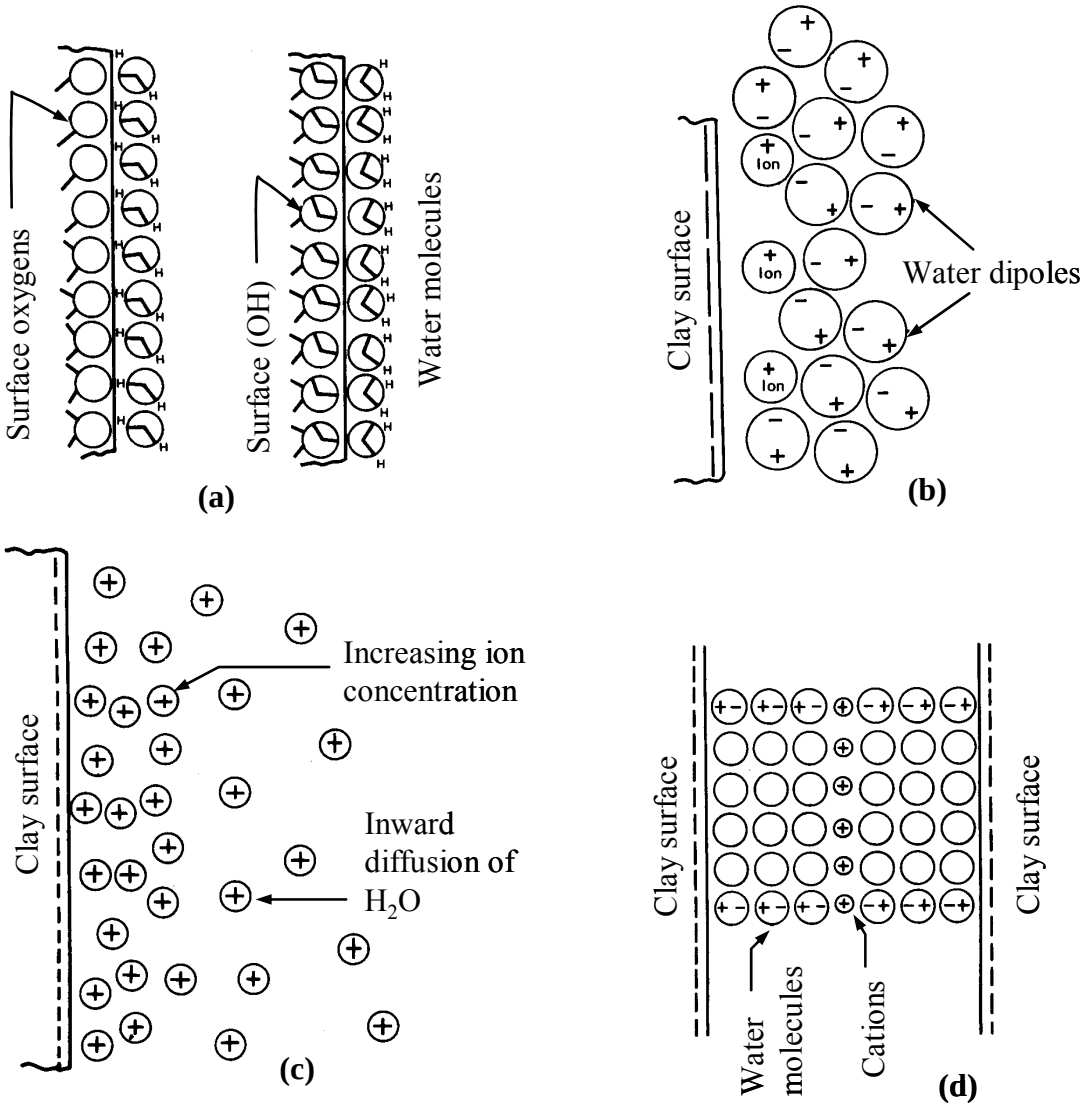

Figure 2.16 Possible Meachanisms of Water Adsorption by Clay Surfaces (a) Hydrogen bonding, (b) Ion hydration, (c) Attraction by Osmosis, and (d) Dipole Attraction. (after Mitchell, 1993)

(d) Charged Surface – Dipole Attraction

As the water is a dipole molecule, even though it is electrically neutral, it is electrostatically attracted to the charged clay surface due to Van der Waals attraction force (Mitchell 1993, Holtz 1981). Water molecules dipoles are directed to the negative charged surfaces, with the degree of orientation decreasing gradually with increasing distance away from the surface.

2.4.2. Diffuse Double Layer

Tightly held interlayer cations within the clay particles, due to electrostatic attraction of the negatively charged surfaces, pull water molecules because of their hydration energy upon wetting. Highly concentrated cations along the charged surfaces try to diffuse away from the surfaces in order to equalize the concentration throughout the clay-water solution. The escaping tendency of cations from the surface and the opposing electrostatic attraction lead to a specific ion distribution along the clay particles in the clay-water suspension. The negative charge of the clay surface and the distribution of cations in the soil solution are known as "Diffuse Double Layer" or DDL (Mitchell, 1993; Shackelford, 1994).

2.4.2.1 Theory and Mathematical Models of DDL

The concept of diffuse double layer has been developed from the basics of the electrical double layer, which describes the variation of electric potential near a charged surface, and plays an important role in the behavior of colloids and other surfaces which are in contact with electrolyte solutions. The earliest concepts of the double layer were proposed and developed by Helmholtz (1853-1879) where the double layer refers to the counterions (cations) and co-ions (anions) in a rigid layer adjacent to the clay charged interfaces (Endo *et al.* 2001). Figure 2.17 illustrates the Helmholtz model which is

analogous to the parallel plate-capacitor in which the negatively charged surface would form one plate and rigidly linked opposite charged cations to the surface would form another plate (Endo *et al.* 2001). In this model no interactions occur further away from the first layer of adsorbed ions, and the electric potential drops sharply from its maximum value at the charged surface to an almost negligible value at the center of the first fixed layer of cations adjacent to the surface, as shown in figure 2.18. Two principal shortcomings were discovered in this model during subsequent research by Gouy and Chapman in 1913 (Mitchell, 1993; Endo *et al.*, 2001; Wikopedia, 2004; Van Olphen, 1977) as follows:

(a) It neglects interactions of cations and anions occurring further away from the charged surfaces and

(b) The extent and thickness of diffuse double layer takes into account no dependence on electrolyte concentration.

Gouy and Chapman (1910-1913) made a significant improvement by introducing a diffuse double layer model, in which the potential decreases exponentially away from the surface due to adsorbed counter-ions (cations) from the solution away from the charged surface. Thus, the double layer would not be compact as in Helmholtz's model, but of variable thickness as the ions are free to move away in the bulk electrolyte solution as shown in figure 2.19 (after Mitchell 1993).

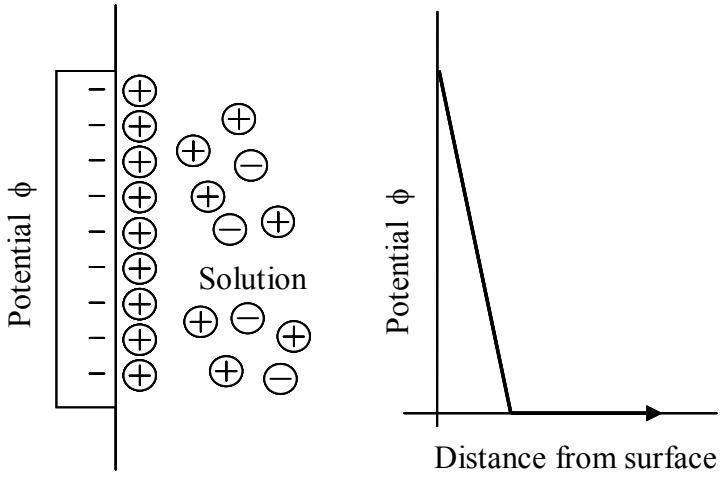

Figure 2.17 Helmholtz Model

The electrical potential of the electrolyte solution decreases exponentially from the face of the charged surface, which gradually extends into the bulk solution, and the concentration of ions have been calculated to be very high at the surface due to the assumption of point ionic charges (van Olphen 1977, Mitchell 1993). The hydrated ionic size is not considered in this model.

Stern, in 1924, developed a model incorporating Helmholtz model and Gouy-Chapman model, commonly known as Stern-Gouy-Chapman model, which is widely acceptable at present (figure 2.19). This model consists of a compact layer of cations of finite radius at the close vicinity of the negatively charged surface known as the "Stern layer", similar to the Helmholtz model, and a diffuse layer of cations and anions extending into the bulk solution similar to the Gouy-Chapman model (van Olphen, 1977; Mitchell 1993). The effect of the stern layer on the surface electrical potential and cationic concentration is shown in figure 2.19 (Mitchell 1993). The thickness of the Stern layer increases with cationic size, and its presence would limit the predicted cation concentration at the surface, as shown in figure 2.19.

Mathematical representations of the diffuse double layer phenomenon were provided using the following assumptions (Mitchell 1993):

(a) Ions are point charges with no interaction among opposite charges within the interlayer and bulk pore spaces,
(b) The charge on the particle surface due to isomorphous substitution is uniformly distributed,
(c) The dimensions of the surface on which the charge deficiency is uniformly distributed are much larger than the diffuse double layer, and
(d) The permittivity of the medium present in between the surfaces is constant regardless of the position.

From electrostatics, Poisson's equation gives the charge balance in an electric field, and the general expression for a homogeneous dielectrical medium in a one-dimensional situation is:

$$\frac{d^2\psi}{dx^2} = -\frac{\rho_{ch}}{\varepsilon_o D} \qquad (2.7)$$

where, ψ is the electrical potential in front of the charged clay surface, ρ_{ch} is the charge volumetric density (C m^{-3}), D is the relative permittivity of the medium, and ε_o is the dielectric constant of the void (C V^{-1} m^{-1}).

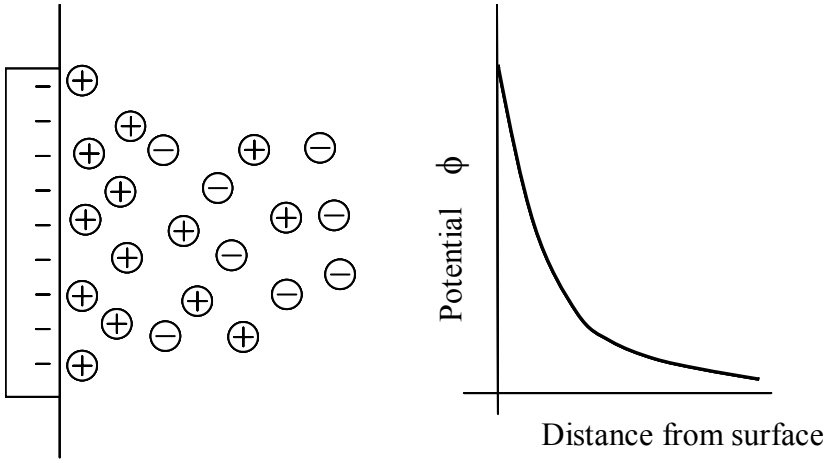

Figure 2.18 Gouy-Chapman Model

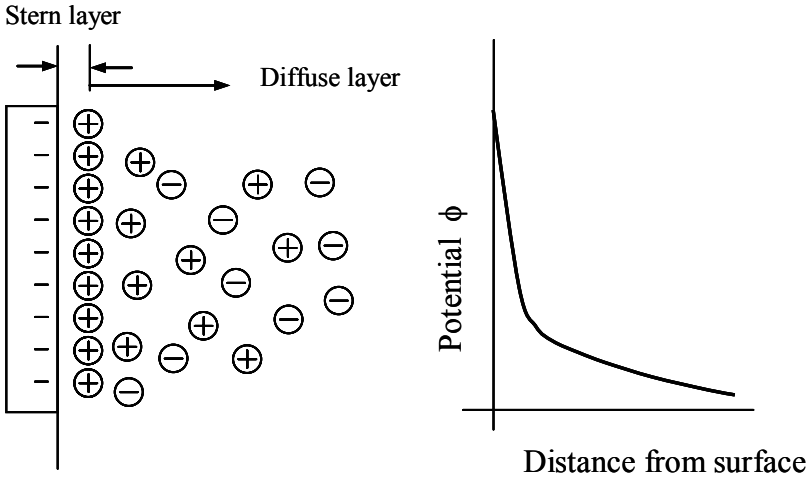

Figure 2.19 Stern Gouy-Chapman Model

On the other hand, the Boltzmann equation represents the distribution of ions within an electrical field:

$$\eta_i = \eta_{io} \exp^{\frac{(\nu_i e\psi_o - \nu_i e\psi)}{kT}} \tag{2.8}$$

where, k is Boltzmann's constant, T the absolute temperature, η_i = ionic concentration of the species i, e = unit electronic charge (16 x 10^{-20} Coulomb), and ψ_o = electrical potential at concentration η_{io}. As the potential at great distance from the interface is equal to zero, the term $\nu_i e\psi_o$ can be set to zero.

The volume charge can be expressed as:

$$\rho_{ch} = e\sum \nu_i \eta_i \tag{2.9}$$

Using equation (2.9), Boltzmann equation (2.8) can be written as:

$$\rho_{ch} = e\sum \nu_i \eta_{io} \exp^{\left(-\frac{\nu_i e\psi}{kT}\right)} \tag{2.10}$$

Substituting into Poisson's equation leads to the general expression for the Poisson-Boltzmann equation in a one-dimensional field:

$$\frac{d^2\psi}{dx^2} = -\frac{e\sum \nu_i \eta_{io} \exp^{\left(-\frac{\nu_i e\psi}{kT}\right)}}{\varepsilon_o D} \tag{2.11}$$

For a solution of single cation and anion species of equal valence, i.e. $i = 2$, $\nu^+ = \nu^- = \nu$, $\eta_o^+ = \eta_o^- = \eta$, and $\sinh p = (e^p - e^{-p})/2$, equation 2.11 can be rewritten as:

$$\frac{d^2\psi}{dx^2} = \frac{2\eta_o \nu e}{\varepsilon_o D} \sinh\left(\frac{\nu e\psi}{kT}\right) \tag{2.12}$$

It is convenient to rewrite the above equation (2.12) in terms of the following dimensionless quantities:

$$y = \frac{\nu e\psi}{kT} \qquad z = \frac{\nu e\psi_o}{kT} \qquad \xi = Kx \tag{2.13}$$

$$\text{where,} \quad K^2 = \frac{2\eta_o e^2 \nu^2}{\varepsilon_o DkT} \tag{2.14}$$

Putting the above relationships of equation (2.13) in equation (2.12), we get:

$$\frac{d^2y}{d\xi^2} = \sinh y \tag{2.15}$$

K, dimensionally a length, is called the Debye-Huckel parameter. Using the boundary conditions for the first integration, $\xi = \infty$, $y = 0$, and $dy/d\xi = 0$, the following can be obtained:

$$\frac{dy}{d\xi} = -\left(2\cosh y - 2\right)^{1/2} = -2\sinh\left(\frac{y}{2}\right) \tag{2.16}$$

This condition holds for a large pore, as it assumes that the double layers of two platelets, one in front of the other, do not overlap.

The boundary condition for the second integration, $\xi = 0$, $y = z$ (i.e. $\psi = \psi_o$), yields:

$$\exp^{y/2} = \frac{\exp^{z/2} + 1 + \left(\exp^{z/2} - 1\right)\exp^{-\xi}}{\exp^{z/2} + 1 - \left(\exp^{z/2} - 1\right)\exp^{-\xi}} \tag{2.17}$$

Equation (2.17) describes the decay of the potential as a function of the distance from the surface at a given surface potential (i.e., z) and at a given electrolyte concentration (i.e., K^2).

If the surface potential is small ($\psi << 25$ mV), then $ve\psi/kT << 1$ (i.e., $z << 1$) and the relation $e^{-x} \approx 1-x$ is often adopted in order to expand the exponential equation (2.11) as follows:

$$\frac{d^2\psi}{dx^2} = -\frac{e\left(\sum \nu_i \eta_{io} - \sum \nu_i^2 \eta_{io} e\psi / kT\right)}{\varepsilon_o D} \tag{2.18}$$

Because of the electrical neutrality of the bulk solution, the first term in the parentheses ($\sum \nu_i \eta_{io}$) has to be equal to zero from the charge equation (2.9), and equation (2.18) then becomes:

$$\frac{d^2\psi}{dx^2} = \mathrm{K}^2\psi \tag{2.19}$$

The solution of the above equation (2.19) can be written as:

$$\psi = \psi_o \exp^{-\mathrm{K}x} \tag{2.20}$$

In this case, the center of gravity of the counter ions (cations) atmosphere coincides with the plane Kx = 1 or x = 1/K. Hence 1/K is often called the double layer thickness; it is also equal to the "characteristics length" in the Debye-Huckel theory of strong electrolytes.

2.4.2.2 Factors Affecting DDL

The thickness of the diffuse double layer (DDL), 1/K, can be rearranged from equation 2.14 as follows:

$$\frac{1}{K} = \left(\frac{\varepsilon_o DkT}{2\eta_o e^2 \nu^2} \right)^{1/2} \qquad (2.21)$$

The variable factors in equation (2.21), which affect the DDL thickness, can be summarized as follows:

(a) Electrolyte Concentration (η_o)

By keeping all other factors constant, an increase in electrolyte concentration will decrease DDL exponentially. A one hundred fold increase in concentration will cause a 10 fold decrease in DDL distance as calculated from equation (2.21), an example of which is shown in figure 2.20 (Mitchell, 1993).

(b) Electrolyte Cation Valance (ν)

It is found from equation (2.21) that the thickness of DDL is inversely proportional to the valence of the electrolyte solution. An increase in valence will suppress the midplane concentrations and potential between interacting plates, which leads to a decrease in interplate repulsion as given in figure 2.20 (after Mitchell, 1993)

(c) Effects of Dielectric Constant (D)

The DDL thickness is directly proportional to the square root of the dielectric constant of the concentrated electrolyte solution. The value of D also affects the electrical potential (ψ_o) as per the hyperbolic expression given in the following equation:

$$\sinh\left(\frac{ve\psi_o}{2kT}\right) = \left(8\eta_o\varepsilon_o DkT\right)^{-1/2}\sigma \qquad (2.22)$$

It is found from equation (2.22) that for a constant value of surface charge density, the electrical potential increases as the dielectric constant decreases.

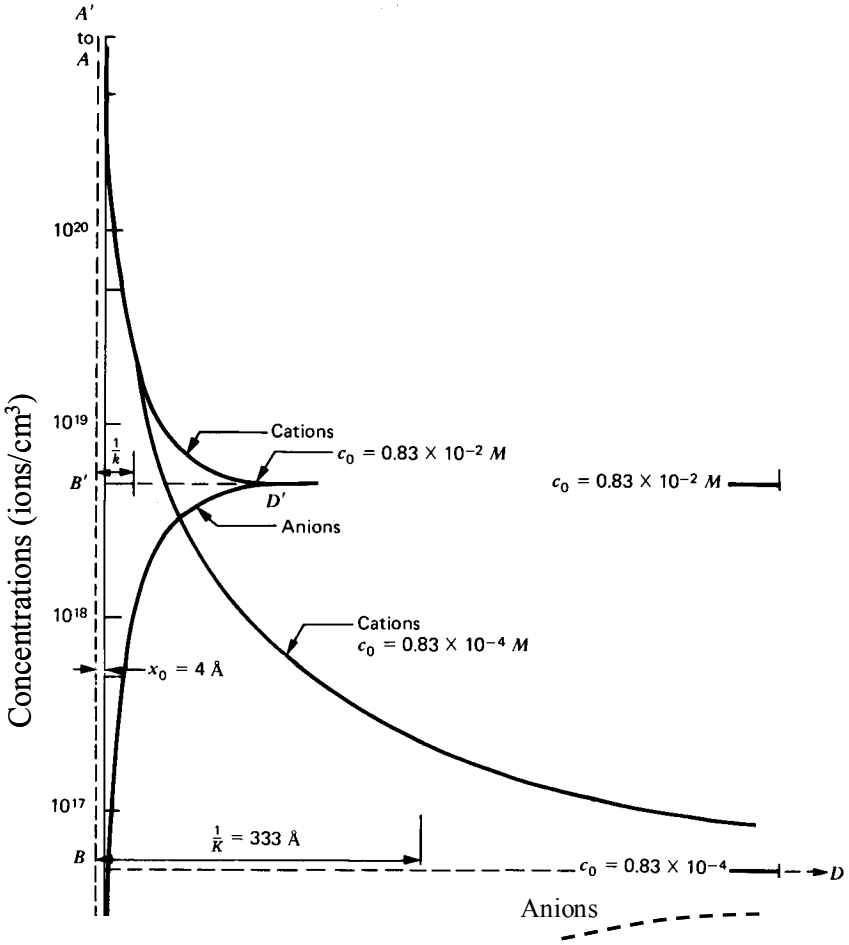

Figure 2.20 Effect of Concentration on Ion Distributions with Distance (after Mitchell, 1993)

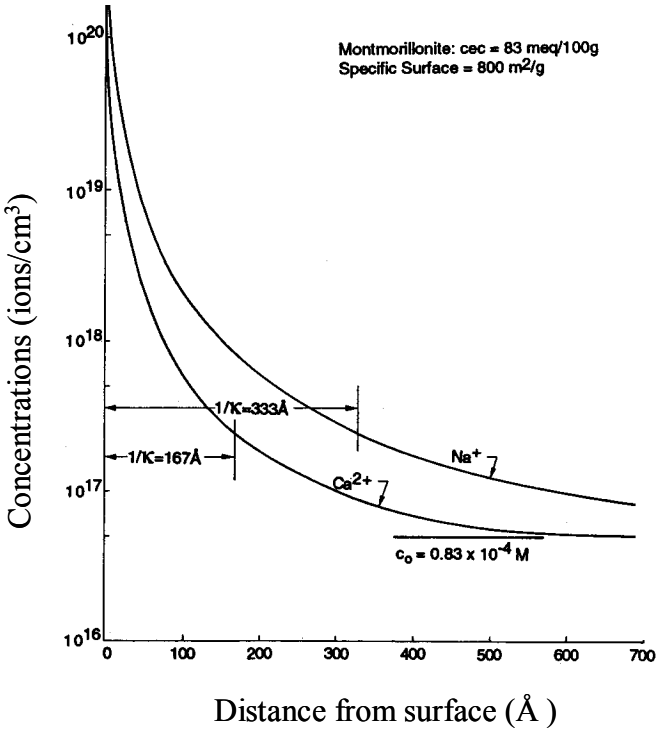

Figure 2.21 Effect of Cation Valence on Double Layer (after Mitchell, 1993)

CHAPTER THREE

BENTONITE CHARACTERIZATION

In this chapter the index and physicochemical properties of bentonite that has been used in this study are highlighted. Geotechnical tests such as Atterberg limits, particle/grain size distribution, specific gravity, and swell index have been conducted using ASTM standards. Modifications have been made to the conventional standards to suit the type of bentonite clay used in this study after thorough investigations of various studies published in the literature.

3.1 Source of Bentonite

Extra High Yield Bentonite powder manufactured by Wyo-Ben, Inc., has been used in this study. Widely known as "Wyoming Bentonite" (sodium montmorillonite), this bentonite is being commercially used in the construction industry for mining exploration, water wells, and directional drilling operations. When one 50-lb bag bentonite powder is mixed with 300 gallons of water, it provides a funnel viscosity of 30-35 seconds.

3.1.1 Mineralogy Through XRD

X-Ray diffraction (XRD) has been used for many years to determine the mineralogy based on basal spacing of the clay minerals (Suzuki *et al*., 2001; Hwang and

Dixon, 2000; Chmielova *et al.*, 2000; Kozaki *et al*., 2001; Song and Sandi, 2001; Mayayo *et al*., 2000; Cases *et al.*, 1997).

X-rays are electromagnetic radiations of wavelength of about 1 Å, which is approximately the same size as an atom. They occur in that portion of the electromagnetic spectrum between gamma-rays and ultraviolet. X-ray diffraction has been in use in two main areas: characterization of crystalline materials and the determination of their structure. Each crystalline solid has its unique characteristic X-ray powder pattern, which may be used as a "fingerprint" for its identification. Once the material has been identified, X-ray crystallography may be used to determine its structure, i.e., atomic packing in the crystalline state and interatomic distances and angles.

X-ray diffraction is a routine method in mineralogy, particularly for fine-grained material study. It is one of the primary techniques used by mineralogists and solid state chemists to examine the physicochemical composition of unknown solids. XRD can provide additional information beyond basic identification. If the sample is a mixture, XRD data can be analyzed to determine the proportion of the different minerals present. Other information obtained can include the degree of crystallinity of the mineral(s) present, possible deviations of the minerals from their ideal compositions (presence of element substitutions and solid solutions), structural state of the minerals, and degree of hydration for minerals that contain water in their structure. Some mineralogical samples analyzed by XRD are too fine-grained to be identified by optical light microscopy. XRD does not, however, provide the quantitative compositional data obtained by electron microprobes or textural and qualitative compositional data obtained by scanning electron microscope.

The XRD technique requires placing a powdered sample of the material in a holder, then illuminating it with X-rays of a fixed wave-length. The intensity of the reflected radiation is then recorded using a goniometer. This data is analyzed for the diffraction angle to calculate the inter-atomic spacing (d value in Angstroms - 10^{-8} cm).

The three-dimensional structure of non-amorphous materials, such as minerals, is defined by regular, repeating planes of atoms that form a crystal lattice. When a focused X-ray beam interacts with these planes of atoms, part of the beam is transmitted, part is absorbed by the sample, part is refracted and scattered, and part is diffracted. Diffraction of an X-ray beam by a crystalline solid is analogous to diffraction of light by droplets of water, producing the familiar rainbow. X-rays are diffracted by each mineral differently, depending on atom make up and arrangement in the crystal lattice.

In X-ray powder diffractometry, X-rays are generated within a sealed tube under vacuum. A current is applied that heats a filament within the tube; the higher the current the greater the number of electrons emitted from the filament. This generation of electrons is analogous to the production of electrons in a television picture tube. A high voltage, typically 15-60 kilovolts, is applied within the tube. This high voltage accelerates the electrons, which then hit a target, commonly made of copper. When these electrons hit the target, X-rays are produced. The wavelength of these X-rays is characteristic of that target. These X-rays are collimated and directed onto the sample, which is a fine powder of particle size of less than 10 microns. A detector detects the X-ray signal; the signal is then processed either by a microprocessor or electronically, converting the signal to a count rate. Changing the angle between the X-ray source, the sample, and the detector at a controlled rate between preset limits, an X-ray scan is obtained. Figure 3.1 shows how X-ray waves reveal the atomic structure of crystals.

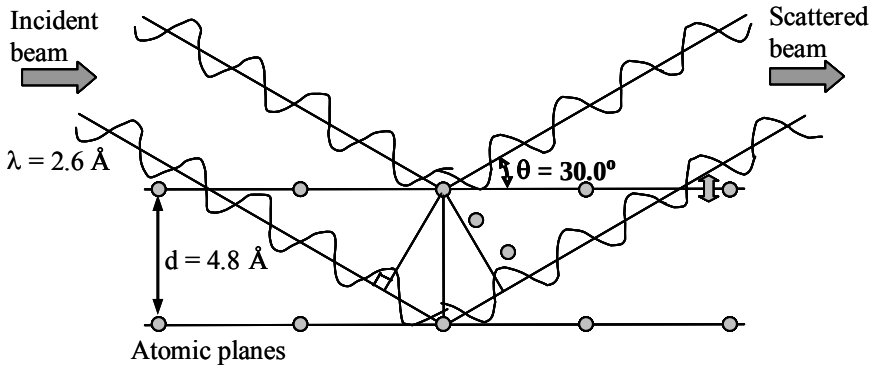

Figure 3.1 Basics of X-ray Diffraction Technique

When an X-ray beam hits a sample and is diffracted, it measures the distances between the planes of the atoms that constitute the sample by applying Bragg's Law as given in the equation (3.1).

$$n\lambda = 2d\sin\theta \qquad (3.1)$$

where the integer n is the order of the diffracted beam, λ is the wavelength of the incident X-ray beam, d is the distance between adjacent planes of atoms (the d-spacing), and θ is the angle of incidence of the X-ray beam. By knowing λ and measuring θ, the d-spacing can be calculated. The characteristic set of d-spacings generated in a typical X-ray scan provides a unique "fingerprint" of the mineral or minerals present in the sample. When properly interpreted, by comparison with standard reference patterns and measurements, this "fingerprint" allows for identification of the material. A typical spectrometer with XRD fundamentals is shown in figure 3.2 where the value of θ or 2θ determines the composition of minerals in the specimen.

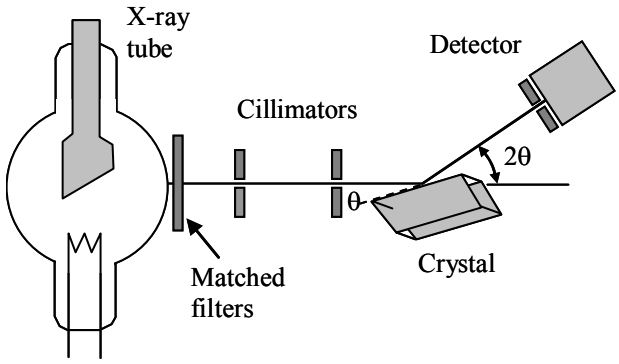

Figure 3.2 XRD Spectrometer Fundamentals

Extra high yield bentonite from Wyo-Ben, Inc. was dried at 105°C to remove all the mobile pore fluid from the sample for XRD analysis. The sample's dry particles were passed through sieve # 200 (particles less than 75 microns) and kept dry until placed

within the holder of XRD device. Copper radiation ($K\alpha = 1.5405$ Å) in the $5 < 2\theta < 65$ range was applied to generate the XRD signature of the material.

3.1.2 Mineral Compositions

Composition of minerals of "Wyo-ben" bentonite from the XRD diffractograms is shown in figure 3.3. Most of the peaks match with those for montmorillonite and quartz minerals.

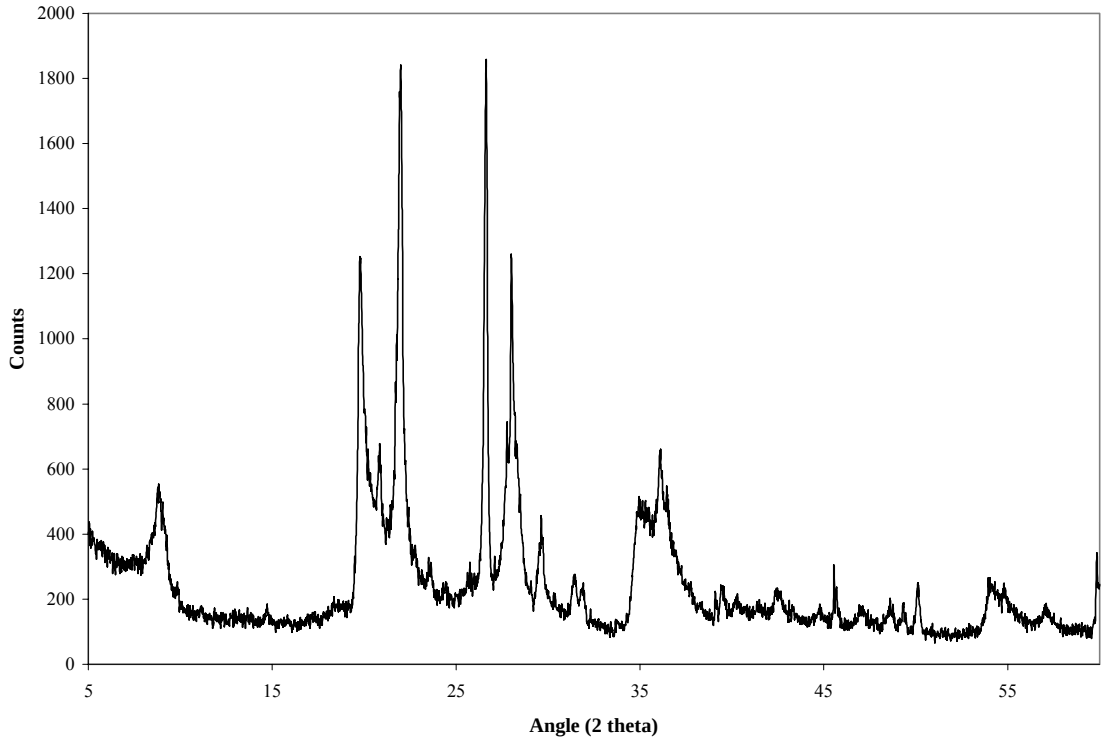

Figure 3.3 XRD Test Results for Bentonite

3.1.3 Chemical Composition

Chemical properties of the bentonite powder were investigated in both dry and colloidal states. Analysis of the chemical composition of bentonite has been carried out on dry specimens using Energy Dispersive Spectroscopy (EDS). Electrical conductivity and pH measurements were conducted on a bentonite-water suspension as described in the following sections.

3.1.3.1 EDS Analysis

Earlier research on chemical composition of various types of bentonite revealed that the major four minerals present in the sodium montmorillonite are silica (SiO_2), alumina (Al_2O_3), sodium oxide (Na_2O), calcium oxide (CaO), and iron oxide (Fe_2O_3). Other minor minerals, which normally constitute less than 1% in total weight, are magnesium oxide (MgO), titanium oxide (TiO_2), potassium oxide (K_2O), manganese oxide (MnO), and trace metals oxide (Kaufhold *et al*., 2002; Nakashima, 2003; Singh *et al*. 2002; Guillaume *et al*., 2003; Christidis, 2001). The four major chemical compounds found in the bentonite are similar to those found in other clay minerals, except for the amount of calcium oxide (CaO) and the relative amounts of other constitutes (Ramirez, 2002; Guillaume *et al*., 2003; Bradbury and Baeyens, 2003; Nakashima, 2003; Benito *et al*., 1998).

In this research, chemical analysis of the as-received bentonite was conducted by Energy Dispersive Spectroscopy (EDS). The as-received samples were oven dried and a 20-gram portion was used for EDS testing.

The EDS technique uses X-rays resulting from interactions between applied fast beam electrons and the specimen atoms. X-rays, which are electromagnetic radiations of extremely short wavelength, are emitted when a specimen is bombarded with fast electrons. The X-ray energy and wavelength are related to the specimen's elemental composition. When the specimen is bombarded by the electron beam of a Scanning

Electron Microscope (SEM), electrons are ejected from the innermost shell of the atoms comprising the specimen. An electron from an outer atomic shell drops into the vacancy in the inner shell in order to return the atom to its normal (balanced) state. This drop results in the loss of energy due to the difference in energy between the vacant shell and the shell contributing the electron. The energy is given up in the form of electromagnetic radiation or X-rays. Since energy levels are different for different elements, characteristic rays are generated accordingly.

Energy Dispersive X-ray microanalysis uses detection equipment to measure the energy values of the characteristic X-rays generated within the electron microscope. An X-ray micro-analyzer system converts X-ray energy into an electronic count by using semiconductor materials that can detect the X-rays. The accumulation of these energy counts creates a spectrum, which is then plotted against relative counts of the detected X-rays and evaluated for qualitative and quantitative determination of the elements present in the specimen. The energy peaks are essentially fingerprints of the specific elements in a specimen. Figure 3.4 illustrates the basic layout of an EDS system. Details of EDS have been described by Russ (1984) and Goldstein *et al.* (1981).

EDS characterization of bentonite was conducted using a Hitachi S-800 spectrometer located at the Metrology Laboratory of the Nanomaterials and Nanomanufacturing Research Center (NNRC) at the University of South Florida. This spectrometer is also fitted with a Scanning Electron Microscope (SEM) as shown in figure 3.5. Bentonite powder was scanned using SEM to find its aggregated particle size, which is also shown in figure 3.6.

Energy peaks for various elements for a bentonite specimen are shown in figure 3.7, which shows the major elements found using EDS. The main chemical elements in the composition of bentonite are found to be oxygen, chlorine, silicon, aluminum, calcium, sodium, iron, sulfur, magnesium and some other trace metals. The chemical compounds that constitute the bentonite powder used in this research are SiO_2, Al_2O_3, Fe_2O_3, Na_2O, MgO, CaO, TiO_2, K_2O, MnO, and some other trace metal oxides. Table 3.1 shows the quantitative chemical composition of all the elements and trace metals derived from EDS.

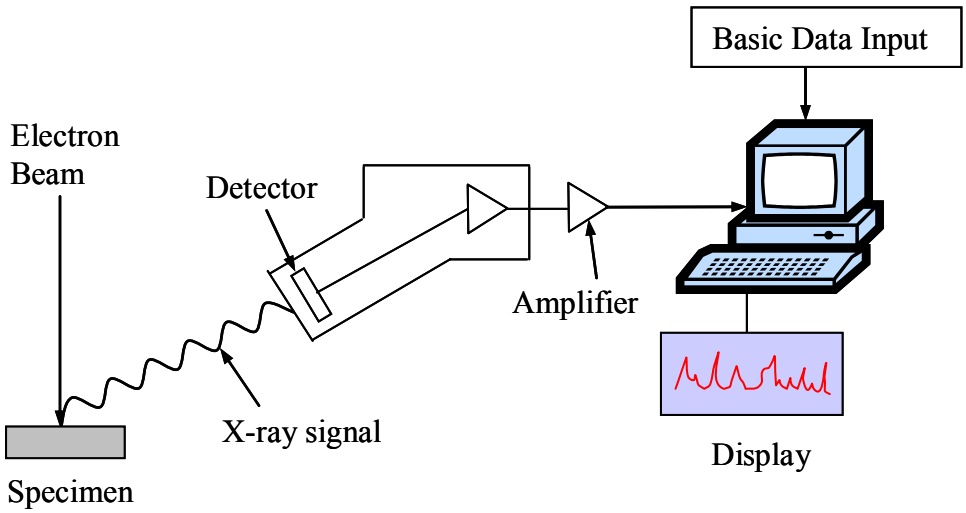

Figure 3.4 Schematic Diagram of EDS System

Figure 3.5 Spectrometer Fitted with Scanning Electron Microscope (HITACHI S-800)

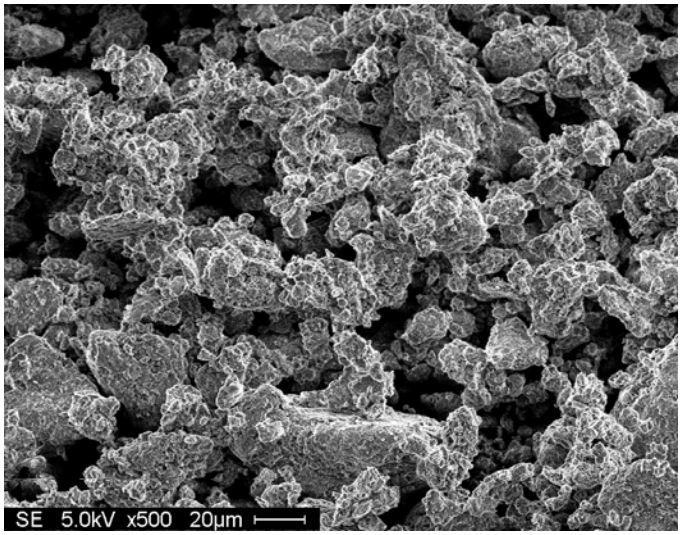

Figure 3.6 Dry Bentonite Powder Under SEM

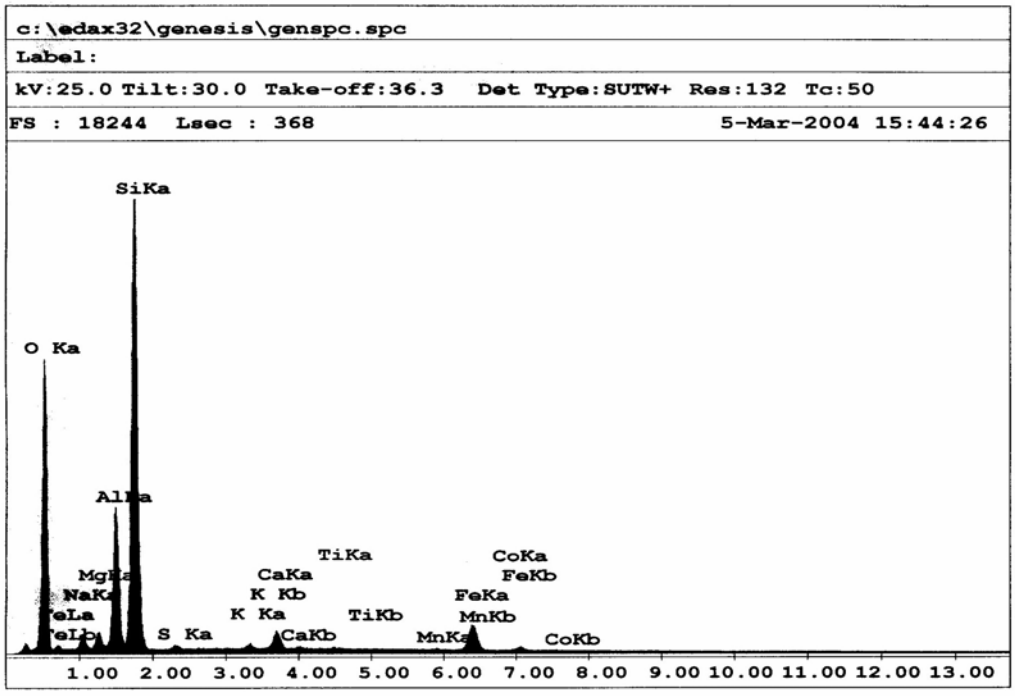

Figure 3.7 Energy Peaks for Bentonite Chemical Elements Using EDS

Table 3.1 Chemical Composition of Bentonite

Major Chemical compounds		Trace metals	
SiO_2	66.5%	Arsenic	0.1 ppm
Al_2O_3	16.9%	Barium	< 1.0 ppm
Fe_2O_3	7.4%	Cadmium	<0.01 ppm
Na_2O	2.3%	Chromium	< 0.05 ppm
MgO	2.3%	Lead	< 0.1 ppm
CaO	2.1%	Mercury	< 0.02 ppm
TiO_2	0.2%	Selenium	< 0.02 ppm
K_2O	0.4%	Silver	< 0.05 ppm

It can be seen from the table that the main exchangeable cations in the double layer space would be sodium, calcium, magnesium and a small amount of potassium.

3.1.4 Electrical Conductivity and pH

Electrical conductivity and pH of a bentonite-water suspension were investigated at various colloidal concentrations. The electrical conductivity was measured by using an Accumet (model AB30) 4-cell conductivity meter (shown in figure 3.8) and two epoxy body electrodes of cell constant 1.0 cm^{-1} and 10.0 cm^{-1}. These electrodes are capable of measuring a wide range of electrical conductivity from 10 to 200,000 microsiemens/cm. Whenever a change of electrodes was required to obtain a measurement within a particular range, it was necessary to recalibrate it using its own standard solution.

Bentonite samples of various amounts were soaked into deionized water for at least 48 hours in order to adsorb as much water as possible with all the pores and interlayer spacing. Quantities of 5g, 10g, 15g, 20g, 30g, and 50g air-dry bentonite powder were mixed with 1 liter of deionized water to obtain 0.5%, 1%, 1.5%, 2%, 3%, and 5% of suspension respectively.

Figure 3.8 Accumet (Model AB30) 4-cell Conductivity Meter

After soaking for at least 48 hours, the bentonite suspension in deionized water was stirred for at least 15 minutes using a mechanical stirrer/mixer before being poured into a 1 liter capacity glass beaker for self flocculation. After flocculation and subsequent settlement, supernatant water samples were collected for electrical conductivity and pH measurement.

Immediately following the sample collection, the pH of the non-acidified original sample was measured using an Accumet portable (model AP63) pH meter and polymerbody combination pH/ATC Ag/AgCl electrode as shown in figure 3.9. The pH meter was calibrated at three levels, using three standard color-coded buffer solutions of pH 4.00, 7.00 and 10.00. The variations of electrical conductivity and pH with respect to the percentage of suspension of bentonite in deionized water are shown in figure 3.10.

The electrical conductivity of bentonite increases with increasing amount of bentonite suspension in a second-order polynomial manner, while the pH decreases with increasing bentonite suspension in a power equation as shown in figure 3.10. At higher suspension concentrations, bentonite aggregate particles are unable to deflocculate and disperse in water, thus contributing less towards the total electrical conductivity of the water solution.

Figure 3.9 Accumet Portable (Model AP63) pH Meter

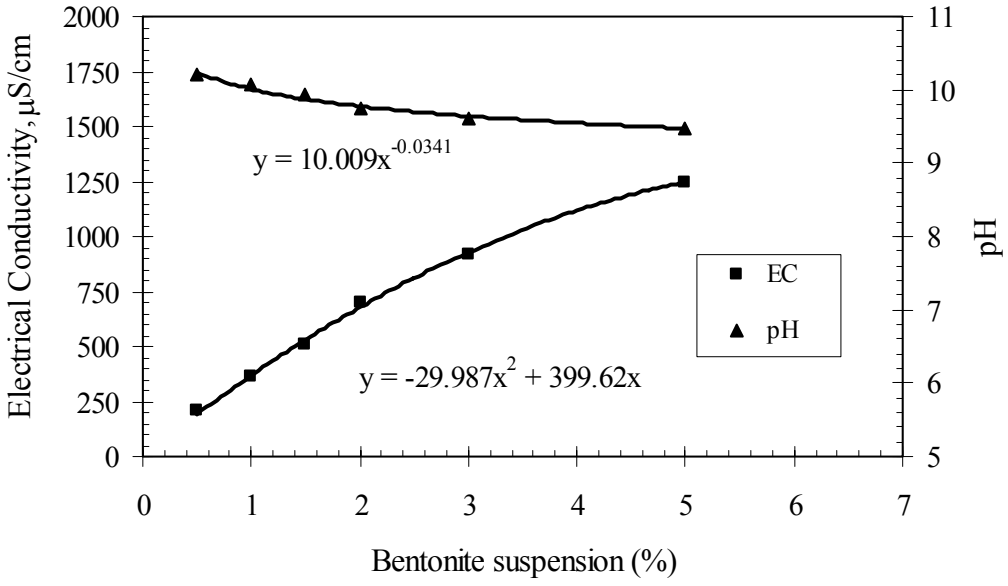

Figure 3.10 Electrical Conductivity and pH of Bentonite Suspension

3.1.5 Loss of Ignition

The amount of organic content in the bentonite powder is indicated by the value of loss of Ignition (LOI), which is traditionally expressed as total percent of the material. LOI of fine grained powdered bentonite is determined by burning at high temperatures in a controlled temperature oven. Loss of ignition has been reported for various types of bentonite within a range of 0.2% to 5% (Keijer and Loch, 2001; Keijer *et al*., 1999; Lehikoinen *et al.*, 1996).

Bentonite clay specimens in this study were burned at two different temperatures (550^{o}C and 1000^{o}C) in two separate specimens, 4.0 g and 2.0 g, respectively. After burning at 550^{o}C temperature, the LOI was found to be 3% while at 1000^{o}C the value rose to 5.6%. According to the technical information provided by the manufacturer of this bentonite (Wyo-Ben, Inc), LOI has been found to be 4.4%, which falls within the range obtained in this study. LOI cannot be measured at very high temperatures because of the evaporation of the volatile components of the bentonite material. Bentonite with higher LOI may or may not interfere with the chemical solutions used during long term diffusion as well as hydraulic conductivity, but would produce organic compounds under long and sustained chemical and hydraulic flow as observed later in some of our experiments.

3.2 Grain Size Distribution

Particle size distribution of bentonite cannot be obtained using either conventional dry sieve or hydrometer testing because of the aggregated nature of the particles. However, both sieve analysis and hydrometer test were carried out in order to investigate the amount of coarse fraction and fine-grained characteristics with various types of inorganic chemical solutions, and to gain a general idea about the relative distribution of clay aggregated particles.

3.2.1 Hydrometer Test

Bentonite particles, because of their high surface charges, repel each other and exist as individual particles when mixed with bulk water. The size of the particle is in the range of 0.01 to 1 μm and can be considered as colloidal. Because of their high colloidal nature, bentonite particle sizes cannot be measured by hydrometer analysis. Nonetheless, a review of the literature show that bentonite particle size distributions were carried out by Kozaki *et al.*, (2001), Eriksen *et al.*, (1999), Zhang *et al.*, (1995), and others, where hydrometer and dry sieve mesh were used.

A clay-water solution is a result of homogeneous dispersion of very small clay particles. The colloidal state lies somewhere between a solution and a suspension. Colloidal clay minerals are among the smallest crystalline particles known to exist, and are neither a suspension nor a solution. Clay colloids are hydrophobic in nature, meaning they have an inherent resistance to interaction with water. Aggregated microscopic clay particles in colloidal solutions are usually less than 2 microns in diameter. Colloidal solutions do not settle under gravity within a reasonable time. When the dispersed particles accumulate into a larger lump or aggregate, which settles relatively rapidly under gravity, then the dispersion is called as "suspension". The distinction in particle size between colloidal solutions and suspensions are arbitrarily taken in geochemistry as a Stokes radius (equivalent spherical radius) of 1 micron (van Olphen, 1977). The equivalent particle size of any shape is computed in hydrometer tests velocity using Stokes Law. Particles smaller than 1 micron are known as colloidal and larger than 1 micron are clay suspensions.

Colloidal clay solutions produce Brownian motion, where the small clay particles display an erratic and random motion in all directions. The water molecules are in constant thermal agitation, and their velocity distribution is determined by the temperature of the system. The motion of the water molecules, due to the fact that the fluid contains heat, causes the molecules to strike the suspended clay particles at random. The impact makes the particles move, and the net effect is an erratic, random motion of the particle through the fluid. Brownian motion is the result of thermal activity of water

molecules around the clay particles. Water molecules in solution constantly collide with clay particles and push the particles in random direction due to the net resultant force.

The mean kinetic energy of a molecule in the liquid, which is equal to the average translational kinetic energy of the particles, is given by:

$$E = \frac{1}{2}mv^2 = \frac{3}{2}kT \qquad (3.2)$$

where, m is the mass of a particle, v is the velocity, k is the Boltzman constant, and T is the temperature. From this formula (equation 3.2) it can be seen that the mean kinetic energy of Brownian motion is proportional to the temperature. Equation (3.2) can also be used to find the velocity of a particle (Van Olphen, 1977). It can be seen from the above energy conservation theory that the average particle velocity decreases with increasing mass, and Brownian motion does not exist for higher clay particles sizes.

Collision with fluid molecules can also make a suspended particle rotate. This phenomenon is called rotational Brownian motion. It has been found that bentonite clay particles can flocculate in the presence of an electrolyte leading to an increase in particle sizes and a reduction in reactivity (Van Olphen, 1977; Sridharan *et al.*, 1999; Zhang *et al.*, 1995; Quirk and Schofield, 1955; Keren and Singer, 1988). To observe the relative particle sizes of clays, the hydrometer technique was used with a dispersing agent in deionized water, and in various synthetic inorganic solutions without a dispersing agent. This method gives the effective particle size in different pore fluids. Though Stoke's law is not strictly valid for non-spherical particles settling at high velocity, it has been used to find out the relative particle sizes in different pore fluids. Six different solutions of various concentrations were used in addition to deionized water with 0.1M NaCl, 0.1M KCl, 0.1M $MgCl_2$, and 0.1M $CaCl_2$ as the lowest electrolyte concentrations.

3.2.2 Test Results and Discussion

Figures 3.11 and 3.12 give the relative particle size distribution of bentonite in 0.1 molar concentration of four different solutions and in NaCl solutions with three different

concentrations respectively. It can easily be observed that, relatively speaking, bentonite is least aggregated and exists as finer particles with 0.1M NaCl and 0.1M KCl solutions in comparison with 0.1M $MgCl_2$ and 0.1M $CaCl_2$ solutions (figure 3.11). It can be concluded that an increase in the solution's ionic valence increases particle aggregation and flocculation. With an increase in electrolyte concentration, the bentonite particles have also become coarser. Compared to NaCl solutions, KCl solutions cause more aggregation of particles. A similar trend was observed where $CaCl_2$ caused more aggregation than $MgCl_2$. Thus 0.1M $CaCl_2$ causes maximum aggregation of particles among all the 0.1 molar solutions.

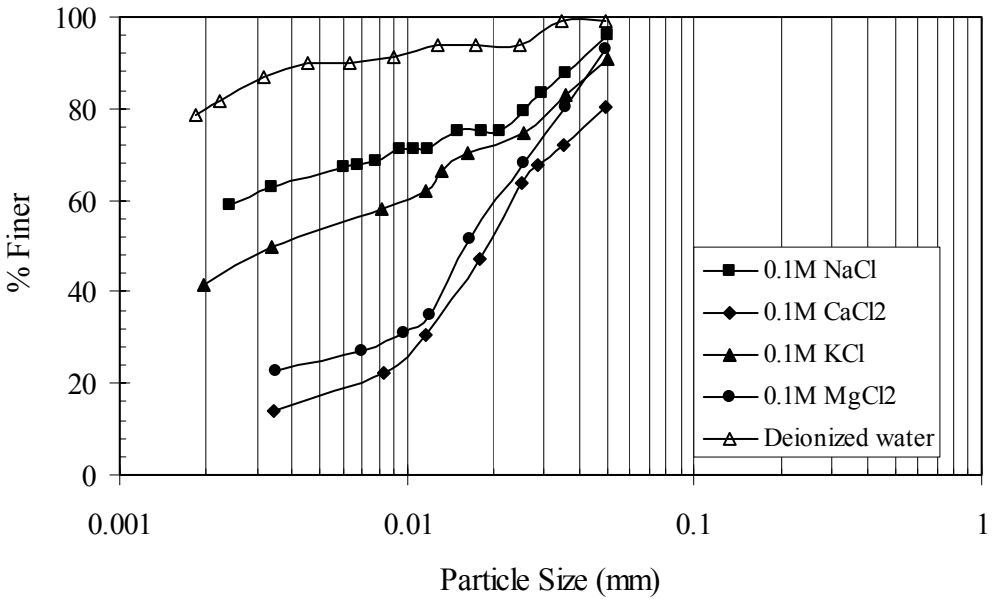

Figure 3.11 Bentonite Particle/Aggregate Distribution with Various Inorganic Chemical Solutions of 0.1 Molar of Concentration

The flocculation increases with an increase in electrolyte concentration, as shown in figure 3.12. Higher concentrated electrolyte solutions reduce the diffuse double layer thickness by attracting the neighboring particles, thus creating aggregated particles which can easily flocculate and settle with time.

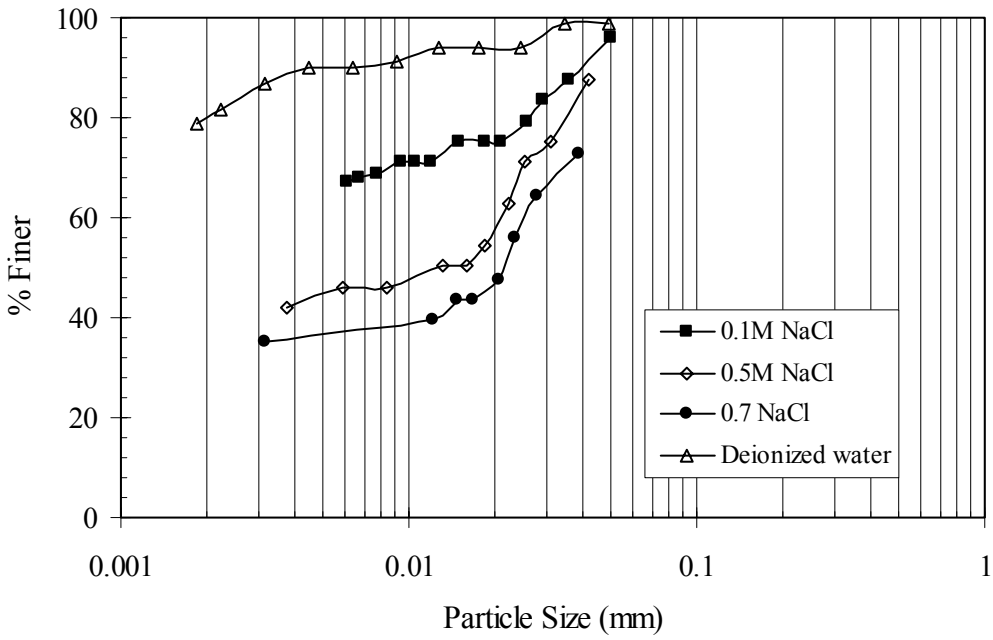

Figure 3.12 Bentonite Particle/Aggregate Distribution with NaCl Solutions of Various Concentrations

3.3 Physical Properties

Physical properties of bentonite in terms of its specific gravity of solids and Atterberg limits, namely liquid limit and plastic limit, are described in this section. Both ASTM standard and British standards have been used in these investigations.

3.3.1 Specific Gravity

Specific Gravity, also known as SG, is a measure of the density of minerals compared to water. Minerals with a specific gravity under 2 are considered light, between 2 and 4.5 average, and greater than 4.5 heavy (Faure, 1998). The specific gravity may slightly vary for a given mineral because of impurities present in the mineral

structure. Many researchers involved with bentonite materials have reported specific gravity values within a range of 2.4 to 2.65, depending on the percentage of montmorillonite mineral content (Malusis and Shackelford, 2002; Keijer and Loch, 2001; Keijer *et al*., 1999).

The specific gravity of the bentonite particles was measured according to ASTM D- 854-02 (2002) using a 500 ml pycnometer volumetric flask. Air-dry samples were soaked in tap water for at least 24 hours under vacuum so as to facilitate the removal of fine pore air bubbles from the water-clay solution. The specific gravity of the solid particles was calculated using the following equation.

$$G_s = \frac{W_s}{W_s + W_{fw} - W_{fs}} \tag{3.3}$$

where, W_s is the weight of the dry bentonite (taken after 24 hrs of oven dry at 105^{o}C), W_{fs} the weight of the flask filled with bentonite and water, and W_{fw} the weight of the flask filled with deaired water only. The average specific gravity of the bentonite used in this study was measured to be 2.55, as shown in the figure 3.13.

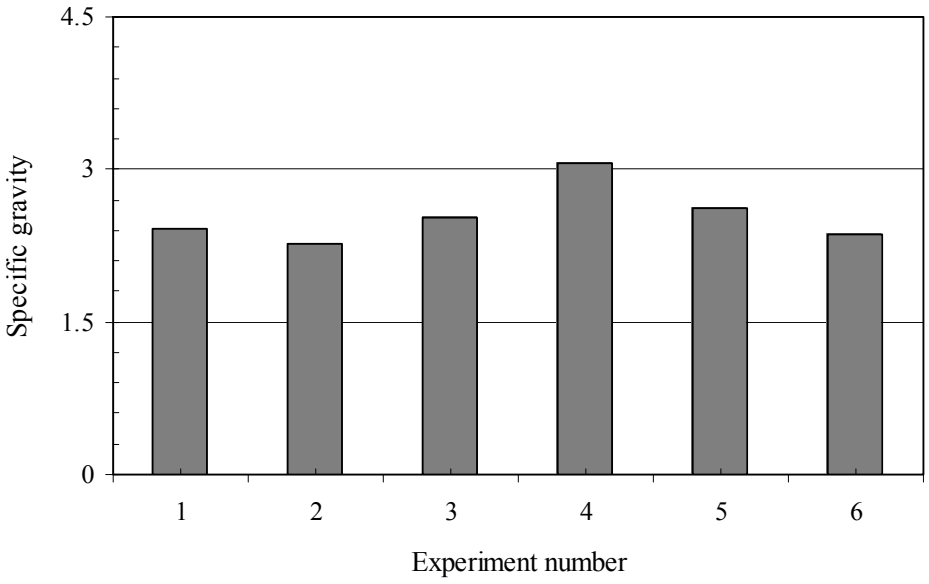

Figure 3.13 Experimental Variation of Specific Gravity

3.3.2 Atterberg Limits

The plasticity behavior of bentonite clay and the effect of pore fluid on the liquid limit help predict the long-term performance of the liner. Atterberg limits of soils can also be used to identify the mineral contents of the soil materials using the plasticity chart shown in figure 3.14 (after Holtz and Kovacs, 1981). The liquid limit of bentonite is very high compared to other clay minerals because of its ability to disperse into extremely small particles with a tremendous amount of potentially absorbing surface. The liquid limit of bentonite is primarily controlled by its diffuse double layer thickness. The numerous factors affecting the thickness of diffuse double layer depend upon the characteristics of the pore fluid which are explained in chapter two, namely dielectric constant, electrolyte concentration, valence of the electrolyte, and temperature. An increase in the diffuse double layer thickness causes an increase in the liquid limit.

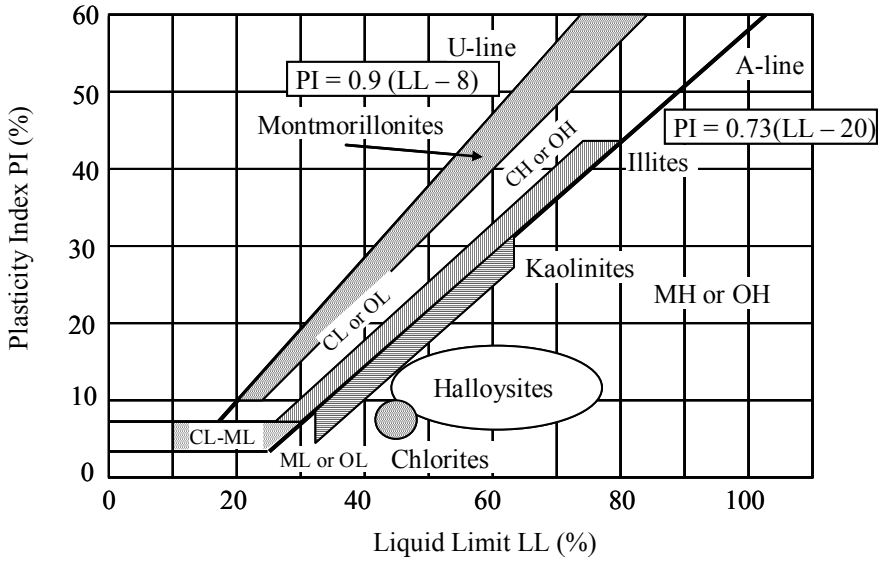

Figure 3.14 Plasticity Chart (after Holtz and Kovacs, 1981)

The liquid limit (LL) of bentonite was determined using water and electrolyte solutions. The Casagrande method for liquid limit testing, as described in ASTM D-4318-00 (2000), was tried unsuccessfully for bentonite. Because of the "stickiness" of

the bentonite particles, no groove can be cut through the material placed in the Casagrande apparatus. Instead the liquid limit of bentonite clay was determined by the cone penetration method (BS1377-1975), where it is defined as the water content corresponding to 20-mm penetration.

The plastic limit of the soil was obtained by ASTM Test Method (D 4318-00) using a rolling apparatus. The test specimens were prepared by mixing with water and storing for at least 24 hrs for uniform absorption. The average values of liquid limit and plastic limit using deionized water as pore fluid for the bentonite used in this research were found to be 546% and 56% respectively. Montmorillonite minerals plot at extreme locations on the plasticity chart, close to the U-line, because of their high absorption capacity (figure 3.15). The bentonite clay used in this study lies slightly above the U-line, which falls out of the montmorillonite mineral zone depicted in the A-chart shown in figure 3.15. This slight deviation of plasticity index (PI) from the theoretical U-line might be due to the arbitrary straight-line definition of the U-line, especially at such high liquid limits. A similar deviation was also reported by Malusis and Shackelford (2002) for the bentonite used in their research. Other researchers have found liquid limit values of smectite minerals as high as 1000% (Mesri and Olson, 1971; Alther *et al*., 1985; Reschke and Haug, 1991).

Deionized water, tap water, and four different inorganic salt solutions with four different concentrations were used in liquid limit investigations of bentonite material in this research study. Figure 3.16 shows the variation of cone penetration with water content for deionized water, tap water, and one molar solutions, while figures 3.17, 3.18, and 3.19 shows the results for 0.5 molar, 0.1 molar, and 0.01 molar salt solutions respectively.

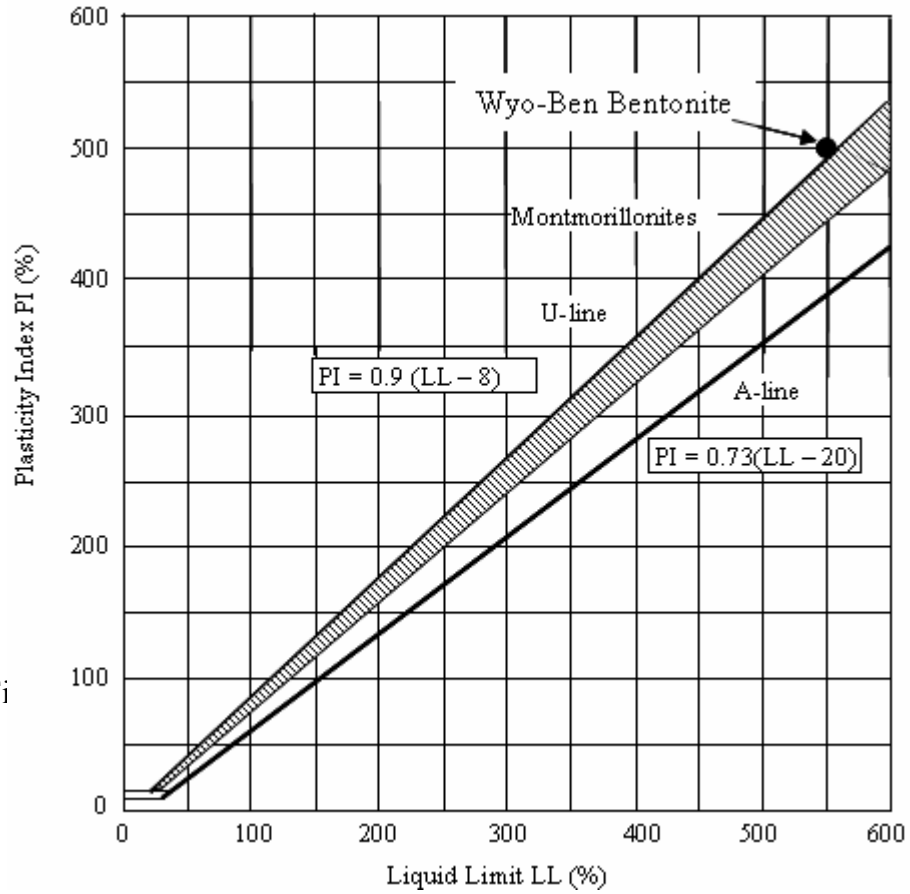

Fi

Figure 3.15 Wyo-Ben Bentonite on the Plasticity Chart

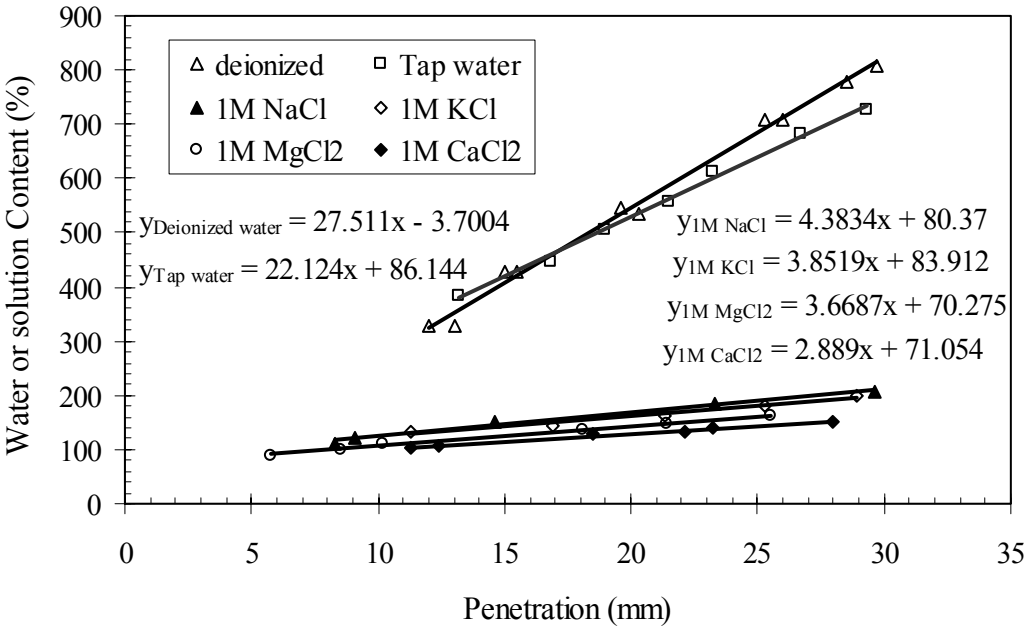

Figure 3.16 Penetration vs. Water/Solution Content (Water and 1 Molar Solution)

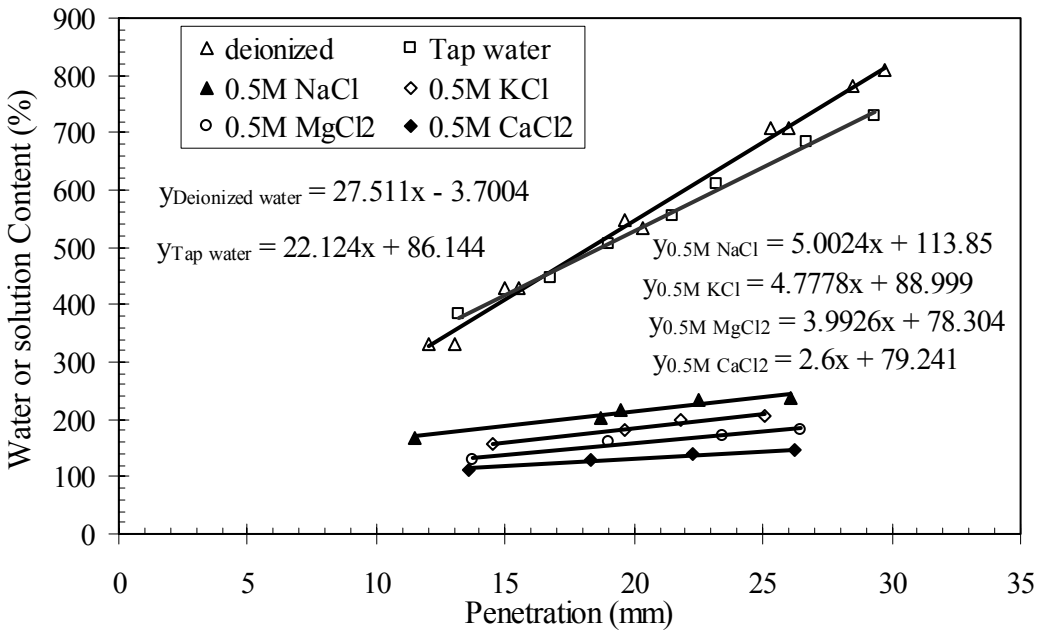

Figure 3.17 Penetration vs. Water/Solution Content (Water and 0.5 Molar Solution)

It can be seen from figures 3.16 and 3.17 that there is a distinct difference between the liquid limit in water and that in higher concentrated salt solutions. This is due to fact that the bentonite particles aggregate due to the reduction in double layer thickness. However, at lower concentrations of salt, the bentonite behavior resembles that of water as seen in figure 3.19. As tap water contains some inorganic ionic compounds, the liquid limit using tap water is slightly lower than that of deionized water, which produces the maximum liquid limit for bentonite clay.

Comparing the liquid limits at various concentrations of salt solutions, it can be concluded that their value decrease with increasing electrolyte concentrations. For monovalent cationic solutions, it can be shown from figures 3.16 – 3.19 that the liquid limit for KCl solutions are lower than those of NaCl, possibly due to stronger ionic linkage of potassium ions with the negative interlayer and inter-particle surface charges, which causes a reduction in diffuse double layer.

The variation of liquid limit for electrolyte solutions of monovalent and divalent cationic solutions can be seen in figures 3.20 and 3.21. Divalent cations are able to replace the exchangeable monovalent cations in the interlayer surfaces, causing a

reduction in double layer thickness, which eventually reduces the absorption capacity of bentonite. As a result, the liquid limit of the material decreases. Liquid limits for $CaCl_2$ solutions were found to be the least among all the solutions because of its higher replacement capacity and its lower water absorption affinity.

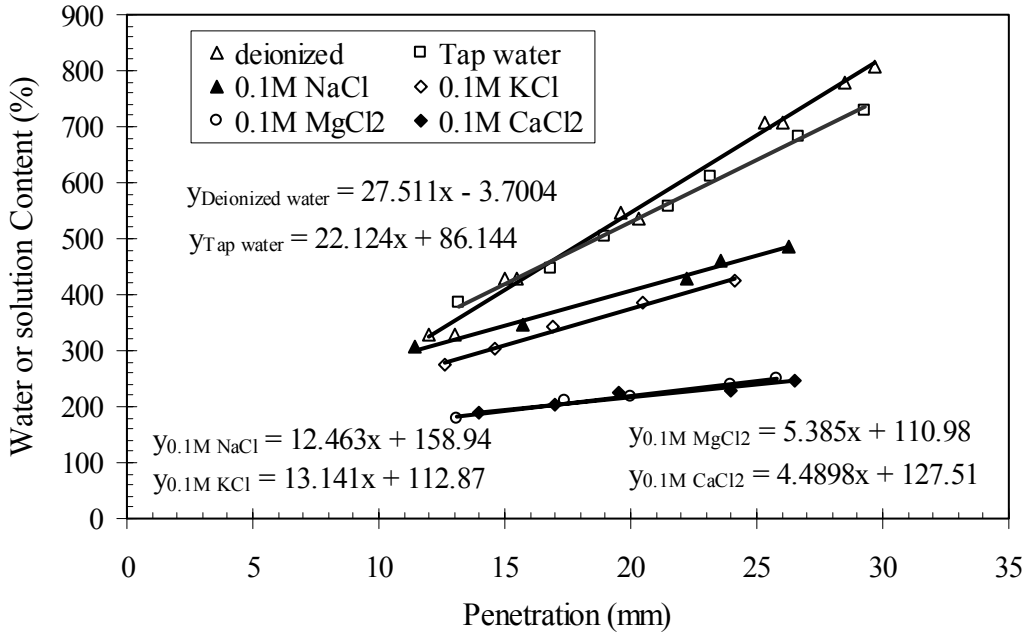

Figure 3.18 Penetration vs. Water/Solution Content (Water and 0.1 Molar Solution)

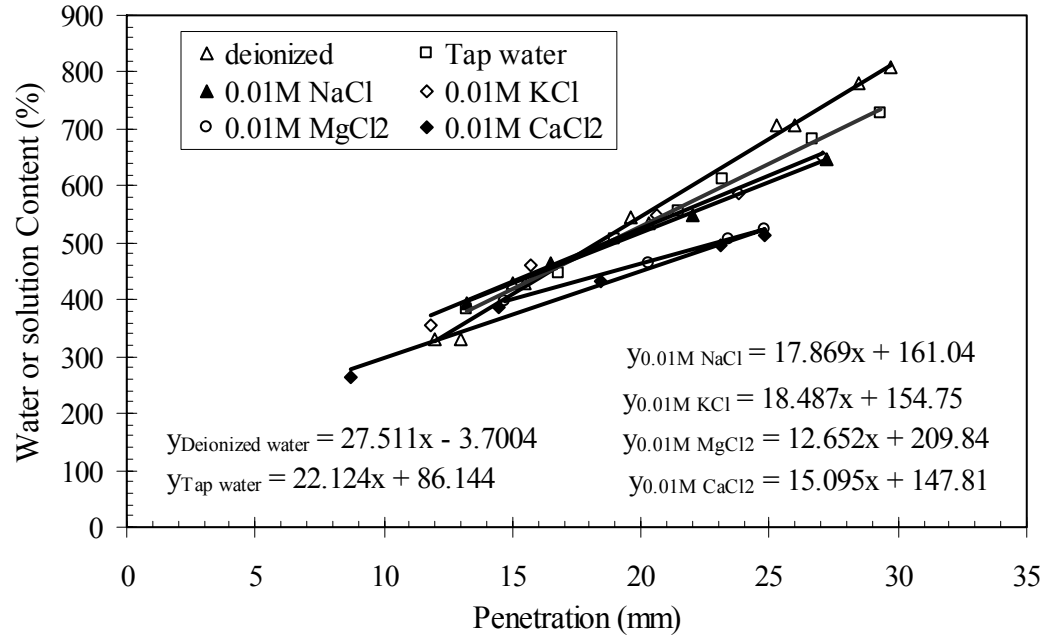

Figure 3.19 Penetration vs. Water/Solution Content (Water and 0.01 Molar Solution)

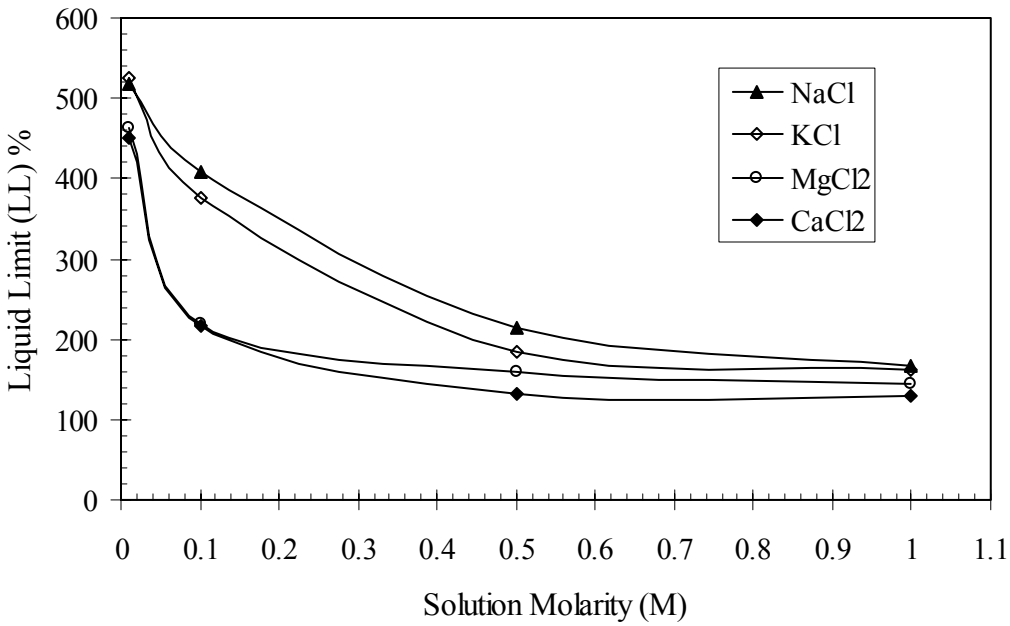

Figure 3.20 Variation of Liquid Limits with Electrolyte Concentration

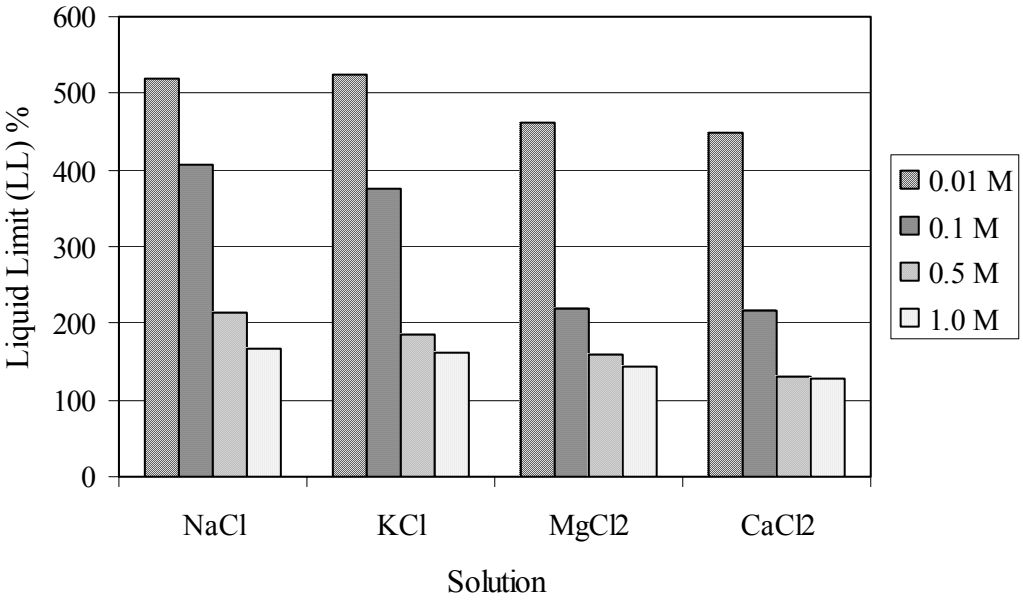

Figure 3.21 Variation of Liquid Limits with Types of Electrolyte Solutions

3.4 Swell Index

Swell index tests were carried out according to the ASTM Standard Method (ASTM D 5890-02) using the various concentration electrolyte solutions which were presented in the previous section. A modified method was used by Reschke and Haug (1991), where 3g of samples were allowed to soak for 24 hours, and the swell index was calculated by dividing the swell volume by the specific gravity of sample. Swell index of Wyoming bentonite has also been investigated by Alther *et al*., 1985, Xeidakis (1996), Zhang *et al.*, (1995), Jo *et al.*, (2001), Stern and Shackelford (1998), Shackelford *et al.*, (2000), and others. It has been found to range between 25 and 65 ml/2g. The main causes of swelling of smectite clay (i.e. bentonite) are (1) the magnitude of cation exchange capacity of the clay mineral interlamellar surface, (2) the type of cations present within the clay surfaces, and (3) the interaction between cations and water molecules (Odom, 1984; Alther *et al*., 1985; Köster, 1996; Kjellander *et al*., 1988; Shackelford *et al*., 2000).

3.4.1 Test Procedure

The newly published ASTM D 5890-02 standard was adopted in determining the swell index of the bentonite. To perform these tests, a 2g sample of dried and finely powdered bentonite clay is dispersed into a 100 ml graduated cylinder in 0.1g increments. A minimum of 10 minutes must pass between additions to allow for full hydration and settlement of the clay to the bottom of the cylinder. These steps are repeated until the entire 2g sample has been added. The sample is then covered and protected for a period of 16 - 24 hours, at which time the level of the settled and swollen clay is recorded to the nearest 0.5 ml. The swell index is expressed in ml/2g of bentonite.

Deionized water and four types of salt solutions at various concentrations were used in swell index experiments. The results and effects of various chemical solutions are discussed in the following sub-section.

3.4.2 Effect of Chemical Solution Species

The swell index of Wyo-Ben bentonite was found to be 60 ml/2g for the suspension in deionized water. However, the maximum swell index of 67 ml/2g has been measured in 0.01 molar NaCl solution as shown in figure 3.22, which could be due to the possibility of more quasi-crystalline water layer formations in and around bentonite particles. As suggested by Odom (1984), the maximum adsorption occurs when Ca and Mg cations together constitute ¼ to ⅕ of the total exchangeable cations, which allows several layers of water to be developed by Na ions. The 0.01 molar NaCl solution may supply the appropriate amount of free sodium ions that could form several layers of quasi-crystalline water layer around the surface of the bentonite, which are responsible for higher swelling and hydration.

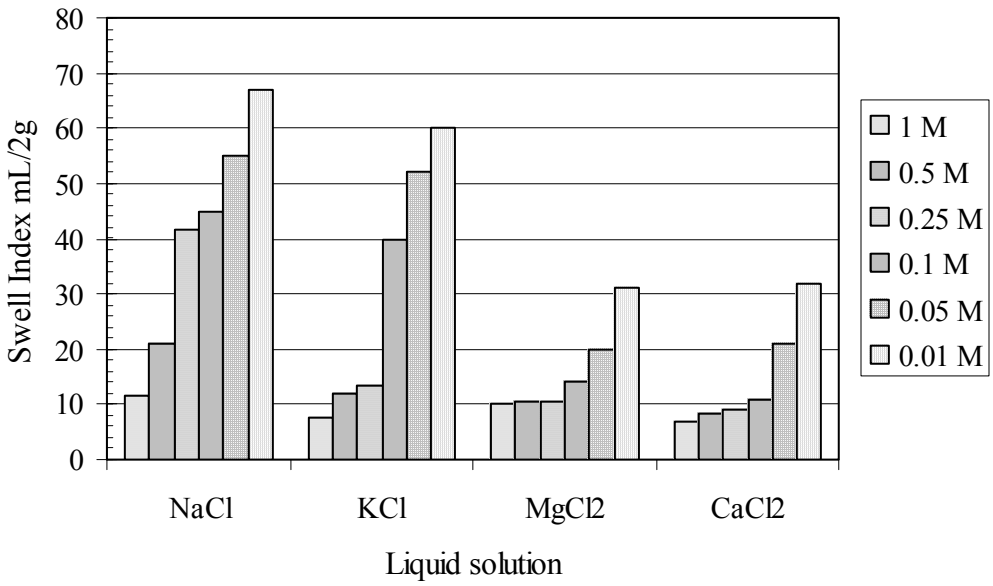

Figure 3.22 Swell Index of Bentonite in Inorganic Chemical Solutions

It can be seen from figure 3.22 that the swell index is higher for monovalent solutions compared to divalent solutions of similar concentrations. Swell index values in KCl solutions are lower than those of NaCl solutions of equal concentrations because of the ability to form rigid linkage between potassium ions and negatively charged clay surfaces. This strong linkage could reduce the diffuse double layer thickness, which is directly responsible for the reduced swelling volume of the bentonite clay materials. In the case of divalent solutions, the divalent cations replace the monovalent cations on the surface exchangeable space and reduce the thickness of the diffuse double layer.

As shown in figure 3.23, minimum swell index values are obtained in the case of higher concentrations of $CaCl_2$ solutions since at higher concentration, calcium cations can substantially replace monovalent cations and water molecules on the surface of the bentonite.

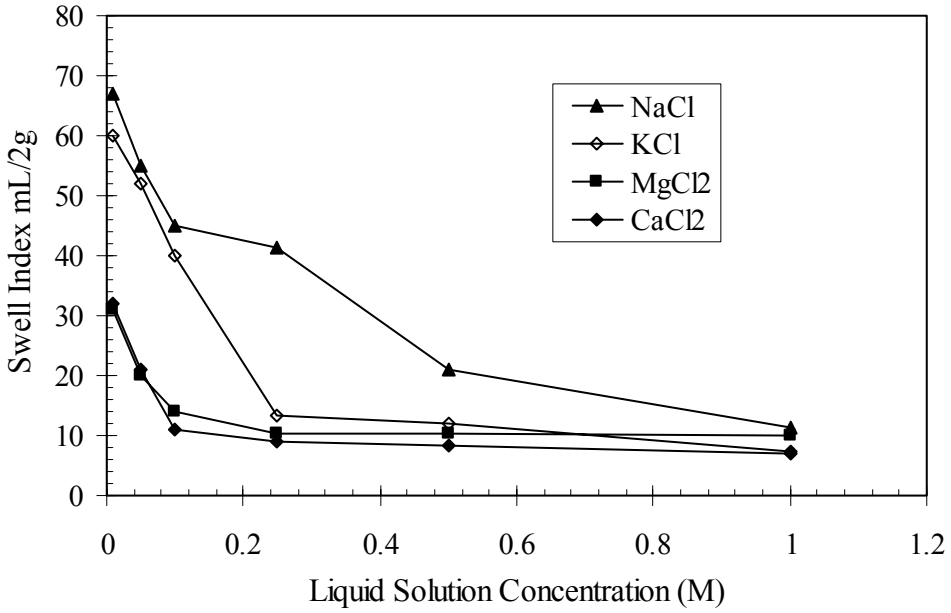

Figure 3.23 Variation of Swell Index with Concentration of Salt Solutions

3.5 Cation Exchange Capacity of Bentonite

Researchers have been measuring the cation exchange capacity (CEC) of clay minerals in many different ways. CEC can be determined by the sodium saturation method as described by Chapman (1965), where the soil sample is first saturated with sodium, and the sodium is subsequently replaced by ammonium ions. The concentration of the recovered sodium is determined by flame photometry which is then expressed in terms of meq/100 g of oven dry soil (Wentink and Etzel, 1972). Other methods used in measuring CEC are X-ray diffraction (Ben *et al*., 2000; Kaufhold *et al*., 2002), infra-red chromatography/spectroscopy (Petit *et al*., 1998; Hwang and Dixon, 2000), cesium chloride adsorption (Itami and Tamamura, 1999), adsorption of a copper ethylenediamine complex (Bergaya and Vayer, 1997), and strontium chloride adsorption ($SrCl_2$) (Schaefer and Steiger, 2002). Research on methylene blue adsorption on clay minerals has been conducted extensively by analyzing clay samples collected from various parts of the world (Hang and Brindley, 1970; Grim 1968; Higgs, 1988; Taylor, 1985; Santamarina *et al*., 2002).

3.5.1 Methylene Blue Test Procedure

Methylene blue (MB) adsorption was found to be one of the most reliable and simple methods to obtain information on the properties of clay minerals, including cation exchange capacity (CEC) of soils and other fine grained minerals. It is also used as an indirect quality indicator for swelling activity of clay materials. If a significant amount of methylene blue is adsorbed by the clay minerals, this may lead to the conclusion that the clay's swelling activity is higher, even though some other minerals which do not swell might also adsorb methylene blue.

The cations in the diffuse double layer are exchangeable with those in the free water. Therefore, methylene blue will exchange cations from both of these sources. In order to eliminate the excessive value of free water cations, clay samples are needed to be

mixed with sufficient deionized water in order to dissolve the precipitated salts and cations existing in the free pore fluid.

The methylene blue molecule consists of an organic base in combination with an acid as shown in figure 3.24. The size of a single molecule of methylene blue as drawn in figure 3.25 has been reported by a number of authors and is tabulated in Table 3.2.

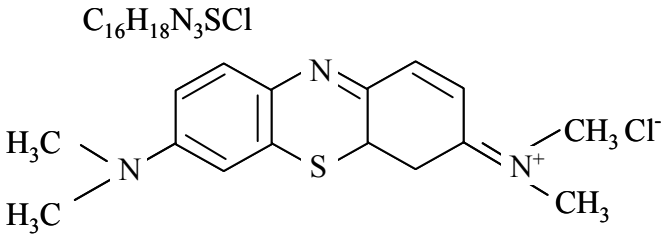

Figure 3.24 Methylene Blue Chemical Structure

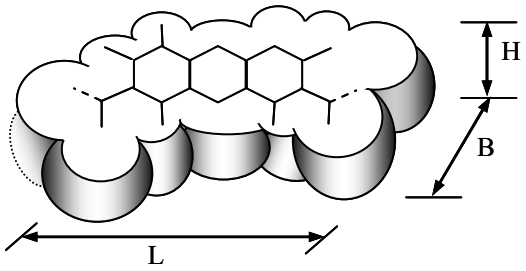

Figure 3.25 Schematic Diagram of Methylene Blue Molecules (after Taylor, 1985)

When methylene blue (dye/powder) is dissolved in water, it will disperse to form a monomer (single molecules) at lower concentrations (less than 10^{-3} mol/m^3), or in monomer-dimer (2 molecules) equilibrium at higher concentrations (about 10^{-2} to 1 mol/m^3) (Taylor, 1985). The chemical formula of $C_{16}H_{18}N_3SCl$ corresponds to a molecular weight of 319.87 g/mol for methylene blue dry die. The methylene blue

molecule contains a negatively charged (Cl^-) ion and a large positively charged ion which drives away the positively charged cations loosely bonded with the clay surfaces at the internal and external faces. The process continues until all the cations have been expelled and replaced by methylene blue molecules with higher fixation attraction.

Table 3.2 Dimensions of Methylene Blue Single Molecule (After Taylor, 1985)

Author	L (nm)	B (nm)	LxB (nm^2)	L (nm)	H (nm)	LxH (nm^2)	B (nm)	H (nm)	BxH (nm^2)
Hofman *et al.*	-	-	1.95	-	-	-	-	-	-
White and Cowen	-	-	1.95	-	-	-	-	-	0.25
Kipling and Wilson	1.6	0.84	1.34	1.60	0.47	0.75	0.84	0.47	0.39
	1.25	0.57	0.71	1.25	0.51	0.64	0.57	0.51	0.29
Hofmann *et al.*	1.50	0.65	0.98	1.50		0.77	0.65		0.33
Hang and Brindley	-	-	1.29	-	-	0.55	-	-	0.25

Methylene blue replaces the clay cations irreversibly as indicated by following reactions.

Ca-Na-Mg clay + Methylene blue (MB) hydrochloride $\rightarrow$ MB Clay + Ca-Na-Mg chloride

Na-bentonite indicates higher CEC because of its higher interlayer spacing as compared to Ca-bentonite where the entry of methylene blue molecules is expected to be restricted because of its limited interlayer (lattice) expansion.

Methylene blue chloride powder (Fisher Scientific, Pittsburgh, PA) was used in this research and the spot method (European standard) has been adopted for measuring CEC for bentonite material. The test procedure can be briefly described as follows:

(a) The methylene blue solution is prepared by mixing methyelene blue powder and deionized water at the ratio of 1g to 200 cc water.

(b) A sufficient amount of deionized water is added to the bentonite clay at about 500 mg to 2 g, so as to produce a suspension or slurry consistency of the clay particles.

(c) A magnetic stirrer with a speed of 400 to 700 rpm is used to stir the bentonite in a glass container continuously until the end of titration by methylene blue.

(d) A methylene blue solution is added to the clay suspension in 0.5 ml increments and stirred for at least 15 minutes.

(e) After each addition of methylene blue, a small amount of clay suspension after stirring is removed by a glass rod and then placed on Fisher brand filter paper P5.

(f) The "end point" is expected to be reached when a permanent light blue halo around the wet soil spot is formed by the unabsorbed methylene blue in excess of the amount required to replace the exchangeable cations of the clay particles.

(g) In order to confirm the end point, step 5 is repeated after a longer stirring for about an hour in order to totally adsorb the methylene blue on the clay surface. If the halo disappears on the filter paper, 0.5 ml of MB is added and steps 5-7 are repeated until a permanent halo appears around the wet clay spot on the filter paper.

The total volume of methylene blue solution added in this process is recorded and used to calculate the cation exchange capacity by the following equation.

$$C.E.C. = MB \text{ added (cc)} \times \frac{\text{MB dry wt (g)}}{319.87} x \frac{1000}{Vol. \text{ of MB solution (cc)}} x \frac{100g}{Clay \text{ dry wt (g)}} \quad \text{(mEq/100 g)} \qquad (3.4)$$

3.5.2 Test Results and Discussion

CEC is normally expressed in meq/100 g of clay sample. The CEC of relatively pure smectite clays ranges between 70 and 130 meq/100 g (Keijer *et al*., 1999; Triantafyllou *et al*., 1999; Shackelford and Lee, 2003; Odom, 1984; Sanchez *et al*., 1999;

Gleason *et al*., 1997; Kahr and Madsen, 1995). However, Malusis and Shackelford (2002) investigated a bentonite having a CEC of 47.7 meq/100 g.

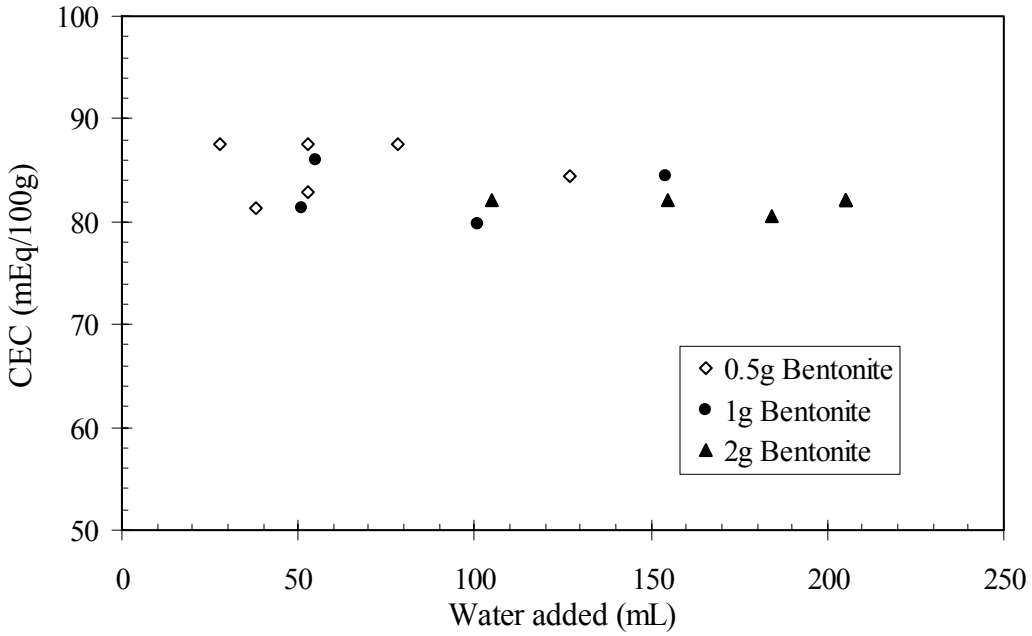

Figure 3.26 Cation Exchange Capacity of Bentonite

CEC values were calculated for various amounts of clay content and MB solution concentrations using the above equation (3.4). Figure 3.26 shows the values of CEC with respect to the amount of water added to the bentonite samples used in this study. Three different amounts of air-dry bentonite samples (0.5 g, 1 g, and 2 g) were mixed and stirred with various amounts of water before adding MB. It can be concluded that no distinct variation of CEC is noticeable due to the amount of bentonite and water added in these experiments. The CEC of the Wyo-Ben bentonite is, therefore, measured to be between 80 and 90 meq/100 g, with an average value of 83 meq/100 g.

CHAPTER FOUR

EQUIPMENT DESIGN & FABRICATION

4.1 Permeability Equipment

Standard pressure panels for permeability tests are commonly used to perform hydraulic conductivity tests, but cannot be used directly with highly corrosive leachates collected from landfill sites and or synthetically mixed chemicals. Aggressive inorganic or organic chemicals can cause the panel tubes and fittings to corrode. To protect the pressure panel, special buffer cells were designed and fabricated as shown in the schematic diagram in figure 4.1. These buffer cells are connected with the various inlets and outlets of the main pressure panels. The main criteria considered during design and fabrication of these cells are

(a) to be used as a substitute for the burette attached to the pressure panels,

(b) to prevent corrosive liquids or leachates from contacting metal fittings and pressure regulators, and thus preventing corrosion, clogging and damaged panel parts,

(c) to accommodate a large quantity of influent to be permeated through the specimen in an uninterrupted fashion,

(d) to fill the cells in an uninterrupted fashion whenever necessary,

(e) to collect the influent and effluent samples at any pore volume of permeation while continuing the permeability test, and

(f) to apply and maintain any specific hydraulic gradient during the test.

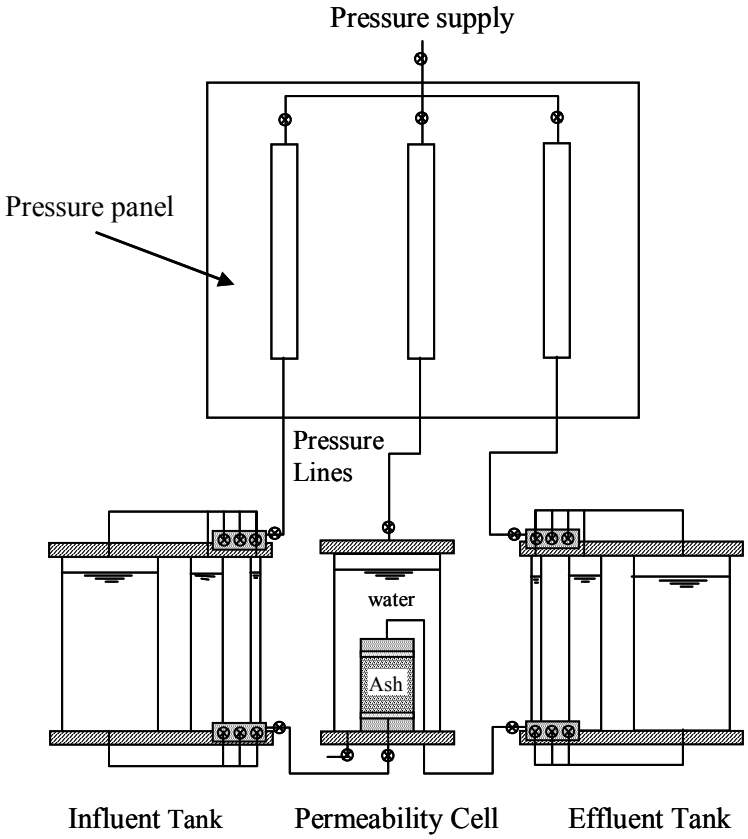

Figure 4.1 Schematic Diagram of Permeability Test Setup

4.1.1 Design Concept

The permeability cells designed and fabricated in this study are suitable for use in both constant head as well as variable head conditions in rigid wall and flexible wall permeameters. The design of the permeability buffer cells has been incorporated to suit the existing pressure panels available in the Geoenvironmental Laboratory at the University of South Florida (USF). Compressed air pressure regulated from the panel can be utilized through the buffer cells. Connections of the cells with the pressure panels were made in such a way that the influent and effluent pressure during the permeability tests can be monitored through the electronic indicator mounted on the main pressure

panel board. Buffer cells were designed to accommodate permeability tests on many different types of soils with a wide range of permeability. Soils with low permeability such as bentonite and other clays, cause small amounts of flow through the specimen even at higher hydraulic gradients while soils with high permeability such as coarse sand generate a high rate of flow under low gradients. Buffer cells have been designed with three chambers of different diameters to indicate with high precision any amounts of flow in the influent and effluent tubes.

Since the duration or pore volume of flow is an important factor in investigating permeability of soils to chemicals, the cells were designed considering a high volume capacity so that the tests could be carried out uninterrupted overnight or for longer intervals.

Uniformity of synthetic chemical solutions can be maintained within the effluent cell for a long duration of time during the permeability since the cell chambers are made of chemically inert materials, and because of their high storage capacity. To verify the chemical composition of synthetic solutions, to monitor leachates quality in the influent cell, and to conduct chemical analysis of the effluent solution, control valves have been provided at the bottom of both influent and effluent cells which provide easy sample collections at any interval of time while running the permeability tests.

Replenishment of influent can be carried out in any quantity through the bottom control valves by hydrostatic force or under pressure, and through the top control valves using a syringe or fill pump connected with the pressure panel. Replenishment from one chamber to another can also be achieved by using a pressure differential across the connecting bridge tubing during the test.

Highly concentrated chemical solutions and contaminant leachates used as permeants might cause chemical precipitation and deposition within the cells as well as in the connecting tubings. Light precipitation and deposition within the cell chambers can be dissolved or removed in one chamber at a time by water jetting or using cleaning solutions without discontinuing the tests. High precipitation can be cleaned after completion of the tests when the individual parts and tubings are dismantled and are typically cleaned using conventional or special acid cleaners.

4.1.2 Materials and Fabrication

The cells, as shown in figure 4.2, consist of three different diameters clear acrylic (Plexiglass) cylinders placed in between two metallic plates. To prevent the chemical corrosion of the metallic plates due to highly concentrated synthetic chemical solutions, the bottom metallic plate was made of highly corrosion-resistance Type 316L stainless steel. Plexiglass cylinders are fitted into grooves cut on the top and bottom plates. The cells are fabricated in such a way that, after tightening, no leakage of liquid is possible even at high applied pressures (100 to 120 psi). All cylinders are 11 inches long and graduated in length and volume, which allows the measurement of the permeants with an accuracy of 1 mm in elevation and 0.1 cm^3 in volume. The cylinders are connected at the top and bottom by flexible transparent rubber tubings to two central blocks, which are made of stainless steel. All the connecting lines are made of transparent nylon tubes of ⅛-inch outside diameter. Stainless steel central blocks were chosen for their high strength and chemical /corrosion resistance characteristics. The top central block is connected to the burette of the pressure panel, through which the pressure is regulated. The other central block, which is attached at the base, is connected to the permeation chamber where the specimen is placed.

The top central block, connecting each of the three buffer cylinders controls the applied pressure from panel regulator with an accuracy of 0.1 psi. However, since no separate regulator is attached to individual buffer cells, the pressure applied on the each of the cylinders is constant. Each cylinder is equipped with a vent valve which is used to release pressure and to facilitate backfilling of the permeant liquid.

The bottom central block connecting each of the three cylinders at their bases controls the flow of permeant in and out of the cylinders. Nickel plated ball valves are connected to each of the outlet nylon tubes at the bottom central block, and are used to control flow of the permeant from individual cylinders and to collect liquid samples at any time during the permeability tests without interrupting flow through other tubes. The required amounts of permeant samples (leachate) before and after passing through

the test specimen are collected from the corresponding (active) cylinder for further chemical analysis.

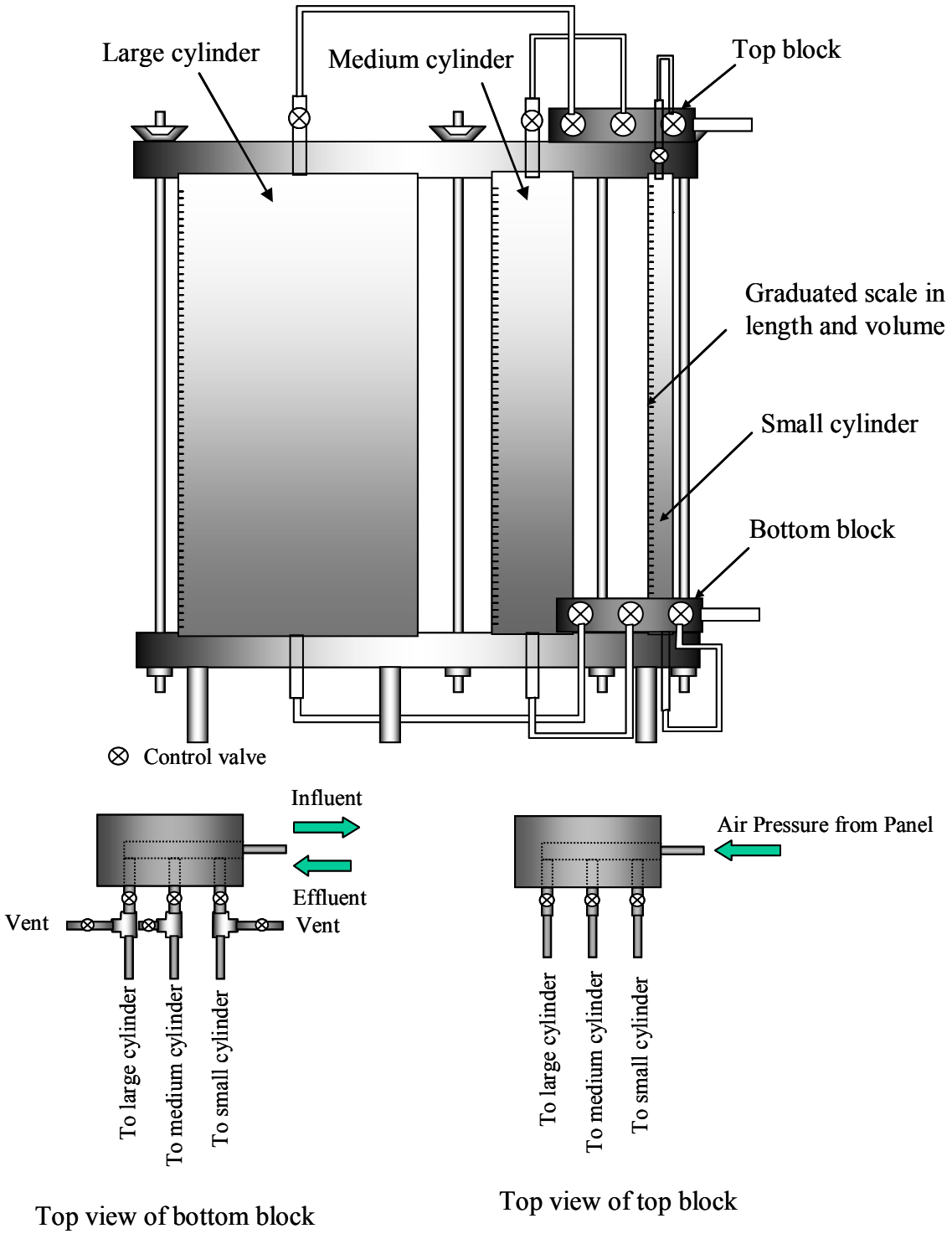

Figure 4.2 Schematic Diagram of Permeameter Cell

Since the inside diameter of the largest cylinder is 5½-inch, over one gallon (4 liters) of permeant can be stored. Each test can therefore, run for quite a substantial period of time depending on the applied hydraulic gradient, soil permeability, and thickness of the test specimen. However, for very low permeability specimens, where the amount of permeant is very small, the small diameter (⅜-inch ID) cylinders are used for flow measurement as well as for collecting the permeant. The small cylinders can also be used for highly permeable specimens to determine the coefficient of permeability (hydraulic conductivity) and to collect small amount of liquid permeants over a short period of time.

The flow of permeant from any cylinder can be cut-off and switched to another cylinder within the same cell using the bottom central block. Throughout the process, the flow remains uninterrupted. By cutting off the flow, the permeant can be collected or replenished up to any desired level while the permeability test is continuing using the other cylinder. Backfilling into the cylinder can be expedited by releasing the attached vent valve placed at the top of the cylinder. Any cylinder can be separately cleaned of any chemical deposition or sedimentation by flushing it with cleaning agents or tap water. The entire cell can also be dismantled after completion of any test, and cleaned and reassembled for subsequent experiments.

The permeameter, as shown in figure 4.3, consist of 5-½-in OD and 5-in ID clear acrylic (Plexiglass) cylinder placed in between two metallic plates and two 4-in diameter stainless steel platens. Plexiglass cylinders are fitted into the grooves cut on the top and bottom plates. The height of the permeameter cylinder is 12 inches which can easily accommodate specimens of up to 8-in long. A control valve at the top plate of the permeameter is connected with the pressure panel through which compressed air is applied to the cell. Pressure applied at the cell liquid surface acts as the cell pressure for the specimen, which is submerged in. Three stainless steel control valves are connected at the base plate of the permeameter as shown in figure 4.3 (b). The middle control valve is connected at the bottom of the platen through which the influent enters into the test specimen. After permeating through the specimen, the effluent flows through the top

platen into the effluent buffer cell. All the connecting lines are of transparent nylon tubes ⅛-inch in outside diameter.

A split mold 4-in ID and 1-in long has been designed and fabricated to be used in preparing the clay specimens onto the bottom platen within the permeameter. The split mold fitted with a rubber membrane is placed flush with the bottom platen so that the loose dry bentonite powder does not slip through the sides of the platen while preparing the specimen. Both top and bottom plates of the permeameter are made anodized iron for corrosion resistance and longer service life.

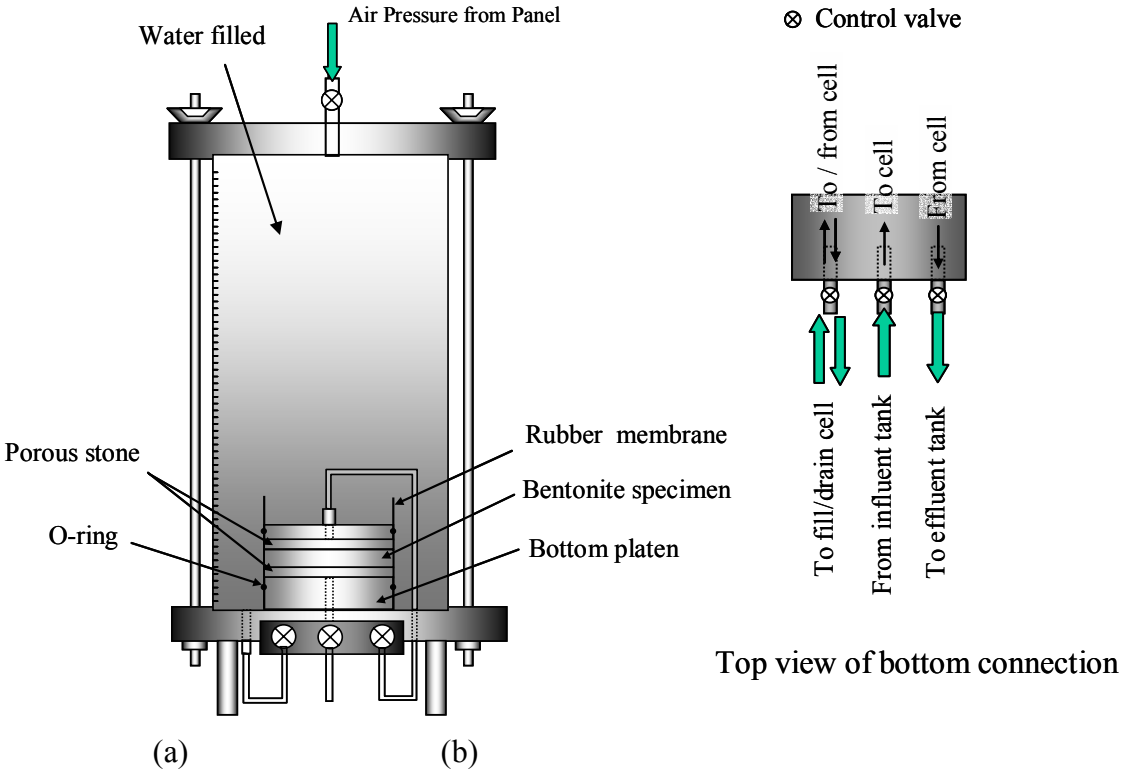

Figure 4.3 Schematic Diagram of Flexible Permeameter (a) Permeameter Cell (b) Bottom Connection

4.2 Diffusion Equipment

Cheung, (1994) described the use of an used apparatus for in-diffusion (electrolyte solution passes through the specimen from high to low concentration) and through-diffusion (electrolyte solution passes over one side of the specimen and is collected from the other side), Eriksen, *et al*., (1999) used a diffusion cell where bentonite was statically compacted in the diffusion cylinder (internal diameter of 10 mm and length of 5 mm) to a dry density of 1800 kg/m^3. Inlet and outlet channels were fitted with a metallic filter (0.82 mm thick), and the clay was equilibrated with the aqueous solution for at least three weeks by pumping a groundwater solution. Higashi *et al*., (1990) investigated the diffusivity of nuclide transport in water (titrated water) through bentonite by using a diffusion cell 4 cm long and 2 cm in diameter. Pre-saturation of samples was carried out by submerging the specimen in water after placing it into the cell. Diffusivity of ions, especially radio-nuclides, through compacted sodium bentonite were investigated by Kim *et al*., (1993) by a method called "back-to-back", where the source solution is allowed to diffuse in plane from the center toward both ends of the specimen. In this method the bentonite clay was saturated with the solution to form a slurry before being dried and cut into slices 2.5 cm in diameter and 2 cm in length. The sliced specimens were then placed into the diffusion circular metallic cells where the specimens were allowed to swell upon saturation with the solution to a predetermined size and volume.

An equipment called "DKS permeameter" (diffusion, convection, sorption) was used to study soil-contaminant transport mechanisms by Mahler and Velloso (2001). In this technique, the soil sample is molded in the middle of the permeameter, and both source solution and distilled water are allowed to percolate into the top and bottom channels, which are made of highly permeable porous materials, thus creating a constant concentration gradient through the specimens.

The diffusion characteristics of compacted sodium bentonite in terms of ionic charges and orientation of clay particles were investigated by Sato (2000) and Sato and Suzuki (2003) using through-diffusion techniques, where bentonite specimens were placed in a diffusion cell and then compacted and saturated with various electrolyte

solutions. Diffusion tests for compacted clay using compaction mold type cells were also used by Shackelford (1988, 1990, 1991, 1994), Shackelford and Daniel (1991), Shackelford *et al*., (1999), where the clay samples were compacted in the mold at optimum water content before being saturated with water for a period of 17 to 160 days.

Lake and Rowe (2000, 1997) devised an apparatus similar to the one used in this study to measure the diffusion coefficient of GCL materials under specified volume diffusion (SVD) condition, where various types of inorganic chemical solutions were used as a source (figure 4.4). Here the clay specimens were allowed to swell by hydration up to any degree, resulting in a wide range of void ratios. SVD allows the comparison of diffusion results in various controlling solutions by controlling the final saturated void ratios of the bentonite clay specimens.

Most of the above diffusion cells were adopted to satisfy the investigators interest in particular factors, field requirements and environmental conditions such as highly traceable chemical elements, long periods of diffusivity, simulating in-situ compaction and saturation, or automation of the set-up among others.

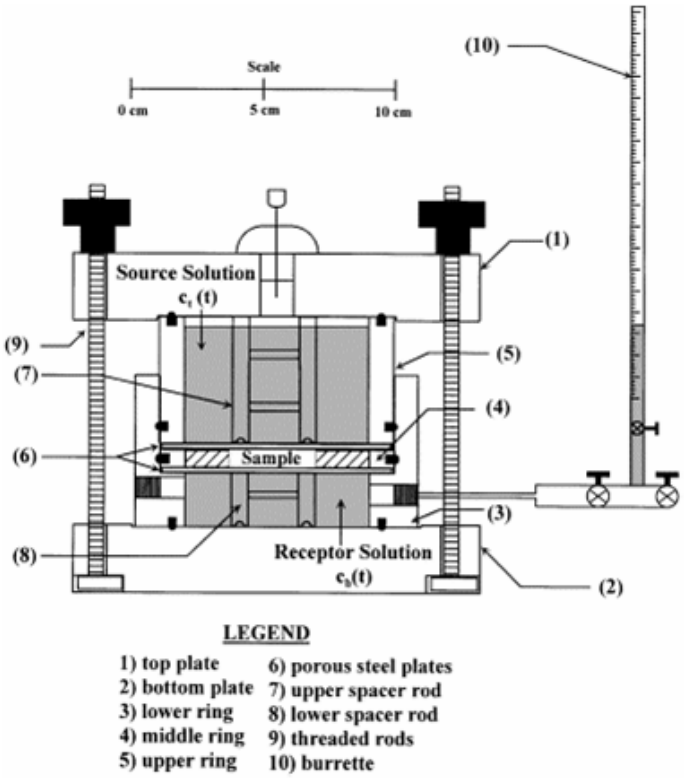

Figure 4.4 Specified Volume Diffusion Cell (After Lake and Rowe, 2000)

4.2.1 Design Concept

The following factors have been considered in designing the diffusion cell in this study.

(a) It is necessary to obtain a uniformity swelling bentonite clay specimen in terms of density and water content.

(b) Full saturation of the clay specimens must be achieved within a short period of time.

(c) The void ratio of the specimens must be varied by controlling the thickness and changing the dry bentonite weight, or by controlling the weight while thickness at full saturation.

(d) Collection of the source and receptor solutions must be easily done while continuing diffusivity testing through the specimen when necessary.

(e) Disturbance to the prepared samples within the mold must be avoided.

(f) Provisions must be made to apply a hydraulic gradient through the specimen for further advection analysis if required.

(g) High storage capacity of the source solution must be secured in order to continue the diffusion experiment for a long period of time without affecting the quality and concentration of the solution.

The diffusion apparatus designed in this study is of the considered to specified volume diffusion (SVD) type as shown in figure 4.5, where the volume of the specimen remains the same throughout the whole diffusion process. Specimens are made by slowing consolidating the slurry samples prepared by mixing bentonite with high amounts of water (above their liquid limit). The idea of making specimens from slurry has come up from the fact that dry bentonite powder starts to swell as soon as it comes into contact with water. An outer sealed layer is created, so uniformity of the specimen cannot be achieved for small amounts of bentonite mixed with water. Furthermore, the amount of swelling bentonite is not uniform across portions of the specimen, which could develop channels for the fluid to pass through during diffusion. It is also not possible to make uniform bentonite samples by mixing with low amount of water (below liquid

limit) because of air bubbles trapped within the specimen during preparation. Preparing the specimens outside the diffusion cell may cause disturbance to specimens, making it difficult to place the specimen uniformly in the cell.

Both source and receptor containers need to be transparent so that the level of fluid can be monitored during diffusion and refilled if necessary to maintain a constant level. It is noted that fluid levels may change due to osmotic flow, thus creating an unwanted hydraulic gradient.

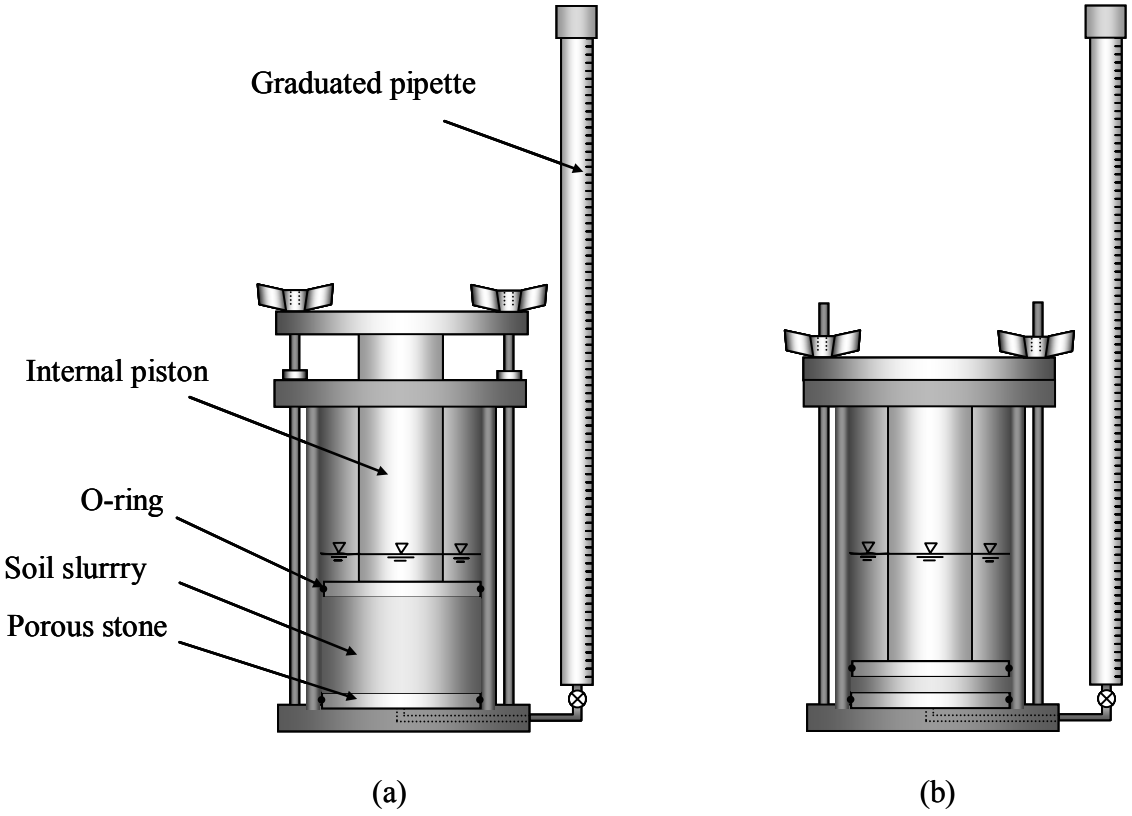

Figure 4.5 Diffusion Set-up with Clay Slurry (a) Initial Before Consolidation (b) Final After Consolidation

4.2.2 Materials and Fabrication

Constant head rigid wall permeameters manufactured according to ASTM D-2434 have been modified to create the diffusion cells as shown in figure 4.5. Rigid permeameter walls which contain the source fluid and the clay specimen have been fabricated in the machine shop at the University of South Florida. The cylinder is made of transparent acrylic material (plexiglass) 6-in long, 3-in ID, and ¼-in thick. A thick O-ring is placed within the groove on both the bottom base plate and the top metallic platen in order to prevent any leakage during diffusion. In order to further prevent leakage, sufficient vacuum grease was pasted in and around the O-rings. The acrylic chamber permits viewing of the sample during testing. The end plates are constructed of anodized aluminum for rust resistance. An internal piston, which is placed inside the diffusion cylinder, is also made of acrylic material and 2-in OD and ¼-in thick. The receptor is a graduated pipette ½-in internal diameter and 10-in long which can contain up to 30 mL of solution. A cap is fitted at the open end of the pipette to prevent any ingress of impurities and evaporation from the solution during testing. A hand-held rubber suction pump with a smaller diameter pipette is used to collect receptor fluid samples for further chemical analysis during diffusion tests.

Both the source chamber and receptor are graduated so as to monitor the level of the fluid. Porous stones 3-in in diameter and ¼-in thick are placed at top and bottom of the clay specimen inside the source chamber to provide filtering during sample preparation and to maintain uniformity of the specimen thickness. Because a tight seal was required, fitting of the porous stones inside the source chamber was one of the most difficult tasks in the whole assembling process. The bottom porous stone had to be placed before the slurry sample was poured into the chamber, while the top one was placed after pouring the slurry. Grooves were cut along the perimeter porous stone so as to fit O-rings as shown in figure 4.6.

A sufficient amount of vacuum grease was pasted along the O-ring and circumference of the top porous stone before placing at the top of the source chamber and subsequently pushing through the plexiglass of the chamber. Tight dimensional

tolerance O-ring is necessary so that the porous stone assembly does not fit too tightly into the chamber which might cause cracking and eventually breaking upon pushing with the internal piston.

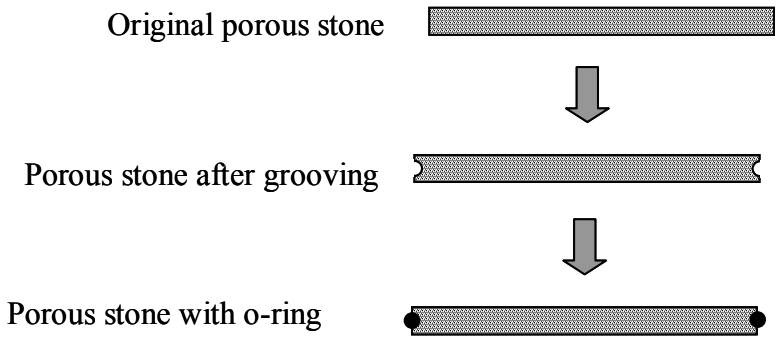

Figure 4.6 Modification of Porous Stone

CHAPTER FIVE

HYDRAULIC CHARACTERIZATION OF BENTONITE

In this chapter, characterization of bentonite in terms of its hydraulic conductivity is presented. Two types of permeameters, namely flexible wall and rigid wall, with various inorganic chemical permeants under various hydraulic gradients and pre-hydration conditions have been used in this study. Chemical analysis of effluent following permeation through bentonite is also reported in this chapter.

5.1 Hydraulic Conductivity of Bentonite

Deionized water, tap water, and synthetic inorganic salt solutions of various concentrations and combinations have been used as permeants for bentonite clay in this investigation. Various chemical permeants, permeameter types, and the effects of various factors controlling conductivity are discussed in this section. Fifty grams of air-dried bentonite samples, 7.5 mm thick and 10.16 cm (4-in) in diameter were used in most of the hydraulic conductivity experiments conducted in the flexible wall permeameter. The corresponding dry density is 0.83 g/cm^3. A different setup was used for rigid wall permeameters, as discussed later in this chapter.

5.1.1 Inorganic Chemical Permeants

Deionized water with less than 5 ppm of impurities, tap water with 200 to 300 ppm of ionic concentration, and four different salt solutions (NaCl, KCl, $CaCl_2$ and $MgCl_2$) of various concentrations and combinations, as shown in Table 5.1, were used in hydraulic conductivity tests as permeants through bentonite clay specimens. All the salts are Fisher Scientific Lab certified brands and have been used according to their formula weights for preparing synthetic inorganic solutions. NaCl, KCl, and $CaCl_2$ are in the form of anhydrous granular salt while $MgCl_2$ is a hexahydrate crystalline salt having the chemical formula of $MgCl_2.6H_2O$. Deionized water, commercially available in plastic one-gallon bottles was used as a solvent for those salt solutions.

The salt solutions have been chosen to investigate the effects of various concentrations, cation size, valence, and ionic strength. Deionized (DI) water is used as the reference and controlling solution, in addition to initial pore fluid saturation. Concentrations of the electrolyte solutions were varied from 0.1M to 5M and were prepared by dissolving crystalline/granular salts with DI water. NaCl and KCl were chosen to investigate the effects of monovalent cations and hydrated ion size (Na^+ and K^+ have different hydrated radius) while $CaCl_2$ and $MgCl_2$ were chosen to investigate the effect of divalent cations (Ca^{2+} and Mg^{2+}) that are commonly found in natural aqueous systems.

Sufficient quantities of solutions were prepared in order to last for the whole period of conductivity experiments so that the uniformity of the solutions can be maintained. The synthetic solutions were transferred to the largest chamber of the cells after being prepared in the lab at normal room temperature ($21^o \sim 22^oC$).

5.1.2 Flexible Wall Permeability

Permeability tests have been performed according to ASTM standard (D-5084) for flexible wall permeameters. Since the effluent (tailwater) level increases with time

during the tests, falling head assumptions with increasing tailwater pressure calculations have been adopted for the calculation of the coefficient of permeability. The modified formula used in the calculation is given in equation (5.1).

$$k = \frac{a_{in} a_{out} L_{sample}}{A_{sample} t (a_{in} + a_{out})} In \frac{(h_{in} - h_{out})_{initial} + \left(\frac{p_{in} - p_{out}}{\gamma_w} \right)_{initial}}{(h_{in} - h_{out})_{final} + \left(\frac{p_{in} - p_{out}}{\gamma_w} \right)_{final}} \qquad (5.1)$$

where a is the area of the apparatus pipette, L_{sample} is the length of the sample, A_{sample} is the cross sectional area of the sample, t is the time between initial and final readings, h is the water elevation in the pipette, p is the pressure in the pipette, and subscripts *in* and *out* denote inflow and outflow, respectively. A schematic diagram has been shown in figure 5.1 to describe all the terms of equation (5.1).

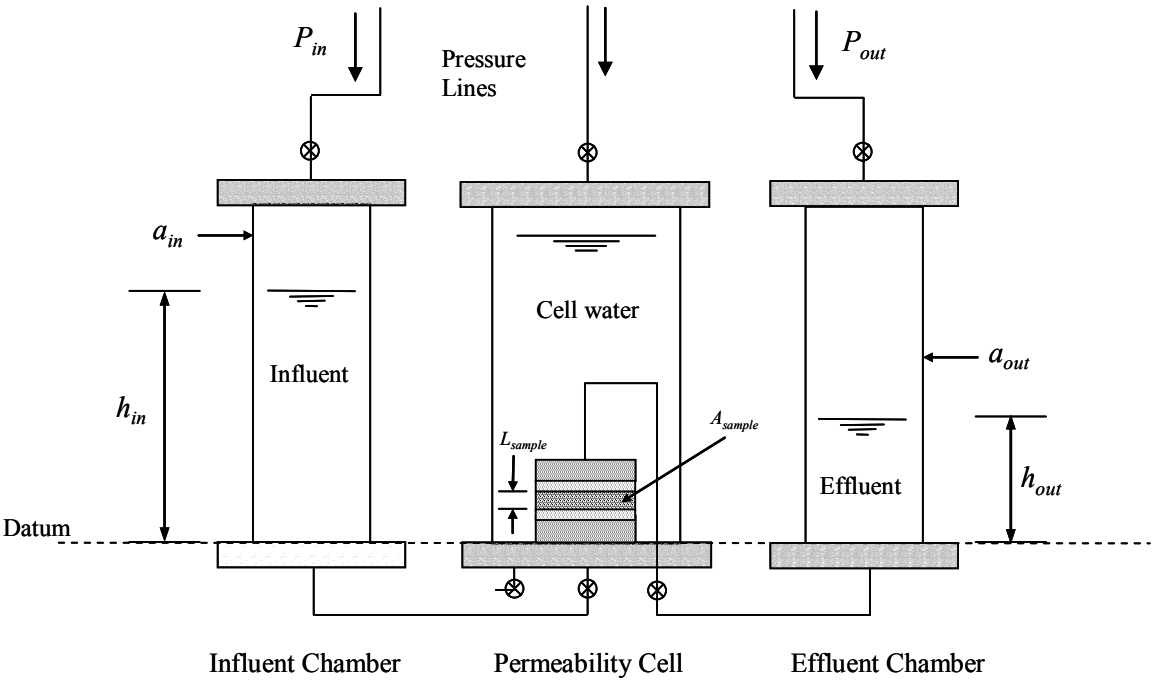

Figure 5.1 Schematic Diagram of Flexible Wall Permeameter Set-up

The detailed description of the test apparatus has been given in Chapter 4. Three stainless steel ball valves are connected with the bottom permeameter plate, which are used to (i) fill and drain the chamber through the base, (ii) supply influent from the influent cell to the specimen through the base platen, and (iii) discharge effluent from the specimen to the effluent cell through the top platen. An opening at the top of the permeameter plate is connected through the ⅛-inch (OD) nylon tubing to the pressure panel through which the regulated air pressure is applied to the cell water. Figure 5.2 shows the connections of all the tubings with various components of influent chamber, permeability cell, and effluent chamber with the pressure panel.

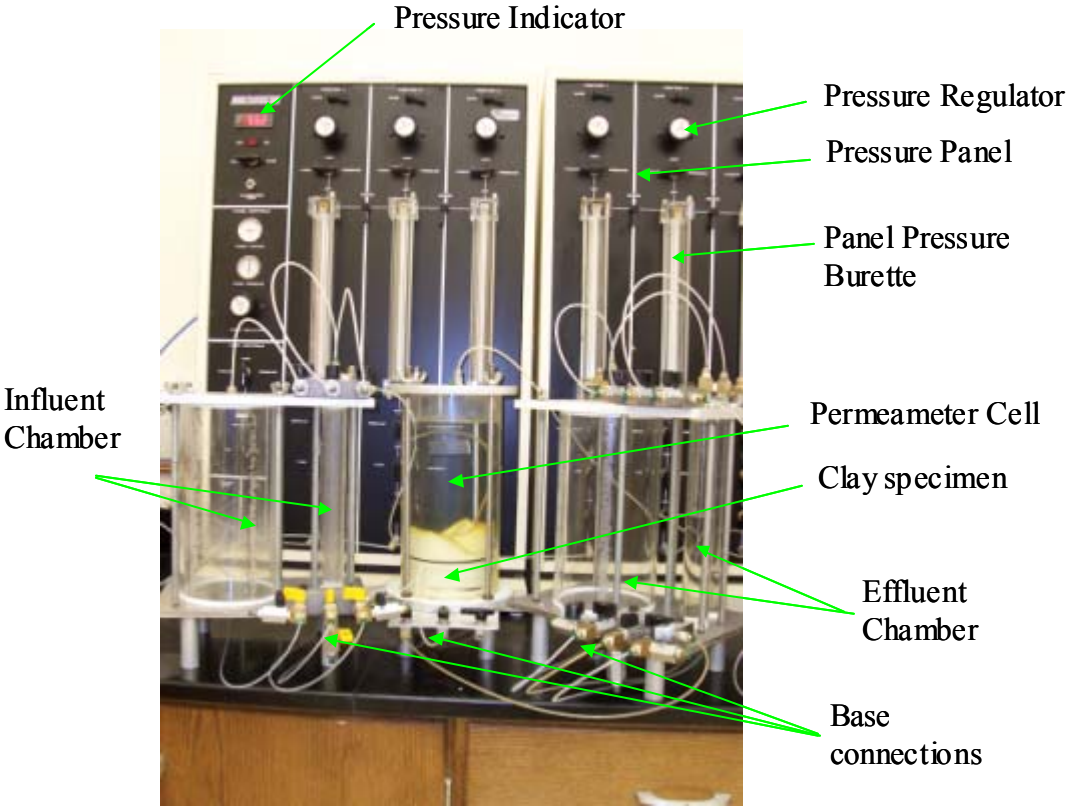

Figure 5.2 Flexible Wall Permeameter

5.1.2.1 Test Procedure

The test procedure described in this section includes sample preparation, sample saturation, permeation phase, and termination criteria. Sample preparation is one of the most critical steps in the flexible wall permeability experiments since proper preparation is crucial in minimizing experimental errors from leakage, sample loss, and disturbance.

5.1.2.2 Sample Preparation

All the components of the permeameter and supporting devices are shown in figure 5.3. A vacuum pump was used during sample preparation for fitting the rubber membrane into the split mold so that the mold can be easily placed on the bottom platen of the permeameter, and to secure the bottom porous stone in place while placing the powdered sample.

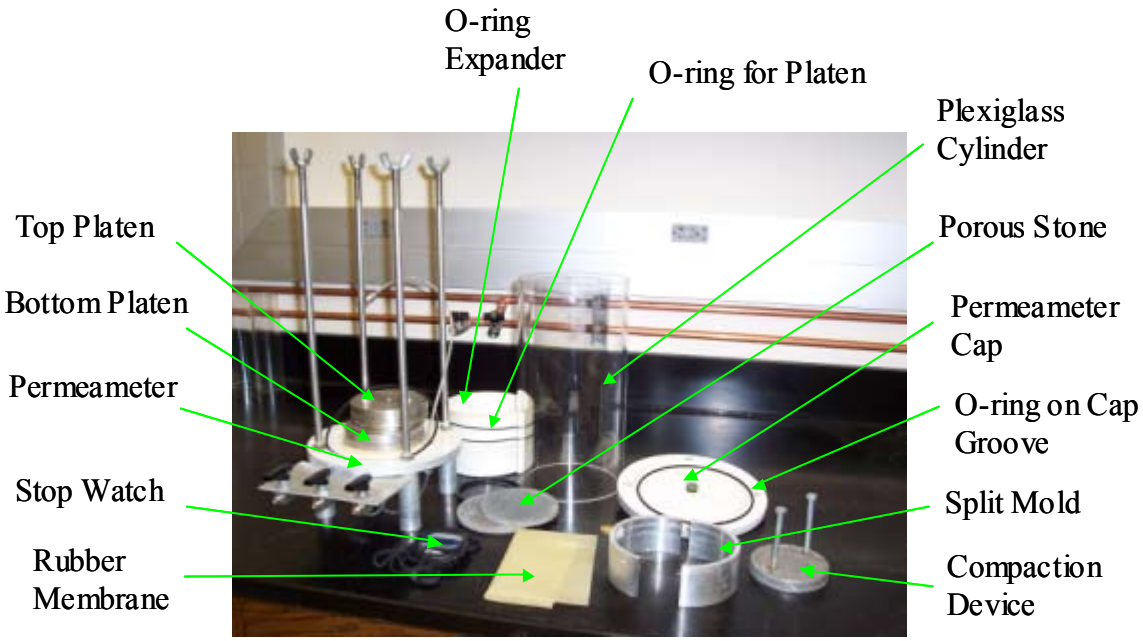

Figure 5.3 Components of Flexible Wall Permeameter

The following steps are carried out in sequence during the preparation of clay specimens in the flexible wall permeameter.

Step 1: The groove of the base plate of permeameter is cleaned thoroughly with a brush and cloth/tissue paper. The O-ring, lubricated with silicon grease, is then fitted to prevent base leakage. A porous stone and filter paper (Fisher Scientific brand) are placed on the bottom platen of the permeameter.

Step 2: A leak free latex membrane is wrapped over the split mold and manually stretched to fit the inner side of the mold in an unwrinkled fashion.

Step 3: A vacuum pump is connected with the mold, and suction is applied to remove air from the space between membrane and mold so that the membrane can follow the inner shape of the mold. The split mold wrapped with the membrane is then placed over the bottom platen while the vacuum pump is kept on.

Step 4: An accurately measured amount (50 g) of air-dried bentonite powder is spread over the filter paper in the mold and is lightly compacted uniformly using a specially designed compaction rod. A spoon can also be used to lightly fill-up any voids left along the perimeter.

Step 5: The top filter paper and porous stone are placed on the bentonite powder carefully to prevent disturbance or loss of clay powder.

Step 6: The top platen is placed on the porous stone and the vacuum pump is then disconnected. The rubber membrane is unrolled from both ends of the split mold and is extended over both top and bottom platens. The mold is then split open and is removed carefully.

Step 7: An O-ring expander whose diameter is at least ½-in larger than that of the specimen is used to place one or two O-rings on the grooves at both top and bottom platens in order to prevent any leakage from the cell into the specimen and to keep the membrane in place.

Step 8: The top platen is connected tightly with the outlet tubings to prevent cell water from seeping through. The plexiglass cylinder is then placed on the O-ring fitted on the chamber base. The top cover of the chamber is tightened to seal the cell while pressure is applied to the chamber during permeability testing.

Step 9: Tap water is filled into the permeameter cell through the bottom opening slowly to minimize disturbance to the newly prepared sample. Water is filled up to a level of 1-2 inches below the top cover.

After completion of sample preparation and water filling, the permeameter is shifted to the pressure panel where the influent and effluent chambers are already assembled. The permeameter is then connected to both chambers through the base tubings as shown in figure 5.2. All the above steps are shown in figure 5.4.

(a) Sample Preparation (Step 1)

(b) Sample Preparation – (Step 2)

Figure 5.4 Sample Preparation for Flexible Wall Permeability Test


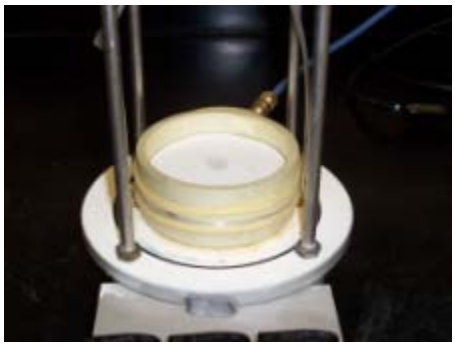

(c) Sample Preparation – (Step 3)

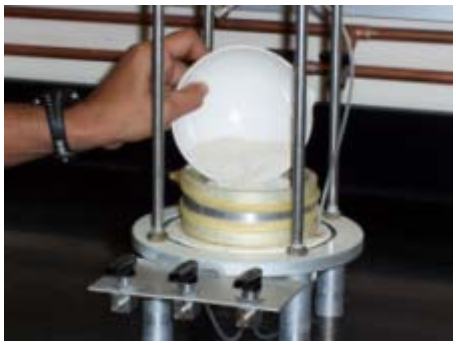
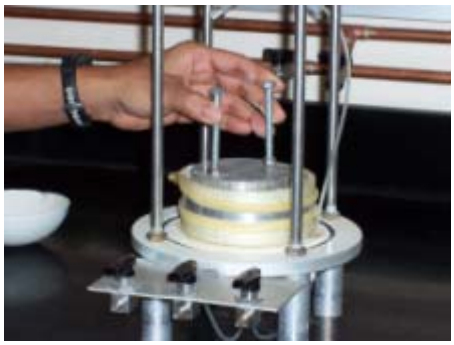

(d) Sample Preparation – (Step 4)

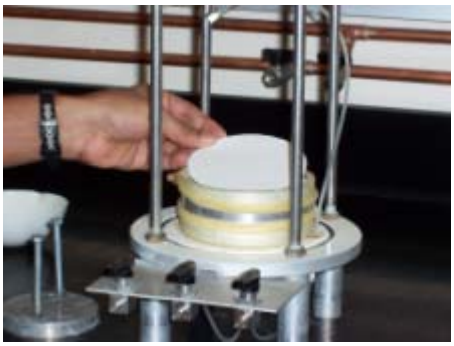
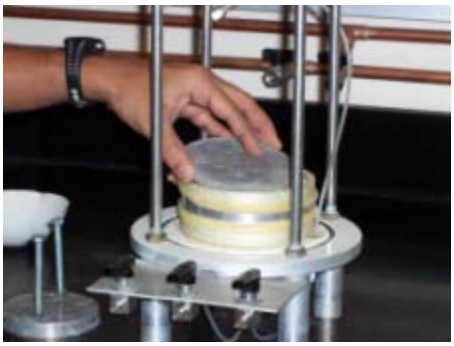

(e) Sample Preparation – (Step 5)

Figure 5.4 Continued

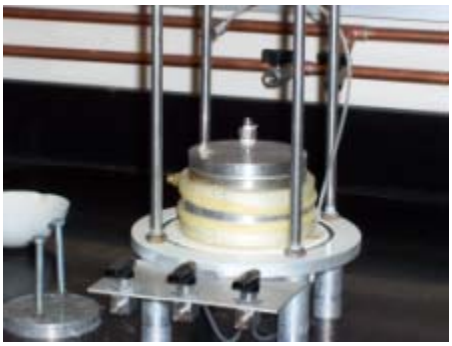

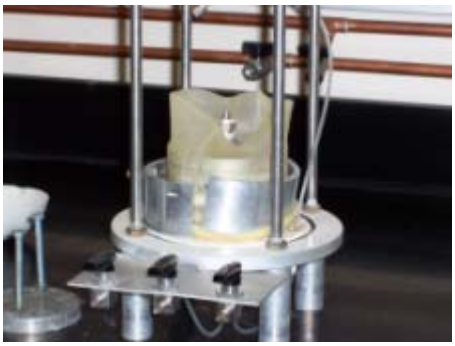

(f) Sample Preparation – (Step 6)

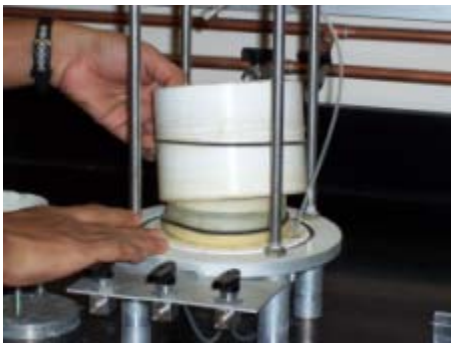

(g) Sample Preparation – (Step 7)

(h) Sample Preparation – (Step 8)

(i) Sample Preparation – (Step 9)

Figure 5.4 Continued

5.1.2.3 Sample Saturation

Back pressure saturation is used as outlined in ASTM D5084 to ensure full saturation. Both influent and effluent chambers are filled up to the same level so that the same pressure head can be maintained during saturation of the specimen. The permeameter cell is also filled with tap water through which the confining pressure is applied to the specimen. All the pressure regulators connected with the chambers and permeameter cell, are turned to zero pressure before opening any controlling valves of the chambers and cell. All the vent valves are closed and the valves that control flow through the specimen are opened so that the water can flow into the specimen and the air bubbles can be flushed out of the specimen. Air pressure is first applied to the permeameter cell so that the cell water can develop an initial confining pressure of about 20 to 35 kPa (3 to 5 psi). Air bubbles will squeeze out of the specimen to the connecting chambers due to this initial confining pressure. Influent and effluent chambers are connected through a bridge on the pressure panel so that the same pressure is applied to both chambers through a single regulator. Air pressure is applied to the chambers as well as to the permeameter cell gradually so as to maintain a pressure difference of 20 to 35 kPa (3 to 5 psi) between the confining pressure and chamber pressures at all times.

It is imperative that the pressure head in both influent and effluent chambers are the same during saturation, so that no flow occurs from one chamber to the other. To achieve this, the same air pressure regulator is used to apply pressure to both chambers through a bridge connection in the pressure panel as mentioned earlier. The pressure in the cells is raised gradually up to 415 kPa (60 psi) and is kept 20 to 35 kPa (3 to 5 psi) below that of the permeameter chamber during the whole period of saturation. A similar backpressure was used by Boynton and Daniel (1985) in flexible wall permeability tests. Backpressure applied to the specimen through the top and bottom platens, is not allowed to surpass the confining chamber pressure to prevent bulging of the specimen. This process of saturation by backpressure was continued for at least 5-7 days to completely dissolve air or gaseous substances from the test specimen and to complete any chemical

primary reaction that might occur with water and chemical compounds present on the surface of the bentonite clay materials.

It is worth noting that removal of air bubbles and gaseous substances from the test specimens by flowing water from one end to the other is not advisable because various dissolved substances will leach out of the specimen with the water flow during saturation. Maximum saturation of the specimen is considered to be accomplished when no significant drop of influent and effluent water levels was observed over a period of 2 to 3 hours.

5.1.2.4 Permeation Phase

Selection of the appropriate hydraulic gradient is of great importance in determining the suitability of flow rate so that no cracks or channels develop through the specimen during the experiment. Variation of the measured coefficient of hydraulic conductivity with hydraulic gradients in excess of 100 was found to be insignificant for clay by Shackelford et al. (2000). Hydraulic gradients in the range of 25 to 100 had also been used by many researchers (Boynton and Daniel, 1985; Jo *et al*., 2001; Stern and Shackelford, 1998; Shackelford and Redmond, 1995; Lin and Benson, 2000;) for clay and sand mix samples. Higher hydraulic gradients in the range of 100 to 600 have also been used for measuring hydraulic conductivity of the clay component of geosynthetic liners (Day and Daniel, 1985; Fernandez and Quigley, 1985; Shackelford, 1994; Petrov *et a*l., 1997; Petrov and Rowe, 1997; Ruhl and Daniel, 1997; Daniel, 1993). Rad *et al*., (1994) used hydraulic gradients as high as 2800 and found that the hydraulic conductivity of GCL was not affected when water is used as permeant. In order to investigate the effects of hydraulic conductivity on bentonite samples, various hydraulic gradients from 250 to 3500 were used in this research study with various inorganic solutions as permeants. The results are presented later.

The effluent cell pressure was reduced from its applied backpressure of 415 kPa (60 psi) during saturation to the required pressure level to develop the pre-calculated

hydraulic gradients. Since the hydraulic gradient also depends on the difference in levels between influent and effluent in addition to the applied regulated pressure, the fluctuation of the actual hydraulic gradient has been accounted for in the calculations. The constant pressure difference of 20 kPa (3.0 psi) between influent and permeameter cell was maintained until the completion of the experiment in order to avoid piping and specimen collapse.

5.1.2.5 Termination Criteria

Since the test set-up represents falling head conditions with increasing tailwater elevation, Eq. 5.5 is again used here to calculate the coefficient of permeability, *k*. Permeation through the bentonite specimen was continued until at least four consecutive values of hydraulic conductivity were obtained over an interval of time (24-hour) in which: (1) the ratio of outflow to inflow rate is between 0.75 and 1.25, and (2) the values of hydraulic conductivity (coefficient of permeability) are steady within ±50% of each other.

Besides the above standard criteria for termination of permeation in permeability tests, electrical conductivity of the effluent was measured until its value exceeded 90% of the influent before termination. This is one way of ensuring that a chemical steady state has been reached before the test is stopped. The coefficient of permeability, and the pH and electrical conductivity of the effluent were plotted with respect to the pore volume of the specimen. A pore volume is defined as the volume of void space in the permeated medium. In these experiments, it represents the total volume of voids available for the leachate to flow through the specimen. The pore volume, V_p, is calculated from the following Equation:

$$V_p = w_c \frac{W_s}{\gamma_w} \qquad (5.2)$$

where w_c is the sample's water content at the end of the test, W_s is the weight of the dry sample, and γ_w is the unit weight of water. In order to allow interactions between

permeant and porous medium to take place, at least one pore volume should be allowed to pass through (Joshi *et al*., 1994).

Termination of the permeability test was carried out by gradually and simultaneously lowering the applied air pressure in the influent, effluent and permeameter cell to zero. Cell pressure was always kept higher than chamber pressure so that the confining rubber membrane does not separate from the specimen surface. Water was then forced out of the cell by slightly increasing the confining pressure through the base opening valve.

After achieving the termination criteria, the specimens were carefully taken out of the permeameter in such a way so as to preserve their structural integrity for further determination of void ratio, physical shape, and size.

5.1.3 Rigid Wall Permeability

Rigid wall permeability experiments were carried out using the diffusion cells described in Chapter 4. The sample preparation was the same as for the diffusion tests, which are described in Chapter 6. Like flexible wall permeability, the effluent (tailwater) level increases with time during the tests and the modified ASTM equation is used in the calculation (equation 5.1). A schematic diagram is shown in figure 5.5 to describe all the terms of equation (5.1).

5.1.3.1 Sample Preparation

Sample preparation steps are the same as those of diffusion tests as described in Chapter 6. After accomplishing a pre-determined thickness of the clay sample due to consolidation, the water from the effluent tube and influent permeameter cell is replaced with deionized water or required permeants. The piston inside the permeameter used during consolidation was kept during the permeability test in order to maintain a constant

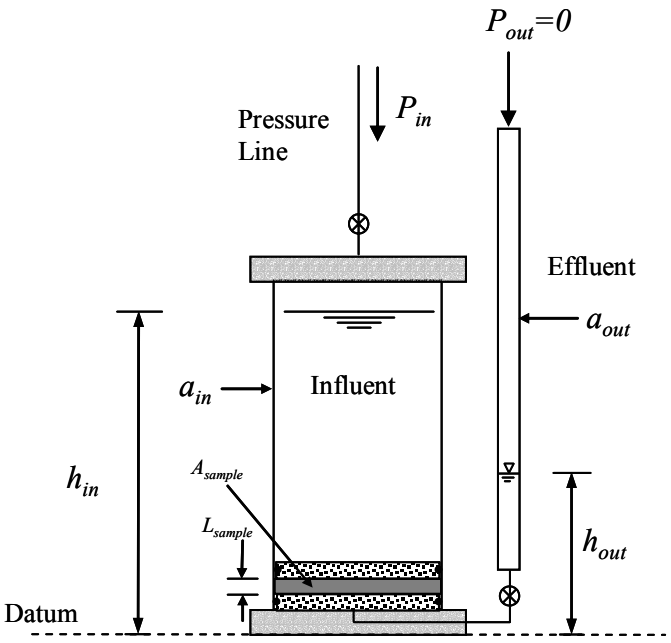

Rigid Wall Permeability Cell

Figure 5.5 Schematic Diagram of Rigid Wall Permeameter Set-up

thickness of the sample. To prevent leakage of influent and compressed air from the bottom and top of the permeameter cell respectively, a sufficient amount of silicon grease was applied on both ends of the plexiglass cylinder of the permeameter cell as well as on the protruded portions of the O-rings placed on both end plates.

5.1.3.2 Permeation Phase

After completion of sample preparation, the cell influent and pipette tube are filled, and the permeameter is shifted to the pressure panel where the influent is subjected to compressed air pressure supplied from the pressure panel. The effluent pipette tube is left open under atmospheric pressure (gauge pressure, $P_{out} = 0$). Lower hydraulic gradients (compared to flexible wall), in the range of 200 to 500, are applied so that the

effluent can be collected without spilling from the pipette within a reasonable time interval.

Termination criteria for the rigid wall permeability are the same as those for flexible wall, except that the test needs to be interrupted should it be necessary to replenish the influent cell before chemical and steady-state flow are achieved. The effluent sample is collected from the pipette at any desired time interval for further analysis for chemical equilibrium in terms of electrical conductivity and pH. The collected sample needs to be diluted for chemical analysis if the amount of effluent collected is insufficient due to slow permeation through bentonite samples.

5.1.4 Factors Affecting Hydraulic Conductivity

Hydraulic conductivity of sodium montmorillonite has been found to be the lowest among most of the clays followed by calcium montmorillonite or other divalent cation montmorillonites as investigated by many researchers (Benson *et al*., 1994; Mitchell, 1976; Lambe, 1953). The various factors that are investigated in this research work are permeant chemical composition, void ratio, hydraulic gradient, first wetting liquid, and boundary conditions.

5.1.4.1 Permeant Chemical Composition

The permeant chemical solution is one of the most important factors affecting permeability of bentonite due to its interaction with the negatively charged clay mineral surfaces, which is responsible for the diffuse double layer variation of bentonite particles. Table 5.1 shows the synthetic chemical solutions with their molarity used in the hydraulic conductivity experiments using flexible wall permeameters. Tests K-1 to K-8 were carried out using single salt solutions while K-9 to K-14 were conducted using multiple solutions in a sequential permeation fashion. Permeability test results for single salt

solutions are shown in figure 5.6 and 5.7 as a function of duration and pore volume, respectively.

Table 5.1 Chemical Solutions Used in Hydraulic Conductivity Using Flexible Wall Permeameter

Test number	Pre-hydration	1st solution	2nd solution	3rd solution
K-1	DI water	1M $CaCl_2$	-	-
K-2	DI water	1M $MgCl_2$	-	-
K-3	DI water	1M KCl	-	
K-4	DI water	1M NaCl	-	-
K-5	DI water	All salts (1M each)	-	-
K-6	DI water	All salts (0.1M each)	-	-
K-7	DI water	All salts (0.01M each)	-	-
K-8	DI water	5M $CaCl_2$	-	-
K-9	1M $CaCl_2$	1M $CaCl_2$	1M NaCl	-
K-10	1M NaCl	1M NaCl	1M $CaCl_2$	-
K-11	DI water	DI water	All salts (0.01M each)	All salts (0.1M each)
K-12	1M $MgCl_2$	1M $MgCl_2$	1M KCl	-
K-13	1M KCl	1M KCl	1M $MgCl_2$	-
K-14	DI water	1M $CaCl_2$	1M $MgCl_2$	-

Note: All salts means NaCl, KCl, $CaCl_2$ and $MgCl_2$

K-11 was also tested for all salts of 1M each solutions following 0.1M solution.

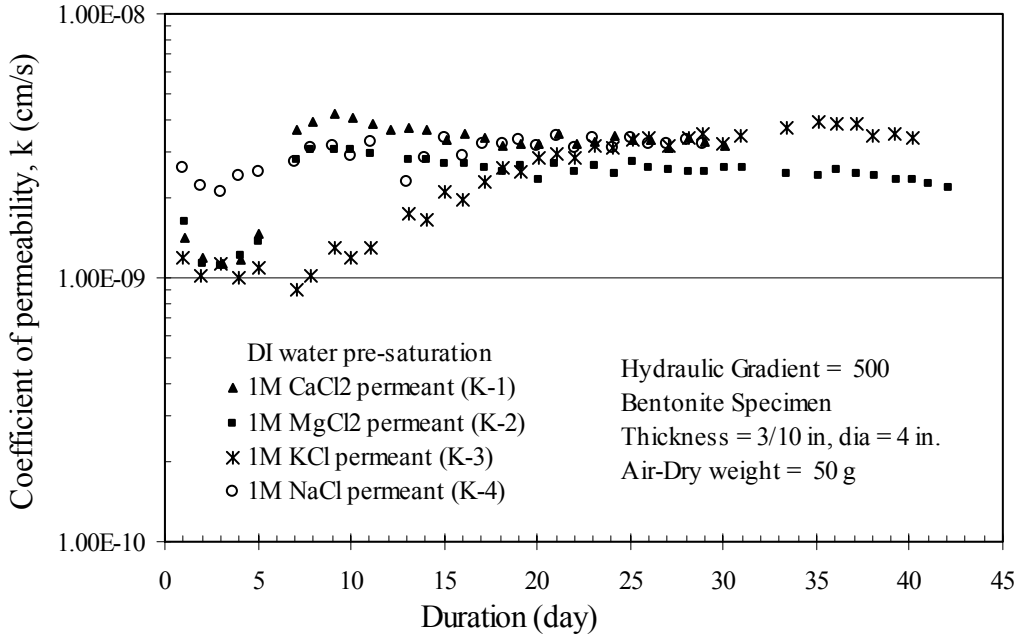

Figure 5.6 Permeability vs. Duration for 1M Salt Solutions Using Flexible Wall Permeameter

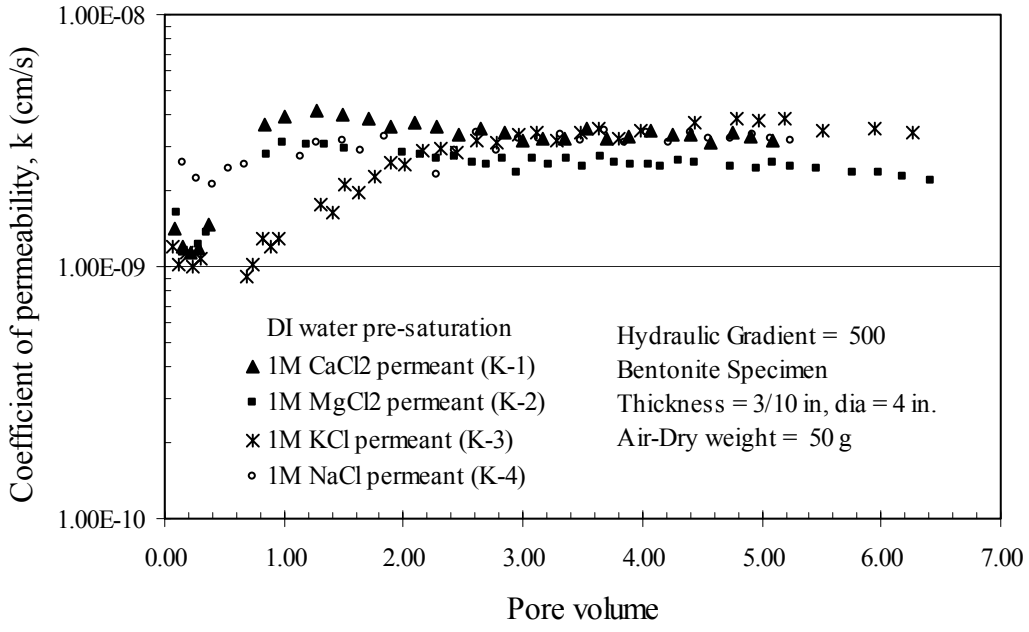

Figure 5.7 Permeability vs. Pore Volume for 1M Salt Solutions Using Flexible Wall Permeameter

It can be seen from figures 5.6 and 5.7, that the variation of steady-state coefficients of permeability (from $2.4x10^{-9}$ cm/s to $3.5x10^{-9}$ cm/s) is not that significant among those four different salt solutions. However, an increase in permeability can be observed initially for $CaCl_2$, $MgCl_2$ and KCl permeants, which could be the results of initial exchange of bentonite surface exchangeable cations. It can also be found that the final stable values of coefficient of permeability are achieved after at most two pore volumes of permeants of all four types of salt solutions.

Permeability test results for experiments K-5, K-6, and K-7 are shown in figures 5.8 and 5.9 with respect to duration and pore volume, respectively. Test K-7, where 0.01 molar of each salt was used as permeant, shows the minimum coefficient of permeability ($k = 1.0x10^{-9}$ cm/s). The variation of permeability with respect to molar concentration of all salts (K-5, K-6, and K-7) permeants is shown in figure 5.8 where a trend of increasing permeability is observed with increasing molarity of the permeants.

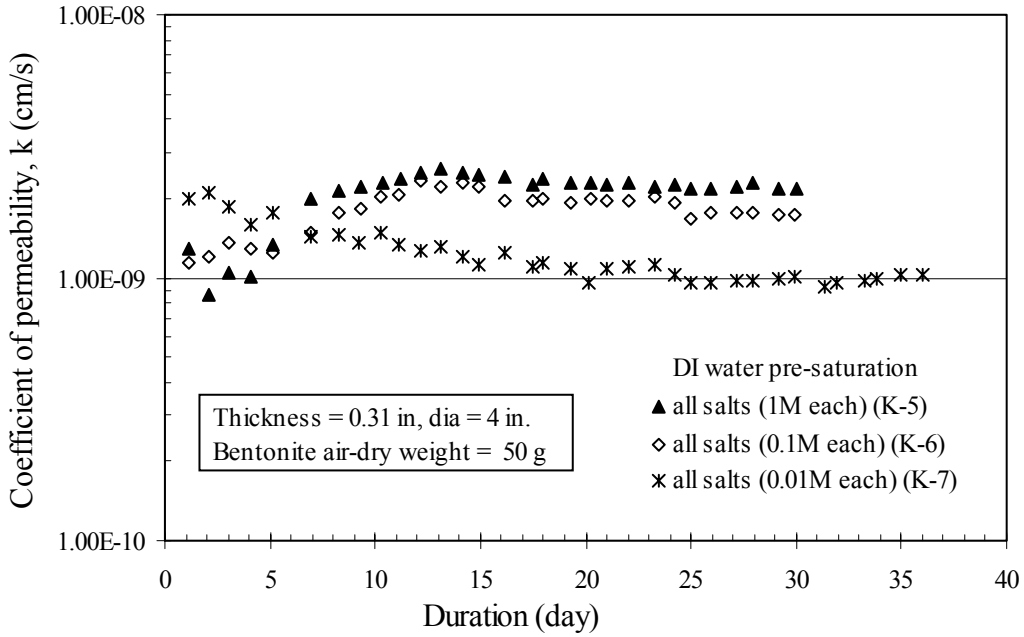

Figure 5.8 Permeability vs. Duration for All Salt Solutions (K-5, K-6, & K-7)

Regardless of applied hydraulic gradient, the final permeability of bentonite clay using various combinations of salt solutions can be achieved after at most two pore

volumes of permeant through the specimens, as shown in figure 5.9. No further variation of permeability is observed until termination at around 9 pore volumes, which lasted for 35 days (figure 5.8)

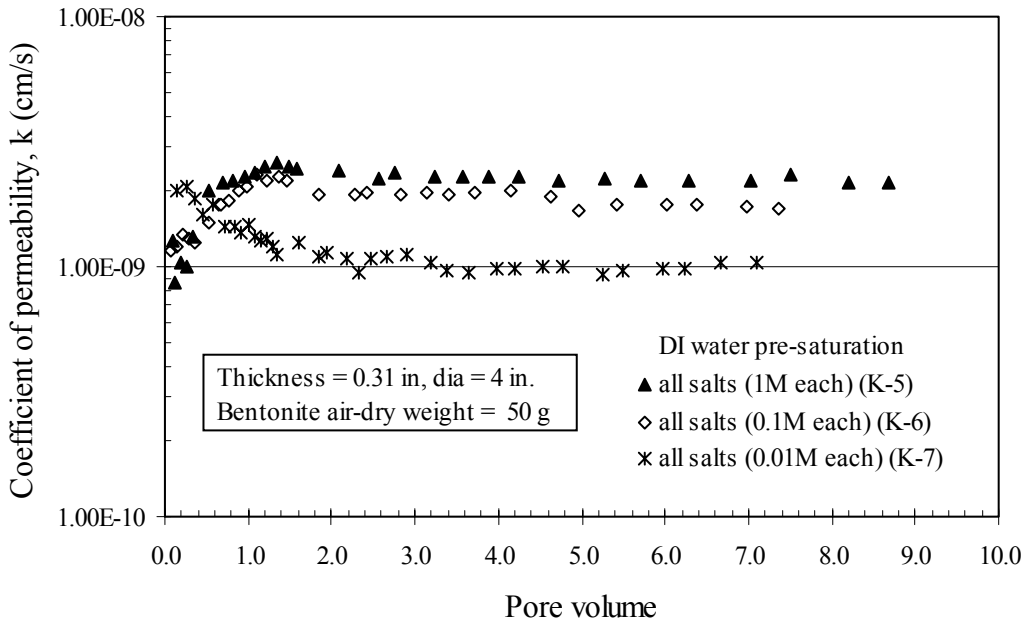

Figure 5.9 Permeability vs. Pore Volume for All Salt Solutions (K-5, K-6, & K-7)

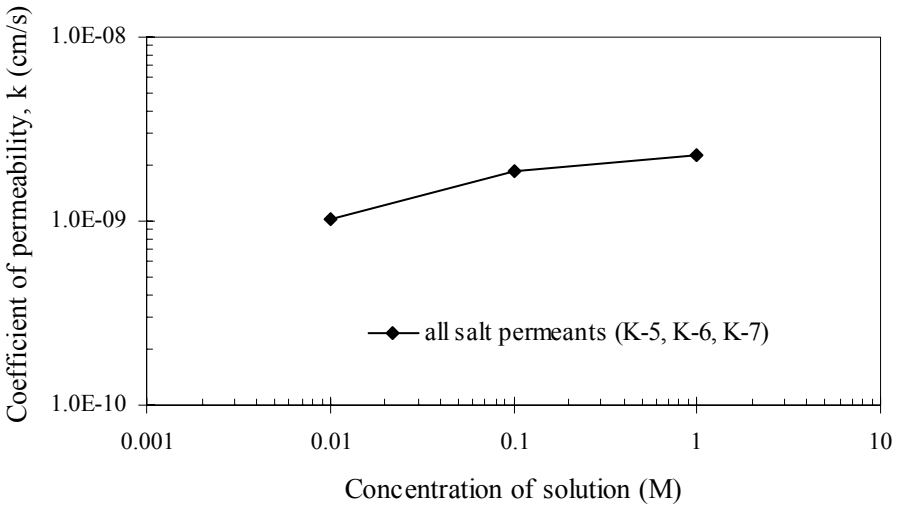

Figure 5.10 Variation of Permeability with Molarity of Combined Salt Solutions

5.1.4.2 Void Ratio

In order to investigate the effect of void ratio of bentonite specimens on permeability using various synthetic chemical solutions, rigid wall permeability tests were carried out with various amounts of air-dry bentonite clay. Table 5.2 lists the tests that were conducted in the laboratory in order to identify the effects of void ratio on $CaCl_2$ and NaCl salt solution permeants.

Table 5.2 Rigid Wall Permeability Tests with Void Ratio Variation

Permeant chemical solution	Test No.	Sample Size (diameter x thickness)	Air-dry sample weight (g)	Void ratio (e)	Coefficient of permeability (k, cm/s)
1M $CaCl_2$	KD-6	76.2 mm x 7 mm	30	1.98	1.26×10^{-9}
	KD-7	76.2 mm x 7 mm	15	4.97	5.84×10^{-9}
	KD-8	76.2 mm x 3 mm	2.5	14.35	6.44×10^{-8}
1M NaCl	KD-5	76.2 mm x 7 mm	30	1.98	6.0×10^{-10}
	KD-9	76.2 mm x 7.84 mm	15	5.69	1.82×10^{-9}
	KD-10	76.2 mm x 7 mm	7.5	10.94	1.55×10^{-8}

Experimental test results of KD-6, KD-7, and KD-8 for 1M $CaCl_2$ permeant are presented in figures 5.11 and 5.12 in terms of duration and pore volume, respectively, while those of KD-5, KD-9, and KD-10 for 1M NaCl permeant are presented in figures 5.13 and 5.14. It can be seen from figure 5.11 that the permeability increases slightly as the test proceeds for 1M $CaCl_2$ permeant, which could be due to the cationic exchange process that results in aggregation of clay particles in higher void ratio specimens. No increase in permeability can be observed for more compacted (i.e. lower void ratio) specimen shown in figure 5.12.

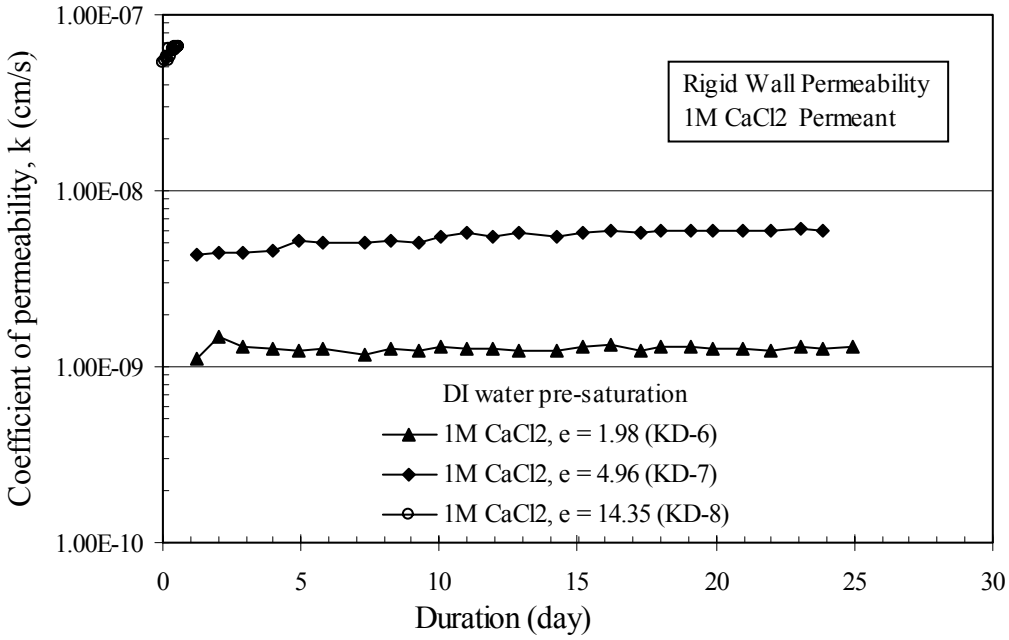

Figure 5.11 Variation of Permeability with Duration of 1M $CaCl_2$ Permeant Used in Bentonite of Various Void Ratios

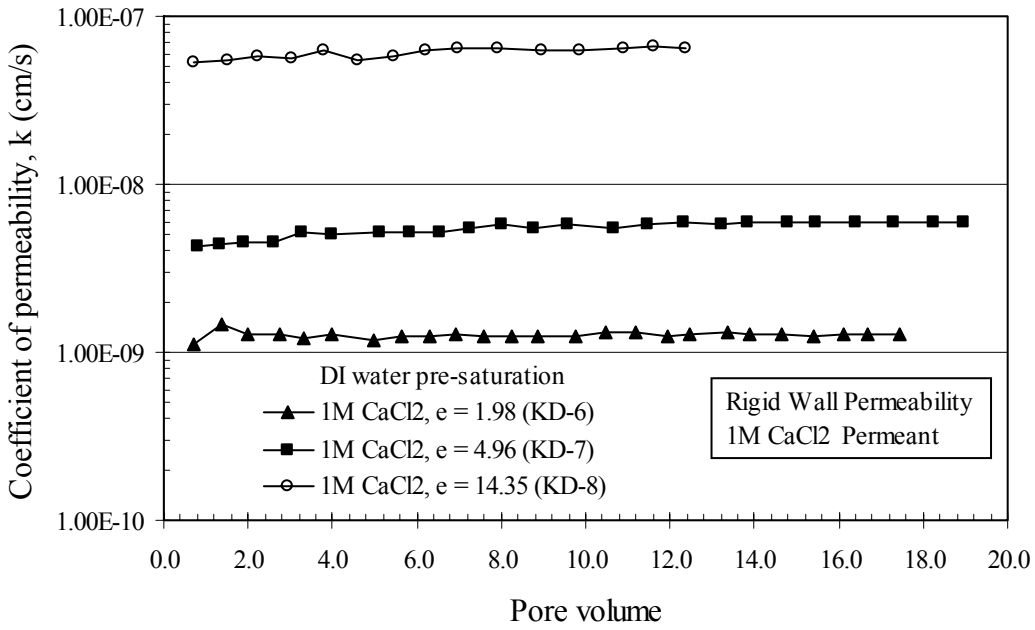

Figure 5.12 Variation of Permeability with Pore Volume of 1M $CaCl_2$ Permeant Used in Bentonite of Various Void Ratios

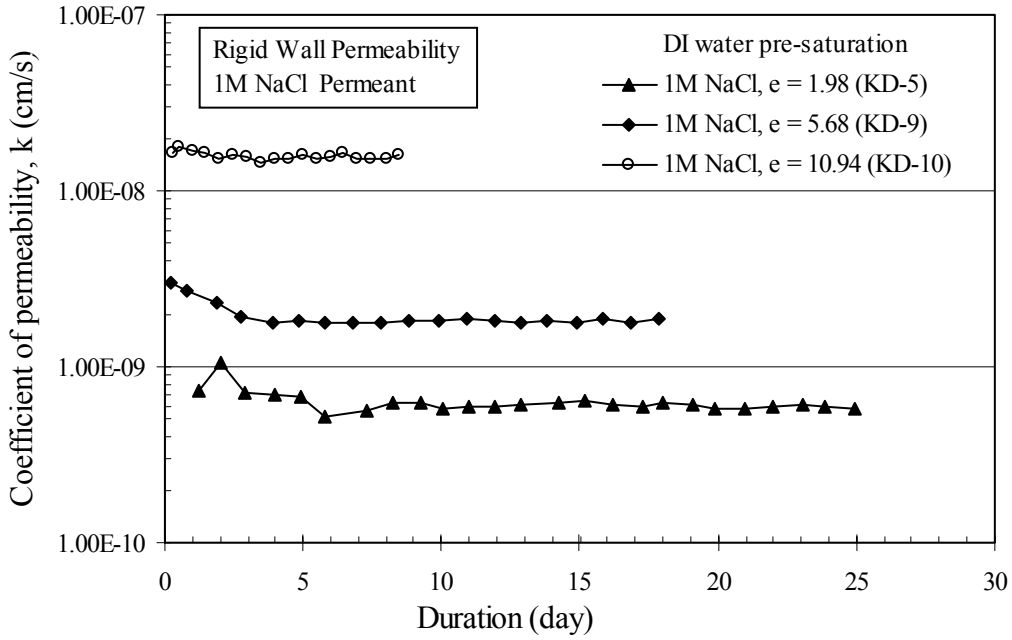

Figure 5.13 Variation of Permeability with Duration of 1M NaCl Permeant Used in Bentonite of Various Void Ratios

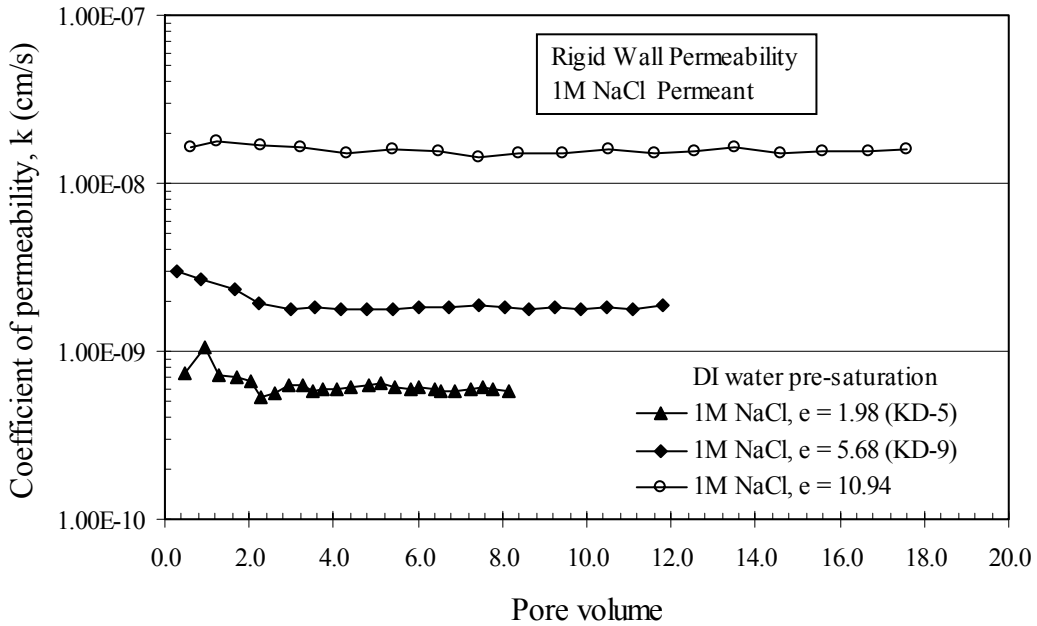

Figure 5.14 Variation of Permeability with Pore Volume of 1M NaCl Permeant Used in Bentonite of Various Void Ratios

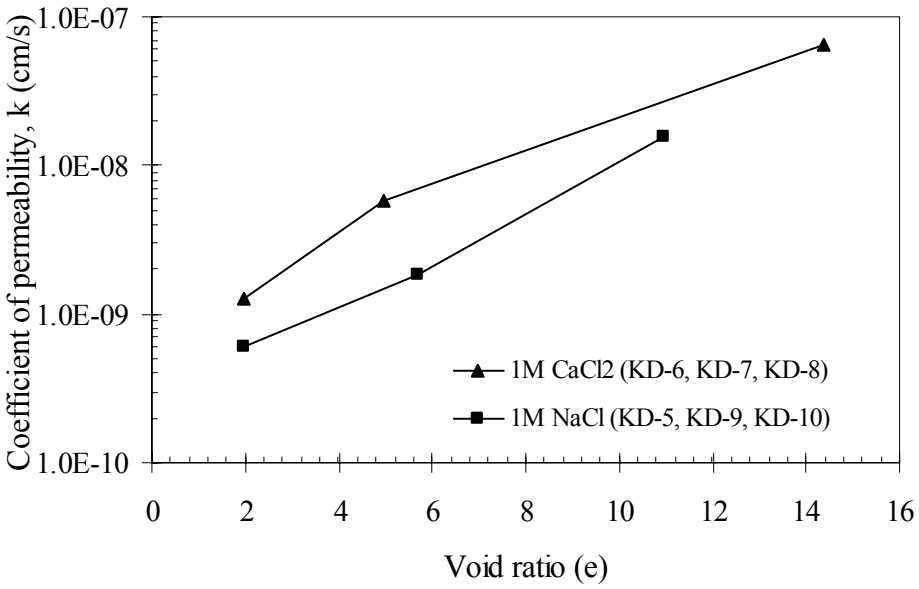

Figure 5.15 Variation of Permeability with Void Ratio for 1M $CaCl_2$ and 1M NaCl Permeants

It is clearly revealed from figure 5.15 that the permeability of bentonite clay increases with increasing void ratios with both permeants of one molar $CaCl_2$ and NaCl salt solutions. The permeability is higher at higher void ratio simply due to the fact that the amount of higher pore volume and space of flow exist in higher void ratio specimens. As divalent cations like calcium Ca^{2+} replace monovalent negatively charged ions like sodium Na^{+}, potassium K^{+}, and others during flow, the diffuse double layer thickness between clay platelets is reduced. Shrinkage of the clay specimens occurs, which causes higher flow of solution during permeability as shown in figure 5.15.

5.1.4.3 Hydraulic Gradient

A combination of salt solutions was used in flexible wall permeability tests (K-5, K-6, and K-7) in order to find the effects of hydraulic gradient on permeability of chemical solution permeants through bentonite clay materials. Hydraulic gradients from

450 to 3115 were applied for this investigation. Table 5.3 shows the coefficient of permeability with respect to the applied hydraulic gradient on various test specimens.

Table 5.3 Flexible Wall Permeability Tests with Hydraulic Gradient Variation

Sample No. & permeant	Hydraulic gradient (i)	Coefficient of permeability (k, cm/s)
K-5 (all salts, 1M each)	450	2.52×10^{-9}
	1320	2.27×10^{-9}
	2190	2.22×10^{-9}
K-6 (all salts, 0.1M each)	445	2.27×10^{-9}
	1310	1.98×10^{-9}
	2165	1.76×10^{-9}
K-7 (all salts, 0.01M each)	455	1.21×10^{-9}
	1335	1.09×10^{-9}
	2230	9.93×10^{-10}
	3115	1.01×10^{-9}

It can be seen from the permeability results listed in Table 5.3 that the coefficient of permeability decreases slightly within the range of 10% to 25% due to 5 to 6 fold increase in hydraulic gradient. The reduction in permeability could be attributed to the effect of clay consolidation at higher seepage forces during permeability experiments. However, the higher applied hydraulic gradient would cause the permeant to flow at a much higher rate, which expedites chemical equilibrium. Chemical equilibrium is required in order to obtain a stable and constant value of k for low permeability clays.

Although ASTM D 5084 recommends a maximum gradient of 30 for fine grained soils of low hydraulic conductivity (k less than 10^{-7} cm/s), higher hydraulic gradient in the range of 50 to 600 are commonly used for measuring hydraulic conductivity of the clay component of geosynthetic liners (Daniel, 1994; Pertrov and Rowe, 1997; Petrov and Rowe, 1997; Petrov *et al*., 1997; Ruhl and Daniel, 1997; Lin, 1998). A high

hydraulic gradient of 2800 was used by Rad *et al*., (1994), for GCL clays using tap water permeant where the k value was found to be insensitive to variations in applied gradients.

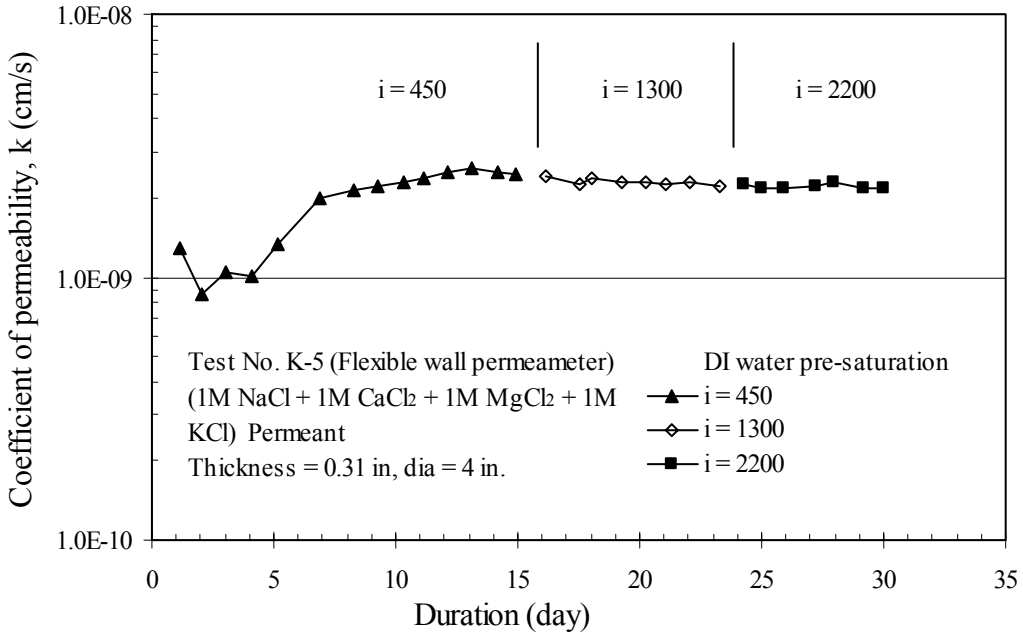

Figure 5.16 Variation of Permeability with Duration of Flow for K-5

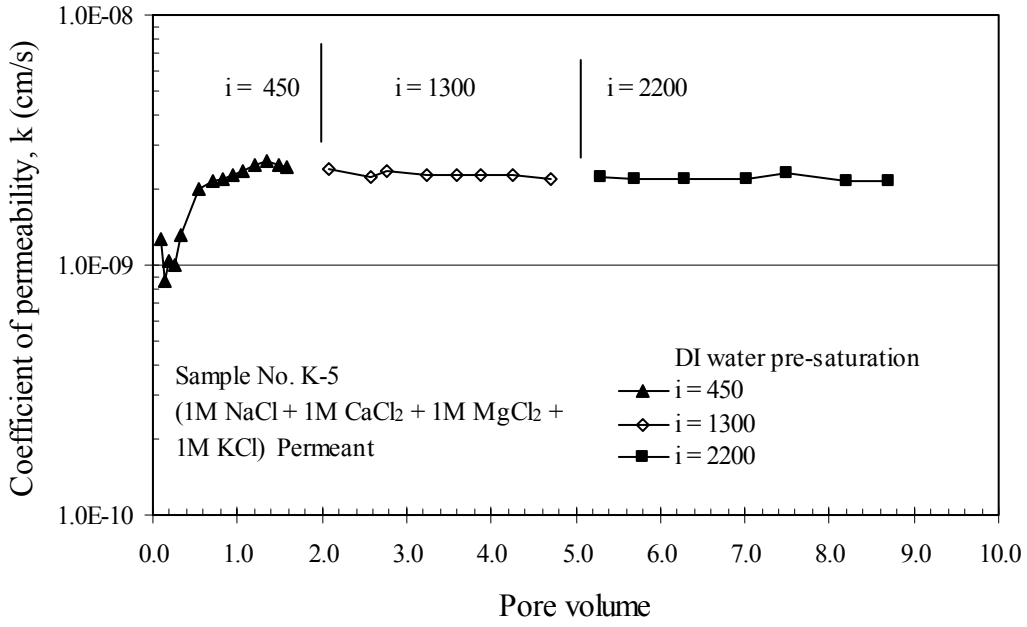

Figure 5.17 Variation of Permeability with Pore Volume of Flow for K-5

Results of the permeability experiments using flexible wall permeameter for K-5, K-6, and K-7 are given in figures 5.16 to 5.21. DI water was used during pre-hydration of the test specimens by applying back pressure.

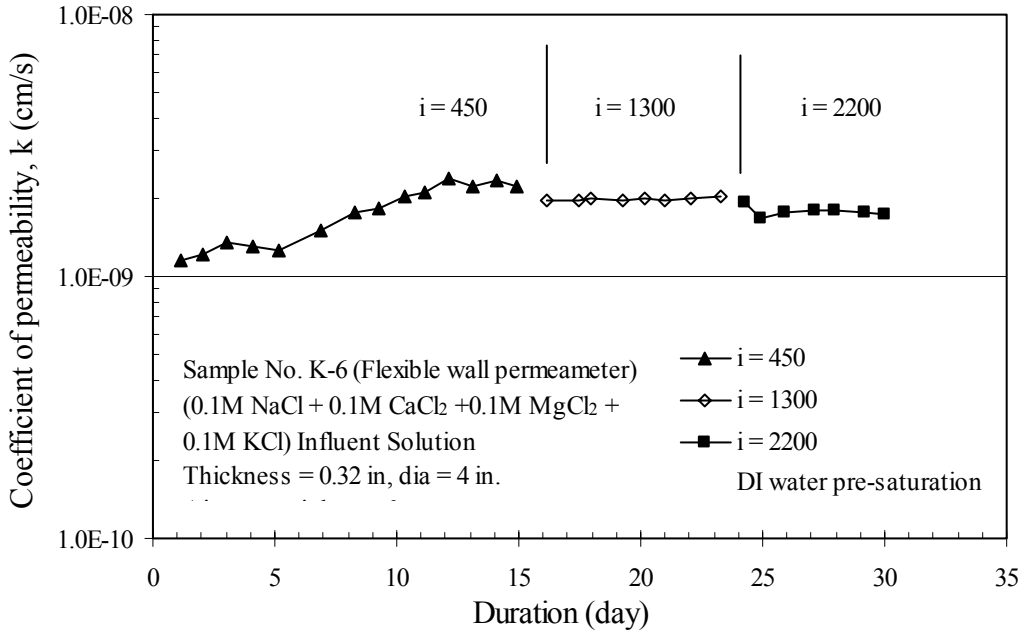

Figure 5.18 Variation of Permeability with Duration of Flow for K-6

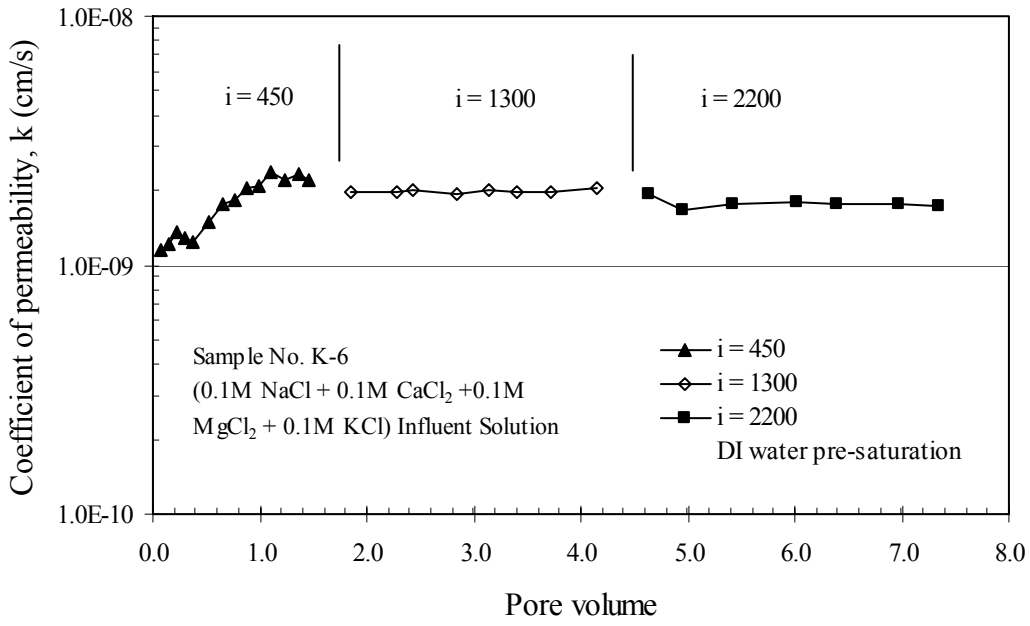

Figure 5.19 Variation of Permeability with Pore Volume of Flow for K-6

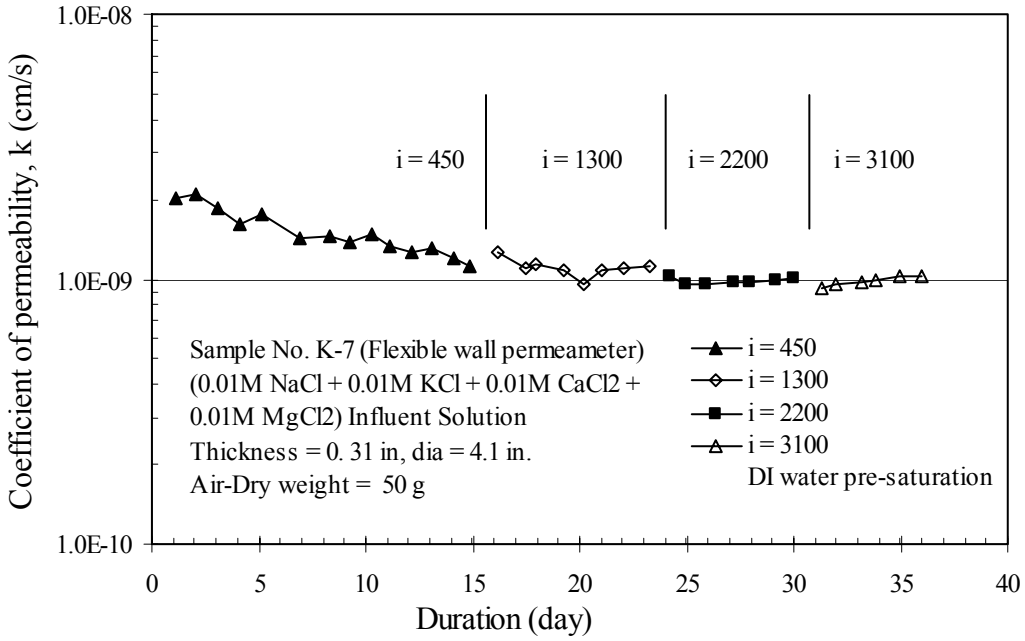

Figure 5.20 Variation of Permeability with Duration of Flow for K-7

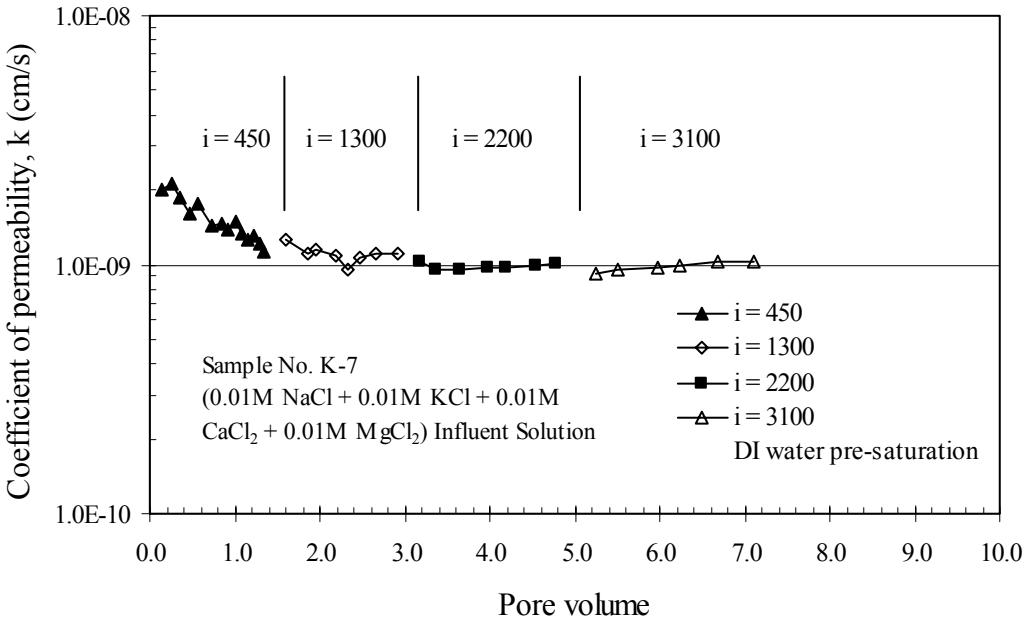

Figure 5.21 Variation of Permeability with Pore Volume of Flow for K-7

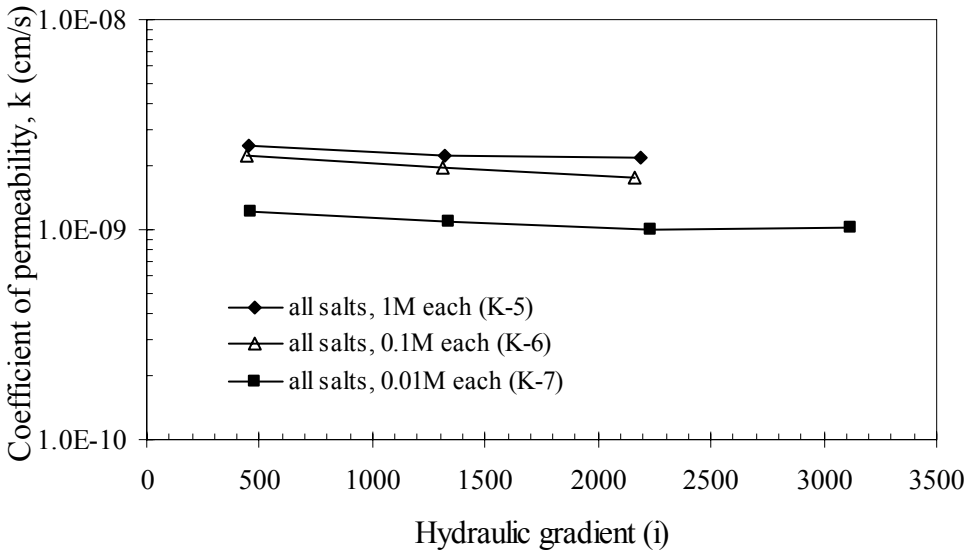

Figure 5.22 Variation of k with Applied Hydraulic Gradient in Combined Salt Solutions

The reduction in permeability is found to be minimal even at an applied hydraulic gradient of around 2000 for the combined salt permeants, as shown in figure 5.22.

5.1.4.4 Pre-hydration

Four pairs of tests are compared to find the effects of pre-hydration on the permeability of bentonite clay as listed in Table 5.4. The same salt solutions applied as permeants are also used as hydration liquid and the "k" test results are compared with those of deionized (DI) water pre-hydrated values.

$CaCl_2$ hydrated clay (K-9) is found to develop a higher k value compared to DI water pre-hydrated clay (K-1), as shown in Table 5.4 and figure 5.23. Structured aggregate particles are assumed to be formed during the process of hydration by $CaCl_2$ solution, which contributes to the higher permeability due to shrinkage of the diffuse double layer and higher pore openings of flow. Hydration by other chemical solutions does not seem to be effective in reorganizing and reorienting the clay platelets, rather

forming more dispersed structure of clay particles and thus reducing the flow of chemical solutions.

Table 5.4 Flexible Wall Permeability Tests with Various Hydration Solutions

Permeant	Sample No.	Pre-hydration	Coefficient of permeability, k (cm/s)
1M $CaCl_2$	K-1	DI water	$3.23x10^{-9}$
	K-9	1M $CaCl_2$	$5.93x10^{-9}$
1M NaCl	K-4	DI water	$3.22x10^{-9}$
	K-10	1M NaCl	$1.43x10^{-9}$
1M KCl	K-3	DI water	$3.55x10^{-9}$
	K-13	1M KCl	$1.55x10^{-9}$
1M $MgCl_2$	K-2	DI water	$2.30x10^{-9}$
	K-12	1M $MgCl_2$	$1.95x10^{-9}$

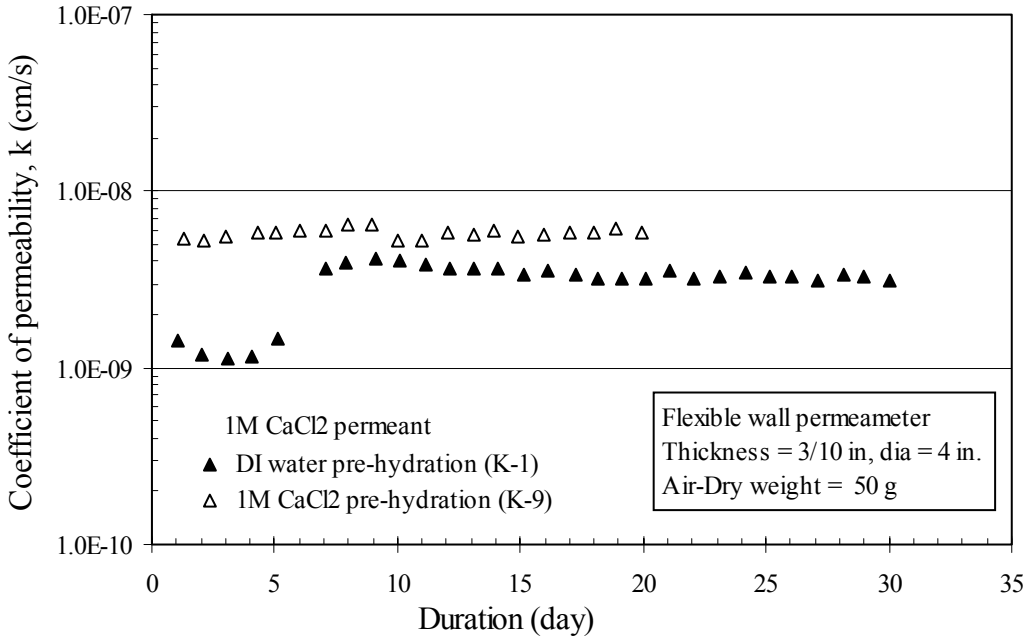

Figure 5.23 Variation of Permeability with Duration of Flow for K-1 & K-9

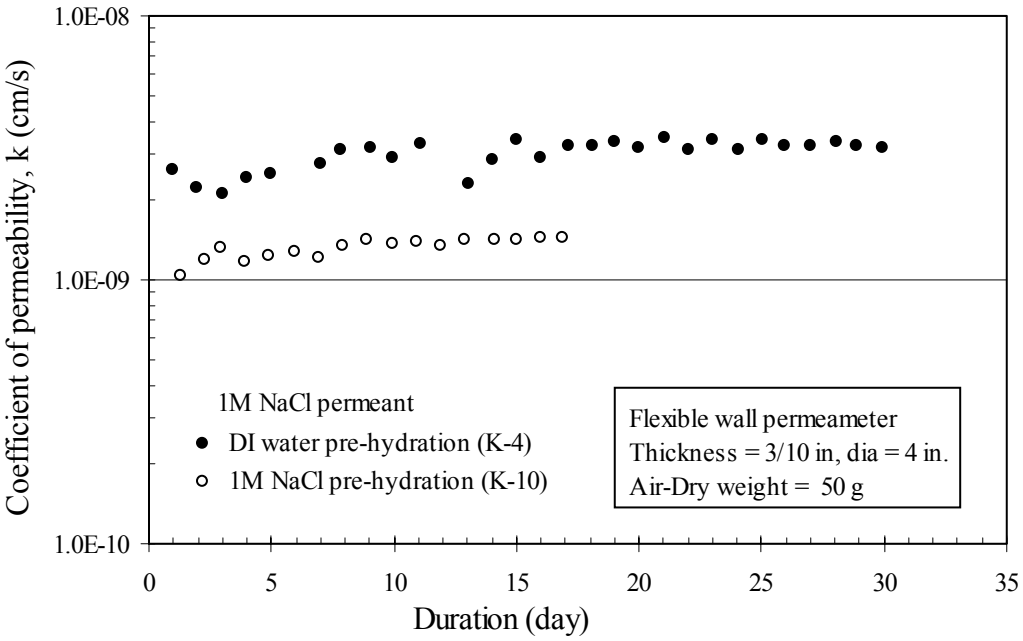

Figure 5.24 Variation of Permeability with Duration of Flow for K-4 & K-10

Permeability test results for 1M NaCl, 1M KCl, and 1M $MgCl_2$ permeants under two different hydration conditions are given in figures 5.23 to 5.26

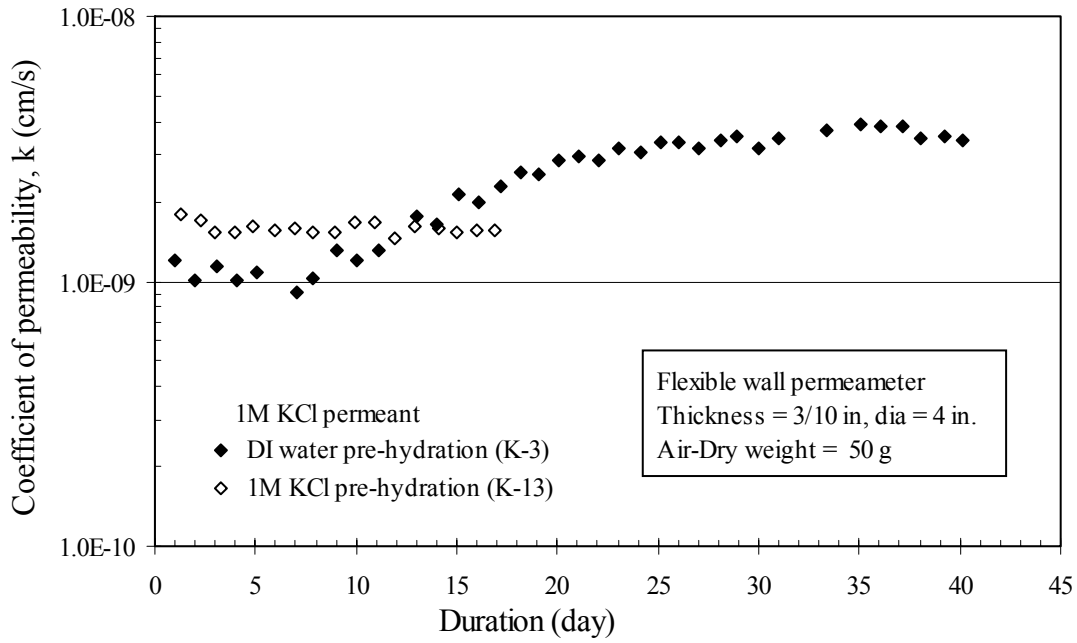

Figure 5.25 Variation of Permeability with Duration of Flow for K-3 & K-13

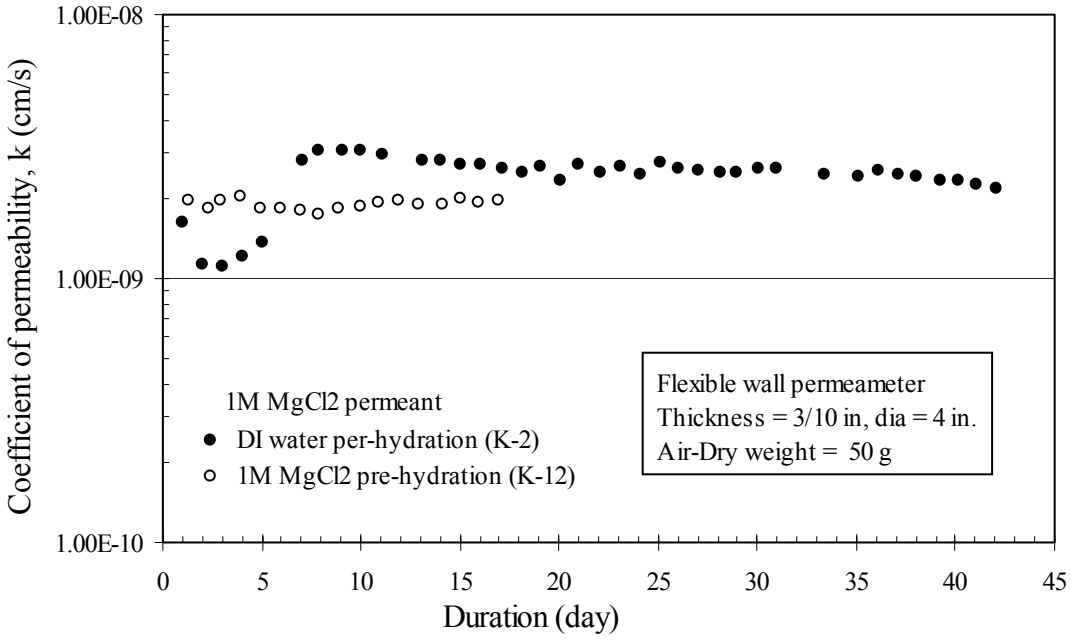

Figure 5.26 Variation of Permeability with Duration of Flow for K-2 & K-12

5.1.4.5 Type of Permeameter

Two types of permeameters, namely, flexible wall and rigid wall, are compared in terms of their performance in achieving the least permeability coefficient values for chemical solution permeation through bentonite clay specimens. Four pairs of tests are compared with the same type of compacted bentonite clay samples (i.e. having same void ratios) under the same pre-hydration conditions (using DI water) and back pressure saturation, as listed in Table 5.5. Two divalent (Ca^{2+} and Mg^{2+}), one monovalent (Na^{+}) cationic salt solutions and DI water were used as permeants in this investigation.

It is clearly found from the test results given in Table 5.5 that the 'k' values due to all types of permeants are lower in rigid wall permeameters than in flexible wall permeameters. During the process of pre-hydration in rigid wall permeameters, bentonite clay particles tend to expand as a result of osmosis pressure due to adsorption but are restrained due to the boundary surfaces of rigid wall and fixed porous plates on both ends

of the specimen. The sides of clay specimen form a seal against the rigid walls and thus prevent development of any side wall leakage, which is quite prevalent in non-expansive clay soils.

Table 5.5 Permeability Tests Using Flexible Wall and Rigid Wall Permeameters

Permeant (DI pre-saturated)	Sample No.	Permeameter type	Coefficient of permeability, k (cm/s)
DI water	K-11	Flexible wall	7.98×10^{-10}
	KD-1	Rigid wall	4.96×10^{-10}
1M $CaCl_2$	K-1	Flexible wall	3.25×10^{-9}
	KD-6	Rigid wall	1.26×10^{-9}
1M $MgCl_2$	K-2	Flexible wall	2.33×10^{-9}
	KD-4	Rigid wall	7.96×10^{-10}
1M NaCl	K-4	Flexible wall	3.22×10^{-9}
	KD-5	Rigid wall	5.94×10^{-10}

In rigid wall permeameters, the void ratio and the physical dimensions of the specimens can be maintained constant as the porous plates are restrained at pre-determined levels, thereby making the permeability calculation less erroneous. The only two disadvantages associated with rigid wall permeameters are that (1) the influent cannot be replenished with the same permeant or replaced with other permeants during progress of permeability tests without disrupting the flow and (2) the influent cannot be collected intermittently for further chemical analysis while the test is in progress.

Four pairs of permeability test results as listed in Table 5.5 and are given in figures 5.27 to 5.30.

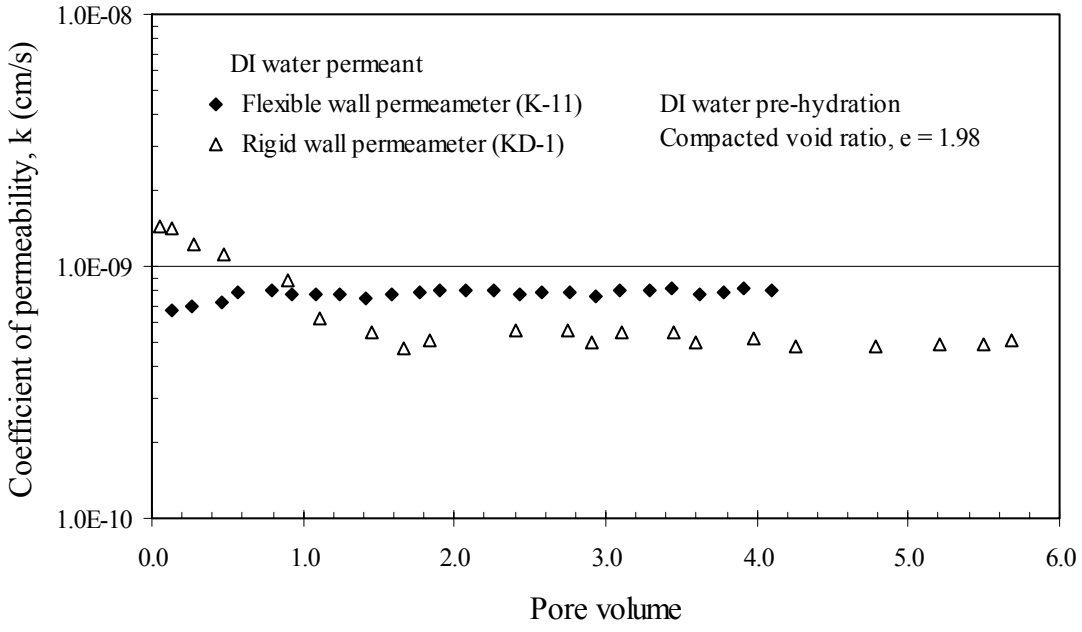

Figure 5.27 Comparison of Permeameters for DI Water Permeant (K-11 & KD-1)

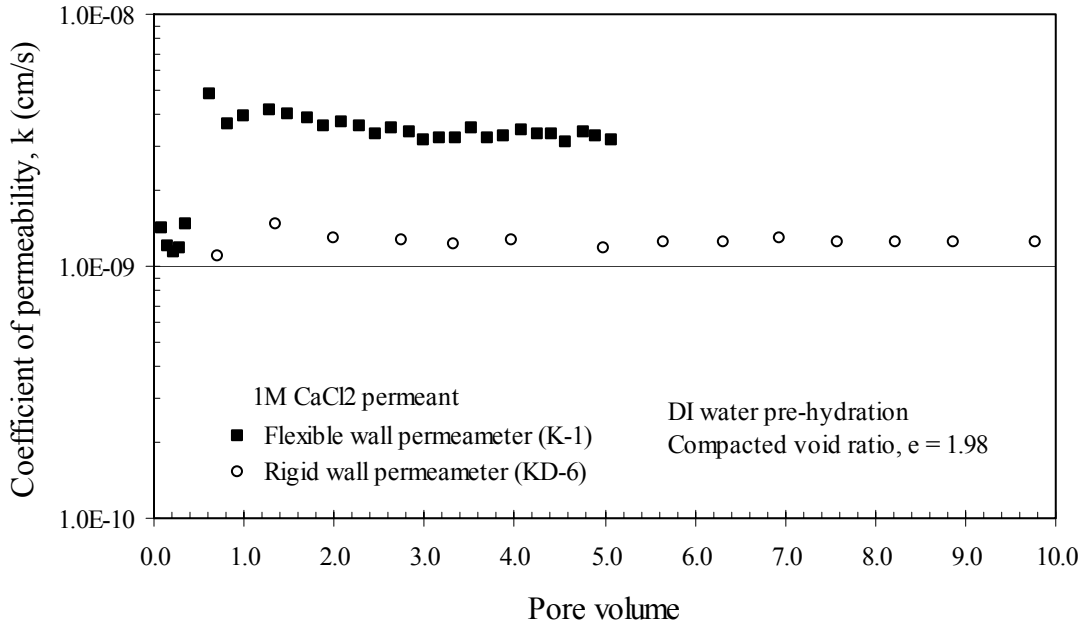

Figure 5.28 Comparison of Permeameters for 1M $CaCl_2$ Permeant (K-1 & KD-6)

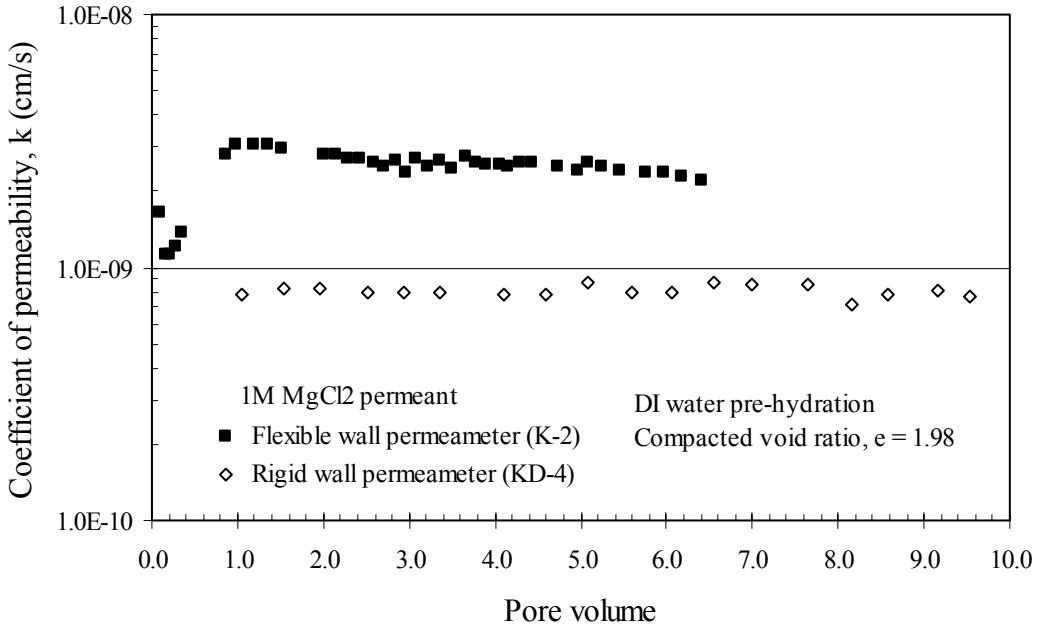

Figure 5.29 Comparison of Permeameters for 1M $MgCl_2$ Permeant (K-2 & KD-4)

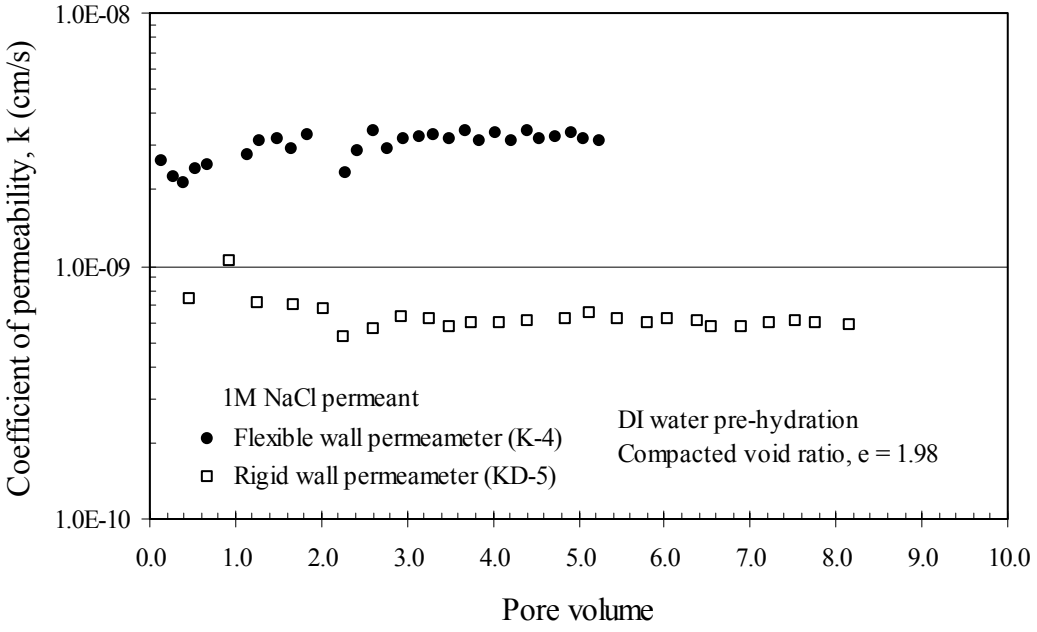

Figure 5.30 Comparison of Permeameters for 1M NaCl Permeant (K-4 & KD-5)

5.2 Chemical Analysis of Effluent

5.2.1 General

Chemical analysis of effluent after permeation in this section includes measurements of pH and electrical conductivity at regular intervals of permeant flow, their ionic analysis, and further analysis in terms of solute storage or retention within the bentonite specimens. Chemical equilibrium in terms of electrical conductivity between influent and effluent is also used as one of the criteria for termination of hydraulic conductivity tests after steady-state permeability is achieved.

Measurements of pH and electrical conductivity (EC) of influent and effluent were carried out in conjunction with flexible-wall as well as rigid wall permeability tests at 24-hour intervals, or in shorter intervals when the permeability was found to be high. The main goal was to obtain a representative profile of the electrical conductivity of chemicals in the leachate as a function of pore volumes of flow until it reaches its chemical equilibrium. During the collection of permeant, the connecting ball valves with the buffer cylinders were kept closed while the permeant was diverted through other tubes to minimize disturbance to the flexible wall permeability test.

In order to conduct full cationic chemical analysis of dissolved solids, 2 ml samples of permeant were collected and transported to the environmental engineering lab upon completion of the collection. To prevent any further chemical reaction in the permeant liquids, care was taken to ensure that handling and transportation time was kept to a minimum. The solution was preserved by adding 1% of nitric acid (HNO_3) and then kept in the refrigerator until the chemical analysis was carried out.

5.2.2 pH Measurement

Immediately following sample collection, the pH of the non-acidified original sample was measured using an Accumet portable (model AP63) pH meter and

polymerbody combination pH/ATC Ag/AgCl electrode. The pH meter was calibrated at three levels, using three standard color-coded buffer solution of pH 4.00, 7.00 and 10.00. As mentioned earlier, DI water was used for pre-hydration and back pressure saturation in the flexible wall permeability tests that are listed in Table 5.6. The figures in Appendix A show the variation of pH of the effluent solution with pore volumes passed through the bentonite specimen with reference to influent pH values. It maybe highlighted that the pH values are found to be slightly higher at the beginning of the experiment, before they gradually reduce to equilibrium values at steady-state conditions. These steady state values are higher than the corresponding influent values, except in the case of $CaCl_2$ permeants. In the case of $CaCl_2$, hydroxyl [OH^-] ions are retained on the clay surfaces during permeability, and therefore the pH of the effluent is reduced.

Table 5.6 Lists of Flexible Wall Permeability Tests with pH Results

Test number	Source solution	Influent pH	Effluent pH range	Effluent Mean pH
K-1	1M $CaCl_2$	7.4	6.81 – 7.74	7.2
K-2	1M $MgCl_2$	6.63	6.27 – 7.59	7.09
K-3	1M KCl	7.1	6.98 – 7.7	7.38
K-4	1M NaCl	7.35	7.28 – 7.92	7.44
K-8	5M $CaCl_2$	8.2	7.25 – 8.25	7.74

5.2.3 Electrical Conductivity

The electrical conductivity of leachates was measured for the same specimens using an Accumet (model AB30) 4-cell conductivity meter and two epoxy body electrodes of cell constant 1.0 cm^{-1} and 10.0 cm^{-1}. These electrodes are capable of measuring a wide range of electrical conductivities from 10 to 200,000 microsiemens. Whenever a change of electrodes was required to obtain a measurement within a particular range, it was necessary to recalibrate it using its own standard solution. The

figures in Appendix A show the variation of EC of the effluent solution with pore volumes passed through the bentonite specimen with reference to influent EC values. From figures A.1 to A.27 (odd numbers), it can be clearly concluded that the EC values reach the influent values at chemical equilibrium after about 3 to 4 pore volumes of flow. Chemical retention in the bentonite specimen can therefore be happening within the first 3 to 4 pore volumes of flow until chemical equilibrium is attained.

In order to calculate the total chemical retention within the bentonite clay specimen during permeability, it can be assumed that the existing chemical elements of the bentonite clay mineral have been "flushed" out within the first pore volume of flow and the influent chemical elements start to accumulate then, until chemical equilibrium is reached. Integrating the area in between the influent EC line and the best fitted effluent EC line from zero pore volume to the pore volume at chemical equilibrium (3 to 4 pore volumes), the total retention capacity of the dissolved salt permeant can be calculated.

The area under the electrical conductivity (EC) curve (μS/cm. pore volume) represents the total amount of solute permeated through the clay specimen. The area under the effluent EC curve within any interval of pore volumes provides the amount of dissolved chemical salts permeated through the specimen, while that under influent EC represents the amount of chemical salts present in the influent that flows into the clay specimen during the same interval of pore volumes. The difference in areas is the amount of chemicals retained within the bentonite clay during permeation of inorganic dissolved chemicals.

Since the testing specimens are saturated with deionized water before the chemical solution permeation is carried out, no chemicals are added to test specimens. After saturation of the clay specimens, EC is measured for the deionized water in the effluent cylinder. Any value measured is due to the diffusion of chemicals present within the specimen during the saturation phase. The total amount of outfluxed chemicals during saturation is to be incorporated in the calculation of actual amounts of chemical retained within the specimen during permeability. In order to obtain a distinct variation of effluent EC, permeation through bentonite clay is required to be carried out following deionized water pre-hydration and back pressure saturation. The calculated amount of

retained chemicals can be checked against the actual amount retained, which is obtained by measuring the dry weight of the specimen after completion of the test.

An example of the calculation of any particular salt permeant is shown below. The influent of the test is one molar $CaCl_2$ solution (test # KD-6) with an electrical conductivity of 128,000 μS/cm. The best fit curve for the effluent EC is obtained using any statistical analysis software ('excel' worksheet in this study). A fourth-order polynomial equation is generated for the effluent EC curve as shown in figure 5.16, which merges with the influent EC line at around 5 pore volumes of flow. The total amount of chemicals present in the effluent, until chemical equilibrium is achieved, is calculated by the area under this curve (area ABCD as in figure 5.31) from a pore volume of zero to a pore volume of five, as given in the following equation (5.3).

Area ABDE =

$$\int_0^5 y\,dx = \int_0^5 \left(-0.0951x^6 - 3.5822x^5 + 185.68x^4 - 2238.5x^3 + 7076.3x^3 + 25288x + 2500\right)dx \quad (5.3)$$

= 379,340 μS/cm . pore volume

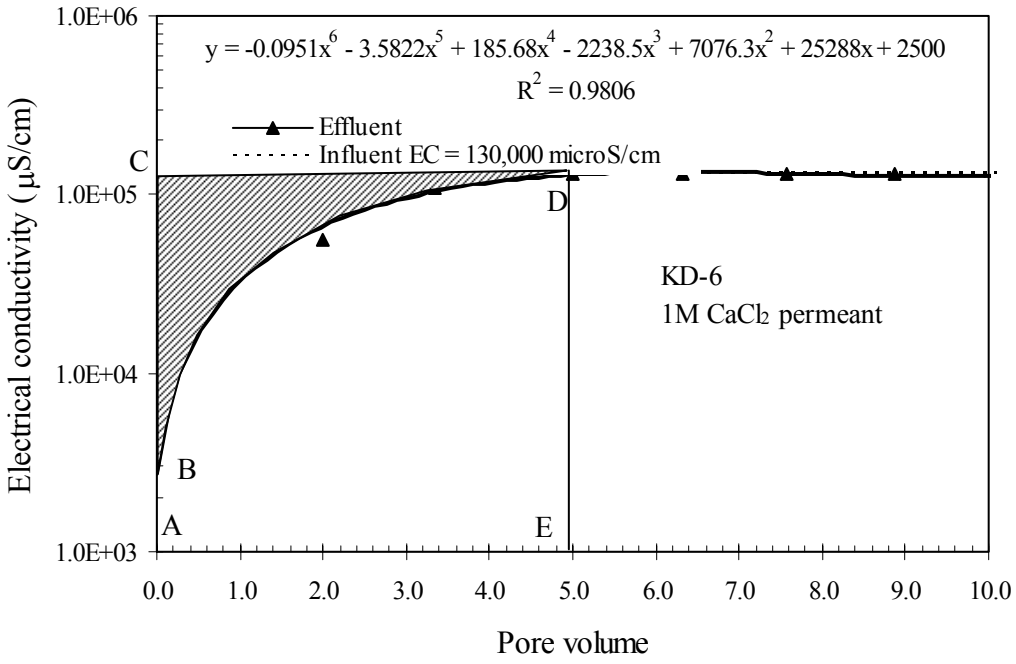

Figure 5.31 Chemical Retention Measurement for KD-6

The total amount of chemicals present in the influent during the same flow volume is the area under the influent EC line from zero to five pore volumes (area ACDE). Therefore, the amount of chemicals influxed into the clay specimen is:

Area ACDE = 130,000 x 5 = 650,000 μS/cm. pore volume

The total of chemicals retained within the specimen

= Area ACDE – Area ABDE

= 650,000 - 379,340 μS/cm. pore volume

= 270,660 μS/cm. pore volume

= 270,660 x 0.66 mg/L x pore volume [since 1 μS/cm = 0.66 ppm]

= 178,635 mg/L x 21.2 ml [since 1 pore volume for KD-6 = 21.2 ml]

= 3,787 mg

= 3.78 g

The actual increase in mass recorded for the test specimen after drying in the oven at 105ºC for 24 hours was found to be 3.2 g which is 15% smaller than the theoretical value, as calculated above from the EC measurements of the effluent and influent solutions. Other values in terms of actual and theoretical chemical retention are given in Table 5.7.

Table 5.7 Theoretical and Actual Chemical Retention During Permeability

Test #	Influent	Size Thickness x mass	Void ratio	Calculated chemical retention (g)	Actual chemical retained (g)
KD-4	1M $MgCl_2$	7mm x 30g	1.98	2.0	1.48
KD-5	1M NaCl	7mm x 30g	1.98	0.8	0.48
KD-6	1M $CaCl_2$	7mm x 30g	1.98	3.78	3.2
KD-11	1M KCl	7mm x 30g	1.98	1.51	1.18
KD-7	1M $CaCl_2$	7mm x 15g	4.96	3.08	2.1
KD-8	1M $CaCl_2$	3mm x 2.5g	14.35	1.86	1.03
KD-10	1M NaCl	7mm x 7.5g	10.94	1.12	0.93

It can be seen from Table 5.7 that the actual amounts of chemical retention are lower than those calculated theoretically from the electrical conductivity plots. These lower values may be attributed to the fact that some loss of clay specimen mass occurs due to the dissolution of chemicals present in the clay during saturation. Also the presence of chemical solution, and the precipitation left within the test apparatus after the completion of permeability test may contribute to the difference.

By comparing the first four tests as listed in Table 5.7 having the same size, mass, and void ratio, it is found that the amount of chemical retained in divalent permeants is higher than that of monovalent permeants since the higher valence cations replace the lower valence cations on the surface of the clay platelets.

5.2.4 Ionic Analysis

All influent and effluent samples were collected in 60 ml polyethylene chemically resistant bottles and mixed with 1% nitric acid (0.6 ml) for preservation at 4^{o}C in the refrigerator until the actual chemical analyses were done. The acidification is a required step in the preservation and chemical analysis of the samples, and does not interfere with the accuracy of the measurement in any way. The acidified samples were analyzed for all major metal ions, namely sodium (Na^{+}), calcium (Ca^{++}), magnesium (Mg^{++}), and potassium (K^{+}). This was done using the "AAnalyst – Atomic Absorption Spectrometer" at the environmental engineering lab of the University of South Florida.

Liquid samples, which were collected and preserved previously during the hydraulic conductivity tests at different EC values, were analyzed, and the amounts (concentration) of their four major chemical elements were determined. Test results obtained from the permeability tests (Test # K-1, K-2, K-3, and K-4) are given in Appendix C. It is found from the plots, in figures C.1 to C.4 of Appendix C, that most of the cation exchange happens until around 2 to 3 pore volumes except in sodium solution where no cation exchange is visible, as shown in figure Appendix C.4 (test # K-4). Sodium and calcium chemical elements are found to be present within the supply

bentonite either in the form of precipitation or exchangeable cations on the clay platelets as evidenced from the ionic analysis plots.

CHAPTER SIX

DIFFUSION IN BENTONITE

In this chapter, test set-up and experimental procedures of diffusion through bentonite is described. A new test procedure and apparatus for diffusion using parts of a rigid wall permeameter is proposed in order to obtain relevant diffusion properties of bentonite clay material. In this study, a number of inorganic chemical permeants were used in diffusivity of bentonite at various solid-water conditions (i.e. various void ratios). Solutions are collected from outflux tubes connected to the diffusion apparatus at regular intervals of time during the progress of diffusion. Test results of chemical analysis of diffusion solutions are also reported in this chapter.

6.1 Experimental Methods

A specially fabricated diffusion cell is used for the diffusion experiments, which was also used in rigid wall permeability experiments (described in Chapter 5). Commercially available deionized water and synthetic inorganic salt solutions of various concentrations and combinations were used as permeants for bentonite clay in this investigation.

Apparatus set-up, test sample preparation and procedure, and sample collection for chemical analysis are described in this section. Test results and chemical analysis of diffused collected samples are discussed in section 6.2. In order to find the diffusivity of various chemical elements in bentonite clay, a number of dissolved salts solutions, used

as permeants, were placed in the highly concentrated source chamber. Bentonite specimens with various thicknesses were prepared to provide different void ratios.

Void ratios of the specimens were varied by taking different amounts of air dry samples for the same physical dimension of the specimens. The thickness of the specimens was kept constant at 3 mm while the weights of air-dried bentonite powder were varied from 2.5 g to 7.5 g. Highly concentrated dissolved salt solutions of one molar and above were prepared and applied as a single salt or a combination of various salts in the source chamber.

6.1.1 Test Set-up

The full description of the test apparatus was given in chapter 4. Diffusion of the highly concentrated solutions through clay was carried out by keeping the liquid levels of both source chamber and receiving tube the same. A schematic diagram in figure 6.1 shows the relevant terms necessary to investigate the diffusion characteristics of bentonite clay materials. The relevant terms are:

L_{sample} = length of the sample

A_{sample} = cross-sectional area of the sample

a_s = area of the source chamber which is equal to the cross-sectional area of the sample

a_r = area of the receptor tube

A stainless steel ball valve connected at the bottom of the receptor tube is used to separate the solution in the tube from that in the source chamber and bottom porous stone. The valve is to be closed while collecting the out-fluxed solution from the receptor tube so that no disturbance or hydraulic gradient is created within the diffusion cell. The connection between the receptor and ball valve is required to be leak proof so that no out-fluxed solution is lost. The grooves on the bottom plate of the diffusion cell need to be cleaned periodically from any deposited solutes by using pressurized tap water and a cleanser. The plexiglass diffusion cylinder, which is placed in between top and bottom

plates, is to be tightened firmly with the bottom plate so that diffusion is prevented through the perimeter of the bottom porous stone. Sufficient vacuum grease is applied on both ends of the plexiglass cylinder in order to prevent any leakage.

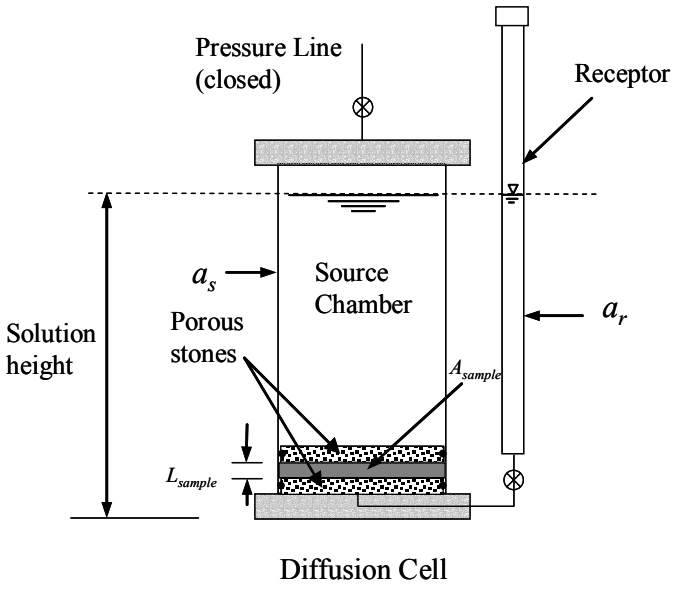

Figure 6.1 Schematic Diagram of Diffusion Cell Set-up

Porous stones are assumed to be non-reactive to the source solutions; however, a small amount of precipitation of dissolved solutes may occur during the process of diffusion. A the end of each diffusion test, each porous stone is thoroughly cleaned of any deposited chemical solutes using commercially available cleanser or diluted acids and flushed with pressurized tap water and then submersed in DI water for at least 48 hours to remove all residue. The neutrality of the DI water with submersed porous stones is checked by a pH meter before being used in any new set-up of diffusion cells.

The porous stones on both sides of the clay specimen are placed in such a way that soft clay slurry does not squeeze out through the joints between the plexiglass and the porous stones while preparing the clay specimen inside the diffusion cell. A sufficient amount of silicon sealant is to be added along the O-ring and circumference of the top and bottom porous stones before being placed inside the chamber. A small

amount of silicon vacuum grease is also applied along the perimeter edge of the porous stones to create frictionless joints so that the stones can be pushed into the top of the specimens with ease. No filter paper is placed in between the specimen and porous stones to reduce any reaction which might occur after a certain period of time between the constituents of the paper, chemical solutions, and clay minerals during the process of diffusion. Choosing the right size O-ring is essential so that the porous stone assembly does not fit too tightly into the chamber, which might cause it to crack and eventually break while pushing the porous stone the internal piston.

A full diffusion set-up picture is given in figure 6.2. A highly concentrated solute flows from the source chamber towards the receptor tube with time due to the concentration gradient.

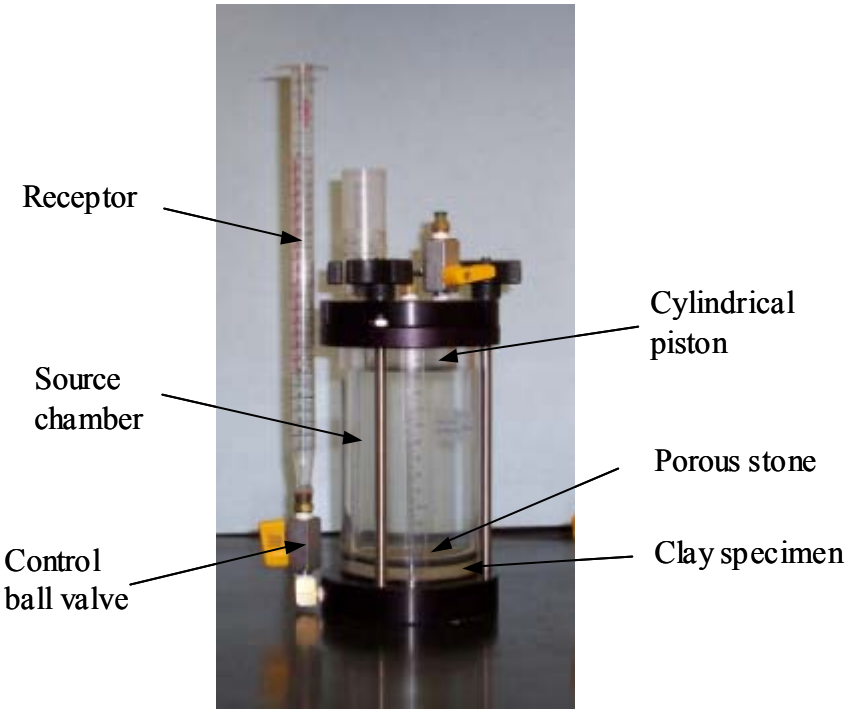

Figure 6.2 Diffusion Set-up

6.1.2 Sample Preparation and Procedure

The sample preparation procedure and test sequence for diffusion experiments were followed strictly in order to obtain reproducible and reliable test results, and minimize experimental errors due to leakage, sample non-uniformity, sample loss, and disturbance.

6.1.2.1 Sample Preparation

A pre-determined amount of air-dried bentonite powder (2.5 g to 7.5 g) is taken in a plastic bowl of sufficient capacity (0.5 liter to 1.0 liter. DI water is slowly added to the bentonite powder and then mixed thoroughly using a high speed mechanical mixer until a slurry consistency bentonite-water suspension is obtained. The bentonite-water slurry is then kept in the bowl with a cover for at least 24 hours so that the water molecules adsorb uniformly on the clay platelets.

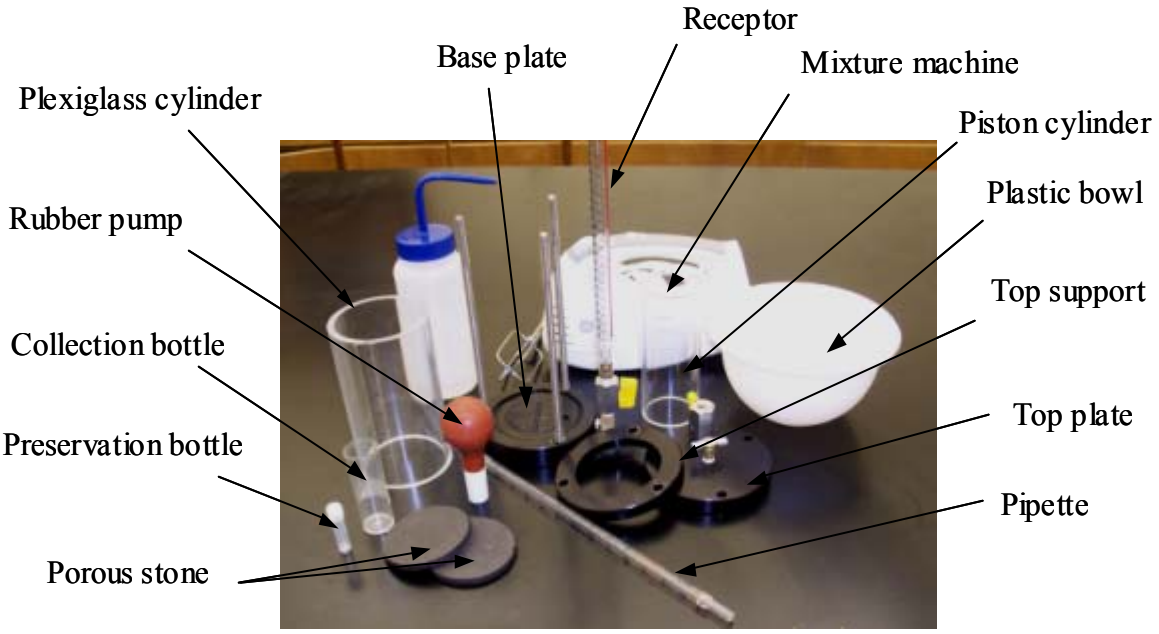

Figure 6.3 Components of Diffusion Cell

After the 24 hour soaking period, the mixer is again used to disintegrate any lumped or aggregated clay particles so that a uniform slurry suspension is achieved before being poured inside the diffusion cell. Constant care is to be taken during the mixing so that no material is lost or left adhering to the parts of the mixer or mixing bowl. All the components of the diffusion cell and its supporting accessories are shown in figure 6.3.

The following steps are carried out in sequence during preparation of clay specimens in the diffusion cell.

Step 1: The grooves of the base plate, connecting fittings of the diffusion cell, and receptor tube are cleaned thoroughly with a brush, pressurized tap water and cloth/tissue paper so that no deposited salt or other impurities are left behind.

Step 2: Sufficient silicon vacuum grease is applied on the perimeter edges of a porous stone and then positioned inside one of the ends of the plexiglass cylinder, flush with the edge of the cylinder.

Step 3: Additional vacuum grease is applied on the both edges of the cylinder. The end with the bottom porous stone from step 2 is then placed on the O-ring seated on the based plate of the diffusion cell.

Step 4: The top support (ring frame) is placed on the top end of the cylinder and tightened with screws so that no leakage is allowed through the bottom connection of the cylinder and the plate.

Step 5: The prepared bentonite slurry is then poured into the plexiglass cylinder (already fitted with the bottom porous stone) in such a way that no bentonite clay is left on the bowl surface or the spoon.

Step 6: After applying vacuum grease along the sides of the O-ring placed on its perimeter edge, the top porous stone is carefully placed on the top side of the cylinder and then pushed into the cylinder with the help of a smaller diameter cylinder until the porous stone touches the top of the bentonite slurry. The porous stone is pressed down inside the cylinder in such a manner that it remains horizontal all the way to the top of the slurry surface. Any inclination in placing the porous stone would allow the bentonite slurry to squeeze out during the subsequent consolidation process. Erroneous results

would be encountered should there be any gap along the perimeter joint of the porous stone and cylinder.

Step 7: After leaving the piston cylinder inside the diffusion cylinder, the top plate of the diffusion cell is placed on the piston cylinder. Three wing nuts are then used to push the top plate down with the piston, which eventually presses the top porous stone down and squeezes the slurry bentonite sample. The three nuts are to be turned slowly and uniformly in order to apply a uniform pressure on the porous stone. During this process of consolidation, the receptor ball valve is kept open so as to create a double drainage flow path.

Step 8: Water accumulated within the receptor tube due to consolidation of the slurry is flushed out. The thickness of the specimen is calculated from the height of the piston when the top plate touches the top support ring after pressing the piston down by turning the screws. The pistons are fabricated in such a length that produces the required thickness of the bentonite specimen at which the diffusion test is performed.

Step 9: The water as well as some suspension clay particles that are squeezed out through the porous stones from top and bottom of the specimen and are accumulated within cylinder and receptor respectively, are collected and dried in an oven overnight. The dried weight of the clay is deducted from the initial amount of the bentonite in order to calculate the final amount of bentonite used in the diffusion experiments.

Step 10: A synthetic inorganic salt solution is prepared by dissolving the required amount of salt in DI water. The concentrated salt solution (about 300 ml to 400 ml) is poured into the source chamber. The top plate is then placed on top of the source chamber and is tightened with the wing nuts so that no opening in the connection is available for air-flow.

Step 11: DI water is poured into the receptor tube up to the same level as the source solution in the chamber. A cap is then placed on top of the receptor tube to prevent any air circulation or evaporation of the receptor solution during the process of diffusion.

Various important steps of the above procedure are shown in figure 6.4. The prepared test assembly with specimen and synthetic solution is then kept in an undisturbed place free of air flow/circulation or temperature variation.

(a) Step 2

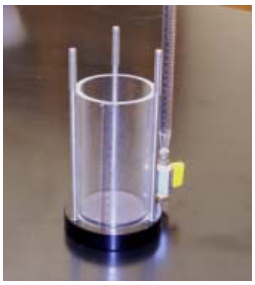

(b) Step 3

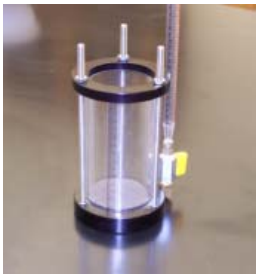

(c) Step 4

(d) Step 5-8

(e) Step 9-11

Figure 6.4 Sample Preparation for Diffusion Test

6.1.3 Synthetic Inorganic Chemicals

Deionized water with less than 5 ppm dissolved ions and four different salt solutions (NaCl, KCl, $CaCl_2$ and $MgCl_2$) of various concentrations and combinations as shown in Table 6.1 were used in diffusion tests as the source solution. All the salts are Fisher Scientific Lab certified brands and were used according to their formula weights for preparing synthetic inorganic solutions. NaCl, KCl, and $CaCl_2$ are anhydrous granular salts while $MgCl_2$ is a hexahydrate crystalline salt having the chemical formula

$MgCl_2.6H_2O$. Deionized water commercially available in one-gallon plastic bottles was used as a solvent for those salt solutions.

The salt solutions have been chosen to investigate the effects of various concentrations, cation size, and valence on the diffusion characteristics of bentonite clay. Concentrations of the electrolyte solutions were varied from 1M to 5M and were prepared by dissolving crystalline/granular salts with DI water. In order to determine the adsorption capacity and replaceabilty of cations on negatively charged clay mineral surfaces, NaCl and KCl were chosen to study the effects of monovalent cations and hydrated ion size (Na^+ and K^+ have different hydrated radius) while $CaCl_2$ and $MgCl_2$ were chosen to investigate the behavior of divalent cations (Ca^{2+} and Mg^{2+}) that are commonly found in natural aqueous systems and at higher concentrations in polluted groundwater and landfill leachate.

6.1.4 Sample Collection for Chemical Analysis

Measurements of pH and electrical conductivity (EC) of outfluxed diffusant were taken at 48-hour intervals, or shorter intervals when the diffusion rate was found to be high. The main goal was to obtain a representative profile of the flow of chemicals through the bentonite clay as a function of time. In order to conduct EC and pH measurements, as well as a full cationic chemical analysis of diffusant, DI water was added to the receptor solution up to a level of 25 ml. By using a long slender pipette and a handheld rubber suction pump, the diffusant was collected from the receptor tube for chemical analysis which includes pH and EC measurements and ionic analysis.

6.2 Chemical Analysis

Chemical analyses in terms of pH, electrical conductivity (EC) and ionic analysis were carried out on the diffusant solution collected from receptor tube. In addition, pH

and EC measurement of source solutions were carried out intermittently in order to verify the uniformity of influx concentration during the whole process of diffusion. Table 6.1 lists the diffusion tests carried out with synthetic inorganic salt solutions of different molarities. Void ratios of the specimens were varied according to their size and the amount of air-dry bentonite in the specimen.

Table 6.1 Lists of Diffusion Samples with Source Solutions

Test number	Source solution	Specimen size Diameter x thickness	Void ratio
D-5	1M NaCl	76.2 mm x 7.84 mm	5.69
D-6	2M $CaCl_2$	76.2 mm x 8 mm	9.23
D-8	2M $MgCl_2$	76.2 mm x 3 mm	14.35
D-9	2M KCl	76.2 mm x 3 mm	14.35
D-10	2M NaCl	76.2 mm x 3 mm	14.35
D-11	2M $CaCl_2$	76.2 mm x 3 mm	14.35
D-12	5M $CaCl_2$	76.2 mm x 3 mm	14.35
D-13	5M $CaCl_2$	76.2 mm x 3 mm	4.11
D-14	5M NaCl	76.2 mm x 3 mm	14.35
D-16	5M NaCl	76.2 mm x 3 mm	6.67
D-17	All salts (1M each)	76.2 mm x 3 mm	14.35

6.2.1 pH Measurement

Immediately following sample collection, the pH of the non-acidified original sample was measured using an Accumet portable (model AP63) pH meter and polymerbody combination pH/ATC Ag/AgCl electrode. The pH meter was calibrated at three levels, using three standard color-coded buffer solutions of pH 4.00, 7.00 and 10.00. During the measurement, the solution must be stirred constantly with the pH probe for at least a minute in order to obtain a stable reading. In each subsequent use of the pH probe,

it is important to wash the probe thoroughly using DI water in order to prevent contamination with previously measured solutions.

The test results for the diffusants collected from the receptor tube are given in a series of figures in appendix B. The results are also summarized in Table 6.2, where the range of pH and their mean pH along with the specimens' void ratios are highlighted. In order to compare the variation of pH values with respect to source solutions, tests results are grouped into three categories as follows:

Group # 1 – Source solution $CaCl_2$ of various molarities (D-6, D-11, D-12 and D-13)

Group # 2 – Source solution NaCl of various molarities (D-5, D-10, D-14 and D-16)

Group # 3 – Source solution of two molars of various salt solutions for same void ratio (e = 14.25) specimens (D-8, D-9, D-10, and D-11).

Combined test results for group 1, 2, and 3 are given in figures 6.5, 6.6, and 6.7 respectively. The values of pH were found to be widely scattered within a range of 5.3 to 10.95, as given in Table 6.2.

It can be seen from figure 6.5 of group # 1 tests, where $CaCl_2$ solutions of various concentrations were used as the source, that pH values of out-fluxed diffusants were found to be slightly higher than those of group # 2 (figure 6.6), where NaCl solutions were used as a source. It can be highlighted that the pH values of $CaCl_2$ source solutions were found to be between 10.0 and 10.5, while those of NaCl solutions were in the range of 7.1 to 7.5. Therefore, it may be concluded that the pH value decreases in the case of $CaCl_2$ source solutions due to retention of hydroxyl ions [OH^-] within the bentonite clay during diffusion. In the case of NaCl source solutions, an increase in pH values can be observed, which could be due to the supply of hydroxyl ions [OH^-] from the bentonite clay during the process of diffusion.

It can be observed from figure 6.7 and Table 6.2 that the pH values for KCl and $MgCl_2$ source solutions are lower than those of NaCl and $CaCl_2$ source solutions, which could be due to the fact that original source pH for KCl and $MgCl_2$ are 6.55 and 6.65 respectively, which are lower than those of NaCl and $CaCl_2$.

Table 6.2 Lists of Diffusion Tests with Out-Fluxed pH Results

Test number	Source solution	Void ratio	pH range	Mean pH
D-5	1M NaCl	5.69	7.33 – 8.86	7.95
D-6	2M $CaCl_2$	9.23	5.85 – 10.95	9.18
D-8	2M $MgCl_2$	14.35	6.32 – 8.87	7.35
D-9	2M KCl	14.35	6.49 – 9.2	7.64
D-10	2M NaCl	14.35	6.6 – 10.67	8.4
D-11	2M $CaCl_2$	14.35	5.3 – 9.74	8.36
D-12	5M $CaCl_2$	14.35	5.74 – 9.8	8.54
D-13	5M $CaCl_2$	4.11	6.62 – 9.35	8.08
D-14	5M NaCl	14.35	7.24 – 8.64	7.98
D-16	5M NaCl	6.67	6.75 – 9.2	8.21
D-17	All salts (1M each)	14.35	7.12 – 8.9	7.68

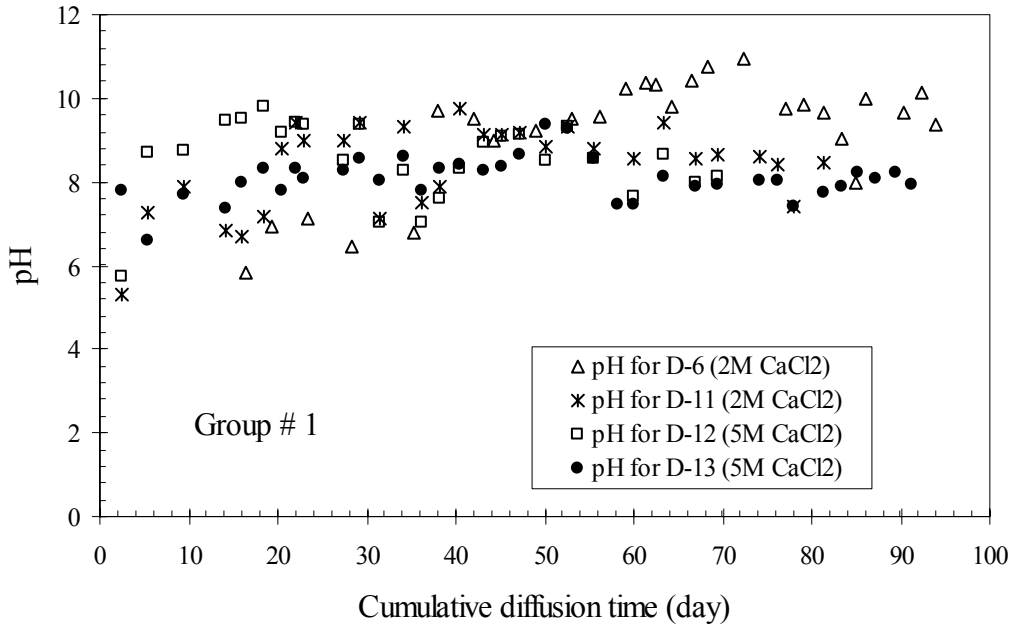

Figure 6.5 Variation of pH for Group #1 Diffusion Tests (D-6, D-11, D-12, and D-13)

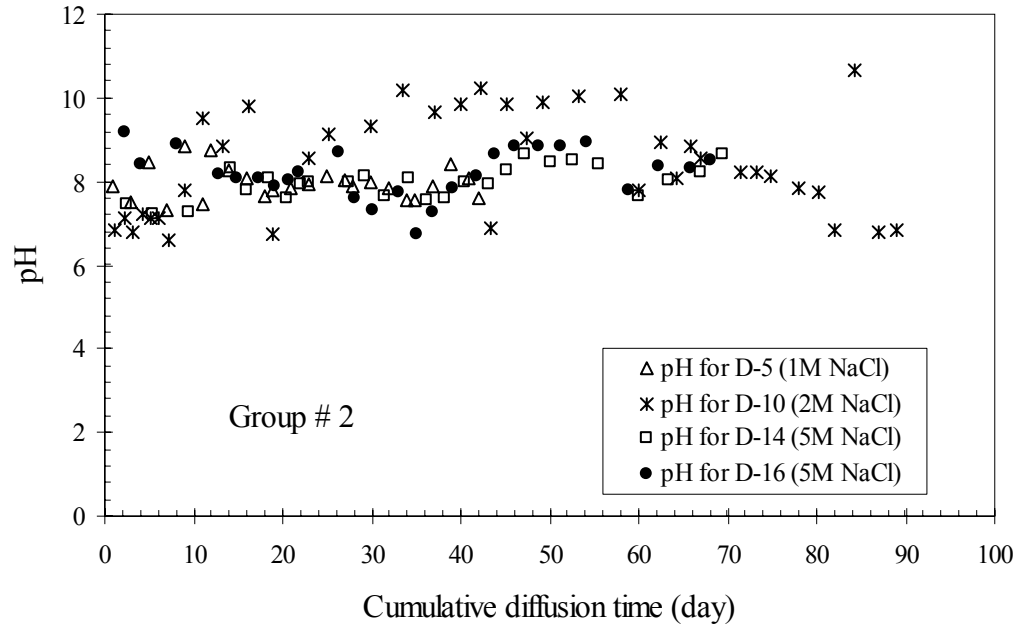

Figure 6.6 Variation of pH for Group #2 Diffusion Tests (D-5, D-10, D-14, and D-16)

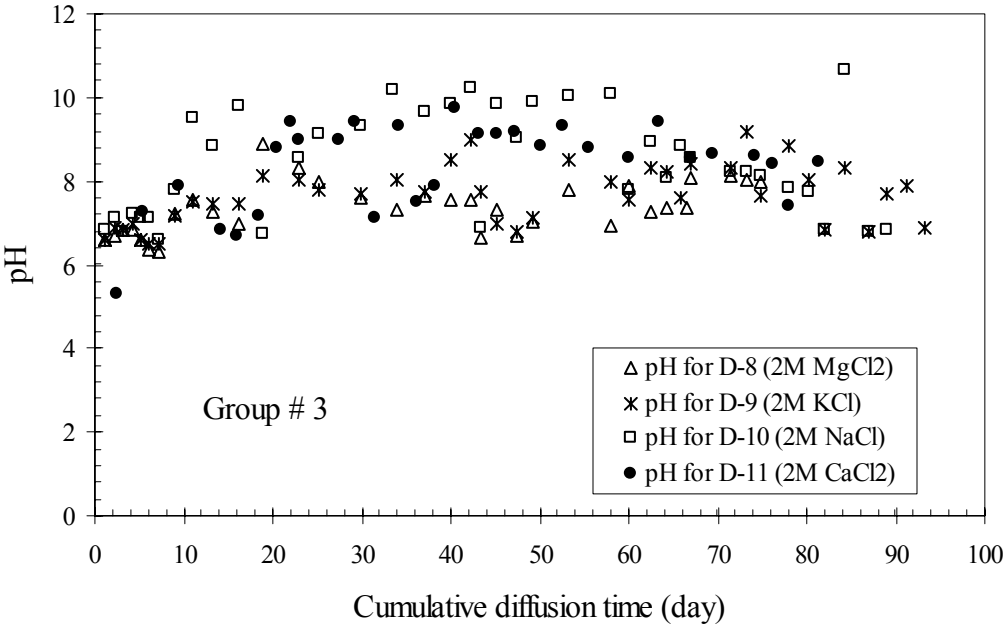

Figure 6.7 Variation of pH for Group #3 Diffusion Tests (D-8, D-9, D-10, and D-11)

6.2.2 Electrical Conductivity

The electrical conductivity of leachates was measured for the same specimens using an Accumet (model AB30) 4-cell conductivity meter and two epoxy body electrodes of cell constant 1.0 cm^{-1} and 10.0 cm^{-1}. These electrodes are capable of measuring a wide range of electrical conductivity from 10 to 200,000 microsiemens. Whenever a change of electrodes was required to obtain a measurement within a particular range, it was necessary to recalibrate it using its own standard known solution before using.

Test results of electrical conductivity measurements for all the diffusion experiments are listed in Table 6.1 and are presented in appendix B. Cumulative diffusion time in days, shown on the horizontal axes of the figures in appendix B, represents the elapsed time from the beginning of the diffusion test. As the receptor tube is replenished with DI water after each collection of diffusant solution, electrical conductivity values presented in the "a" series of figures in appendix B measure the EC for the duration between two consecutive sample collections. In the "b" series of the figures in appendix B, the cumulative electrical conductivity values, which are calculated from the raw data of the "a" series, are plotted on the vertical axis. A diffusion test is considered to have reached at steady-state condition when the curve of cumulative EC versus cumulative diffusion time starts to take the shape of a straight line. After achieving a constant variation of cumulative EC with respect to elapsed diffusion time, as shown by the dotted straight lines in figures "b" in appendix B, diffusion tests were terminated and the bentonite clay specimens were collected and dried in the oven for further analysis.

Three groups of tests, as outlined in section 6.2.1, were also considered for comparison of out-fluxed cumulative electrical conductivity with respect to diffusion duration. The results are tabulated in Table 6.3, along with their duration intercept known as the "Lag Time", and their steady-state equation. Combined test results of EC for groups 1, 2, and 3 are also given in figures 6.8, 6.9, and 6.10 respectively.

Table 6.3 Comparison of Diffusion Tests with 'Lag Time' and Steady-State Equation

Group #	Test number	Source solution	Void ratio	Lag Time	Steady-state equation
1	D-6	2M $CaCl_2$	9.23	39	Y= 382.82X - 14913
	D-11	2M $CaCl_2$	14.35	25	Y = 847.67X - 20905
	D-12	5M $CaCl_2$	14.35	8	Y = 1664.1X - 13584
	D-13	5M $CaCl_2$	4.11	54	Y = 756.82X – 40684
2	D-5	1M NaCl	5.69	16.5	Y = 59X – 984
	D-10	2M NaCl	14.35	40	Y = 453.78X – 17907
	D-14	5M NaCl	14.35	14	Y = 1116.7X – 15682
	D-16	5M NaCl	6.67	19	Y = 677.77X – 13165
3	D-8	2M $MgCl_2$	14.35	45	Y = 566.66X – 25387
	D-9	2M KCl	14.35	40	Y = 359.66X – 14468
	D-10	2M NaCl	14.35	40	Y = 453.78X – 17907
	D-11	2M $CaCl_2$	14.35	25	Y = 847.67X - 20905

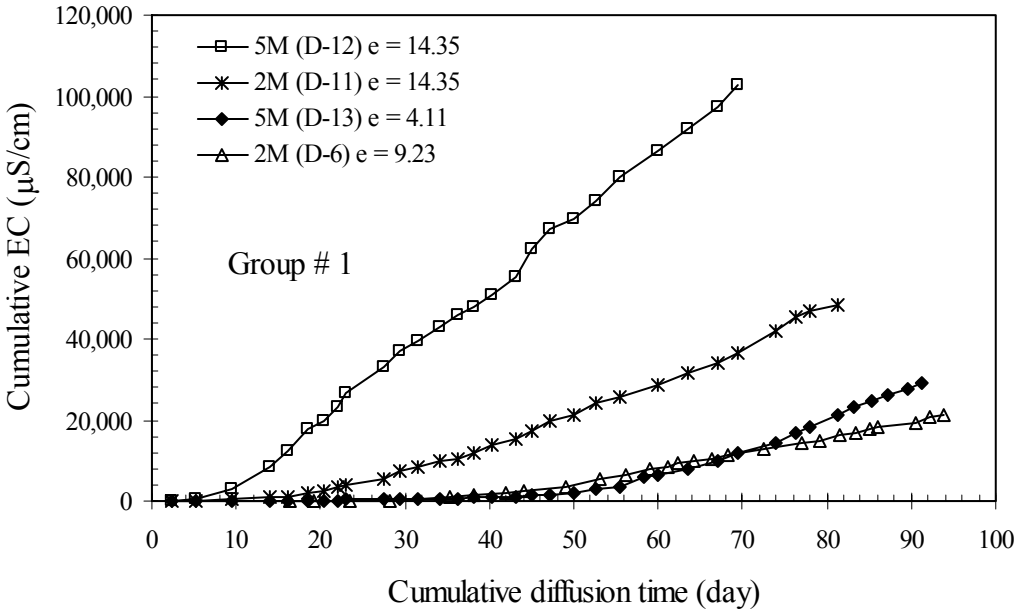

Figure 6.8 Cumulative EC for Group #1 Diffusion Tests (D-6, D-11, D-12, and D-13)

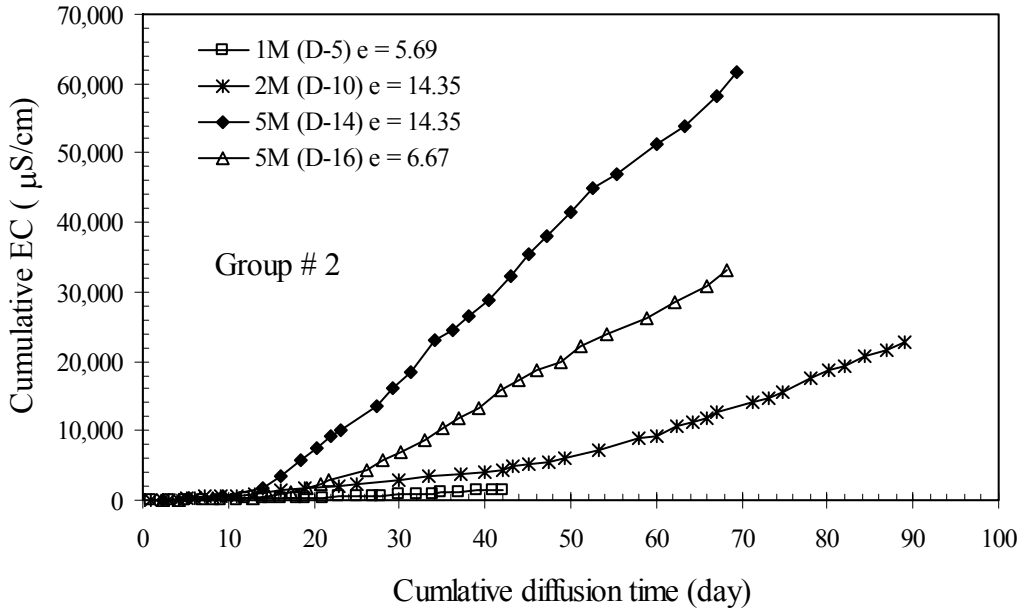

Figure 6.9 Cumulative EC for Group #2 Diffusion Tests (D-5, D-10, D-14, and D-16)

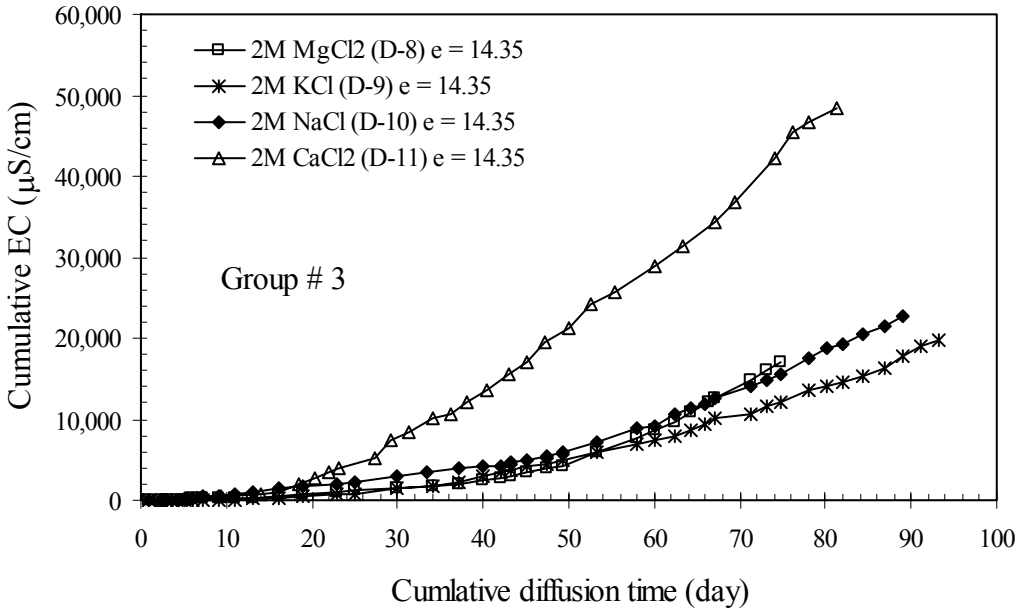

Figure 6.10 Cumulative EC for Group #3 Diffusion Tests (D-8, D-9, D-10, and D-11)

It can be seen from figure 6.8 that the fastest diffusion rate and shorter lag time were achieved for test D-12 where the bentonite specimen had higher void ratio (e = 14.35) with a higher concentrated source solution of 5 molars. For consolidated bentonite clays of lower void ratios, lower rates of diffusion and longer lag times were found, even at higher concentrated source solutions, as shown in figure 6.8.

The same trend can also be observed for NaCl source solutions used in diffusion through bentonite clay specimens, as shown in figure 6.9. The rate of diffusion of one molar NaCl solution through bentonite clay of void ratio 5.69 was so slow that it was terminated after 45 days of diffusion. By comparing figures 6.8 and 6.9, it can be concluded that the rate of diffusion is much faster in $CaCl_2$ solutions than in NaCl solutions.

In group # 3 diffusion tests, various salt solutions of the same molarity (2M) were used as source solutions for bentonite clay specimens of the same void ratio (e = 14.35). The results are given in figure 6.10. It can be clearly seen from figure 6.10 that the rate of diffusion is much higher and lag time is much shorter for $CaCl_2$ solution in comparison with other source solutions.

6.2.3 Ionic Analysis

All diffusant samples were collected in 2 ml polyethylene chemically resistant bottles and mixed with 1% nitric acid for preservation at 4^oC in the refrigerator until the actual chemical analyses were done. The acidification is a required step in the preservation and chemical analysis of the samples, and does not interfere with the accuracy of the measurement in any way. The acidified samples were analyzed for all the relevant cations, namely sodium (Na^+), calcium (Ca^{2+}), magnesium (Mg^{2+}), and potassium (K^+). This was done in the USF environmental lab using the "Optical Emission Spectrometer" which is known to be a highly accurate method for that purpose.

Table 6.4 Ionic Analysis of Diffusant of Two Molar Solutions Through Bentonite

Test #	Time lapsed (days)	Na^+ (mg/l)	K^+ (mg/l)	Mg^{++} (mg/l)	Ca^{++} (mg/l)	Total (mg/l)
D-8 2M $MgCl_2$	1.05	9	5.5	3	3.3	20.8
	9.09	0.6	0.7	0	0.5	1.8
	13.16	3.3	1.1	11.1	1.2	16.7
	16.1	5.8	1.1	20.4	1.6	28.9
	22.92	3.5	0.5	12.5	0.8	17.3
	29.99	2	6.7	49	1.6	59.3
	42.15	2.2	0.4	300	2	304.6
	53.31	2.3	14.8	351	3	371.1
	71.35	4	2.9	608.8	3.8	619.5
D-9 2M KCl	1.04	1.1	8.5	4.2	7.1	20.9
	2.3	0.3	8.7	3.4	2.7	15.1
	16.1	7.2	10	0.3	0.5	18
	18.96	2.2	36.5	0.4	1.1	40.2
	22.92	1.8	58.4	0.5	0.7	61.4
	29.99	1.3	163.4	0.3	0.9	165.9
	39.91	1.8	212.3	0.5	1.3	215.9
	53.31	1.8	244.9	1.5	3.3	251.5
D-10 2M NaCl	1.03	7.2	4.5	2.2	2.2	16.1
	2.3	4.6	5	1.6	1.5	12.7
	5.14	11	3.2	0.4	0.3	14.9
	13.16	45	2.2	2.1	1.6	50.9
	16.1	99.3	1.03	0.2	0.3	100.8
	22.92	90	1.4	0.2	1	92.6
	33.53	108	1	0.3	1.4	110.7
	78.08	2666	2	0.4	5.8	2674.2
D-11 2M $CaCl_2$	5.31	4.1	3.6	0.5	16.5	24.7
	9.38	11	19.4	0.9	0.9	32.2
	18.44	7.5	10.4	5.1	108	131
	29.27	22.9	45.3	1	643.6	712.8

Solutions, which were collected and preserved previously during the diffusion tests at different EC values, were analyzed, and the amounts (concentrations) of their major four chemical elements were determined. Table 6.4 shows the test results of ionic analysis conducted on various diffusants collected from receptor tubes. By comparing the diffusants of 2M $MgCl_2$ and 2M $CaCl_2$ in tests # D-8 and D-11, respectively, it is found that calcium divalent cations replace more monovalent cations from the negatively charged surface of clay platelets than magnesium divalent cations. This may be

attributed to the larger hydrated radius of magnesium cations compared to calcium. Small amounts of divalent cations were detected, even when using monovalent diffusants, as shown in test # D-9 and D-10 in Table 6.4. This may be due to the presence of loose precipitated divalent cations mixed in the bentonite powder. However, no significant traces of cations are encountered at the steady-state condition other than those of the diffusant solutions.

CHAPTER SEVEN

TRANSPORT THEORY AND ANALYSIS OF DIFFUSION IN BENTONITE CLAY

7.1 Fluid Transport Mechanisms

There are four different types of flow which occur through soils, namely, fluids, electricity, chemicals, and heat flow. These flows occur due to the variation in their respective potentials at various locations. In addition, coupled flow is defined as the flow of one type due to the flow potential of another type. Water flow, chemical flow and coupled hydraulic-chemical flow are investigated in this research.

Transport of dissolved chemicals or solutes in the subsurface is generally considered to be the result of three important processes: advection, dispersion, and diffusion. The following sections are designated to describe the advection and diffusion flow theories and their related characteristics.

7.1.1 Advection Flow

Advection is defined as a movement (flow) of fluid (or leachate) through a porous medium due to a potential (hydraulic gradient) as shown in figure 7.1. Advection occurs in the pore fluid where the flowing fluid is responsible for carrying chemicals in the form of dissolved or suspended particles.

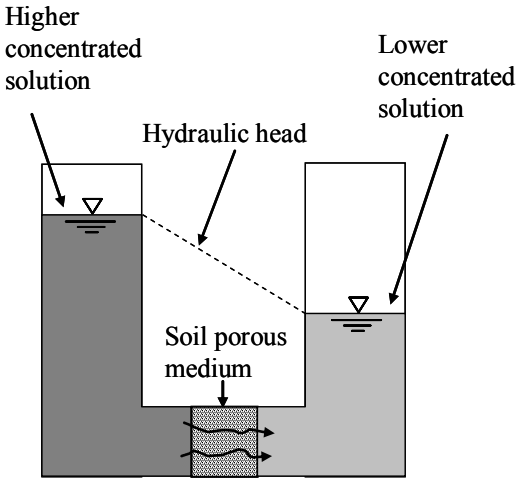

Figure 7.1 Advection of Solute Transport

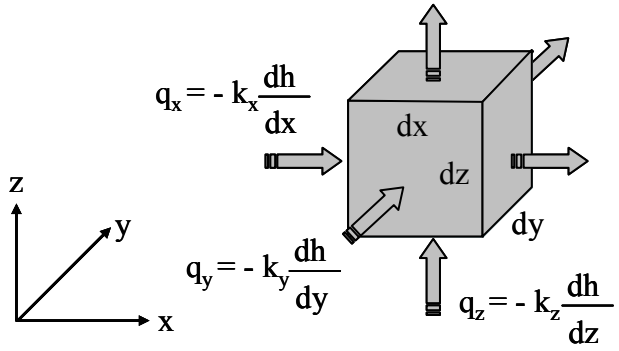

Figure 7.2 Mathematical Representation of Advection

The mathematical representation of 3-D advection is shown in figure 7.2, where *dh* is the change of hydraulic head across an infinitesimal distance *dx, dy*, or *dz*. The terms *q* and *k* with subscripts in their respective directions are known as Darcy flux [LT^{-1}] and hydraulic conductivity or coefficient of permeability [LT^{-1}], respectively. The chemical flux, J_a [$MT^{-1}L^{-2}$] through a unit area due to a hydraulic influx of a solution of concentration *C* [ML^{-3}] can be written as (Malusis, 2001; Mitchell, 1993):

$$J_a = Cq \tag{7.1}$$

The mass of chemical solute accumulated by advection during any time interval t_1 to t_2 can be calculated by integrating equation (7.1) as follows:

$$M_a = \int_{t_1}^{t_2} J_a \cdot dt = \int_{t_1}^{t_2} C(t) \cdot q \cdot dt \tag{7.2}$$

In equation (7.2), $C(t)$ is the concentration of the chemical during the time interval, and *q* is the Darcy flux defined as $k(dh/dx)$.

7.1.2 Diffusion Flow

Transport of chemicals through a porous medium by dispersion consists of two processes, namely, molecular diffusion (commonly known as diffusion) and mechanical (or hydrodynamic) mixing. Diffusion is defined as the process whereby ionic or molecular constituents are transported under the influence of their kinetic activity in the direction of their concentration gradient as shown by the schematic diagram in figure 7.3. The solute (chemicals) still flows through the porous medium even when the hydraulic gradient is zero, as shown in figure 7.3.

Dissolved chemicals flow from the high concentration location to the low concentration location. The amount of mass flux, J_d [$MT^{-1}L^{-2}$], depends on its chemical concentration gradient. Figure 7.3 shows the variation of concentration gradient (also known as chemical potential gradient) where it changes with time and eventually reaches a constant at steady state condition. No concentration gradient, and accordingly no net solute flow, exists when the concentration on both sides of the medium is the same. Diffusion flux, J_d, as given by the Fick's first law for steady state condition, is written in equation 7.3 (Mitchell, 1993; Malusis, 2001, 2004; Shackelford, 1993, 1996, 2001).

$$J_d = -D_o \frac{dC}{dx} \tag{7.3}$$

D_o [L^2T^{-1}] is known as the coefficient of diffusion in "free solution" (normally when the chemical is in infinite dilution). Several investigators have studied the influential factors controlling the value of D_o as expressed in equation (7.4) (Shackelford and Daniel, 1991; Robinson and Stokes, 1959; Beek, *et al.* 1999)

$$D_o = f\left(\frac{T}{|z| \cdot \eta \cdot r}\right) \tag{7.4}$$

where |z| is the absolute value of the ionic valence, η is the absolute viscosity of the solution, r is the molecular or hydrated ionic radius, and T is the absolute temperature of the solution.

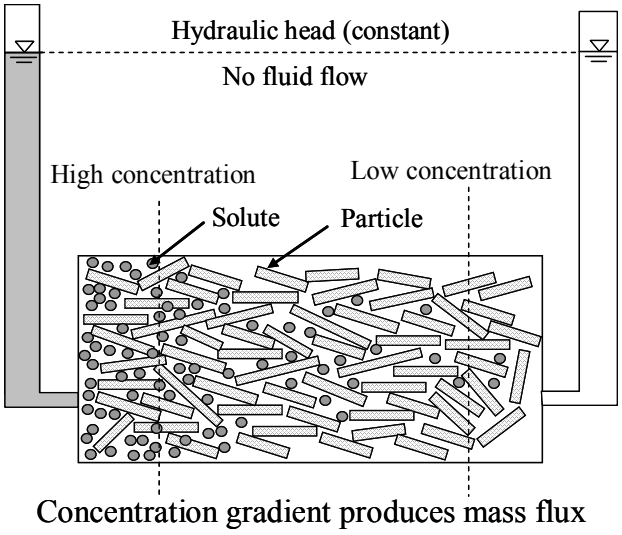

Figure 7.3 Molecular Diffusion of Solute

In order to incorporate Fick's first law in a soil medium, modifications to equation (7.3) have been introduced by many researchers, (e.g., Cheung and Gray, 1989; Eriksen, *et al.* 1999; Foose, 2002; Shackelford and Lee, 2003; Malusis and Shackelford, 2004). Chemical diffusion in soils is much slower than in the free solution because of the effect of porosity, especially in fine grained soils where the permeability is lower and where a tortuous pore channels exist. Further reduction of diffusivity happens in clays since the particles are adsorptive due to the negatively charged particle surface. Factors affecting the diffusivity of chemical solutes through a soil mass can be summarized as follows:

(a) Cross-sectional area of flow within the soil mass: The availability of the flow path depends on the porosity of the soil and the degree of saturation. Diffusivity is directly proportional to the values of porosity (n) and degree of saturation (S_r). The maximum flux for liquid phase diffusion occurs when the soil is fully saturated (degree of saturation, $S_r = 1.0$).

(b) Flow path tortuosity: Tortuosity (τ) of a soil mass, which depends on the shape and arrangement of clay/soil particles, reduces the flow rate of

chemical solutes through diffusion. Since it is not possible to measure the tortuous flow path directly, the effect of tortuosity is typically incorporated into the value of diffusivity coefficient of solute flow as suggested by many researchers (Shackelford and Daniel, 1991; Quigley and Rowe, 1986; Quigley, *et al.* 1987).

(c) Fluidity or mobility of the fluid adjacent to clay particles: The viscosity of the fluid adjacent to the clay mineral surfaces is higher than that of bulk fluid because of the immobility of the clay surface water and the higher adsorption capacity of the negatively charged clay particle surfaces. A fluidity factor (α) has been introduced by Kemper *et al.*, (1964), Olsen *et al.*, (1965) which reduces the diffusivity of chemical solutes through fine-grained adsorptive clay particles.

(d) Anion exclusion: Electrical imbalance might occur on clay mineral surfaces due to the exclusion of anionic charges which are expelled from the pores between diffuse double layers when subjected to high stresses (Porter *et al.*,1960; Freeze and Cherry, 1979; Drever, 1982; Shackelford and Daniel, 1991). However, it is not quite possible to separate the anion exclusion factor (γ) from other factors in determining the diffusivity.

The only factor from the above list that can be readily measured for any clay material is porosity. Therefore, the chemical mass flux due to diffusion through fine-grained (non-reactive) clay can be written by adopting an effective diffusion coefficient, D^*, which incorporates all other controlling factors as given in equation (7.5).

$$J_d = -D^* n \cdot \frac{\partial C}{\partial x} \qquad (7.5)$$

The effective diffusion coefficient, D^*, can be expressed with all the relevant factors including those expressed in equation (7.4) as given in the following equation (7.6).

$$D^* = f\left(\frac{T}{|z| \cdot \eta \cdot r} + \tau \cdot \alpha \cdot \gamma\right) \tag{7.6}$$

However, the transport of solutes that are subjected to chemical reactions or chemical exchanges (cation exchange for bentonite clay minerals), which are analogous to "reactive solutes," differ from the transport of nonreactive solutes as calculated using equation (7.5). In order to accommodate the effects of cation exchange on the clay mineral surfaces, an additional factor known as "retardation factor", R_d, has been added in the diffusion formulation which inversely affects the flow of solutes as given in equation (7.7).

$$J_d = -\frac{D^* n}{R_d} \cdot \frac{\partial C}{\partial x} \tag{7.7}$$

The retardation factor can be defined in terms of partition coefficient K_p, as given by equation (7.8).

$$R_d = 1 + \frac{\rho_d}{n} \cdot K_p \tag{7.8}$$

The partition coefficient, K_p, is defined as the amount of a given constituent that is adsorbed or desorbed by a soil for a unit increase or decrease in the equilibrium concentration in solution (Mitchell, 1993, Shackelford and Daniel, 1991).

Fick's first law is only applicable for diffusive flux of solutes under steady-state condition when the concentration gradient within the medium does not change with time. The rate of change in concentration with time and distance within the transport medium, as shown in figure 7.4, is described by Fick's second law which can be expressed mathematically for non-reactive solute diffusion as follows:

$$\frac{\partial C}{\partial t} = D^* \frac{\partial^2 C}{\partial x^2} \tag{7.9}$$

Fick's second law for reactive solutes, where adsorption on clay mineral surfaces occurs during diffusive transport in clay soil, can be expressed by equation (7.10) incorporating the retardation factor (Freeze and Cherry, 1979, Shackelford and Daniel, 1991, Mitchell, 1993; and many others).

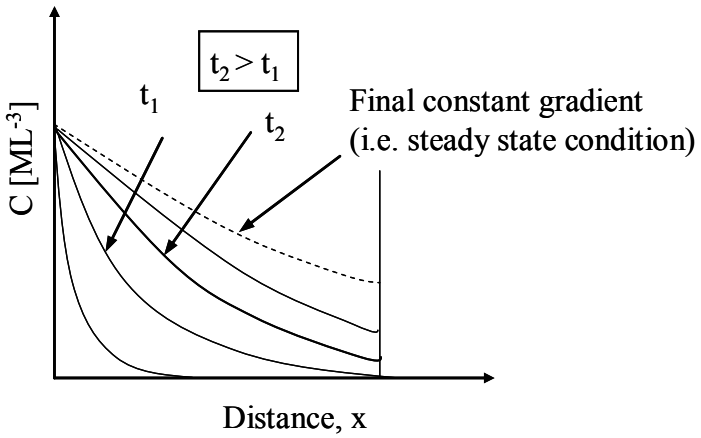

Figure 7.4 Diffusion as a Function of Distance and Time

$$\frac{\partial C}{\partial t} = \frac{D^*}{R_d} \cdot n \cdot \frac{\partial^2 C}{\partial x^2} = D^*_A \left(\frac{\partial^2 C}{\partial x^2} \right) \tag{7.10}$$

The value of ($D^* n/R_d$), replaced by D^*_A, is defined as the "apparent diffusion coefficient" by many researchers (Quigley *et al.* 1987; Li and Gregory, 1974).

7.1.2.1 Mathematical Solution to Diffusion Equation

The partial (second order) differential equation (7.10) which has been solved mathematically by various researchers in the form of equation (7.11) as suggested by Ogata (1970) and Freeze and Cherry (1979) is most popular among engineers.

$$\frac{C}{C_O} = erfc\frac{x}{2\sqrt{D^*_A t}} = 1 - erf\frac{x}{2\sqrt{D^*_A t}} \qquad (7.11)$$

where C is the concentration at any time, C_o is the constant supply concentration, and x is the distance of travel at time t. The initial concentration of the medium through which diffusion occurs is considered to be zero at t = 0. Equation (7.11) can also be fitted to a forward difference numerical solution which can be easily implemented in a spreadsheet as outlined below.

The purpose of solving the differential equation would be to calculate the concentration of solute ($C_{x,t}$) at any depth of the clay medium as time progresses. The subscripts (x,t) of concentration C, have been changed so as to provide more arithmetic representation as follows:

$$C_{x,t} \Rightarrow C_{i,j} \quad \text{where,} \quad i \rightarrow x \ \text{(depth)}$$
$$j \rightarrow t \ \text{(time)}$$

Since the solution is required for 1-D vertical diffusion flow, the clay layer has been divided into a number of thin layers with a distance or depth of Δx. It is first required to calculate the concentration at $C_{i,j+1}$ based on neighboring locations on previous time as $C_{i-1,j}, C_{i,j},$ and $C_{i+1,j}$ as follows:

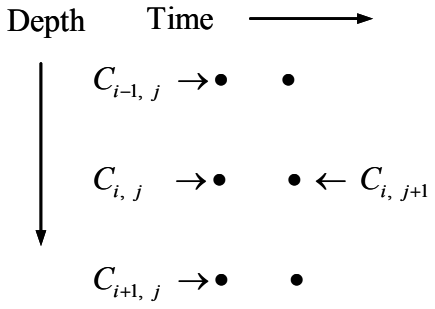

To find $\left(d^2C/dx^2\right)$ in a finite difference scheme, the concentration function $C = f(x)$ about point i can be expanded using Taylor's series expansion.

$$C_{(i+1)} = C_i + \Delta x\left(\frac{\partial C}{\partial x}\right)_i + \frac{\Delta x^2}{2!}\left(\frac{\partial^2 C}{\partial x^2}\right)_i + \frac{\Delta x^3}{3!}\left(\frac{\partial^2 C}{\partial x^2}\right)_i + \frac{\Delta x^4}{4!}\left(\frac{\partial^2 C}{\partial x^2}\right)_i + \ldots \quad (7.12)$$

$$C_{(i-1)} = C_i - \Delta x\left(\frac{\partial C}{\partial x}\right)_i + \frac{\Delta x^2}{2!}\left(\frac{\partial^2 C}{\partial x^2}\right)_i - \frac{\Delta x^3}{3!}\left(\frac{\partial^2 C}{\partial x^2}\right)_i + \frac{\Delta x^4}{4!}\left(\frac{\partial^2 C}{\partial x^2}\right)_i - \ldots \quad (7.13)$$

Adding equations (7.12) and (7.13) would result in equation (7.14).

$$C_{(i+1)} + C_{(i-1)} = 2C_i + \Delta x^2\left(\frac{\partial^2 C}{\partial x^2}\right)_i + 2\frac{\Delta x^4}{4!}\left(\frac{\partial^2 C}{\partial x^2}\right)_i + \ldots \quad (7.14)$$

Since the value of Δx^2 is small, the value of Δx^4 is even smaller and can therefore be neglected. By rearranging equation (7.14), the expression of $\left(\partial^2 C / \partial x^2\right)$ can be written as follows:

$$\frac{\partial^2 C}{\partial x^2} = \left[\frac{C_{(i+1),t} + C_{(i-1),t} - 2C_{(i,t)}}{\Delta x^2}\right] \quad (7.15)$$

The partial differential term on the left side of Fick's second law in equation (7.10) can be refined as follows:

$$\frac{\partial C}{\partial t} = \left[\frac{C_{(i,t+\Delta t)} - C_{(i,t)}}{\Delta t}\right] \quad (7.16)$$

By substituting equations (7.15) and (7.16) into equation (7.10), the concentration of solute at any location *i* after an infinitesimal time interval Δt can be calculated using equation (7.17).

$$C_{(i,t+\Delta t)} = C_{(i,t)} + \frac{\Delta t \cdot D^*_A}{\Delta x^2}\left[C_{(i+1),t} + C_{(i-1),t} - 2C_{(i,t)}\right] \quad (7.17)$$

It can be seen from equation (7.17) that the value of concentration at a node at the next time step ($t + \Delta t$) is determined from the values at the current time at the three adjacent nodes (i-1, i, and i+1). In this formulation, Δt is the incremental time step in the numerical solution, and Δx is the increment in space in the direction, x.

Boundary conditions on the sides of the clay medium during diffusion play an important role in calculating and representing graphically the diffusion profile with the variation of time during the transient period before achieving steady-state condition. In this research, a source of constant concentration, C_o, has been applied and the

concentration at a depth is presented in proportion to the initial concentration, in the form of C/C_o, as shown later in the chapter. Graphs are plotted to show the change in concentration as isochrones of C/C_o with respect to elapsed time.

7.1.3 Chemico-Osmotic Flow

Osmosis flow is considered when the clay material acts like a semipermeable membrane. Osmosis is a process when a membrane restricts the passage of solutes while allowing the flow of solvent due to the difference in concentration of the solvent between the both sides. The transport of solvent (eg. water) stops when the concentrations of the solutions on both sides are the same, or when the hydraulic pressure across the membranes equals the osmotic pressure difference between the two solutions, as sketched in figure 7.5.

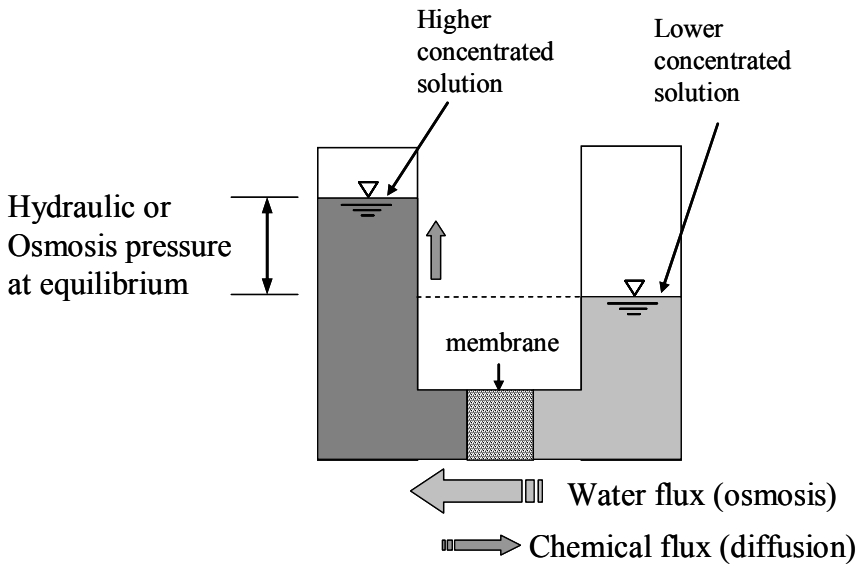

Figure 7.5 Chemico-Osmosis of Solute Transport

It can be seen from figure 7.5 that the chemico-osmosis phenomenon counteracts the flow of solute and therefore reduces the contaminant outward flux (Malusis *et al.,* 2001; Shackelford *et al.*, 2001).

The chemico-osmosis efficiency coefficient, ω, also known as the reflection coefficient, σ, is defined as the ratio of the pressure difference induced across the membrane as a result of prohibiting chemico-osmotic flux of solution (ΔP) to the theoretical chemico-osmotic pressure difference across an 'ideal' semipermeable membrane (Δπ) subjected to an applied difference in solute concentration as shown in equation (7.18) (Malusis *et al.* 2003; Keijer, 2000).

$$\omega = \frac{\Delta P}{\Delta \pi} \tag{7.18}$$

It can also be defined as the ratio of the developed hydraulic pressure over the applied osmotic pressure after equilibrium i.e. at zero solution flux (Keijer, 2000). The chemico-osmotic efficiency coefficient, ω, ranges from zero (ω =0) for non-membranes to unity (ω =1) for 'ideal' membranes that completely restrict the passage of solutes. Clay minerals can be considered to be 'non-ideal' membranes with ω < 1.

The theoretical value of osmotic pressure (Δπ) is calculated with respect to concentration variation at the membrane boundaries by the van't Hoff equation (7.19) (Malusis and Shackelford, 2002; Mitchell, 1993).

$$\Delta \pi = RT \sum_{i=1}^{N} \left(C_{i,H} - C_{i,L} \right) \tag{7.19}$$

where, R = the universal gas constant [8.314 J $mol^{-1}K^{-1}$ or 0.0821 atm $mol^{-1}K^{-1}$], T = the absolute temperature [K], $C_{i,H}$ = the initial high concentration of solute *i* species [mol L^{-3}], and $C_{i,L}$ = the initial low concentration of solute *i* species on the other side of the membrane. The induced hydraulic pressure can be calculated or measured from the levels of the standpipes connected to the solutions on both sides of the membrane, which varies with time until it reaches equilibrium with constant elevations of solution on both sides.

A steady-state solute flux through the semipermeable clay specimen is established and maintained when (a) the osmotic pressure is counterbalanced by the hydraulic pressure and (b) constant flow of solute diffusion occurs due to the difference in concentration gradient.

7.1.4 Determination of Diffusion Parameters

The developed hydraulic pressure due to osmosis can be measured by observing the solution levels of the higher concentrated standpipe or by using a differential pressure transducer placed on both sides of the membrane (Shackelford and Lee, 2003). The pressure gradually increases with time until it reaches its peak value and then decreases due to diffusion of solute until it reaches its steady-state condition. A typical graph of these processes with respect to induced chemico-osmotic pressure (ΔP) and elapsed time is drawn in figure 7.6 (Shackelford and Lee, 2003).

During the process of solute transport due to diffusion and chemico-osmosis, the concentration of the solution is measured from the concentration of individual species of solute. In the steady-state condition, the measured concentrations for a given solute are converted to cumulative mass per unit cross-sectional area, Q_t, as given in equation (7.20) (Malusis *et al.* 2001; Shackelford and Lee, 2003).

$$Q_t = \frac{1}{A}\sum_{i=1}^{N}\Delta m_i = \frac{1}{A}\sum_{i=1}^{N} C_i \Delta V_i \qquad (7.20)$$

where, A = cross-sectional area of the specimen, Δm_i = mass increment of the solute species *i* collected over a time increment (Δt), ΔV_i = increment volume of the solution from which the outflow flux is collected, C_i = the concentration of the solute species in the incremental volume, and N = number of incremental samples (solution) collected during the total elapsed time, *t*. The values of Q_t calculated from equation (7.20) with respect to elapsed time can be plotted as shown in figure 7.6 (Shackelford and Lee, 2003; Malusis *et al.*, 2001).

It is seen from figure 7.7 that the constant slope line, which represents the steady-state diffusion, intersects with the time axis at t_L , commonly known as lag time (Shackelford, 1991; Malusis *et al.*, 2001). The time, t_{ss}, in figure 7.7 denotes the time required for steady-state diffusion or the time until which transient diffusion occurs within the specimen due to chemico-osmosis of the semipermeable clay membrane.

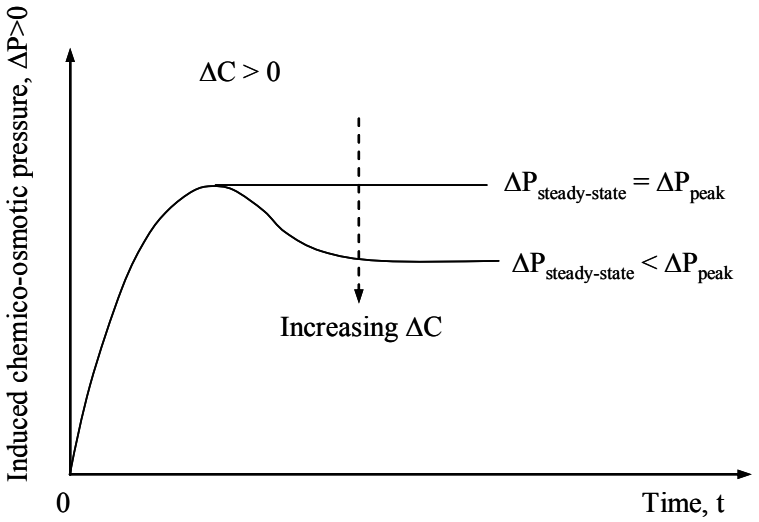

Figure 7.6 Induced Chemico-Osmotic Pressure Observed for Clay Membranes (Shackelford and Lee, 2003)

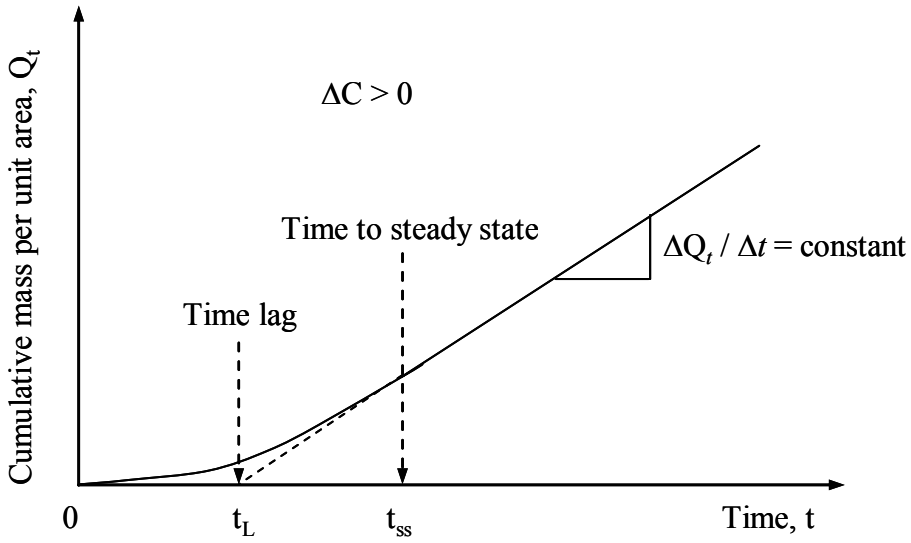

Figure 7.7 Cumulative Solute Mass Through Clay Specimen due to Diffusion (Shackelford and Lee, 2003; Malusis *et al*., 2001)

The analytical solution for cumulative mass flux (Q_t) due to diffusion in 1-D direction under steady-state condition has been investigated by many researchers. The expression given in equation (7.21) by Crank (1975) and Shackelford (1991) is applicable for a constant source concentration, C_o, and a perfectly flushing boundary condition (concentration of solute is kept zero).

$$Q_t = \frac{nD^* C_o}{L} t - \frac{nR_d L C_o}{6} \tag{7.21}$$

where, n = the specimen porosity, L = length or thickness of the specimen, D* = effective diffusion coefficient, R_d = the retardation factor, and t = total elapsed time of diffusion flow. The slope $(\Delta Q_t / \Delta t)$ of figure (7.6) which represents the steady-state diffusion condition is obtained by best-fit regression of the straight portion of the graph. The value of effective diffusion coefficient, D*, of any solute species can be computed using equation (7.21) by considering the term $(nR_d LC_o / 6)$ as zero at steady-state condition, which gives the following equation (7.22)

$$D^* = \left(\frac{\Delta Q_t}{\Delta t}\right)\left(\frac{L}{nC_o}\right) \tag{7.22}$$

The value of retardation factor, R_d, of any solute species can be computed by using equation (7.21) and lag time, t_L, at time intersection when $Q_t = 0$ as follows:

$$R_d = \frac{6D^*}{L^2} t_L \tag{7.23}$$

The value of D* calculated from equation (7.22) is used to evaluate the value of R_d from equation (7.23).

The total solute mass flux of any dissolved chemical species (i), J_i, through low permeability clay due to advection, chemico-osmosis, and diffusion can be written as follows (Mitchell, 1993; Malusis and Shackelford, 2002, 2004):

$$J_i = J_{a,i} + J_{\pi,i} + J_{d,i} = (1-\omega) q_h C_i + q_\pi C_i - nD^*_{A,i} \frac{\partial C_i}{R_d \partial x} \tag{7.24}$$

where, $J_{a,j}$ = advection solute flux due to hydraulic gradient (i_h), ω = chemico-osmotic efficiency coefficient ($0 \le \omega \le 1$), q_h = Darcy's flux (=$k_h i_h$, where k_h = hydraulic coefficient), J_π = chemico-osmotic solute flux, q_π [= $\omega k_h i_\pi$, where i_π = the gradient in chemico-osmotic pressure head] is the chemico-osmotic solute flux for a unit difference in concentration from lower solute concentration to higher solute concentration (i.e.,

opposite to the direction of solute diffusion), n = porosity, $D^*_{A,i}$ = effective salt-diffusion coefficient, and C_i = initial influent molar solute concentration.

The chemico-osmotic coefficient controls the types of flow to be considered for evaluating the solute mass through the semipermeable membrane barriers. If the value of ω is close to zero (i.e. non-membrane, permeable layer), then, $q_\pi \rightarrow 0$, and equation (7.24) would become the conventional advection-diffusion solute mass flux expression as given in equation (7.25).

$$J_i\big|_{\omega=0} = J_{a,i} + J_{d,i} = q_h C_i - nD^*_{A,i} \frac{\partial C_i}{R_d \partial x} \qquad (7.25)$$

However, when the value of ω is close to unity (i.e. ideal membrane, impermeable layer), then, the advection flow would be zero and the chemico-osmotic flux and diffusion will become the same which would cancel each other, eventually causing the resultant solute flux of equation (7.24) to become zero (J →0) (Malusis and Shackelford, 2003).

7.2 Analysis of Diffusion Test Results

Analysis of diffusion test results was carried out in order to determine the various diffusion parameters, namely, effective diffusion coefficient of inorganic chemical elements (D*), retardation factor (R_d), partition coefficient (K_p), and apparent diffusion coefficient (D^*_A). The following sub-sections describe these diffusion parameters in detail.

7.2.1 Lag Time and Time to Steady-State

In order to obtain the lag time and time to steady-state as explained in figure 7.6, electrical conductivity values taken at regular interval of time were accumulated with

time of diffusion and plotted as cumulative electrical conductivity vs diffusion time, as shown in figures B.1(b) to B.11(b) in appendix B. A straight line was drawn for each graph using linear regression, and the intercept of the straight line on the diffusion time axis was taken as the lag time. The point where the curve generated during the initial stage of diffusion joins the straight line is known as time to steady-state. The lag time and time to steady-state of diffusion tests carried out in this study are tabulated in Table 7.1.

Since the values of lag time and time to steady-state vary with the void ratio, specimen thickness, and concentration of diffusant, diffusion tests were divided into three groups, as shown in Table 6.3 of Chapter six. Lag time and time to steady-state are required to be measured as accurately as possible using consistent statistical methods. Because of the slight scattering in data from a theoretical straight line, even after attaining the steady-state condition, a sequential linear regression method was used to obtain the best possible straight line for the steady-state condition. The sequential linear regression was carried progressively from the last 3 data points of the EC versus time data with an increment of one additional data point in successive regression cycles. In each regression cycle, the coefficient of determination, R^2, was calculated and compared with the next regression analysis coefficient until a significant deviation in R^2 was found. The data point corresponding to the location where R^2 starts to drop significantly from the previous regression cycle represents the time when the transient diffusion ends. This data point also represents the transition from the initial non-linear curve to the linear slope line. Therefore, the elapsed time associated with the earliest maximum R^2 value of the regression analysis represents the time required to establish steady-state diffusion of the solute, t_{ss}, as explained in figure 7.6.

The straight line representing the steady-state diffusion, obtained from the sequential linear regression, is then extended to the horizontal (time) axis, and the intercept value on the time scale is established as the lag time, t_L, of the diffusion solute. A summary of the statistical methods for all the diffusion tests with R^2 values are tabulated in Table 7.1.

Table 7.1 Summary of Statistical Method for Steady-State Diffusion

Test No.	Number of data points used	R^2	Steady-state equation
D-6	18	0.9982	Y = 382.82X - 14913
D-8	9	0.9978	Y = 566.66X – 25387
D-9	16	0.9896	Y = 359.66X – 14468
D-10	15	0.9959	Y = 453.78X - 17907
D-11	17	0.9940	Y = 847.67X - 20905
D-12	24	0.9979	Y = 1664.1X – 13584
D-13	7	0.9904	Y = 756.82X – 40684
D-14	23	0.9973	Y = 1116.7X – 15682
D-16	17	0.9979	Y = 677.77X - 13165

The time to steady-state and lag time obtained using the above statistical methods for all the diffusion tests conducted in this study are listed in Table 7.2 with corresponding void ratios of the test specimens. The times to steady state are compared to theoretical values generated from the numerical analysis as explained later in this chapter. The amount of influx coming out of the specimen after achieving the steady-state condition is found to be constant for any interval of time as defined by the slope of the straight line drawn on the graphs shown in figures B.1(b) to B.11(b). From the test results of group #3 of equal void ratio of test specimens, it was found that the lag time of cations follows the sequence $Ca^{2+} < Na^{+} < K^{+} < Mg^{2+}$, which means that the calcium cations lag time is the shortest, followed by sodium, potassium, and magnesium.

Table 7.2 Lag Time and Time to Steady-State of Various Diffusants

Group #	Test number	Source solution	Void ratio	Lag Time (days)	Time to Steady-state (days)
1	D-6	2M $CaCl_2$	9.23	39	53
	D-11	2M $CaCl_2$	14.35	25	36
	D-12	5M $CaCl_2$	14.35	8	9
	D-13	5M $CaCl_2$	4.11	54	63
2	D-10	2M NaCl	14.35	40	58
	D-14	5M NaCl	14.35	14	18
	D-16	5M NaCl	6.67	19	26
3	D-8	2M $MgCl_2$	14.35	45	58
	D-9	2M KCl	14.35	40	58
	D-10	2M NaCl	14.35	40	58
	D-11	2M $CaCl_2$	14.35	25	36

7.2.2 Diffusion Coefficient

Two types of diffusion coefficient, namely, effective diffusion coefficient (D^*) and apparent diffusion coefficient (D^*_A) are calculated in this study. The effective diffusion coefficient (D^*) of any cation is calculated using equation 7.22 as follows:

$$D^* = \left(\frac{\Delta Q_t}{\Delta t}\right)\left(\frac{L}{nC_o}\right) \tag{7.22}$$

The slope of the steady-state line as shown in figures B.1(b) to B.11(b) is converted from a change in electrical conductivity per unit time [microSiemen/day] to change of mass flux per unit area per unit time [mg/(cm^2 x s)]. This conversion is carried out according to the following steps:

(a) The electrical conductivity in microsiemens is multiplied by 0.66 to obtain the mass flux concentration in ppm (mg/liter).

(b) The mass flux in ppm (mg/liter) is multiplied by the volume of receptor solution (after dilution) to calculate the total mass flux in mg.

(c) The total mass flux is distributed among its cations and anions components. At steady-state condition, in order to fulfill the electroneutrality requirement, the charge flux of the anions (in this case is the chloride anion, Cl^-) is of the same magnitude as the charge flux of the cations (that constituents the salt solution, namely, Na^+,K^+,Mg^{2+}, and Ca^{2+}) according to the following equation 7.26.

$$J_{anion}|z_{anion}| = J_{cation}|z_{cation}| \qquad (7.26)$$

where J_{anion} and J_{cation} are the steady-state diffusive molar fluxes of anions and cations, and z_{anion} and z_{cation} are the charges of anions and cations respectively. The steady-state diffusive molar flux of chloride (Cl^-) anion will therefore be the same magnitude of the steady-state diffusive molar flux of monovalent cations and twice the magnitude of divalent cations. However, in order to obtain the mass fluxes of Cl^-, the above ratios are required to be multiplied by the ratio of atomic weight of cation to the atomic weight of Cl^-. For example, for the NaCl solution, the magnitude of the steady-state diffusive mass flux of Cl^- will be [= 1 x (23/35.453)] 0.648 times the magnitude of the sodium (Na^+) cation mass flux. Similarly, for $CaCl_2$ solution, the ratio of mass flux for Ca^{2+} and Cl^- at steady-state will be 1:2.26.

(d) The value obtained in step 2 is divided by the cross-sectional area [cm^2] of the clay specimen.

(e) The units are them converted to a consistent set of unties to finally attain the unit of mg/(cm^2 x s).

After calculating the slope of the steady-state line in mg/(cm^2 x s) for a particular cation mass flux per unit area per duration of diffusion, the source concentration of the same cation, C_o, is then calculated in mg/cm^3. For example, for a 2M $CaCl_2$ solution, the

theoretical value of C_o would be [= 80,000 ppm = 80,000 mg/liter = 80,000 mg / 1000 cm^3] = 80 mg/cm^3. The value of [$L/(nC_o)$] is then calculated in cm^4/mg, since the porosity, n, is dimensionless, and the length or thickness of the specimen is in cm. The units of the effective diffusion coefficient is therefore [$mg/(cm^2$ x s) x cm^4/mg] or cm^2/s which is then converted to the more commonly used unit of cm^2/day as shown in the Table 7.3. The source concentration, Co, was calculated based on individual cation concentration of the synthetic salt solution. For example, for the 2M $CaCl_2$ source solution, the concentration C_o is 40,000 x 2 = 80,000 ppm or mg/l.

Table 7.3 Worksheet for the Calculation of Effective Diffusion Coefficient, D* of Various Cations

Test No.	Source Solution	Porosity n	L (cm)	Slope (EC/day)	Receptor Vol. (ml)	Outflux (mg)	Cations (mg)	$(\Delta Q/\Delta T)$ $mg/cm^2/s$	C_o (mg/l)	(L/nC_o) cm^4/mg	D* (cm^2/s) (Cations)	D* (m^2/s) (Cations)
D-6	2M $CaCl_2$	0.902	0.8	382.82	250	63.1653	19.3698	4.9E-06	80000	0.011086	5.45E-08	5.45E-12
D-8	2M $MgCl_2$	0.935	0.3	566.66	250	93.4989	39.4325	1.0E-05	48600	0.006602	6.61E-08	6.61E-12
D-9	2M KCl	0.935	0.3	359.66	250	59.3439	28.2212	7.2E-06	78200	0.004103	2.94E-08	2.94E-12
D-10	2M NaCl	0.935	0.3	453.78	250	74.8737	45.4125	1.2E-05	46000	0.006975	8.04E-08	8.04E-12
D-11	2M $CaCl_2$	0.935	0.3	847.67	250	139.866	42.8901	1.1E-05	80000	0.004011	4.37E-08	4.37E-12
D-12	5M $CaCl_2$	0.935	0.3	1664.1	250	274.577	84.1995	2.1E-05	200000	0.001604	3.43E-08	3.43E-12
D-13	5M $CaCl_2$	0.935	0.3	756.82	250	124.875	38.2933	9.7E-06	200000	0.001863	1.81E-08	1.81E-12
D-14	5M NaCl	0.935	0.3	1116.7	250	184.256	111.755	2.8E-05	115000	0.002790	7.91E-08	7.91E-12
D-16	5M NaCl	0.935	0.3	677.77	250	111.832	67.8285	1.7E-05	115000	0.002999	5.16E-08	5.16E-12

In order to calculate the apparent diffusion coefficient, (D^*_A), the relationships of retardation factor, R_d, with diffusion coefficients as given in equations 7.10 and 7.23 were rearranged and the following expression was deduced in terms of the lag time and the physical dimensions of the test specimen.

$$D^*_A = \frac{nL^2}{6t_L} \tag{7.27}$$

The values of apparent diffusion coefficients, (D^*_A), of various cations used as source solution during the diffusion tests through bentonite are calculated using equation 7.27 and are tabulated in Table 7.4. By comparing the tests D-8, D-9, D-10, and D-11 of the same porosity and thickness specimens using the same concentrated diffusants, it can be found that the apparent diffusion coefficient of Ca^{2+} (i.e. 6.49×10^{-13} m^2/s) is higher than those of other cations due to its higher replaceability capacity as compared with others cations used in bentonite.

Table 7.4 Apparent Diffusion Coefficient for Various Cations in Bentonite

Test No.	Source Solution	Porosity n	L (cm)	Lag Time (days)	D^*_A (m^2/s) (Cations)
D-6	2M $CaCl_2$	0.902	0.8	39	2.86E-12
D-8	2M $MgCl_2$	0.935	0.3	45	3.61E-13
D-9	2M KCl	0.935	0.3	40	4.06E-13
D-10	2M NaCl	0.935	0.3	40	4.06E-13
D-11	2M $CaCl_2$	0.935	0.3	25	6.49E-13
D-12	5M $CaCl_2$	0.935	0.3	8	2.03E-12
D-13	5M $CaCl_2$	0.805	0.3	54	2.59E-13
D-14	5M NaCl	0.935	0.3	14	1.16E-12
D-16	5M NaCl	0.87	0.3	19	7.95E-13

7.2.3 Retardation Factor

Lag time is again used to calculate the retardation factor, R_d, of individual cations using the expression given in equation 7.23. Retardation factor is directly proportional to both effective diffusion coefficient and lag time. The values of retardation factor of all the cations used in this study are given in Table 7.5.

Table 7.5 Retardation Factor of Various Cations in Bentonite

Test No.	Source Solution	L (cm)	Porosity n	Lag Time (days)	D* m^2/s (Cations)	R_d (Cations)
D-6	2M $CaCl_2$	0.8	0.902	39	5.45E-12	1.722
D-8	2M $MgCl_2$	0.3	0.935	45	6.61E-12	17.126
D-9	2M KCl	0.3	0.935	40	2.94E-12	6.771
D-10	2M NaCl	0.3	0.935	40	8.04E-12	18.522
D-11	2M $CaCl_2$	0.3	0.935	25	4.37E-12	6.287
D-12	5M $CaCl_2$	0.3	0.935	8	3.43E-12	1.580
D-13	5M $CaCl_2$	0.3	0.805	54	1.81E-12	5.633
D-14	5M NaCl	0.3	0.935	14	7.91E-12	6.381
D-16	5M NaCl	0.3	0.87	19	5.16E-12	5.649

The retardation factor of all the individual cations is found to be more than unity, as listed in Table 7.4, which indicates that adsorption happens on the surface of clay platelets due to diffusion flow of the cations (Ca^{2+}, Mg^{2+}, K^+, and Na^+). The smallest retardation factor was obtained for calcium cations with a highly porous bentonite specimen (D-12), probably because of its minimum resistance to diffusion on bentonite clay platelets at steady-state condition. The 2M NaCl source solution produces the maximum retardation factor (test. D-10) indicating a maximum resistance to diffusion on bentonite clay platelets at steady-state condition. The thickness of diffuse double layer is higher in sodium concentrated solution than in calcium concentrated solution, which

results in a zone of immobility within the pore spaces. By comparing test D-10 and D-14 for 2M NaCl and 5M NaCl source solutions, respectively, it can be concluded that the higher concentrated solutions generate lower retardation factors because of the lower diffuse double layer thickness which eventually creates more available pore spaces for solute mobility. The same trend can be observed in calcium solutions where higher concentrated source solution (D-12) develops lower retardation factor compared to lower concentrated source solution (D-11) for bentonite of the same porosity.

7.2.4 Partition Coefficient

The partition coefficient, K_p, is defined as the ratio of the adsorbed concentration on the clay surfaces to the concentration of solution in equilibrium. It be calculated using equation 7.8 after calculating the value of retardation factor of each individual cations. The values of partition coefficient of all the cations used in this study are given in Table 7.6.

It can be highlighted from Table 7.6 that the minimum partition coefficient was found in calcium source solutions (e.g. $K_p = 0.492$ from D-12 of 5M $CaCl_2$) which represents the minimum adsorption on the clay platelet surfaces. The maximum partition coefficient (Kp = 14.88) was found in test D-10 with the 2M NaCl solution, indicating the maximum adsorption on the clay platelet surfaces. It can be concluded, from tests D-11 and D-12 on 2M $CaCl_2$ and 5M $CaCl_2$ diffusants, respectively, that for clay specimens of the same porosity, the higher concentrated diffusant results in a lower partition coefficient due to the collapse of clay platelets as a result of shrinkage in the diffuse double layer and the formation of more aggregated particles where the total adsorption capacity per unit surface area decreases compared with the increasing concentration of pore fluid in equilibrium. The 2M $MgCl_2$ diffusant also resulted in a higher partition coefficient, which could be due to its higher hydrated ionic radius that gets obstructed in the diffuse double layer. More diffusion tests are necessary in order to

conclude the mechanism of diffusivity of magnesium and potassium cations in bentonite clay.

Table 7.6 Partition Coefficient of Various Cations in Bentonite

Test No.	Source solution	porosity n	Bulk density ρ_b (g/ml)	R_d (Cations)	K_p (Cations)
D-6	2M $CaCl_2$	0.902	1.152	1.722	0.565
D-8	2M $MgCl_2$	0.935	1.101	17.126	13.694
D-9	2M KCl	0.935	1.101	6.771	4.901
D-10	2M NaCl	0.935	1.101	18.522	14.880
D-11	2M $CaCl_2$	0.935	1.101	6.287	4.490
D-12	5M $CaCl_2$	0.935	1.101	1.580	0.492
D-13	5M $CaCl_2$	0.805	1.303	5.633	2.862
D-14	5M NaCl	0.935	1.101	6.381	4.570
D-16	5M NaCl	0.87	1.202	5.649	3.365

7.2.5 Diffusion Coefficient Through Numerical Solution

The apparent diffusion coefficient (D^*_A) obtained from the lag time method can be used in calculating the time to steady-state using numerical method, as explained in section 7.1.2.1. By knowing the boundary conditions and dividing the specimen into a number of thin layers, the time to steady-state of any particular diffusant can be obtained by the forward numerical difference method, as expressed in equation (7.17). A simple spreadsheet was formulated to calculate the diffusion mass flux at any particular time interval and location within the test specimen. The process of calculating the diffusion mass flux through the bentonite clay specimen continues until a steady-state condition is reached which satisfies the constant mass flux of diffusant obtained from the

experiments. In theory, complete steady state will never be reached, but a condition where the variation in concentration is almost linear with distance could be viewed as steady state.

The diffusion profile of Mg^{2+} cations using the 2M $MgCl_2$ diffusant through bentonite is shown in figure 7.8. Using the value of D^*_A obtained from the time-lag method, it can be found that the time required to achieve a constant diffusion mass flux at the receptor end is 56 days as compared to 58 days as calculated from lag time method given in Table 7.2 (D-8).

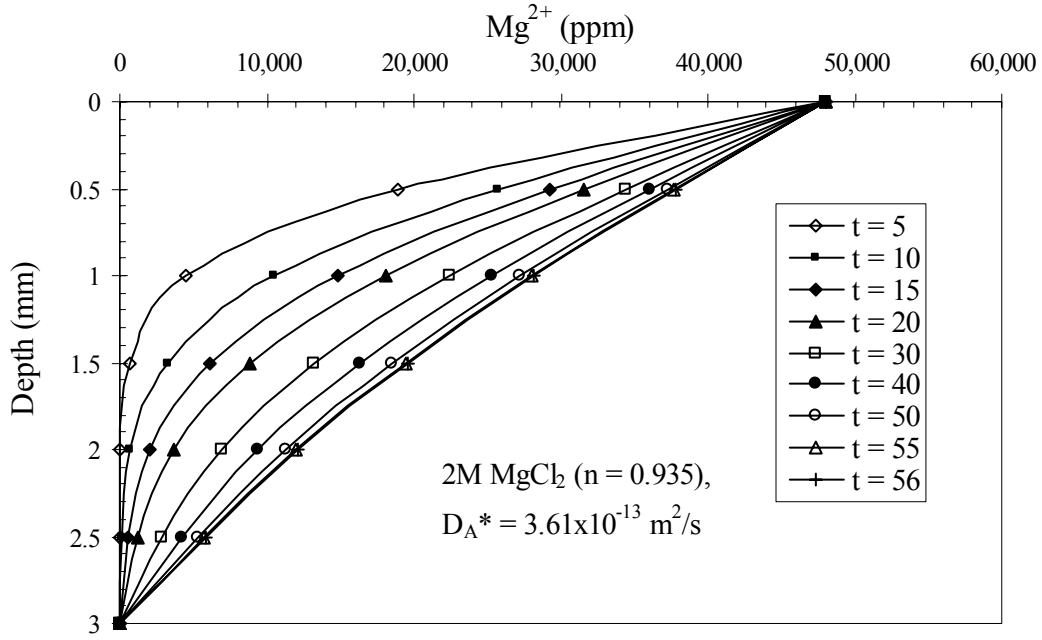

Figure 7.8 Diffusion Profile of Mg^{2+} Ions Using Numerical Method

The time required to satisfy the conditions of steady-state, which were derived from the lag time method for K^+ cations using a 2M KCl diffusant through bentonite specimen layer is 47 days as shown in figure 7.9. However, it took about 58 days to reach the steady-state condition using the lag time analysis as shown in Table 7.2.

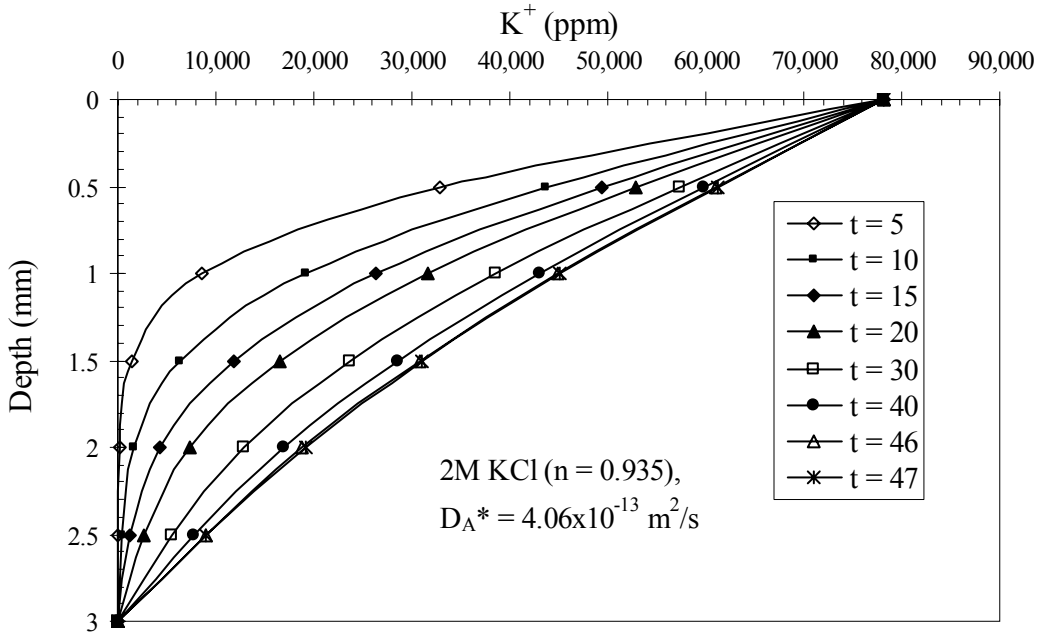

Figure 7.9 Diffusion Profile of K^+ Ions Using Numerical Method

Figures 7.10 and 7.11 show the diffusion profiles of Na^+ and Ca^{2+} cations respectively using numerical methods at various depths and durations until steady-state conditions as obtained by the lag time method were satisfied. The time to steady-state with Na^+ cation using the numerical method was found to be 41 days while that for Ca^{2+} cation was about 35 days, compared to 58 days and 36 days, respectively, from the lag time method (Table 7.2). It is therefore concluded that the numerical method under-predicts the time to steady state, compared to the lag time method. However, it can be seen from the slope of the diffusion profiles (figures 7.8 to 7.11) that further diffusion would result in a condition that better approximates the theoretical steady-state condition (straight line).

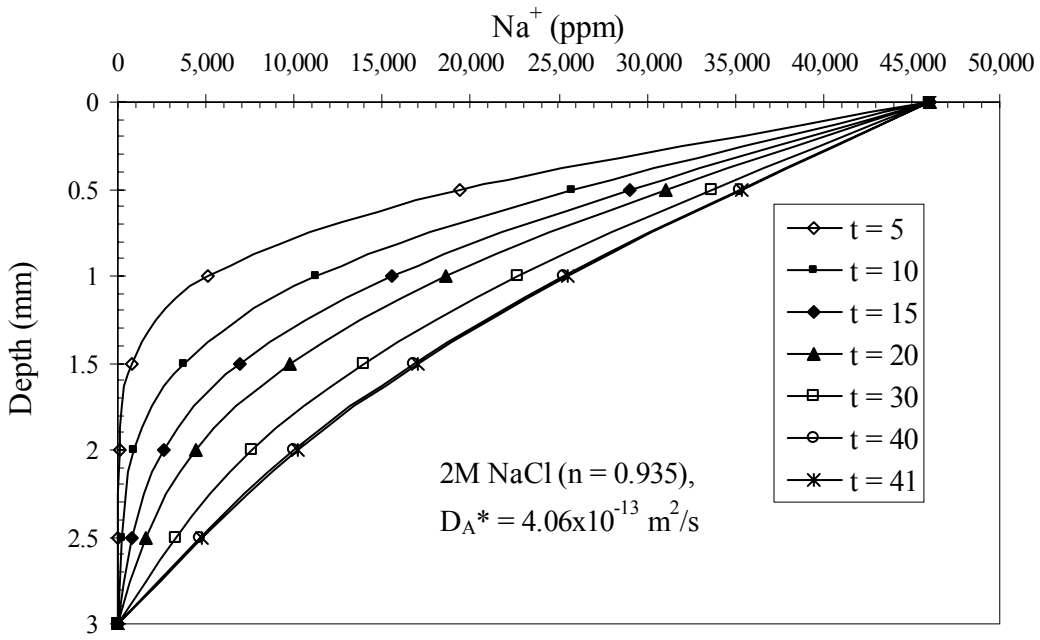

Figure 7.10 Diffusion Profile of Na^+ Ions Using Numerical Method

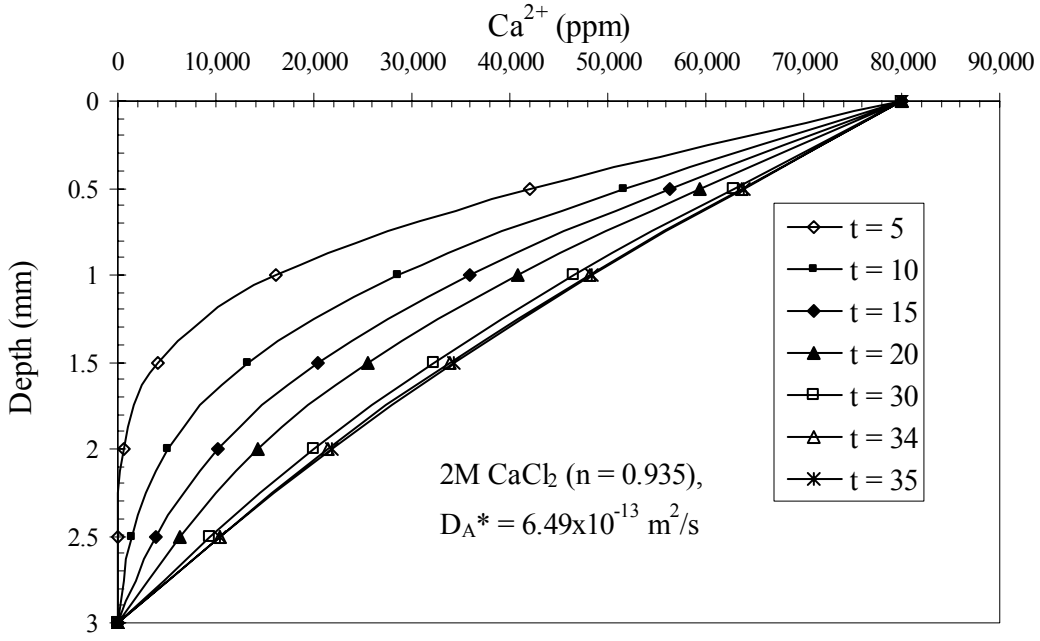

Figure 7.11 Diffusion Profile of Ca^{2+} Ions Using Numerical Method

CHAPTER EIGHT

SUMMARY AND RECOMMENDATIONS

8.1 Summary

While bentonite has been used as a flow barrier in many applications, its performance has been found to deteriorate when in contact with inorganic chemicals present in the leachate. Attempts have been made to find a relation between bentonite performance, in terms of coefficient of permeability, and its geotechnical properties. Aggregated platelets size distribution obtained using hydrometer tests were found to be inconsistent with the liquid limits tests obtained using the cone penetrometer, with finer aggregated platelets producing higher liquid limit in the sequence of Na>K>Mg>Ca. However, this finding was limited to 0.1 molar concentrated electrolyte solutions of the above inorganic salts.

No distinctive relationship was found to exist between the liquid limits and the coefficient of permeability obtained using both flexible wall and rigid wall permeameters. However, a strong correlation was found to exist between swell index and hydraulic conductivity and was attributed to the fact that similar mechanisms control both the swelling behavior and the hydraulic conductivity. Swell index values obtained using 1 molar concentration of various salt solutions (figure 3.22) were found to be in sequence with the values of coefficients of permeability obtained using rigid wall permeameter (Na<Mg<K<Ca). It is therefore possible to compare the permeability of bentonite qualitatively by simply performing swell index tests with various electrolyte solutions at 1 molar concentration.

Hydraulic equilibrium was found to occur at around 2 to3 pore volumes of flow, which is earlier than the flow required for chemical equilibrium determined using

electrical conductivity measurements. The coefficient of permeability measured from the flexible wall permeameter was found to be erratic because of the unpredictable and immeasurable shape of the swelling clay specimen during testing. Significant swelling of specimen occurred, especially while performing permeability tests using water and lower concentrated electrolyte solutions. Sidewall leakage channels, normally developing in rigid wall type experiments, can easily be eliminated when the bentonite clay specimens are hydrated and saturated for at least 48 hours before the actual permeation is carried out. Swelling of the bentonite upon hydration acts as a self sealing mechanism for all internal and sidewall channels.

Other than the type of permeameter, the most important factors affecting the permeability of bentonite are permeant chemical composition, void ratio, and initial hydration condition. A distinct variation in coefficient of permeability is observed between permeants containing sodium and calcium cations. Higher k values for permeants containing calcium is attributed to the fact that Ca^{2+} replaces monovalent cations, such as Na+, K+ and others attached on to the negatively charged clay surface, and thereby reduces the thickness of the diffuse double layer. Relationships for the variation in coefficient of permeability between sodium and calcium solutions, as well as void ratio relationships, were established. No significant variation of k of bentonite clay was observed upon applying hydraulic gradients at high as 3100, which discredits the concept of consolidation of bentonite at higher gradients.

Pre-hydration of bentonite clay plays an important role in its permeability. Different structures of the platelets are formed when hydrating with water and various inorganic electrolyte solutions before the actual permeation of the solution through the specimen.

Electrical conductivity of the effluent can be used as an indicator to monitor the amount of chemical retention during permeation by various inorganic electrolytes. No significant correlation could be found between pH and electrical conductivity of the effluent during permeation with various electrolyte solutions.

Various diffusion parameters, namely effective and apparent diffusion coefficients, retardation factor, and partition coefficient, of four different inorganic

chemical diffusants were investigated in this study. The time to steady-state determined from the lag time method was found to be slightly shorter than that from the forward numerical difference method. Calcium cations were found to diffuse faster than the other three cations (Na^+, K^+, Mg^{2+}), as identified by their retardation factor values. Higher sodium retardation factors indicate its strong affinity for the negatively charged clay surface for a longer period of time. Maximum sodium cation adsorption on the clay surface was also confirmed by its highest partition coefficient compared to other cations used in this study. Partition coefficients of the cations were found to be in the order of $Ca^{2+} < K^+ < Mg^{2+} < Na^+$.

8.2 Design Recommendation

Design recommendation can be made to bentonite clay of similar physical and engineering characteristics to be used as hydraulic barriers in the field. The relevant physical, chemical and engineering properties necessary for design are Atterberg limits, and swell index. Particle or aggregated clay platelets size distribution from hydrometer tests could be misleading because of the changes in specific gravity of the aggregated particles formed upon hydrated. Other limitations of the hydrometer test stem from the use of Stokes' law, which assumes the aggregated particle to be solid single spherical particle of pre-determined specific gravity.

Liquid and plastic limits of the bentonite used in this study were found to be 546% and 56%, respectively, while the free swell index determined using deionized water was 60 ml/2g of dry bentonite. The free swell index can also be measured using various inorganic salt solutions to provide a rapid indicator of the coefficient of permeability of the bentonite when permeated with the corresponding solutions. However, the coefficients of permeability of bentonite with various inorganic chemical permeants should be applied with caution since statistical confidence levels are not available. More data are required to validate the reproducibility of the test results before they can be used in design.

The amounts of chemicals retained in the saturated bentonite clay during permeation can be calculated using electrical conductivity measurements of the effluent, as described in Chapter 5, and correlate well with the weight increase of the actual bentonite clay after at the end of the test. An equivalent flow of five pore volume permeation is required in order to predict the maximum chemical retention within the bentonite clay during advection flow. The amounts of chemical retained in the case of divalent permeants are higher than in monovalent permeants. If the total amount of chemicals in the total influent of any containment can be calculated by the designer, the chemical outflux can be predicted by subtracting the total amounts of chemical retained in the bentonite clay during the first five pore volumes or so. The designer can also choose the thickness of the bentonite layer such that the retention capacity meets certain performance limits or criteria.

Diffusion profiles of various inorganic chemicals can be simulated up to steady-state conditions and allow the calculation of mass flux and diffusant concentration at any elapsed time and at any location within the bentonite clay barrier. By plotting the normalized concentration in terms of initial concentration of inorganic source chemical [C/C_o] versus depth factor normalized with respect to total depth [d/d_o], the diffusion mass flux can be predicted for any concentration of source diffusants at any depth within the bentonite clay medium. The solution can be easily adapted to varying source concentrations since it can be easily programmed in a spreadsheet.

REFERENCES

1. ASTM D 5890-02, "Standard Test Method for Swell Index of Clay Mineral Component of Geosynthetic Clay Liners," *Annual Book of ASTM Standards* 2002, Vol. 04.13, American Society for Testing and Materials, Philadelphia, PA.

2. ASTM D 422-63 (2002), "Standard Test Method for Particle-Size Analysis of Soils," *Annual Book of ASTM Standards*, 2002, Vol. 04.08, American Society for Testing and Materials, Philadelphia, PA.

3. ASTM D854-02 (2002) "Standard Test Methods for Specific Gravity of Soil Solids by Water Pycnometer" *Annual Book of ASTM Standards*, Vol. 04.08, American Society for Testing and Materials, Philadelphia, PA.

4. ASTM D 4318-00 (2000) "Standard Test Methods for Liquid Limit, Plastic Limit, and Plasticity Index of Soils," *Annual Book of ASTM Standards*, Vol. 04.08, American Society for Testing and Materials, Philadelphia, PA.

5. D2434-68(2000) "Standard Test Method for Permeability of Granular Soils (Constant Head)", *Annual Book of ASTM Standards*, Vol. 04.08, American Society for Testing and Materials, Philadelphia, PA.

6. D5084-00e1 "Standard Test Methods for Measurement of Hydraulic Conductivity of Saturated Porous Materials Using a Flexible Wall Permeameter", *Annual Book of ASTM Standards*, Vol. 04.08, American Society for Testing and Materials, Philadelphia, PA.

7. BS 1377-1975 Test 2(A), "Determination of Liquid Limit, Preferred Method using Cone Penetrometers," *British Standard Institution*.

8. ASTM C837-99 (2003) Standard Test Method for Methylene Blue Index of Clay.

9. Alther, G., Evans, J., Fang, H., and Witmer, K. (1985), "Influence of Inorganic Permeants upon the Permeability of Bentonite," *Hydraulic Barriers in Soil and Rock*, ASTM STP 874, A.I. Johnson et al., eds., ASTM, West Conshohocken, Pa., pp. 64-73.

10. Anderson, D.C., Crawley, W., and Zabcik, J.D. (1985), "Effects of Various Liquids on Clay Soil : Bentonite Slurry Mixtures," *Hydraulic Barriers in Soil and Rock*, ASTM STP 874, A.I. Johnson et al., eds., ASTM, West Conshohocken, Pa., pp. 93-103.

11. Anderson, D., and Brown, K.W. (1981), "Organic Leachate Effects on the Permeability of Clay Liners," in Landfill disposal: Hazardous Waste, *Proceedings of the 7th Annual Research Symposium*, Washington, D.C., U.S. Environmental Protection Agency, pp. 119-130.

12. Anderson, D., Brown, K.W., and Green, J. (1982), "Effects of Organic Fluids on the Permeability of Clay Soil Liners," in Landfill disposal: Hazardous Waste, *Proceedings of the 8th Annual Research Symposium*, Fort Mitchell, Kentucky, U.S. Environmenatl Protection Agency, pp. 179-190.

13. Ashmawy, A.K., El-hajji, D., Sotelo, N., and Muhammad, N. (2002), "Hydraulic Performance of Untreated and Polymer-Treated Bentonite in Inorganic Landfill Leachates", *Clays and Clay Minerals*, Vol. 50, No. 5, pp. 546-552.

14. Barbour, S.L. and Fredlund, D.G. (1989), "Mechanisms of Osmotic Flow and Volume Change in Clay Soils," *Canadian Geotechnical Journal*, vol. 26, pp. 551-562.

15. Beek, W.J., Muttzall, K.M.K., and Van Heuven, J.W. (1999), Transport Phenomena, 2nd edition, *John Wiley and Sons Ltd.*, West Sussex, England.

16. Ben, R.H., Tessier, D., and Ben H. A.A., (2000), "Mineralogy of the <2 micron Fraction of Three Mixed-Layer Clays from Southern and Central Tunisia," *Clay Minerals*, vol.35, no.2, pp.375-381.

17. Bennett, R.H., and Hulbert, M.H., (1986), Clay Microstructure, International Human Resources Development Corporation, Publishers, Boston, MA, USA. chapters 1, 2 & 3.

18. Benson, C.H. and Daniel, D.E. (1994a), "Minimum Thickness of Compacted Clay Liners: I. Stochastic Models," *Journal of Geotechnical Engineering*, ASCE, vol. 120, no. 1, pp. 129-152.

19. Benson, C.H. and Daniel, D.E., (1994b), "Minimum Thickness of Compacted Clay Liners: II. Analysis and Case Histories," *Journal of Geotechnical Engineering*, ASCE, vol. 120, no. 1, pp. 153-172.

20. Benson, C.H., Zhai, H., and Wang, X. (1994), "Estimating Hydraulic Conductivity of Compacted Clay Liners," *Journal of Geotechnical Engineering*, ASCE, vol. 120, no. 2, pp. 366-387.

21. Benson, C.H., Gunter, J.A., Boutwell, G.P., Trautwein, S.J., and Berzanskis, P.H., (1997), "Comparison of Four Methods to Assess Hydraulic Conductivity," *Journal of Geotechnical and Geoenvironmental Engineering*, ASCE, vol. 123, no. 10, pp. 929-937.

22. Bergaya, F, and Vayer, M. (1997), "CEC of clays; measurement by adsorption of a copper ethylenediamine complex," *Applied Clay Science*, vol.12, no.3, pp.275-280.

23. Bogardi, I., Kelly, W.E., and Bardossy, A. (1989), "A Reliability Model for Soil Liners: Initial Design," *Journal of Geoetchnical Engineering*, ASCE, vol. 115, no. 5, pp. 658-669.

24. Bogardi, I., Kelly, W.E., and Bardossy, A. (1990), "Reliability Model for Soil Liner: Postconstruction," *Journal of Geoetchnical Engineering*, ASCE, vol. 116, no. 10, pp. 1502-1520.

25. Bourg, I.C, Bourg, A.C.M, Sposito, G. (2003), "Modeling diffusion and adsorption in compacted bentonite; a critical review", *Journal of Contaminant Hydrology*, vol. 61, no. 1-4, pp. 293-302.

26. Boynton, S.S. and Daniel, D.E. (1985), "Hydraulic Conductivity Tests on Compacted Clay," *Journal of Geotechnical Engineering*, ASCE, vol. 111, no. 4, pp. 465-478.

27. Bradbury, M. H. and Baeyens, B. (2003), "Porewater Chemistry in Compacted Re-saturated MX-80 bentonite," *Journal of Contaminant Hydrology*, vol.61, no.1-4, pp.329-338.

28. Broderick, G.P. and Daniel, D.E. (1990), "Stabilizing Compacted Clay Against Chemical Attack," *Journal of Geotechnical Engineering, ASCE*, vol. 116, no. 10, pp. 1549-1567.

29. Brownlow, A.H. (1970), Geochemistry, Prentice-Hall, Inc., Englewood Cliffs, New Jersey.

30. Bruno, H. (2002), "Geosynthetic Clay Liners Offer Many Advantages for Containment Applications", http://www.esemag.com/0102/clay.html, Accessed 01/17/2004.

31. Bujdak, J., Janek, M., Madejova, J., Komadel, P. (2001), "Methylene Blue Interactions with Reduced-Charge Smectites," *Clays and Clay Minerals*, vol.49, no.3, pp.244-254, Jun 2001.

32. Cadena, F., Rizvi, R., and Peters, R. W. (1990), "Feasibility Studies for the Removal of Heavy Metals from Solution Using Tailored Bentonite," *Hazardous and Industrial Wastes Hazardous and Industrial Wastes - Proceedings of the Mid-Atlantic Industrial Waste Conference.* Publ by Technomic Publ Co Inc, Lancaster, PA, USA. p 77-94.

33. Canty, G.A., Atalay, A., Laguros, J.G., Robertson, J., and Pandey, K. K. (1995), "A Preliminary Assessment of Utilizing Fluidized Bed Ash in Landfill Liner Applications," *Journal of Environmental Science and health, Part A: Environmental Science & Engineering and Toxic & Hazardous Substance Control*, vol. 30, no. 2, Feb, pp. 439-459.

34. Cases, J.M., Berend, I., Francois, M., Uriot, J.P., Michot, L.J., Thomas, F. (1997), "Mechanism of Adsorption and Desorption of Water Vapor by Homoionic Montmorillonite; 3, The Mg^{2+}, Ca^{2+}, and Ba^{3+} exchanged forms," *Clays and Clay Minerals*, vol.45, no.1, pp.8-22.

35. Chapman, H.D. (1965), "Cation Exchange Capacity," In Methods of Soil Analysis – Part 2, *American Society of Agronomy*, Inc., Madison, Wisconsin.

36. Chapuis, R.P. (1990), "Sand-Bentonite Liners: Permeability from Laboratory Tests," *Canadian Geotechnical Journal*, vol. 27, pp. 47-57.

37. Chapuis, R.P. (2002), "The 2000 R.M. Hardy Lecture: Full-Scale Hydraulic Performance of Soil-Bentonite and Compacted Clay Liners," *Canadian Geotechnical Journal*, vol. 39, pp. 417-439.

38. Chen, K.Y. and Bowerman, F.R. (1974) "Mechanisms of Leachate Formation in Sanitary Landfills, in Recycling and Disposal of Solid Wastes: Industrial , Agricultural, Domestic," Yen, T.F. Ed.;56 Ann Arbor Science Pub., Ann Arbor.

39. Cheung, S.C.H. (1994), "Modeling of Inorganic Contaminant Transport in Dense Bentonite," *Journal of Soil Contamination*, vol. 3, no. 2, pp. 137-157.

40. Cheung, S.C.H. and Gray, M.N. (1989), "Mechanisms of Ionic Diffusion in Dense Bentonite," *Proceedings of Scientific Basis for Nuclear Waste Management XII symposium*, Materials Research Society, Pittsburgh, Pennsylvania, vol. 127, pp. 677-681.

41. Cheung, S.C.H., Oscarson, D.W., and Lopez, R.S. (1984), "Factors Influencing Mass Diffusion in Bentonite and Mixtures of Bentonite and Sand," *Materials Research Society Symposium*, Boston, MA, vol. 26, pp. 711-718.

42. Chmielova, M., Malac, Z., Merinska, D., Capkova, P., and Weiss, Z., (2000), "XRD analysis and modelling of Na-montmorillonite intercalated with octadecylamine," *Sixteenth conference on Clay mineralogy and petrology* in Karlovy Vary (Czech Republic) Acta Universitatis Carolinae. Geologica, vol.44, no.2-4, pp.91-93.

43. Christidis, G.E. (2001), "Formation and Growth of Smectites in Bentonites; a Case Study from Kimolos Island, Aegean, Greece," *Clays and Clay Minerals*, vol.49, no.3, pp.204-215.

44. Christidis, G.E. (1998), "Physical and Chemical Properties of Some Bentonite Deposits of Kimolos Island, Greece," *Applied Clay Science*, vol.13, no.2, pp.79-98.

45. Crank, J. (1975), The Mathematics of Diffusion, 2nd edition, *Clarendon Press*, Oxford, England.

46. du Plessis, J.P. and Ross, L.I. (1993), "Permeability Prediction for Water Seepage Through Low Porosity Granular Porous Media," *Water South Africa*, vol. 19, no. 2, Apr. pp. 147-152.

47. Daniel, D.E. (1984), "Predicting Hydraulic Conductivity of Clay Liners," *Journal of Geotechnical Engineering*, ASCE, vol. 110, no. 2, pp. 285-300.

48. Daniel, D.E. (1985), "Predicting Hydraulic Conductivity of Clay Liners," Reply. *Journal of Geotechnical Engineering*, ASCE, vol. 111, no. 12, pp. 1466-1467.

49. Daniel, D.E. (1989), "In Situ Hydraulic Conductivity Tests for Compacted Clays," *Journal of Geotechnical Engineering*, ASCE, vol. 115, no. 9, pp. 1205-1227.

50. Daniel, D.E. (1990), "A Rational Basis for Determining Safety of Containment," *Proceedings of the ASCE 17th Annual National Conference on Optimizing the Resources for Water Management*, Forth Worth, TX, pp. 489-493.

51. Daniel, D.E., et al. (1984), "Permeability Testing with Flexible-Wall Permeameters," *Geotechnical Testing Journal*, vol. 7, no. 3, pp. 113-122.

52. Daniel, D.E. (1993), "Clay Liners," Geotechnical Practice for Waste Disposal, D.E. Daniel, ed., *Chapman & Hall*, London, England, pp. 137-163.

53. Daniel, D.E. (1994), "State-of-the-Art: Laboratory Hydraulic Conductivity Tests for Saturated Soils," *In Hydraulic Conductivity and Waste Contaminant Transport*, ASTM, STP 1142, D.E. Daniel and S.J. Trautwein, eds., ASTM, West Conshohocken, Pa., pp. 30-78.

54. Daniel, David E., (1995), "Soil Barrier Layers Versus Geosynthetic Barriers in Landfill Cover Systems," *Proceedings of the 1995 Conference of the Geotechnical Engineering Division of ASCE in conjunction with the ASCE Convention,* San Diego, CA, Geotechnical Special Publication, no. 53, pp. 1-18.

55. Daniel, D.E. and Benson, C.H. (1990): "Water Content-Density Criteria for Compacted Soil Liners", *Journal of Geotechnical Engineering, ASCE,* vol. 116, no. 12, pp. 1811-1830.

56. Day, S.R. and Daniel, D.E. (1985), "Hydraulic Conductivity of Two Prototype Clay Liners," *Journal of Geotechnical Engineering*, ASCE, vol. 111, no. 8, pp. 957-970.

57. Dorsey, J.D., Ward, A.D., Fausey, N.R., and Blair, E.S. (1990), "A Comparison of Four Methods for Measuring Saturated Hydraulic Conductivity," *Transactions of the American Society of Agricultural Engineers* (ASE), vol. 33, no. 6, pp. 1925-1931.

58. Drever, J.I. (1982), The Geochemistry of Natural Waters, Prentice-Hall, Inc., Englewood Cliffs, N.J.

59. Edil, T.B. and Berthouex, P.M. (1990), "Earthen Barriers Technology For Waste Containment", *Journal of Waste Management*, vol. 10, pp. 147-153.

60. Edil, T. B., Sandstrom, L. K., and Berthouex, P.M. (1992), "Interaction of Inorganic Leachate with Compacted Pozzolanic Fly Ash", *Journal of Geotechnical Engineering*, vol. 118, no. 9, September 1992, pp. 1410-1430.

61. Egloffstein, T. (1995), "Properties and Tests Methods to Assess Bentonite Used in Geosynthetic Clay Liners," *Geosynthetic Clay Liners*, Balkema, Rotterdam, The Netherlands, pp. 51-72.

62. Endo, T., Yamamoto, S., Honna, T., Eneji, A.E. (2002), "Sodium-Calcium Exchange Selectivity as Influenced by Clay Minerals and Composition", *Soil Science*, vol. 167, no. 2, pp.117-125.

63. Eriksen, T.E., Jansson, M., and Molera, M. (1999), "Sorption Effects on Cation Diffusion in Compacted Bentonite," *Journal of Engineering Geology,* vol. 54, pp. 231-236.

64. Faure, G. (1998), Principles and Applications of Geochemistry, 2nd edition, *Prentice-Hall*, Inc., New Jersey.

65. Fernandez, F. and Quigley, R.M. (1986), "Organic Liquids and the Hydraulic Conductivity of Barrier Clays," *Proceedings of the International Conference on Soil Mechanics and Foundation Engineering*, June 22-26, Cambridge, MA, pp. 1867-1870.

66. Fernandez, F. and Quigley, R.M. (1985), "Hydraulic Conductivity of Natural Clays Permeated with Simple Liquid Hydrocarbons," *Canadian Geotechnical Journal*, vol. 22, pp. 205-214.

67. Fletcher, P. and Sposito, G. (1989), "The Chemical Modeling of Clay/Electrolyte Interactions for Montmorillonite," *Journal of Clay Minerals*, vol. 24, pp. 375-391.

68. Fletcher, P., Sposito, G., and LeVesque, C.S. (1984), "Sodium-Calcium-Magnesium Exchange Reactions on a Montmorillonitic Soil: I. Binary Exchange Reactions," *Soil Sci Soc Am J* vol. 48 no. 5 Sep-Oct 1984. p 1016-1021.

69. Foose, G. J. (2002), "Transit-Time Design for Diffusion Through Composite Liners," *Journal of Geotechnical and Geoenvironmental Engineering, ASCE,* vol. 128, no. 7, pp. 590-601.

70. Freeze, R.A. and Cherry, J.A. (1979), Groundwater, *Prentice-Hall, Inc*., Englewood Cliffs, N.J. USA.

71. Gleason, M.H., Daniel, D.E., and Eykholt, G.R., (1997), "Calcium and Sodium Bentonite for Hydraulic Containment Applications," *Journal of Geotechnical and Geoenvironmental Engineering, ASCE*, vol. 123, no. 5, pp. 438-445.

72. Goldstein, J.I., Newbury, D.E., Echlin, P., Joy, D.C., Fiori, C., and Lifshin, E. (1981) Scanning Electron Microscopy and X-Ray Microanalysis, Plenum Press.

73. Gordon, B.B. and Forrest, M. (1981), "Permeability of Soils Using Contaminated Permeant," *In Permeability and Groundwater Contaminant Transport*, ASTM, Special Technical Publication, STP 746, pp. 101-120.

74. Grim, R.E. (1968), Clay Mineralogy, 2nd edition, *McGraw-Hill Book Company*.

75. Grim, R.E. and Guven, N. (1978), Bentonites: Geology, Mineralogy, Properties, and Uses, Elsevier Science Publishing Co., Inc., New York, N.Y.

76. Grube, W.E. J. (1990), "Measuring Performance of Clay Containment Barriers," *Proceedings of the ASCE 17th Annula National Conference on Optimizing the Resources for Water Management*, Forth Worth, TX, pp. 482-488.

77. Guillaume, D., Neaman, A., Cathelineau, M., Mosser, R.R., Peiffert, C., Abdelmoula, M., Dubessy, J., Villieras, F., Baronnet, A., and Michau, N., (2003), "Experimental Synthesis of Chlorite from Smectite at 300^{o}C in the Presence of Metallic Fe," *Clay Minerals*, vol.38, no.3, pp.281-302.

78. Güngör, N. and Ece, Ö.I. (1999), "Effect of the Adsorption of Non-Ionic Polymer Poly(vinyl) Pyrolidone on the Rheological Properties of Na-Activated Bentonite," *Materials Letters*, vol 39, pp. 1-5.

79. Gymer, R.G. (1973), Chemistry: an Ecological Approach, *Harper & Row, Publishers*, New York.

80. Hajjaji, M., Kacim, S., Alami, A., El B.A., and El M.M. (2001), "Chemical and Mineralogical Characterization of a Clay taken from the Moroccan Meseta and a Study of the Interaction Between its Fine Fraction and Methylene Blue", *Applied Clay Science*, vol.20, no.1-2, pp.1-12.

81. Hajra, M.G., Reddi, L.N., Glasgrow, L.A., Xiao, M., and Lee, I.M. (2002), "Effects of Ionic Strength on the Fine Particle Clogging of Soil Filters," *Journal of Geotechnical and Geoenvironmental Engineering, ASCE*, vol. 128, no. 8, Aug., pp. 631-639.

82. Hang, P.T. and Brindley, G.W. (1970), "Methylene Blue Absorption by Clay Minerals Determination of Surface Areas and Cation Exchange Capacities (Clay-Organic Studies)," *Clays and Clay Minerals*, vol. 18, pp. 203-212.

83. Hermann, J.G. and Elsbury, B.R. (1987), "Influential Factors in Soil Practice for Waste Disposal '87," edited by R.D. Woods, ASCE, NY, pp. 522-536.

84. Hettiaratchi, J.P.A., Achari, G., Joshi, R.C., and Okoli, R.E. (1999), "Feasibility of Using Ash Admixtures in Landfill Bottom Liners or Vertical Barriers at Contaminated Sites," *Journal of Environmental Science and Health, Part A: Toxic/Hazardous Substances and Environmental Engineering*, vol 34, n 10, pp. 1897-1917.

85. Higashi, K., Yamaguchi, T., Takabatake, M. N., and Fujita, H. (1990), "Diffusion of Water in Bentonite," *Memoirs of the Faculty of Engineering, Kyoto University*, vol. 52, no. 2, pp. 106-113.

86. Higgs, N.B. (1988), "Methylene Blue Adsorption as a Rapid and Economical Method of Detecting Smectite," *Geotechnical Testing Journal*, vol. 11, no. 1, pp. 68-71.

87. Holtz, R.D. and Kovacs, W.D. (1981), An Introduction to Geotechnical Engineering, *Prentice-Hall, Inc.*, New Jersey.

88. Holtz, W.G. (1985), "Predicting Hydraulic Conductivity of Clay Liners," *Discussion: Journal of the Geotechnical Engineering Division*, ASCE, vol. 111, no. 12, pp. 1457-1459.

89. Hwang, J.Y. and Dixon, J.B., (2000), "Flocculation Behavior and Properties of Na-Montmorillonite Treated with Four Organic Polymers," *Clay Science*, vol. 11, no. 2, pp.137-146.

90. Itami, K. and Tamamura, T. (1999), "Evaluation of Cation Exchange Capacity of Montmorillonite using Caesium Chloride," *Clay Science*, vol. 10, no. 6, pp. 469-476.

91. James, A.N., Fullerton, D., and Drake, R. (1997), "Field Performance of GCL under Ion Exchange Conditions," *Journal of Geotechnical and Geoenvironmental Engineering*, ASCE, vol. 123, no. 10, pp. 897-901.

92. Jo, H.Y., Katsumi, T., Benson, C.H., and Edil, T.B. (2001), "Hydraulic Conductivity and Swelling of Nonprehydrated GCLs Permeated with Single-Species Salt Solutions," *Journal of Geotechnical and Geoenvironmental Engineering, ASCE*, vol. 127, no. 7, pp. 557-567.

93. Johnson, G.W., Crumley, W.S., and Boutwell, G.P. (1994), "Field Verification of Clay Liner Hydraulic Conductivity," *In Hydraulic Conductivity and Waste Contaminant Transport in Soils*, edited by D.E. Daniel and S. Trautewein, ASTM, Special Technical Publication STP 1142, pp. 226-245.

94. Joshi, R.C., Hettiaratchi, J.P.A., and Achari, G. (1994**),** "Properties of Modified Alberta Fly Ash in Relation to Utilization in Waste Management Applications", *Canadian Journal of Civil Engineering*, vol. 21, no. 3, Jun 1994, pp. 419-426.

95. Jurcek, P., Krizova, V. J., Ivanova, P., and Aguete, E.C. (1999), "Study of Sorption and Diffusion Processes in Natural Bentonites," *Acta Universitatis Caroliae*, Geologica, vol. 43, no. 3, pp. 581-585.

96. Kacimov, A.R. and Obnosov, Y.V. (2000), "Two-Dimensional Seepage in Porous Media with Heterogeneities," *Journal of Geochemical Exploration*, vol. 69, pp. 251-255.

97. Kahr, G. and Madsen, F. T. (1995), "Determination of Cation Exchange Capacity and the Surface Area of Bentonite. Illite, and Kaolinite by Methylene Blue Adsorption," *Applied Clay Science*, vol. 9, pp. 327-336.

98. Kemper, W.D., Maasland, D.E.L., and Porter, L.K. (1964), "Mobility of Water Adjacent to Mineral Surfaces," *Proceedings of Soil Science Society of America*, vol. 28, no. 2, pp. 164-167.

99. Kaufhold, S., Dohrmann, R., Ufer, K., and Meyer, F. M. (2002), "Comparison of methods for the quantification of montmorillonite in bentonites," *Applied Clay Science*, vol. 22, no.3, pp.145-151.

100. Kayabali, K. (1997), "Engineering Aspects of a Novel Landfill Liner Material: Bentonite-Amended Natural Zeolite," *Journal of Engineering Geology*, vol. 46, pp. 105-114.

101. Keijer, T.J.S. (2000), "Chemical Osmosis in Natural Clayey Materials," Geologica Ultraiectina, 1996, Ph.D. Thesis, Universiteit Utrecht, The Netherlands, pp. 166.

102. Keijzer, T.J.S and Loch, J.P.G. (2001), "Chemical Osmosis in Compacted Dredging Sludge," *Soil Science Society of America Journal*, vol. 65, no. 4, pp.1045-1055.

103. Keijzer, T.J.S., Kleingeld, P.J., and Loch, J.P.G. (1999), "Chemical Osmosis in Compacted Clayey Material and the Prediction of Water Transport," *Journal of Engineering Geology*, vol. 53, pp. 151-159.

104. Keren, R. and Singer, M.J. (1988), "Effect of Low Electrolyte Concentration on Hydraulic Conductivity of Sodium/Calcium-Montmorillonite-Sand System," *Soil Science Society of America Journal*, vol. 52, no. 2, pp. 368-373.

105. Kim, H.T., Suk, T.W., and Parks, S.H. (1993), "Diffusivities for Ions Through Compacted Na-Bentonite with Varying Dry Bulk Density," *Waste Management*, vol. 13, pp. 303-308.

106. King, K.S., Quigley, R.M., Fernandez, F., Readers, D.W., and Bacopoulos, A., (1993), "Hydraulic Conductivity and Diffusion Monitoring of the Keele Valley Landfill Liner," Maple, Ontario, *Canadian Geotechnical Journal*, vol. 30, pp. 124-134.

107. Kitsopoulos, K.P. (1997), "Comparison of the Methylene Blue Absorption and the Ammonium Acetate Saturation Methods for Determination of CEC Values of Zeolite-Rich Tuffs", *Clay Minerals*, vol. 32, no. 2, pp.319-322.

108. Kjellander, R., Marcelja, S., and Quirk, J. (1988), "Attractive Double-Layer Interactions Between Calcium Clay Particles," *Journal of Colloid and Interface Science*, vol. 126, no. 1, pp. 194-211.

109. Koch, D. (2002), "Bentonites As A Basic Material For Technical Base Liners And Site Encapsulation Cut-Off Walls", *Applied Clay Science*, vol. 21, no.1-2, pp.1-11.

110. Koerner, R.M. (1999), Designing with Geosynthetics, 4th edition, *Prentice-Hall, Inc.*, Upper Saddle River, N.J.

111. Koerner, R.M. and Soong, T.Y. (2000), "Leachate in Landfills: The Stability Issues," *Journal of Geotextiles and Geomembranes,* vol. 18, pp. 293-309.

112. Köster, H. M. (1996), "Mineralogical and Chemical Heterogeneity of Three Standard Clay Mineral Samples," Clay Minerals, vol. 31, pp. 417-422.

113. Kozaki, T., Inada, K., Sato, S., and Ohashi, H. (2001), "Diffusion Mechanism of Chloride Ions in Sodium Montmorillonite," *Journal of Contaminant Hydrology*, vol.47, no.2-4, pp.159-170.

114. Lake, C.B., and Rowe, R.K. (2000), "Diffusion of Sodium and Chloride Through Geosynthetic Clay Liners," *Journal of Geotextiles and Geomembranes*, vol. 18, pp. 103-131.

115. Lehikoinen, J., Carlsson, T., Muurinen, A., Olin, M., and Salonen, P. (1996), "Evaluation of Factors Affecting Diffusion in Compacted Bentonite," Scientific Basis for Nuclear Waste Management XIX Materials Research Society Symposium Proceedings vol. 412, Materials Research Society,USA., pp. 675-682.

116. Lambe, T.W. (1953), "The Structure Of Inorganic Soil," *Proceedings of the American Society of Civil Engineers*, vol. 79, no. 315, 49 pp.

117. Li, Y.H. and Gregory, S. (1974), "Diffusion of Ions in Sea Water and in Deep-sea Sediments," *Geochimica et Cosmochimica Acta*., vol 38, no. 5, pp. 703-714.

118. Lide, D.L. (2002), CRC Handbook of Chemistry and Physics, 82nd ed, CRC Press LLC., FL.

119. Lin, L.C. and Benson, C.H. (2000), "Effect of Wet-Dry Cycling on Swelling and Hydraulic Conductivity of GCLs," *Journal of Geotechnical and Geoenvironmental Engineering, ASCE*, vol. 126, no. 1, pp. 40-49.

120. Lu, J.C.S. et al., Ed. (1985), Leachate from Municipal Landfills, Production and Management, Noyes Pub., Park Ridge.

121. Mahler, C.F. and Velloso, R.Q. (2001), "Diffusion and Sorption Experiments Using a DKS Permeameter," *Journal of Engineering Geology*, vol. 60, pp. 173-179.

122. Malusis, M.A. and Shackelford, C.D. (2004), "Predicting Solute Flux through a Clay Membrane Barrier," *Journal of Geotechnical and Geoenvironmental Engineering*, vol. 130, no. 5, pp. 477-487.

123. Malusis, M.A. and Shackelford, C.D. (2002a), "Chemico-Osmotic Efficiency of a Geosynthetic Clay Liner," Journal of Geotechnical and Geoenvironmental Engineering, vol. 128, no. 2, pp. 97-106.

124. Malusis, M.A. and Shackelford, C.D. (2002b), "Coupling Effects During Steady-State Solute Diffusion Through A Semipermeable Clay Membrane," Environmental Science and Technology, vol. 36, pp. 1312-1319.

125. Malusis, M.A., Shackelford, C.D., and Olsen, H.W. (2001), "A Laboratory Apparatus to Measure Chemico-Osmotic Efficiency Coefficients for Clay Soils," *Geotechnical Testing Journal*, vol. 24, no. 3, pp. 229-242.

126. Mayayo, M. J., Bauluz, B., and Gonzalez, L.J.M. (2000), "Variations in the chemistry of smectites from the Calatayud Basin (NE Spain)," *Clay Minerals*, vol. 35, no. 2, pp.365-374.

127. McBean, E.A., Rovers, F.A., and Farquhar, G.J. (1995), Solid Waste Landfill Engineering and Design.Prentice, Hall PTR, Englewood Cliffs.

128. McBride, M.B. (1994), Environmental Chemistry of Soils, Oxford University Press, New York, Oxford.

129. McNeal, B.L. and Coleman, N.T. (1966), "Effect of Solution Composition on Soil Hydraulic Conductivity," *Proceedings of Soil Science Society of America*, vol. 30, pp. 308-312.

130. McNeal, B.L., Norvell, W.A., and Coleman, N.T. (1966), "Effect of Solution Composition on the Swelling of Extracted Soil Clays," *Journal of Soil Science Society of America*, vol. 30, pp. 313-317.

131. Mesri, G. and Olson, R..E. (1971), "Mechanisms Controlling the Permeability of Clays," *Clays and Clay Minerals*, vol. 19, no. 3, pp. 151-158.

132. Miller, W.L., Townsend, T., Earle, J., Lee, H., and Reinhart, D.R. (1994) "Leachate Recycle and the Augmentation of Biological Decomposition at Municipal Solid Waste Landfills," *Presented at the Second Annual Research Symposium, Florida Center for Solid and Hazardous Waste Management*, Tampa, FL.

133. Mitchell, J.K. (1993), Fundamentals of Soil Behavior, *John Wiley and Sons, Inc*., New York, N.Y.

134. Mitchell, J.K. and Madsen, F.T. (1987), "Chemical Effects on Clay Hydraulic Conductivity," *Geotechnical Practice foe Waste Disposal '87, Proceedings of Specialty Conference*, Ann Arbor, Michigan, June 15-17, Geotechnical Special Publication, no. 13, pp. 87-116.

135. Muhammad, N. and Ashmawy, A.K, (2003), "Compatibility of Incinerator Ash-Soil Mix as an Alternative Material for Landfill Liners and Covers," *report submitted to Florida Center For Solid And Hazardous Waste Management*, Gainesville, FL, pp. 72.

136. Mundell, J.A. (1985), "Predicting Hydraulic Conductivity of Clay Liners," *Discussion: Journal of Geotechnical Engineering*, ASCE, vol. 111, no. 12, pp. 1459-1464.

137. Mundell, J.A. and Bailey, B. (1985), "The Design and Testing of a Compacted Clay Barrier Layer to Limit Percolation Through Landfill Covers," *In Hydraulic Barriers in Soil and Rock*, edited by A.I. Johnson, R.K. Frobel, N.J. Cagalli, and C.B. Petterson, ASTM, Special Technical Publication, STP 874, pp. 246-262.

138. Nakashima, Y. (2003), "Diffusivity Measurement of Heavy ions in Wyoming Montmorillonite Gels by X-ray Computed Tomography," *Journal of Contaminant Hydrology*, vol.61, no.1-4, pp.147-156.

139. Nordquist, J.E. (1990), "Comparison of Laboratory and Field Measured Hydraulic Conductivities of Soil Liners," *Proceedings of the 1990 Annual Symposium on Engineering Geology and Geotechnical Engineering*, no. 26, April 4-6, Pocatello, Idaho, pp. 11/1-11/5.

140. Odom, I.E. (1984), "Smectite Clay Minerals; Properties and Uses," *Philosophical Transactions of the Royal Society of London, Series A: Mathematical and Physical Sciences*, vol.311, no.1517, pp.391-409.

141. Ogata, A. (1970), "Theory of Dispersion in a Granular Medium, U.S. Geological Survey Professional Paper, no. 411-1.

142. Olsen, S.R., Kemper, W.D., and van Schaik, J.C. (1965), "Self-Difusion Coefficients of Phosphorous in Soil Measured by Transient and Steady-State Methods," *Proceedings of Soil Science Society of America*, vol. 29, no. 2, pp. 154-158.

143. Peterson, S.R., and Gee, G.W. (1985), "Interactions between Acidic Solutions and Clay Liners: Permeability and Neutralization," *Hydraulic Barriers in Soil and Rock*, ASTM STP 874, A.I. Johnson et al., eds., ASTM, West Conshohocken, Pa., pp. 229-245.

144. Petit, S., Righi, D., Madejova, J., and Decarreau, A. (1998), "Layer Charge Estimation of Smectites using Infrared Spectroscopy," *Clay Minerals*, vol. 33, no. 4, pp. 579-591.

145. Petrov, R.J. and Rowe, R.K. (1997), "Geosynthetic Clay Liner (GCL) – Chemical Compatibility by Hydraulic Conductivity Testing and Factors Impacting Its Performance," *Canadian Geotechnical Journal*, vol. 34, pp. 863-885.

146. Petrov, R.J., Rowe, R.K., and Quigley, R.M. (1997), "Selected Factors Influencing GCL Hydraulic Conductivity," *Journal of Geotechnical and Geoenvironmental Engineering*, ASCE, vol. 123, no. 8, pp. 683-695.

147. Picornell, M. (1985), "Predicting Hydraulic Conductivity of Clay Liners," *Discussion: Journal of Geotechnical Engineering*, ASCE, vol. 111, no. 12, pp. 1464-1465.

148. Porbaha, A., Pradhan, T.B.S., and Yamane, N. (2000), "Time Effect on Shear Strength and Permeability of Fly Ash", *Journal of Energy Engineering*, vol. 126, no. 1, April 2000, pp. 15-31.

149. Porter, L.K., Kemper, W.D., Jackson, R.D., and Stewart, B.A. (1960), "Chloride Diffusion in Soils as Influenced by Moisture Content," *Proceedings of Soil Science of America*, vol. 24, no. 6, pp. 400-403.

150. Qasim, S.R. and Chiang, W. (1994) Sanitary Landfill Leachate, Technomic Publishing Co., Inc., Lancaster.

151. Quigley, R.M. and Rowe, R.K. (1986), "Leachate Migration Through Clay Below a Domestic Waste Lanfill, Sarnia, Ontario, Canada: Chemical Interpretation and Modeling Philosophies," *Hazardous and Industrial Solid Waste Testing and Disposal*, STP 933, Lorenzen, et al., (eds.), ASTM, Philadelphia, PA., pp. 93-103.

152. Quigley, R.M., Yanful, E.K., and Fernandez, F. (1987), "Ion Transfer by Diffusion Through Clay Barriers," *Geotechnical Practice for Waste Disposal*, A.S.C.E. Geotechnical Special Publication, vol. 13, pp. 137-158.

153. Quirk, J.P. and Schofield, R.K. (1955), "The Effect of Electrolyte Concentration on Soil Permeability," *Journal of Soil Science*, vol. 6, no. 2, pp. 163-178.

154. Rad, N.S., Jacobson, B.D., and Bachus, R.C. (1994), "Compatibility of Geosynthetic Clay Liners with Organic and Inorganic Permeants," *Proceedings of the 5th International Conference on Geotextiles, Geomembranes and Related Products*, September 5-9, Singapore, pp. 1165-1168.

155. Ramirez, S., Cuevas, J., Petit, S., Righi, D., and Meunier, A. (2002), "Smectite Reactivity in Alkaline Solutions Geologica Carpathica (Bratislava)," vol. 53, no. 2, pp. 87-92.

156. Reinhart, D.R. and Grosh, C.J. (1998), "Analysis of Florida MSW Landfill Leachate Quality," *State University System of Florida, Florida Center for Solid and Hazardous Waste Management*, Gainesville, FL, Report #97-3, pp. 108.

157. Reschke, A.E. and Haug, M.D. (1991), "The Physico-Chemical Properties of Bentonites and the Performance of Sand-Bentonite Mixtures," *Proceedings of the 44th Annual Canadian Geotechnical Conference*, Calgary, Alberta, September 29-October 02, vol. 2, paper no. 62, pp. 62/1-62/10.

158. Rogowski, A.S. (1986), "Hydraulic Conductivity of Compacted Clay Soils," *Proceedings of the 12th Annual Research Symposium on Land Disposal, Remedial Action, Incineration, and Treatment of Hazardous Waste*, U.S.EPA, Cincinnati, Ohio, pp. 29-39.

159. Rogowski, A.S. (1990), "Comparison Between the Field and Laboratory Measured Properties of a Clay Liner," *Proceedings of the 17th Annual National Conference on Optimizing the Resources for Waste Management*, Forth Worth, TX, pp. 476-481.

160. Rowe, R.K. and Booker, J.R. (1985), "1-D Pollutant Migration in Soils of Finite Depth," *Journal of Geotechnical Engineering*, ASCE, vol. 111, no. 4, pp. 479-499.

161. Rowe, R.K., Lake, C.B., and Petrov, R.J. (2000), "Apparatus and Procedures for Assessing Inorganic Diffusion Coefficients Through Geosynthetic Clay Liners," *ASTM Geotechnical Testing Journal*, vol. 23, pp. 206-214.

162. Rowe, R.K., Petrov, R.J., and Lake, C. (1997), "Compatibility Testing and Diffusion Through Geosynthetic Clay Liners (GCL)," *Proceedings of Sardinia 97, Sixth International Landfill Symposium*, Cagliari, Italy, October 13-17, pp. 301-310.

163. Rowe, R.K., Quigley, R.M., and Booker, J.R. (1995), "Clayey Barrier Systems for Waste Disposal Facilities," *E & FN Spon (Chapman and Hall)*, London.

164. Ruhl, J.L. and Daniel, D.L. (1997), "Geosynthetic Clay Liners Permeated with Chemical Solutions and Leacheates," *Journal of Geotechnical and Geoenvironmental Engineering, ASCE*, vol. 123, no. 4, pp. 369-381.

165. Russ, J.C. (1984), Fundamentals of Energy Dispersive X-Ray Analysis, *Butterworths & Co (Publishers) Ltd*.

166. Sai, J.O. and Anderson, D.C. (1991), "State-of-the-Art: Field Hydraulic Tests for Compacted Soil Liners," *Geotechnical Testing Journal*, vol. 13, no. 3, pp. 215-225.

167. Sällfors, G., and Öberg, H., and Anna, L. (2002), "Determination of Hydraulic Conductivity of Sand-Bentonite Mixtures for Engineering Purposes," *Journal of Geotechnical and Geological Engineering*, The Netherlands, vol. 20, pp. 65-80.

168. Sanchez, A.G., Alastuey, A., and Querol, X. (1999), "Heavy Metal Adsorption by Different Minerals: Application to the Remediation of Polluted Soils," *The Science of the Total Environmental Journal*, vol. 242, pp. 179-188.

169. Santamarina, J.C., Klein, K.A., Wang, Y.H., and Prencke, E. (2002), "Specific Surface: Determination and Relevance," *Canadian Geotechnical Journal*, vol. 39, no. 1, pp. 233-241.

170. Sato, H. (2000), "Effect of Ionic Charge on Effective Diffusion Coefficient in Compacted Sodium Bentonite," *Proceedings of Materials Research Society Symposium*, vol. 608, pp. 267-274.

171. Sato, H. and Suzuki, S. (2003), "Fundamentals Study on the Effect of an Orientation of Clay Particles on Diffusion Pathway in Compacted Bentonite," *Applied Clay Science*, vol. 23, pp. 51-60.

172. Schaefer, M. and Steiger, M., (2002), "A Rapid Method for the Determination of Cation Exchange Capacities of Sandstones; Preliminary Data," *Geological Society Special Publications*, vol.205, pp.431-439.

173. Schulze, D.G. (1989), "An Introduction to Soil Mineralogy", Dixon, J.B. and Weed, S.B. (eds.), *In Minerals in Soil Environments*, Madison, WI, Soil Science Society of America, pp. 1-34.

174. Shackelford, C.D. (1988), "Diffusion of Inorganic Chemical Wastes in Compacted Clay," thesis presented to the University of Texas, at Austin, TX, in partial fulfillment of the requirements for the degree of Doctor of Philosophy.

175. Shackelford, C.D. (1990), "Transit-time Design of Earthen Barriers," *Journal of Engineering Geology*, vol. 29, no. 1, pp. 79-94.

176. Shackelford, C.D. (1991), "Laboratory Diffusion Testing for Waste Disposal – A Review," *Journal of Contaminant Hydrology*, vol. 7, pp. 177-217.

177. Shackelford, C.D. (1994), "Waste Soil Interactions that alter Hydraulic Conductivity," *In Hydraulic Conductivity and Waste Contaminant Transport, ASTM*, STP 1142, D.E. Daniel and S.J. Trautwein, eds., ASTM, West Conshohocken, Pa., pp. 111-168.

178. Shackelford, C.D. and Daniel, D.E. (1991a), "Diffusion in Saturated Soil, I: Background," *Journal of Geotechnical Engineering*, ASCE, vol. 117, no. 3, pp. 467-484.

179. Shackelford, C.D. and Daniel, D.E. (1991b), "Diffusion in Saturated Soil, II: Results for Compacted Clay," *Journal of Geotechnical Engineering*, ASCE, vol. 117, no. 3, pp. 485-506.

180. Shackelford, C.D. and Lee, J.M. (2003), "The Destruction Role of Diffusion on Clay Membrane Behavior," *Journal of Clays and Clay Minerals*, vol. 51, no. 2, pp. 186-196.

181. Shackelford, C.D. and Redmond, P.L. (1995), "Solute Breakthrough Curves for Processed Kaolin at Low Flow Rates," *Journal of Geotechnical Engineering*, ASCE, vol. 121, no. 1, pp. 17-32.

182. Shackelford, C.D., Malusis, M.A., and Stern, R.T. (1999), "Electrical Conductivity Breakthrough Curves," *Journal of Geotechnical and Geoenvironmental Engineering, ASCE*, vol. 125, no. 4, pp. 260-270.

183. Shackelford, C.D., Benson, C.H., Katsumi, T., Edil, T.B., and Lin, L. (2000), "Evaluating the Hydraulic Conductivity of GCLs Permeated with Non-Standard Liquids," *Journal of Geotextiles and Geomembranes*, vol. 18, pp. 133-161.

184. Singh, S. K., Baser, B. L., and Shyampura, R. L. (2002), "Chemical composition and charge behaviour of smectites in Vertisols of Rajasthan," *Journal of the Indian Society of Soil Science*, vol.50, no.1, pp.106-110.

185. Snyder, K.A. (2001), "The Relationship Between the Formation Factor and the Diffusion Coefficient of Porous Materials Saturated with Concentrated Electrolytes: Theoretical and Experimental Considerations," *Concrete Science and Engineering*, vol. 3, pp. 216-224.

186. Song, K. and Sandi, G. (2001), "Characterization of montmorillonite surfaces after modification by organosilane," *Clays and Clay Minerals*, vol.49, no.2, pp.119-125.

187. Sposito, G. (1981), "The Thermodynamics of Soil Solutions", *Oxford University Press*, Oxford, London.

188. Sposito, G. (1989), The Chemistry of Soils, *Oxford University Press*, Oxford, London.

189. Sposito, G. and Fletcher, P. (1985), "Sodium-Calcium-Magnesium Exchange Reactions on a Montmorillonite Soil: III. Calcium-Magnesium Exchnage Selectivity," *Soil Science Society of America Journal*, vol. 49, pp. 1160-1163.

190. Sivapullaiah, P.V. and Savitha, S., (1999), "Index Properties of Illite-Bentonite Mixtures in Electrolyte Solutions," *Geotechnical Testing Journa*l, GTJODJ, vol. 22, no. 3, September pp. 257–265.

191. Stern, R.T. and Shackelford, C.D. (1998), "Permeation of Sand-Processed Clay Mixtures with Calcium Chloride Solutions," *Journal of Geotechnical and Geoenvironmental Engineering, ASCE*, vol. 124, no. 3, pp. 231-241.

192. Stewart, J.P. and Nolan, T.W. (1987), "Infiltration Testing for Hydraulic Conductivity of Soil Liners," *Geotechnical Testing Journal*, vol. 10, no. 2, pp. 41-50.

193. Suzuki, S., Fujishima, A., Ueno, K., Ichikawa, Y., Kawamura, K., Shibata, M., Sato, H., and Kitayama, K. (2001) "Microstructural Modeling of Compacted Sodium-Bentonite and Application of Unified Molecular Dynamics/Homogenization Analysis for Diffusion Process," *Journal of the Clay Science Society of Japan*, vol. 41, no. 2, pp.43-57.

194. Taylor, R.K. (1985), "Cation Exchange in Clays and Mudrocks by Methylene Blue," *Journal of Chemical Technology and Biotechnology*, Vol. 35A, pp. 195-207.

195. Tissa H.I. (2004), Environmental Science and Engineering and Center for Experimental Study of Subsurface Environmental Processes (CESEP), Colorado School of Mines, www.hsrc.org/hsrc/html/ssw/rio/tissa2.pdf, Accessed April 03, 2004.

196. Trautwein, S. and Boutwell, G. (1994), "In Soil Hydraulic Conductivity Tests for Compacted Liners and Caps," *In Hydraulic Conductivity and Waste Contaminant Transport in Soils*, edited by D.E. Daniel and S. Trautwein, ASTM, Special Technical Publication, STP 1142, pp. 184-226.

197. Triantafyllou, S., Christodoulou, E., and Neou-Syngouna, P. (1999), "Removal of Nickel and Cobalt from Aqueous Solutions by Na-Activated Bentonite," *Journal of Clays and Clay Minerals*, vol. 47, no. 5, pp. 567-572.

198. Van Olphen, H. (1977), Clay Colloid Chemistry, 2nd edition, *John Wiley & Sons*, Inc., New York.

199. Volzone, C., Rinaldi, J.O., and Ortiga, J., (2000), "Swelling of TMA (tetramethylammonium)- and HDP (hexadecylpyridinium) – Montmorillonites in Water and Toluene Media: Influence of the Type Montmorillonites," *Journal of Materails Research,* vol. 3, no. 4, pp. 115-118.

200. Walter, C. E. (1976), "Practical Refuse Recycling," *Journal of Environmental Engineering Division, ASCE,* vol. 102, no. 1, pp. 139-148.

201. Warshaw, C.M. and Roy, R. (1961), "Classification And A Scheme For The Identification Of Layer Silicates", *Geological Society of America Bulletin*, vol. 72, no. 10, pp.1455-1492.

202. Weaver, C.E. and Pollard, L.D. (1975), The Chemistry of Clay Minerals, 1st edition, Elsevier Scientific Publishing Company, Amsterdam, The Netherlands.

203. Wen S., Yang D., and Chen J. (2001), "X-ray diffraction characterization of bentonite and acidation of bentonite, alkalization of bentonite, and surface characteristics under scanning electron microscope," *Acta Mineralogica Sinica*, vol. 21, no. 3, pp. 453-456.

204. Wentink, G.R. and Etzel, J.E. (1972), "Removal of Metal Ions by Soil," *Journal of Water Pollution Control Federation*, vol. 44, no. 8, pp. 1561-1574.

205. Xeidakis, G.S. (1996), "Stabilization of Swelling Clays by $Mg(OH)_2$. Changes in Clay Properties after Addition of Mg-hydroxide," *Journal of Engineering Geology,* vol. 44, pp. 107-120.

206. Xiao, S., Moresoli, C., Bovenkamp, J., and Kee, D.D. (1997), "Sorption and Permeation of Organic Environmental Contaminants Through PVC Geomembranes," *Journal of Applied Polymer Science,* vol. 63, no. 9, Feb 1997, pp. 1189-1197.

207. Zhang, F., Low, P., and Roth, C. (1995), "Effects of Monovalent Exchangeable Cations and Electrolytes on the Relation Between Swelling Pressure and Interlayer Distance in Montmorillonite," *Journal of Colloid and Interface Science., Academic Press*, New York, vol. 173, pp. 34-41.

208. Zimmie, T.F. (1981), "Geotechnical Test Considerations in the Determination of Laboratory Permeability for Hazardous Waste Disposal Siting", *American Society for Testing and Materials,* Special Technical Publications 760. 1981. ASTM pp. 293-304.

APPENDICES

Appendix A: Test Results of pH and EC of Permeability Tests

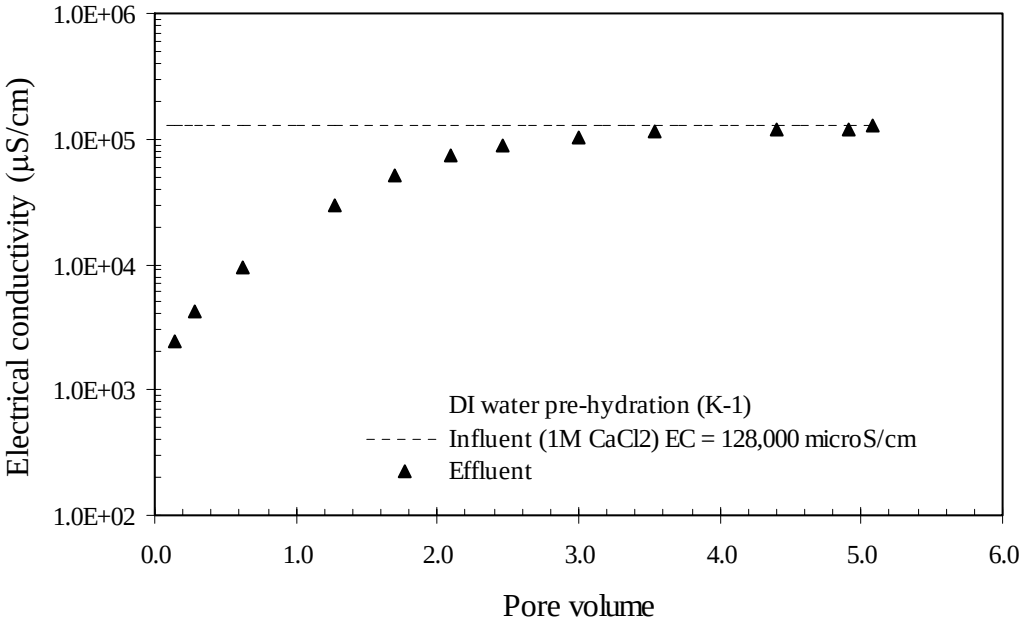

(a)

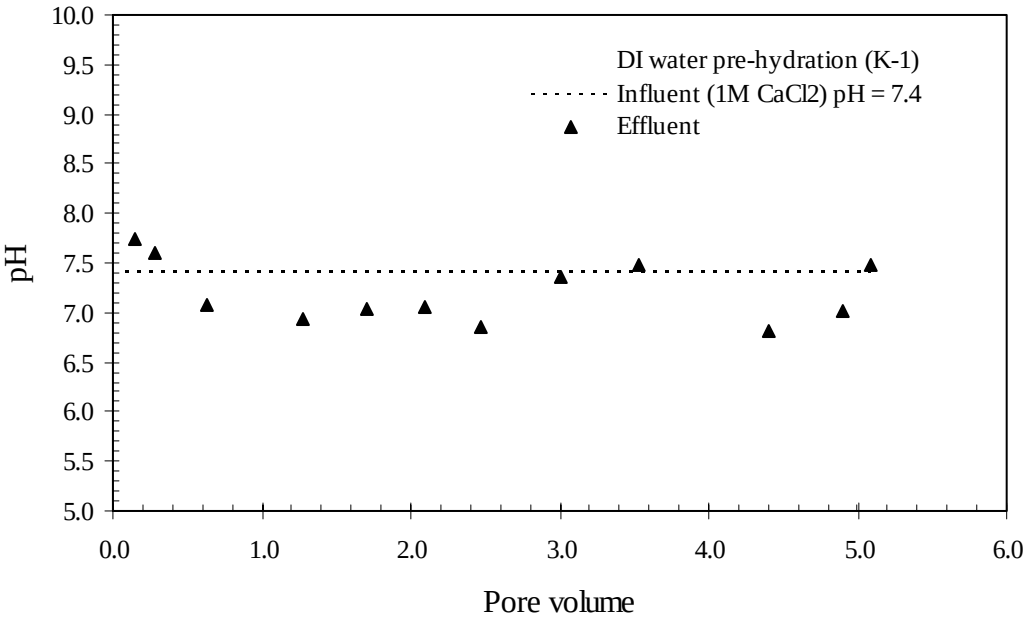

(b)

Figure A.1 Ionic Analysis of Permeability Test K-1 (a) Electrical Conductivity vs. Pore Volume and (b) pH vs. Pore Volume

Appendix A: (Continued)

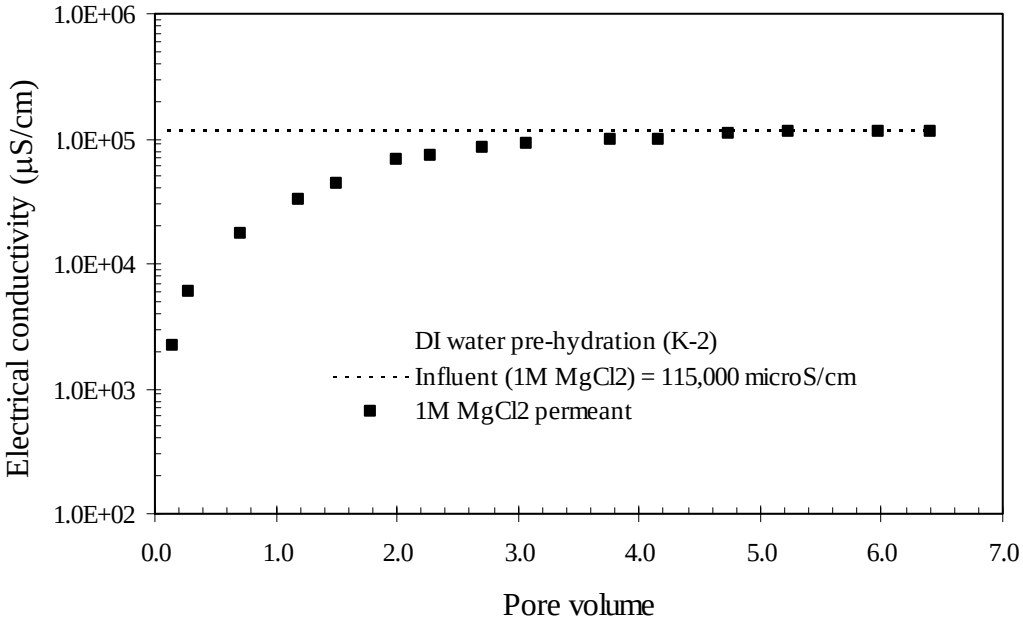

(a)

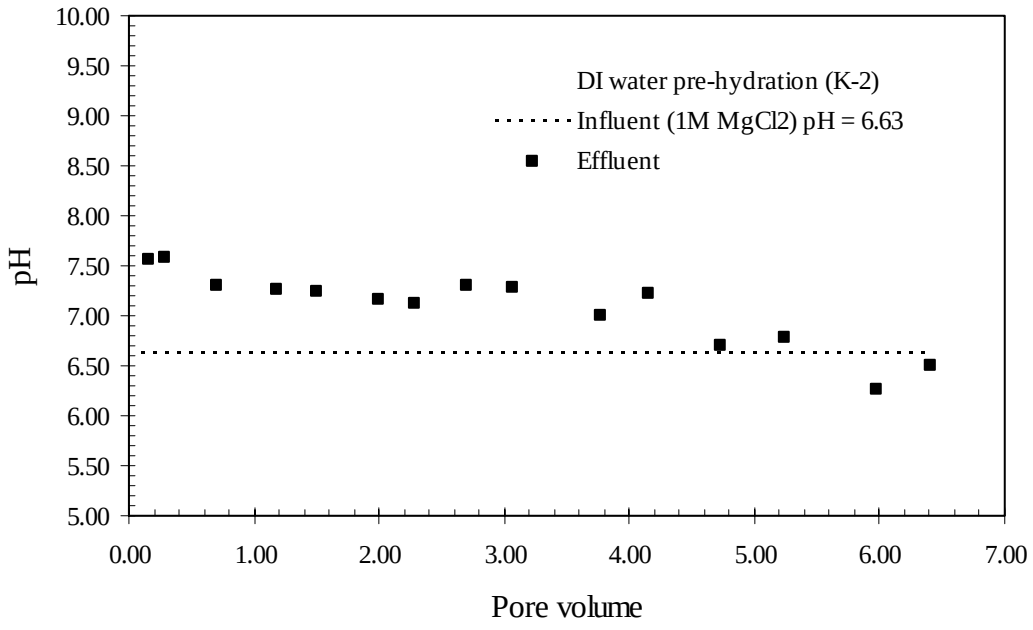

(b)

Figure A.2 Ionic Analysis of Permeability Test K-2 (a) Electrical Conductivity vs. Pore Volume and (b) pH vs. Pore Volume

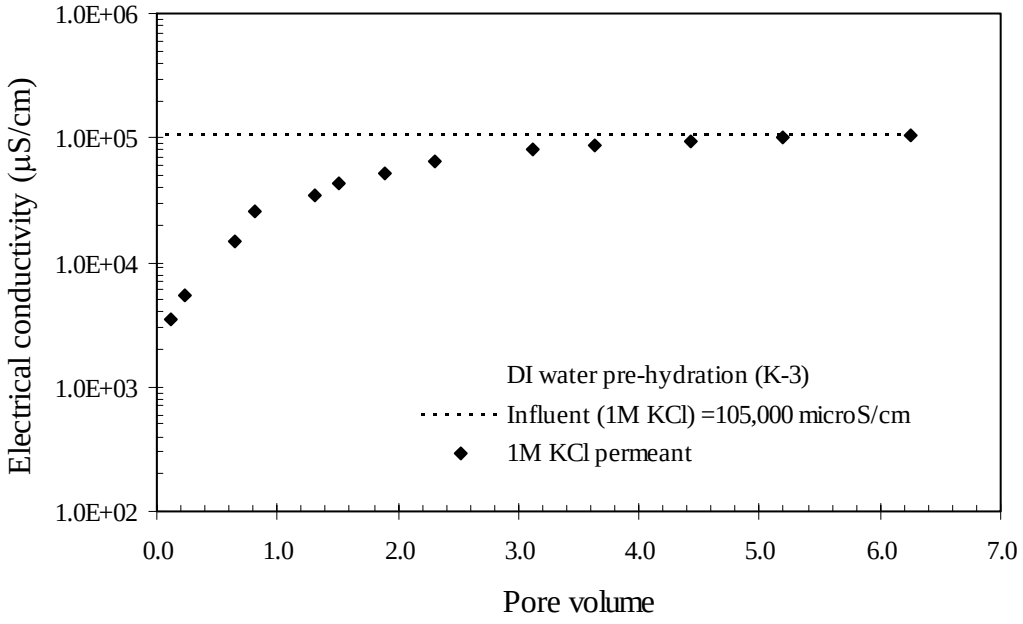

(a)

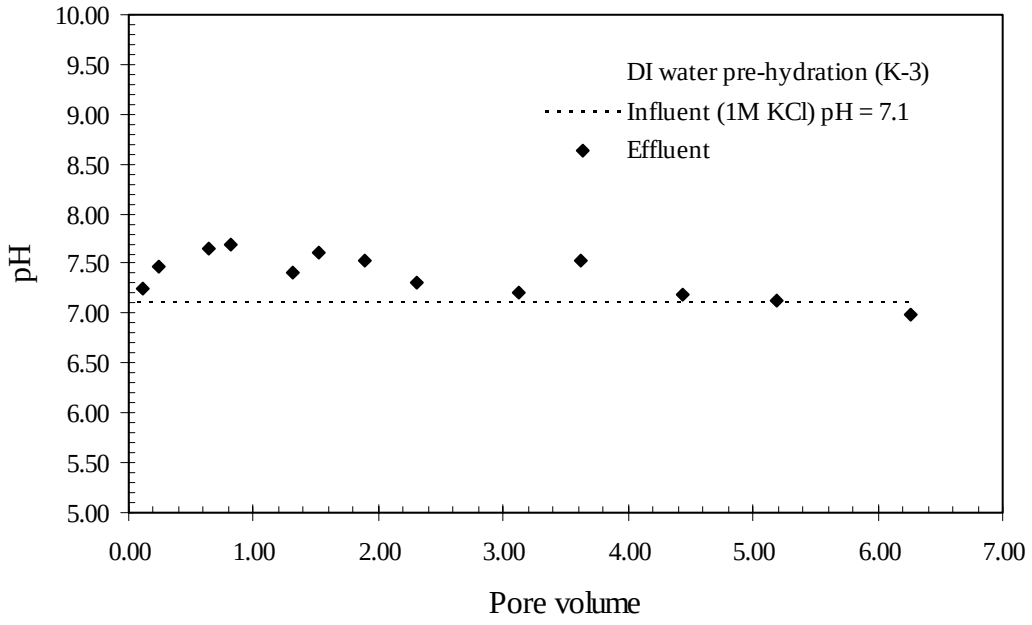

(b)

Figure A.3 Ionic Analysis of Permeability Test K-3 (a) Electrical Conductivity vs. Pore Volume and (b) pH vs. Pore Volume

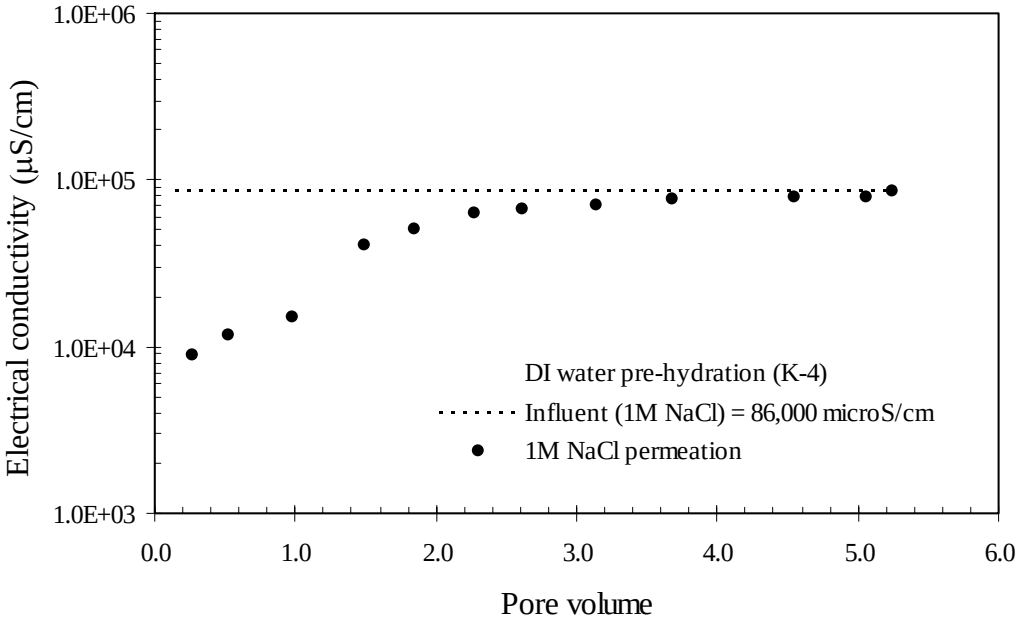

(a)

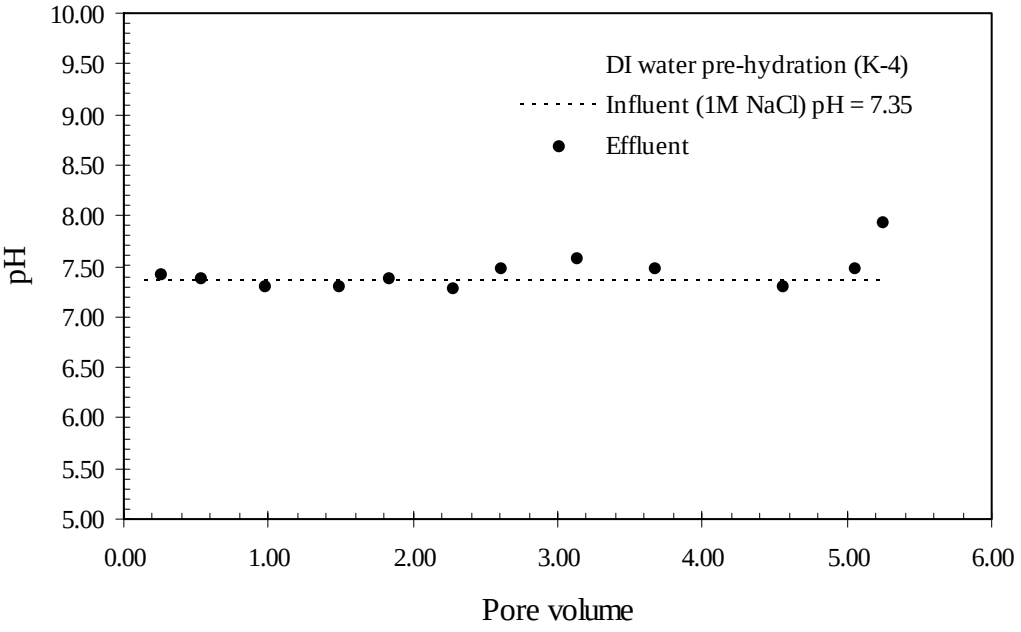

(b)

Figure A.4 Ionic Analysis of Permeability Test K-4 (a) Electrical Conductivity vs. Pore Volume and (b) pH vs. Pore Volume

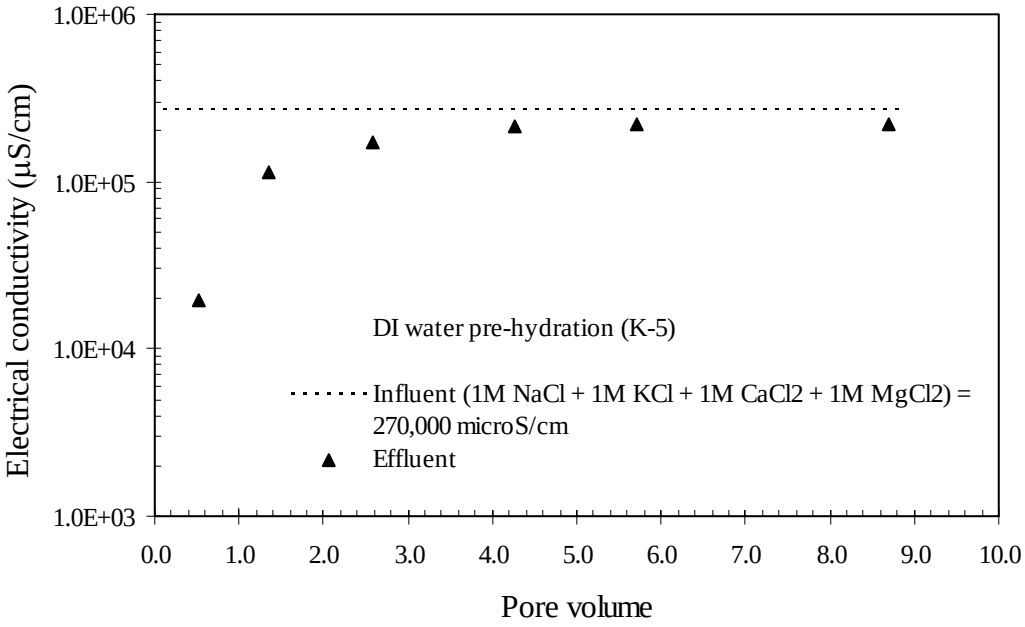

(a)

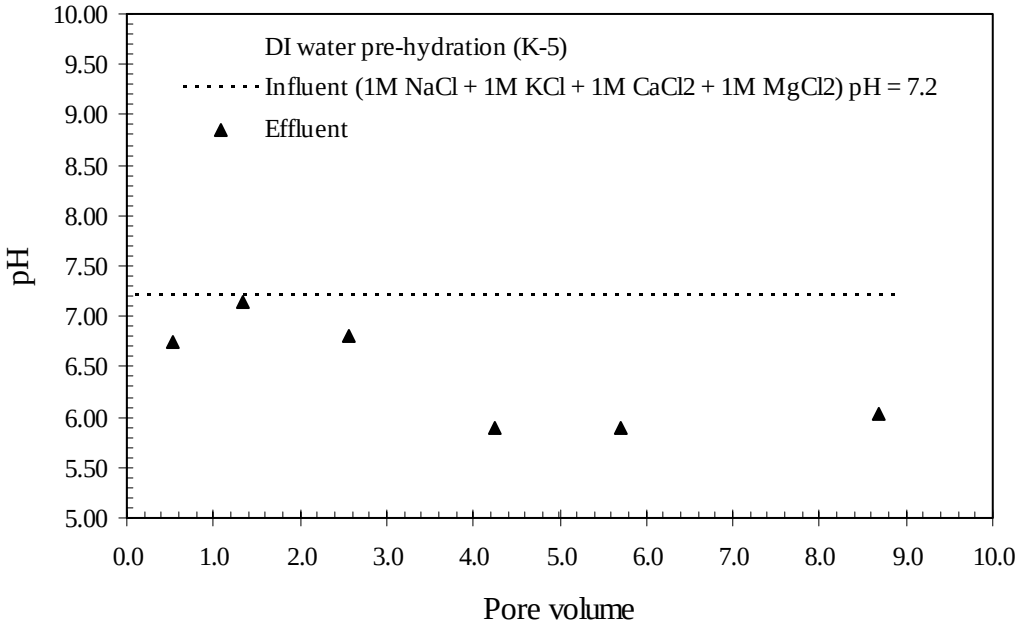

(b)

Figure A.5 Ionic Analysis of Permeability Test K-5 (a) Electrical Conductivity vs. Pore Volume and (b) pH vs. Pore Volume

Appendix A: (Continued)

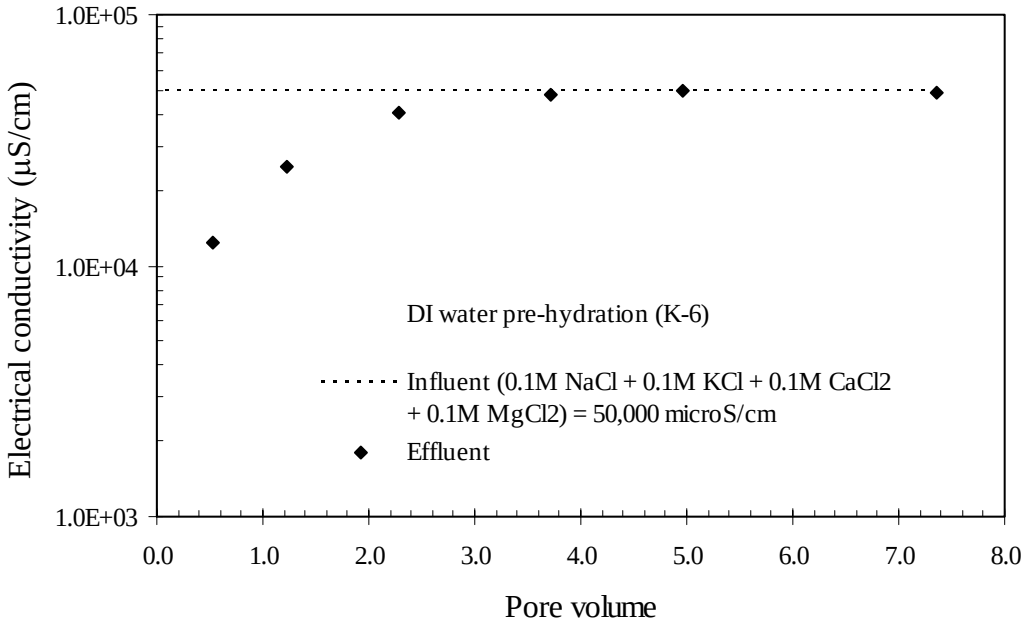

(a)

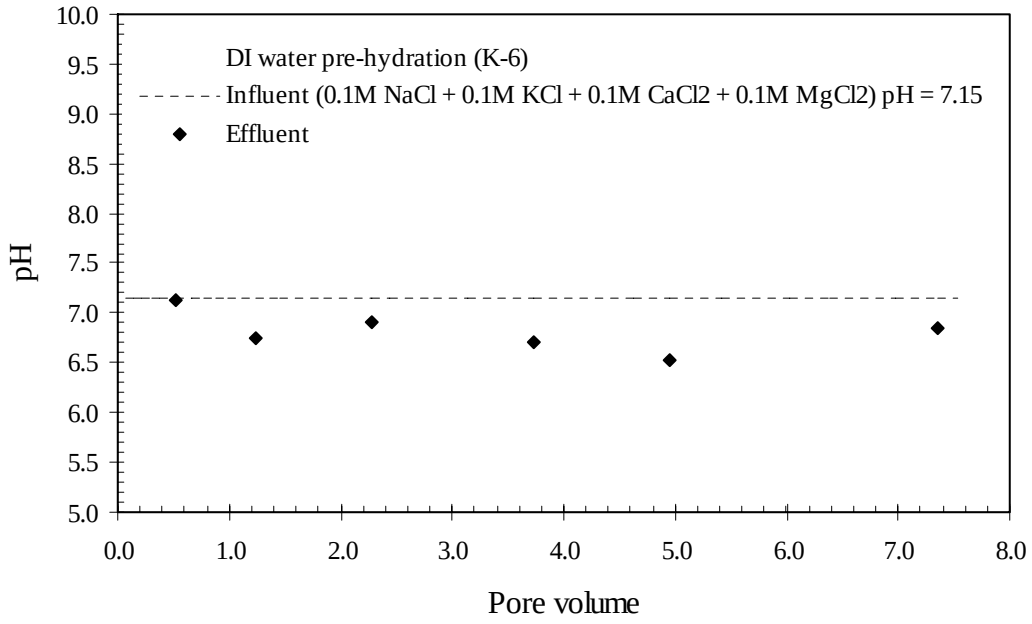

(b)

Figure A.6 Ionic Analysis of Permeability Test K-6 (a) Electrical Conductivity vs. Pore Volume and (b) pH vs. Pore Volume

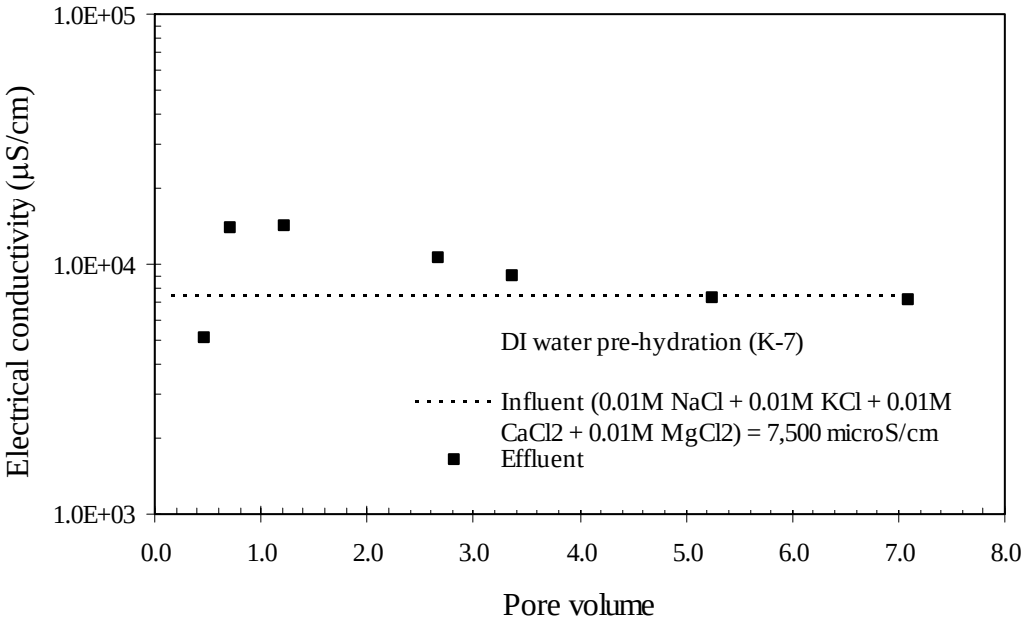

(a)

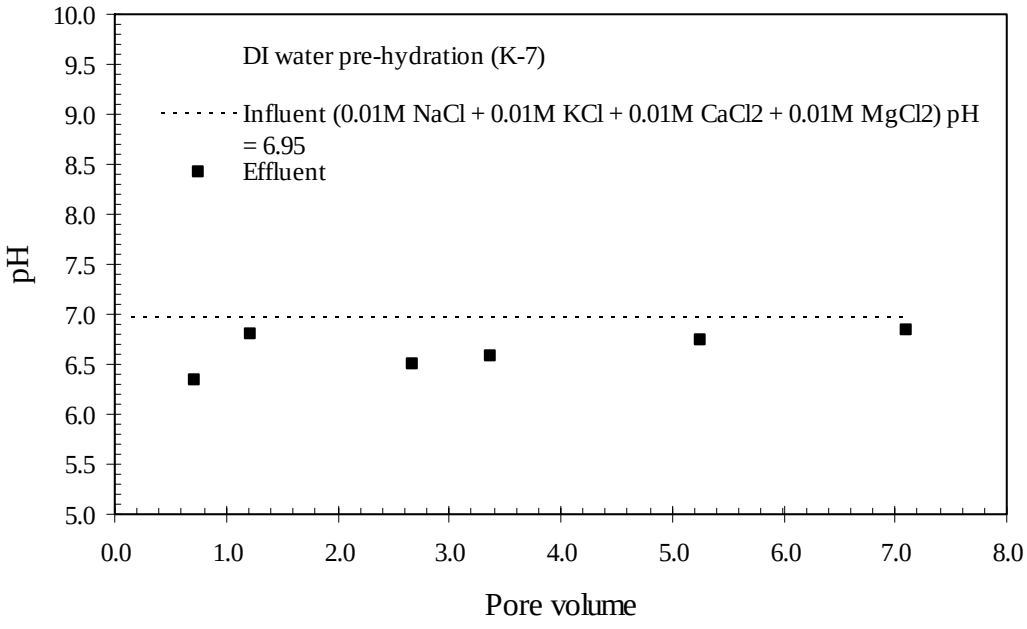

(b)

Figure A.7 Ionic Analysis of Permeability Test K-7 (a) Electrical Conductivity vs. Pore Volume and (b) pH vs. Pore Volume

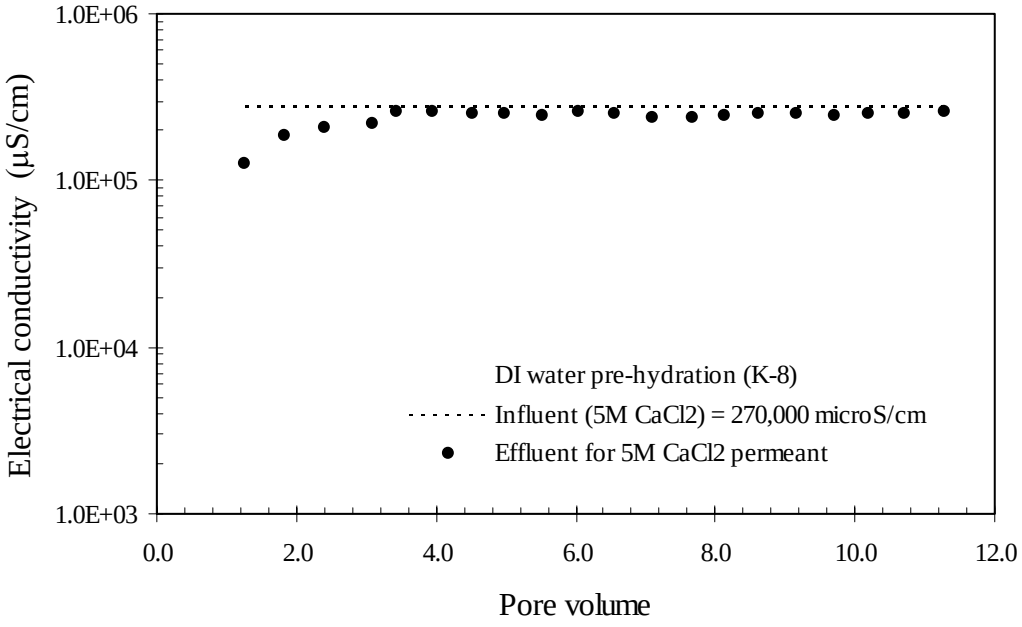

(a)

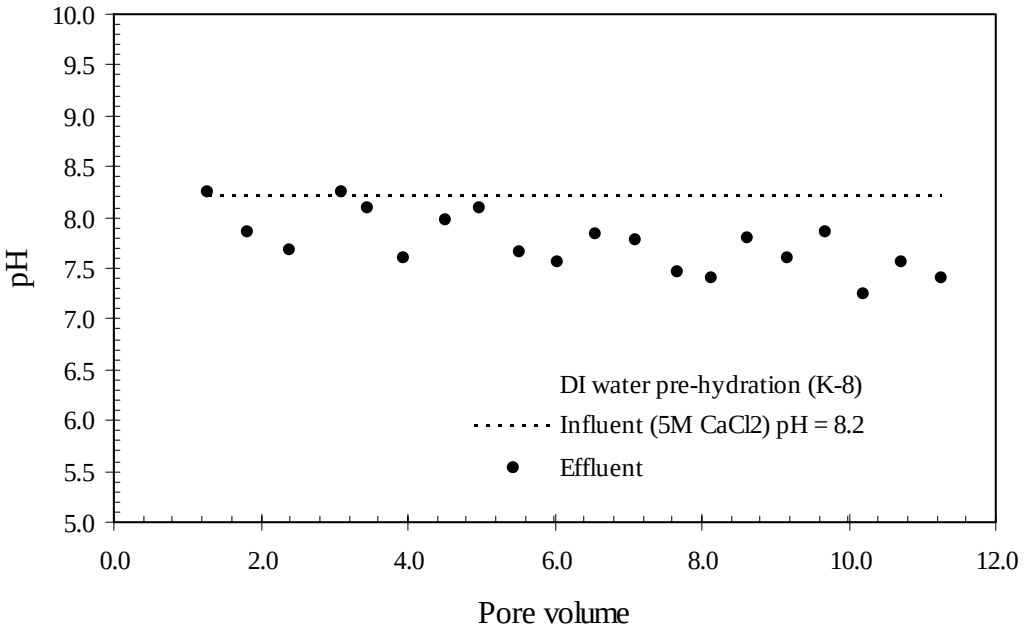

(b)

Figure A.8 Ionic Analysis of Permeability Test K-8 (a) Electrical Conductivity vs. Pore Volume and (b) pH vs. Pore Volume

Appendix A: (Continued)

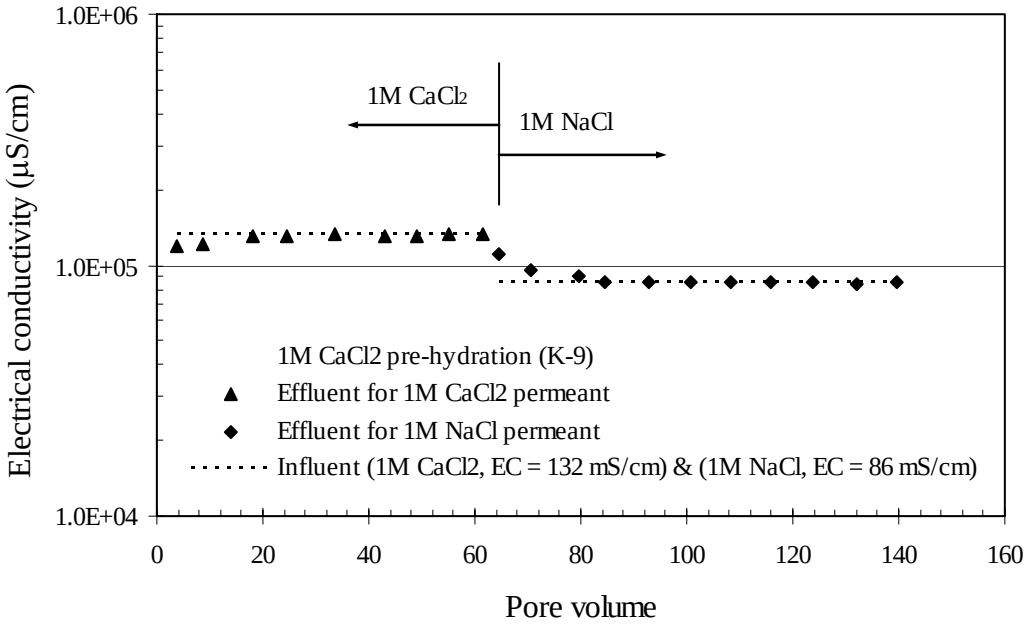

(a)

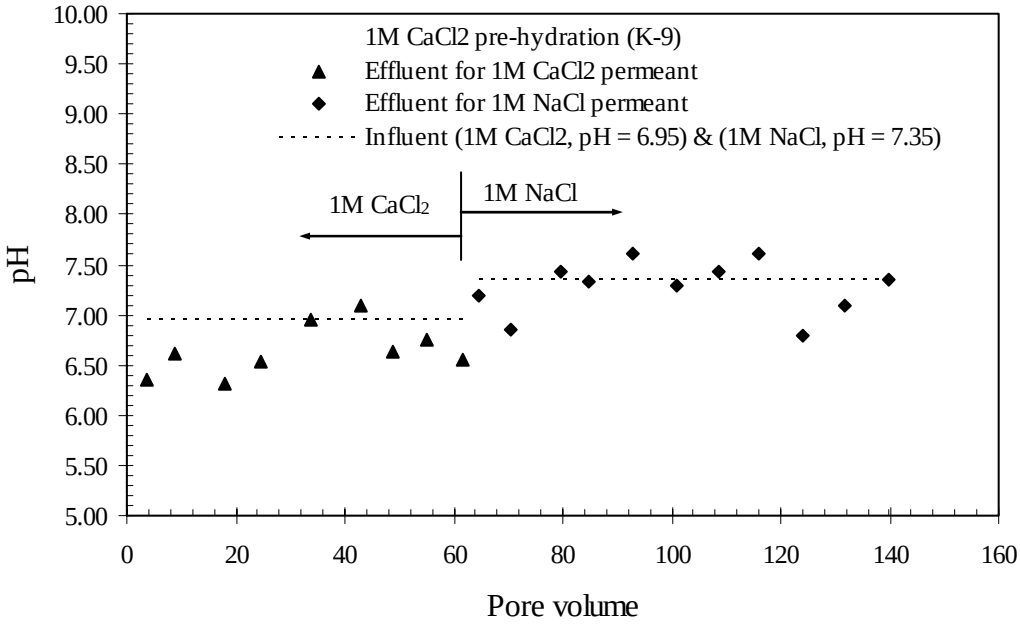

(b)

Figure A.9 Ionic Analysis of Permeability Test K-9 (a) Electrical Conductivity vs. Pore Volume and (b) pH vs. Pore Volume

Appendix A: (Continued)

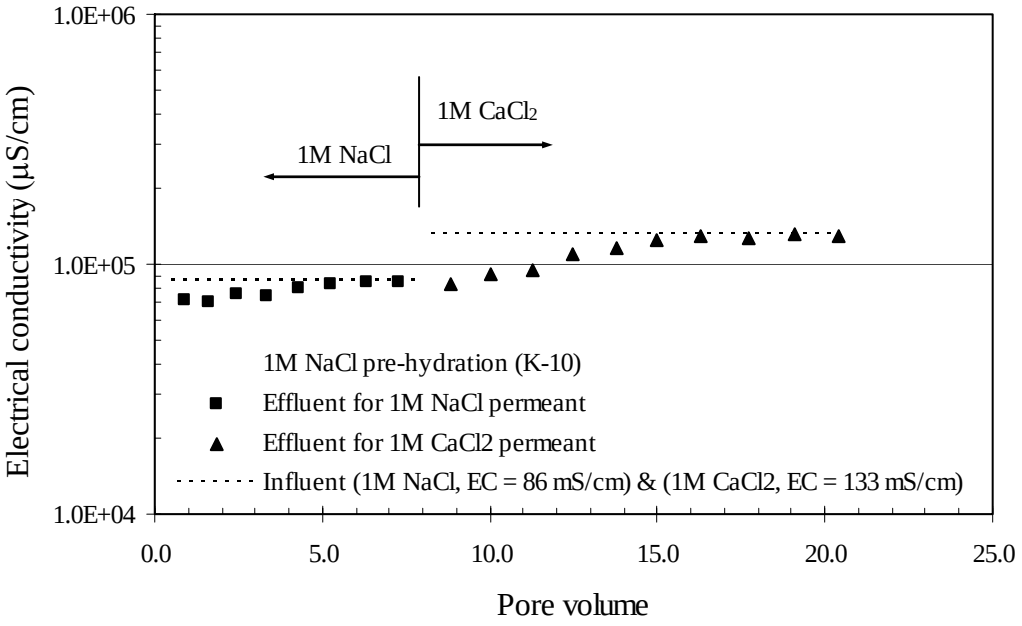

(a)

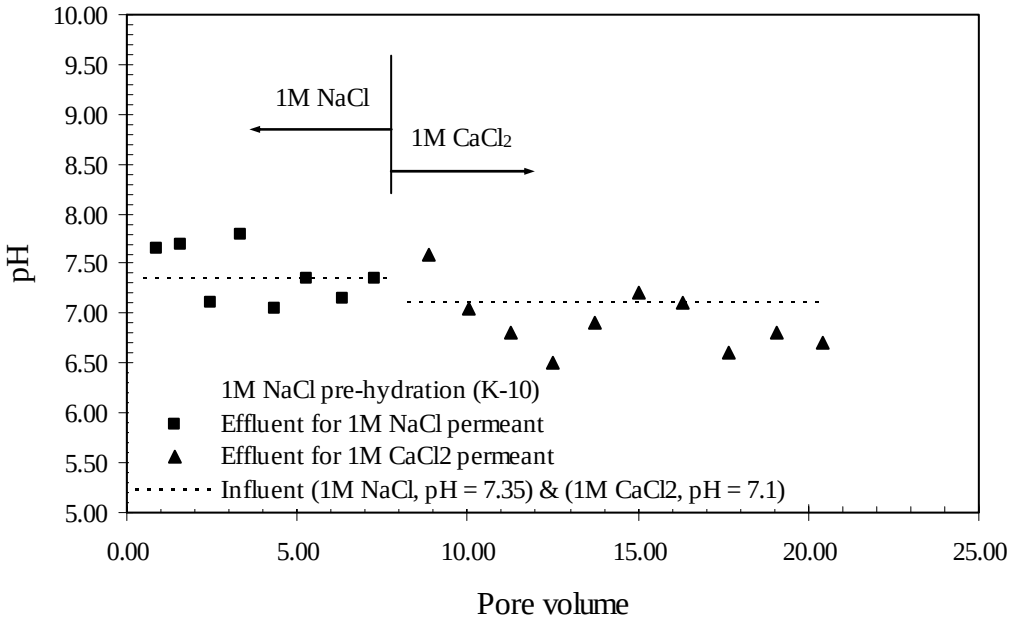

(b)

Figure A.10 Ionic Analysis of Permeability Test K-10 (a) Electrical Conductivity vs. Pore Volume and (b) pH vs. Pore Volume

Appendix A: (Continued)

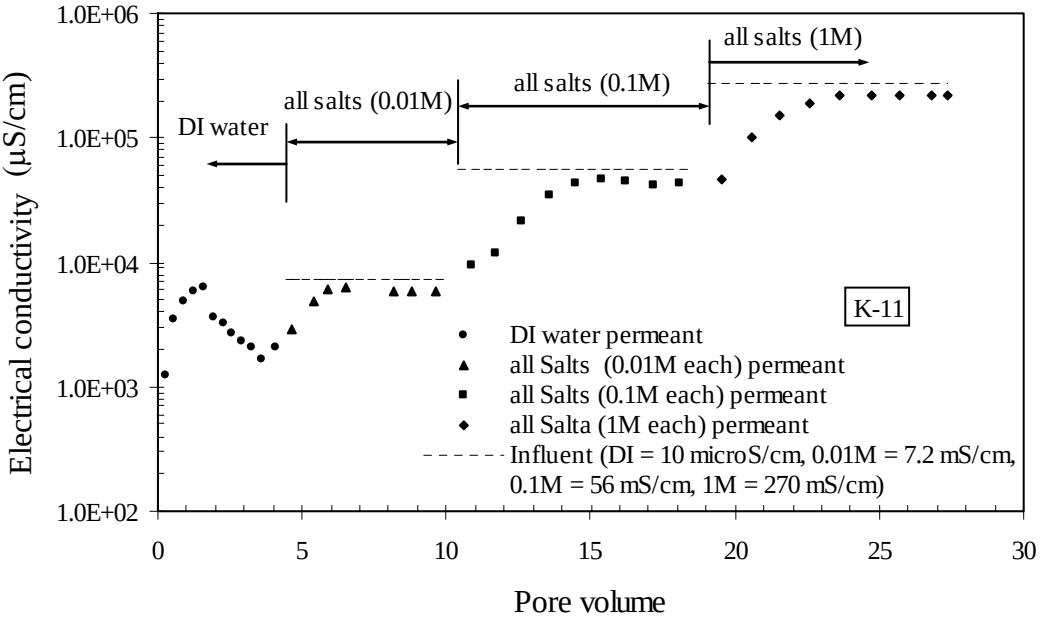

(a)

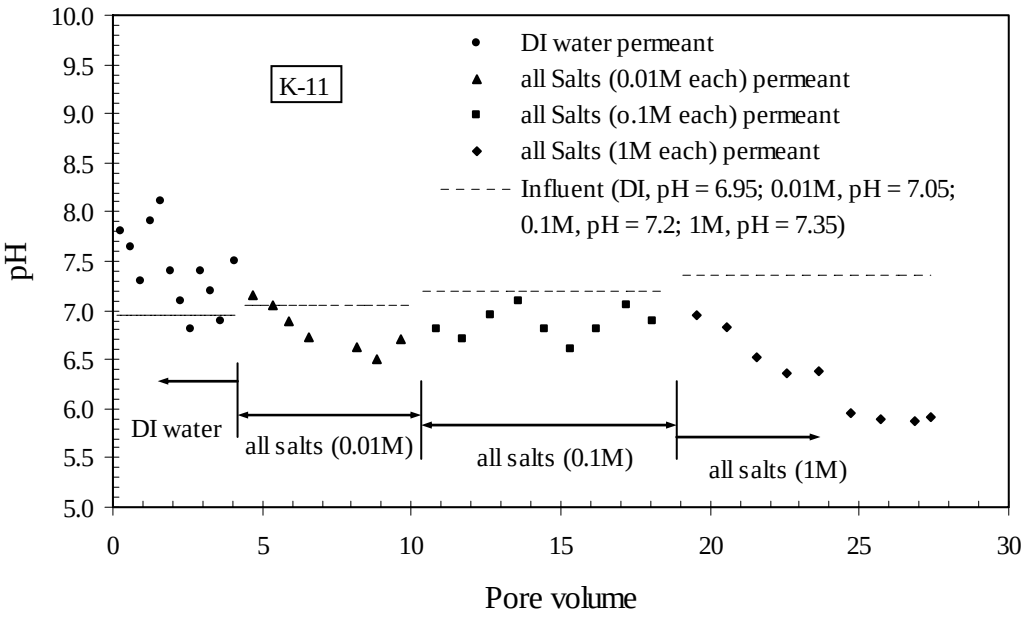

(b)

Figure A.11 Ionic Analysis of Permeability Test K-11 (a) Electrical Conductivity vs. Pore Volume and (b) pH vs. Pore Volume

Appendix A: (Continued)

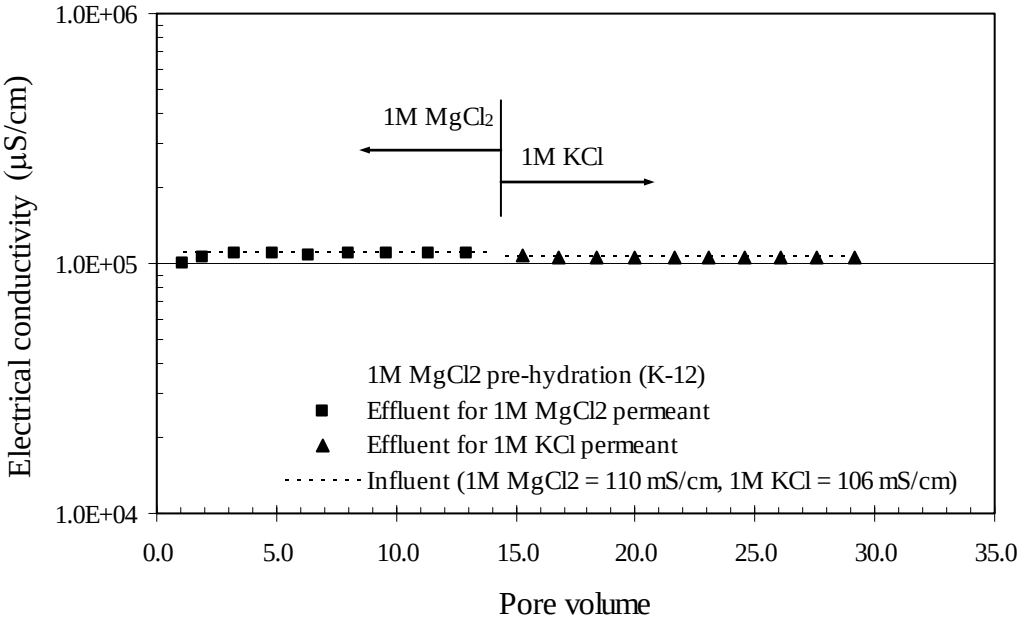

(a)

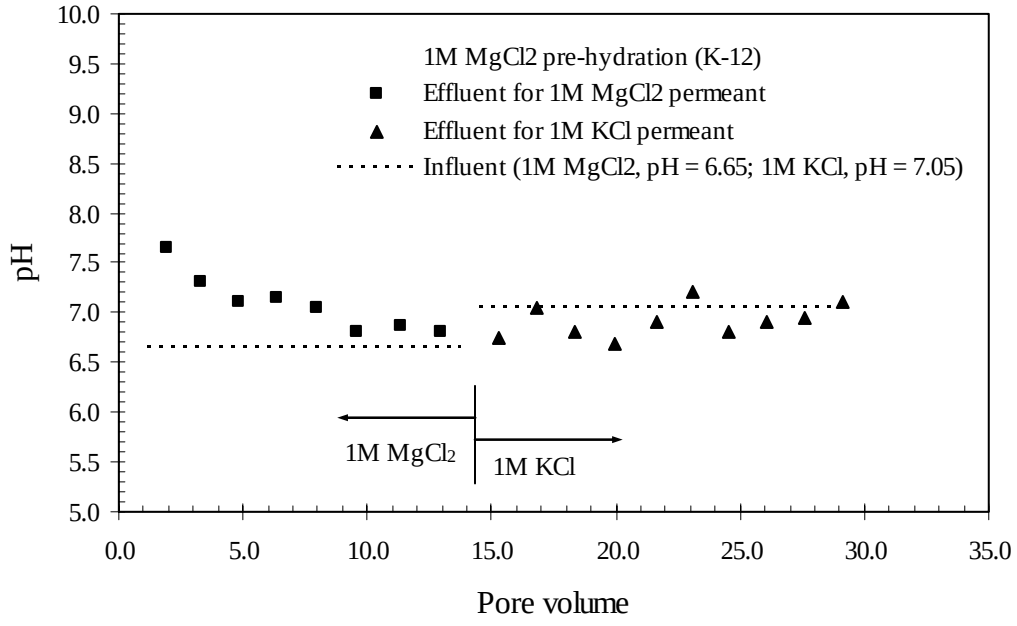

(b)

Figure A.12 Ionic Analysis of Permeability Test K-12 (a) Electrical Conductivity vs. Pore Volume and (b) pH vs. Pore Volume

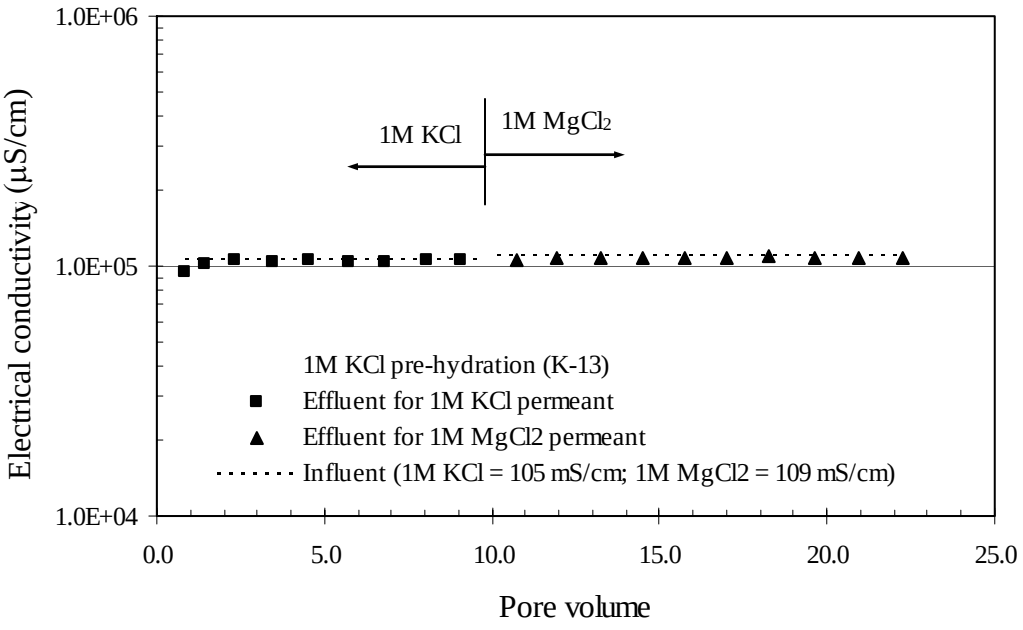

(a)

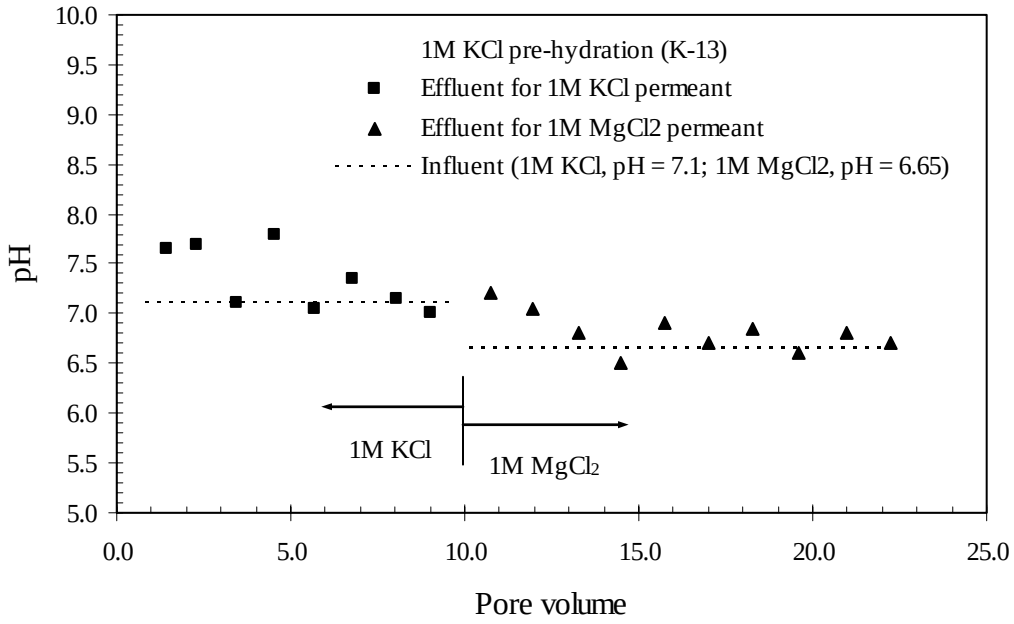

(b)

Figure A.13 Ionic Analysis of Permeability Test K-13 (a) Electrical Conductivity vs. Pore Volume and (b) pH vs. Pore Volume

Appendix A: (Continued)

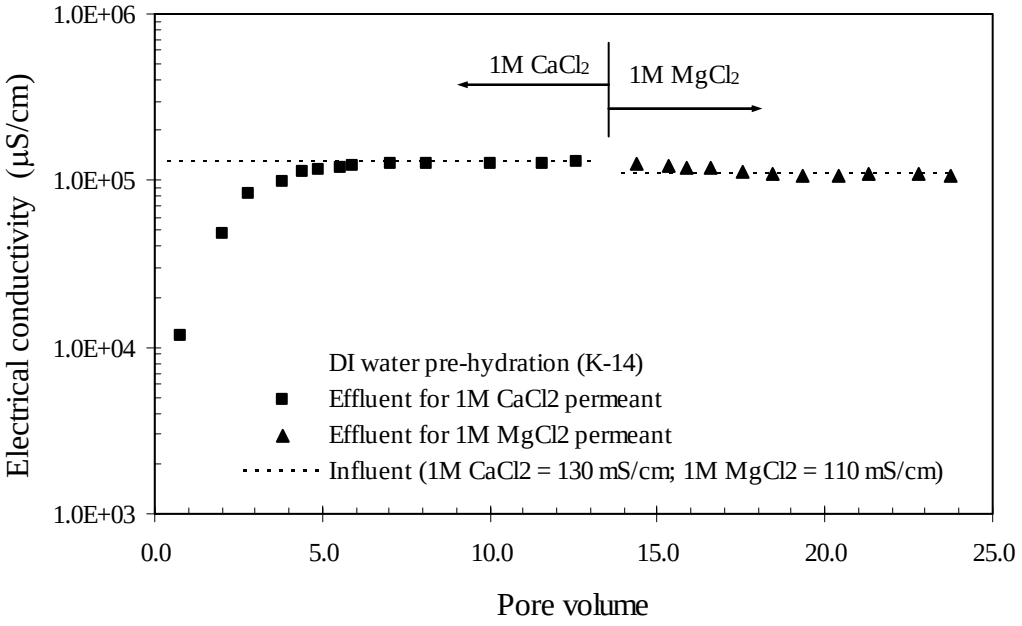

(a)

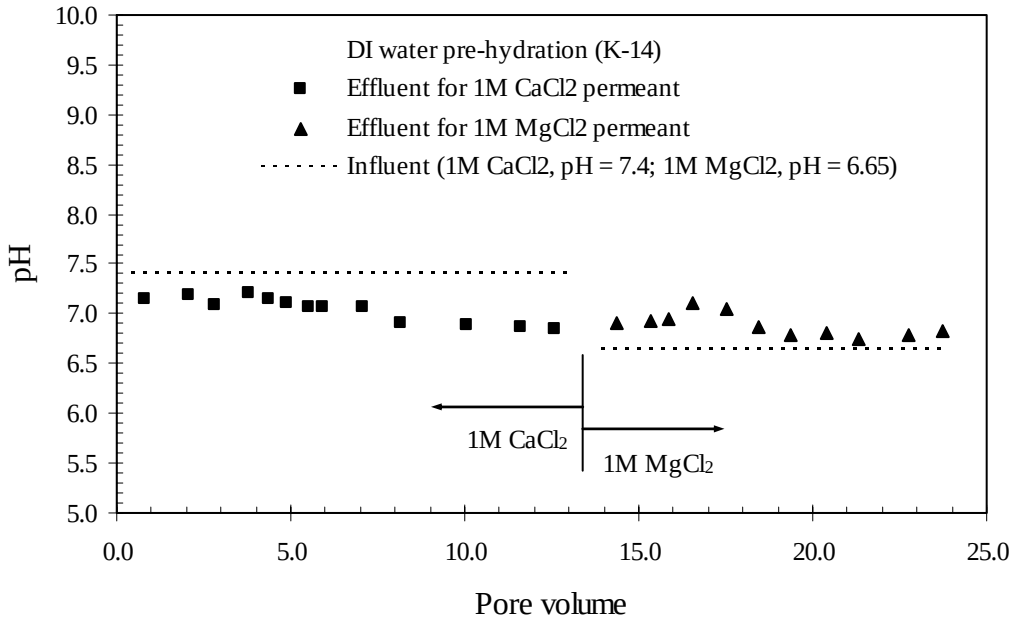

(b)

Figure A.14 Ionic Analysis of Permeability Test K-14 (a) Electrical Conductivity vs. Pore Volume and (b) pH vs. Pore Volume

Appendix B: Test Results of pH and EC of Diffusion Tests

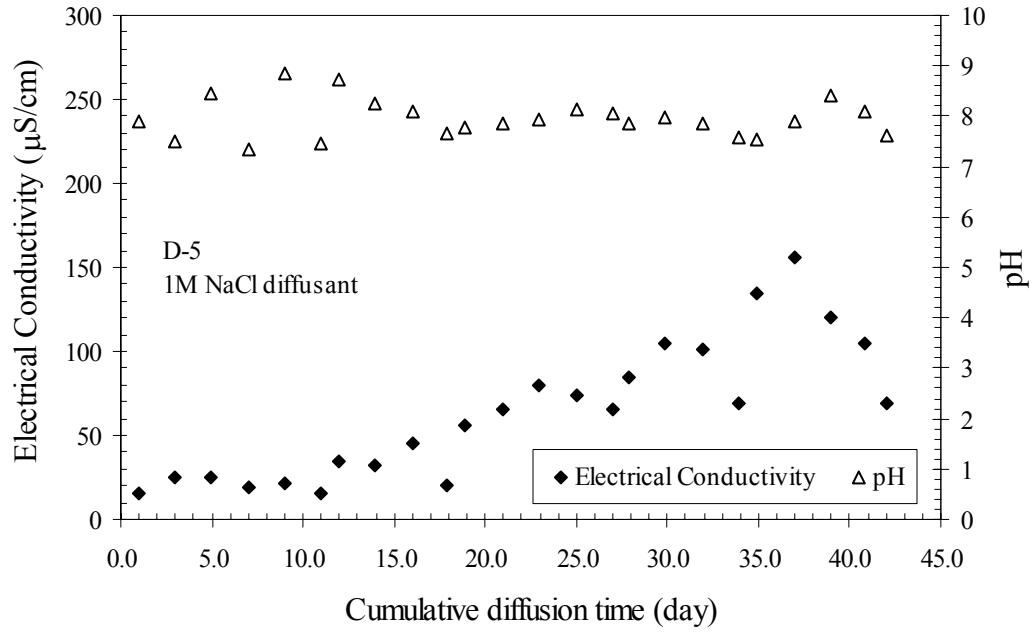

(a)

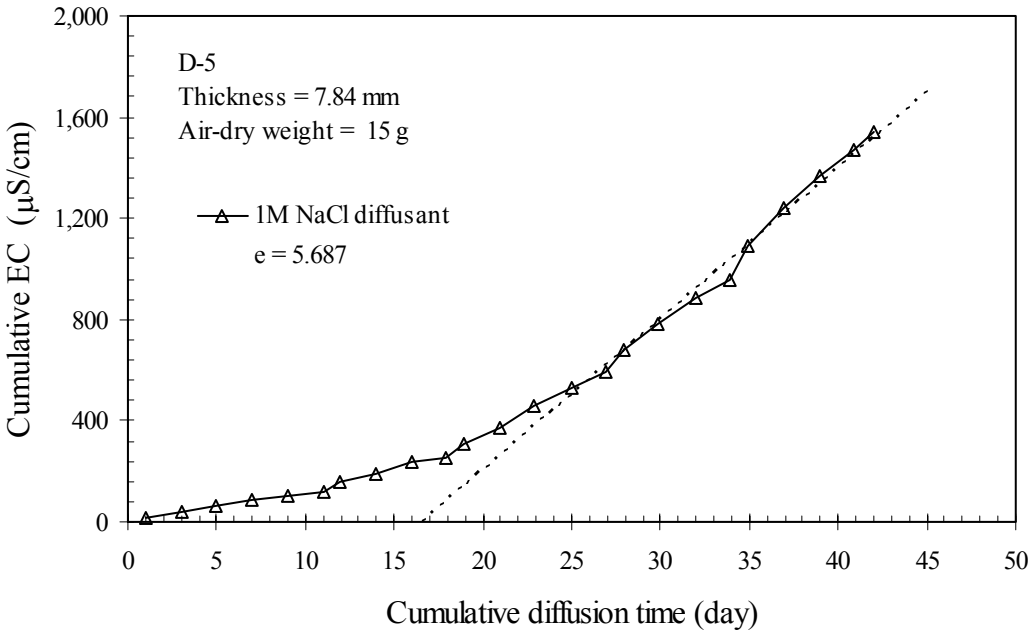

(b)

Figure B.1 Diffusion Test Results for D-5 (a) pH and Electrical Conductivity and (b) Cumulative EC versus Cumulative Diffusion Time

Appendix B: (Continued)

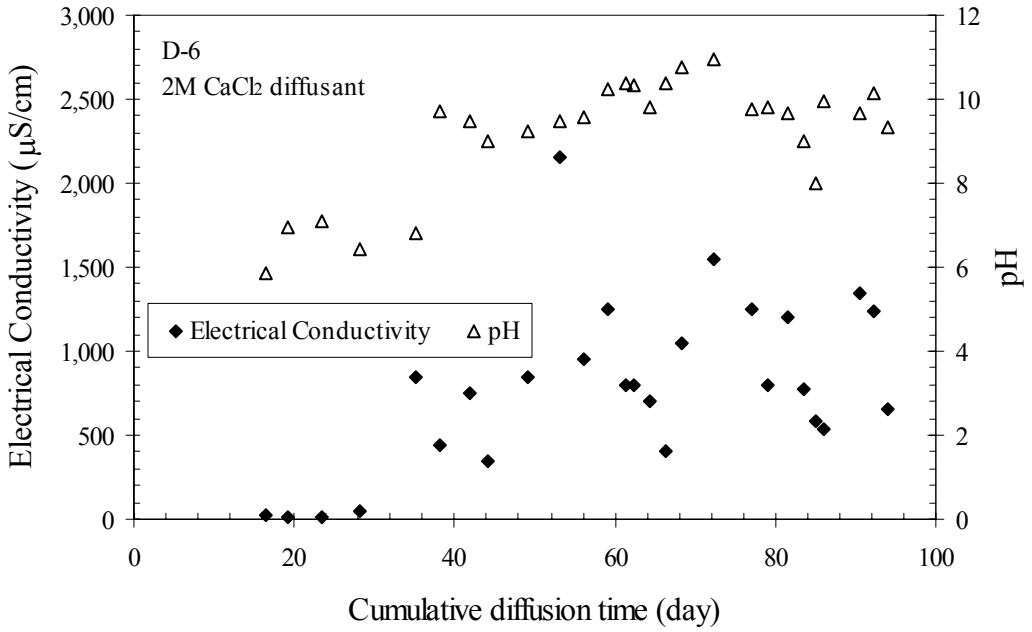

(a)

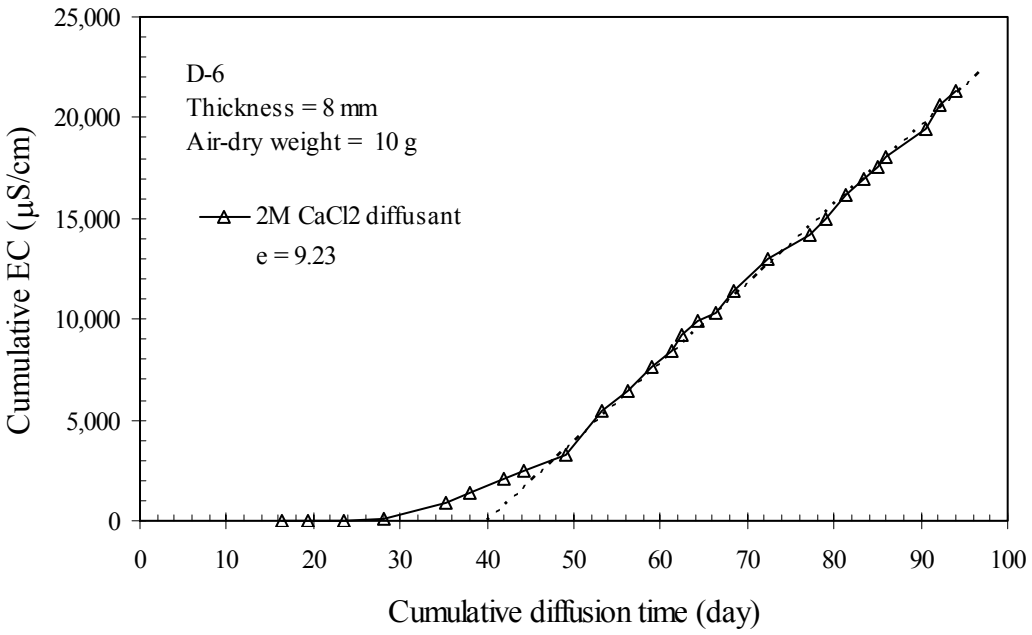

(b)

Figure B.2 Diffusion Test Results for D-6 (a) pH and Electrical Conductivity and (b) Cumulative EC versus Cumulative Diffusion Time

Appendix B: (Continued)

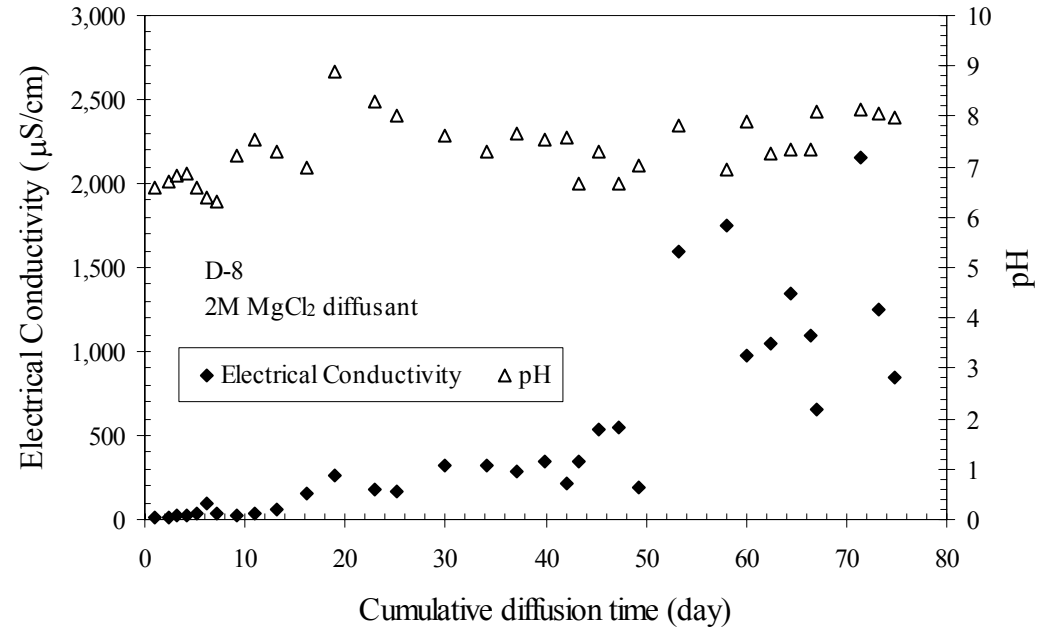

(a)

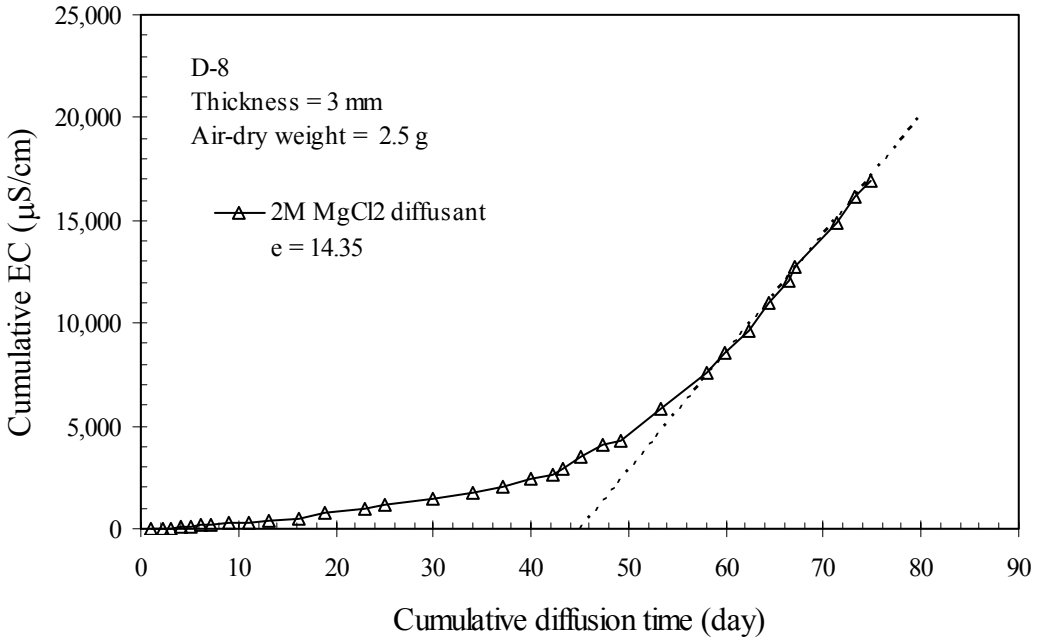

(b)

Figure B.3 Diffusion Test Results for D-8 (a) pH and Electrical Conductivity and (b) Cumulative EC versus Cumulative Diffusion Time

Appendix B: (Continued)

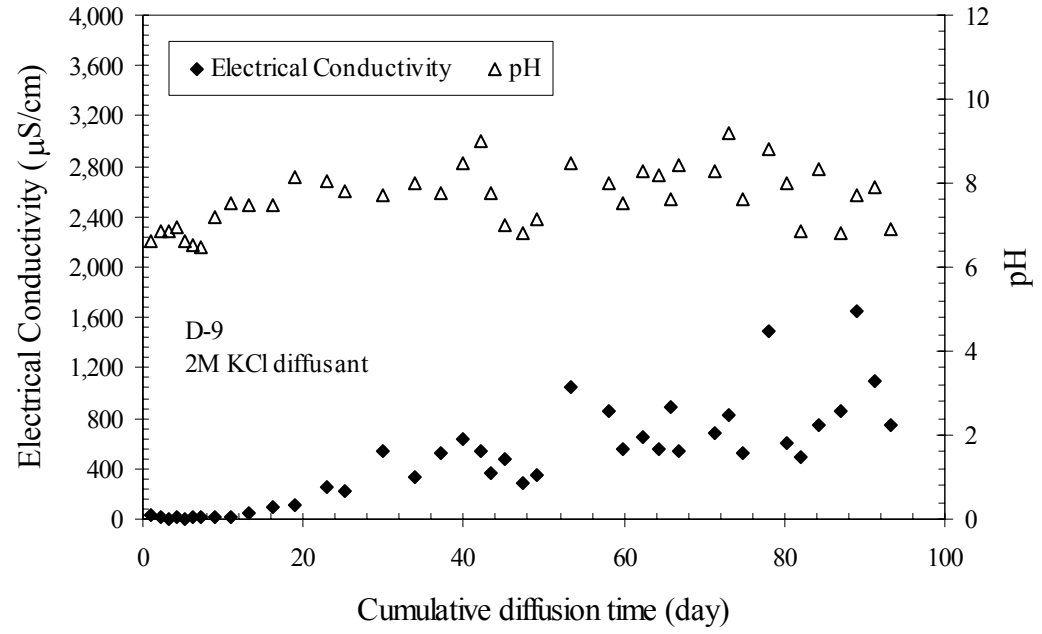

(a)

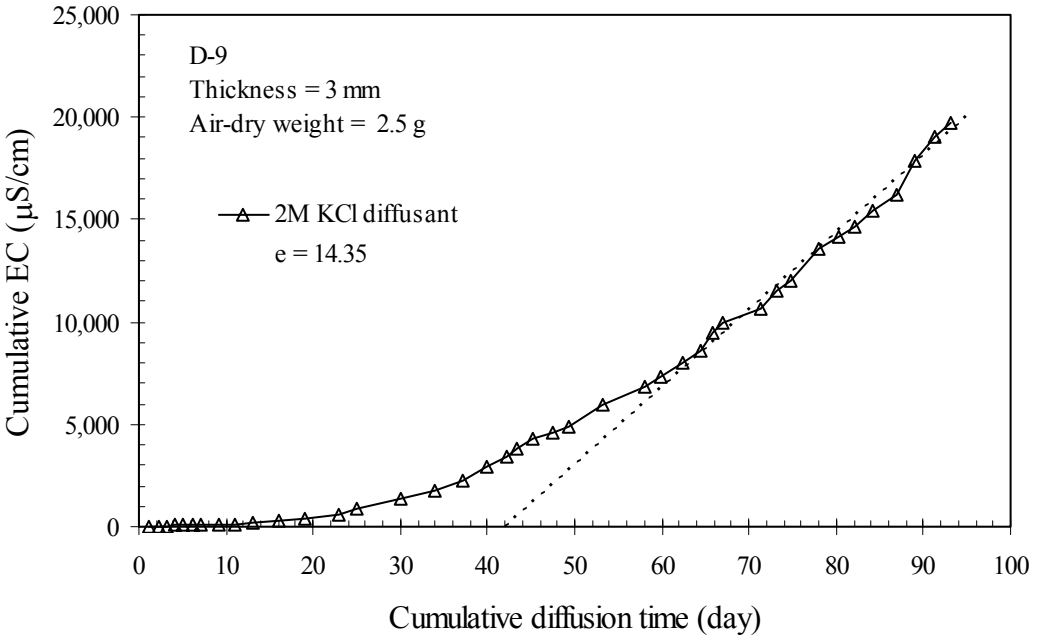

(b)

Figure B.4 Diffusion Test Results for D-9 (a) pH and Electrical Conductivity and (b) Cumulative EC versus Cumulative Diffusion Time

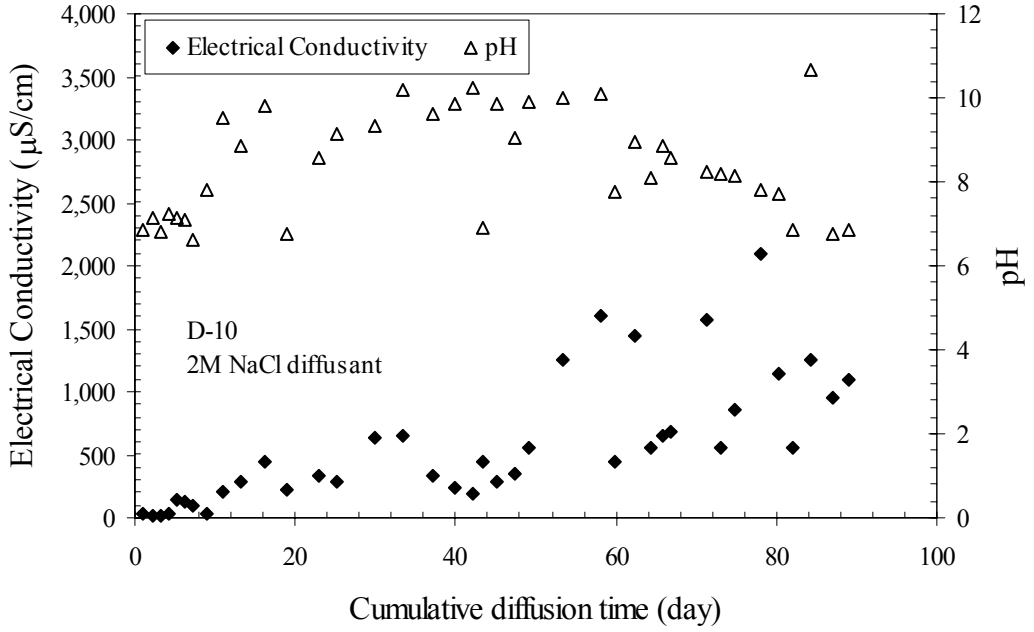

(a)

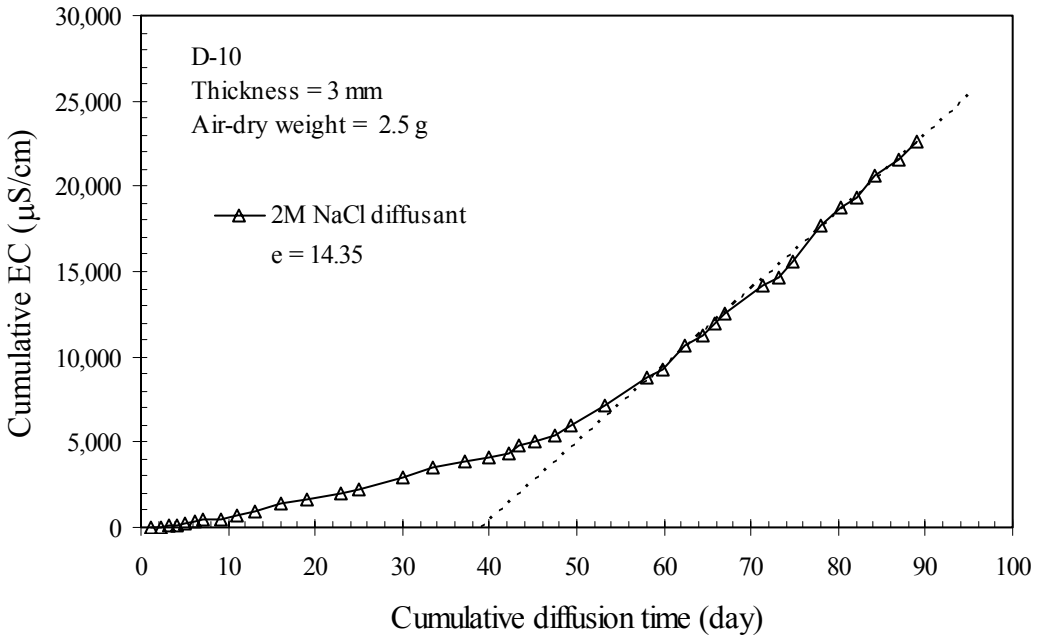

(b)

Figure B.5 Diffusion Test Results for D-10 (a) pH and Electrical Conductivity and (b) Cumulative EC versus Cumulative Diffusion Time

Appendix B: (Continued)

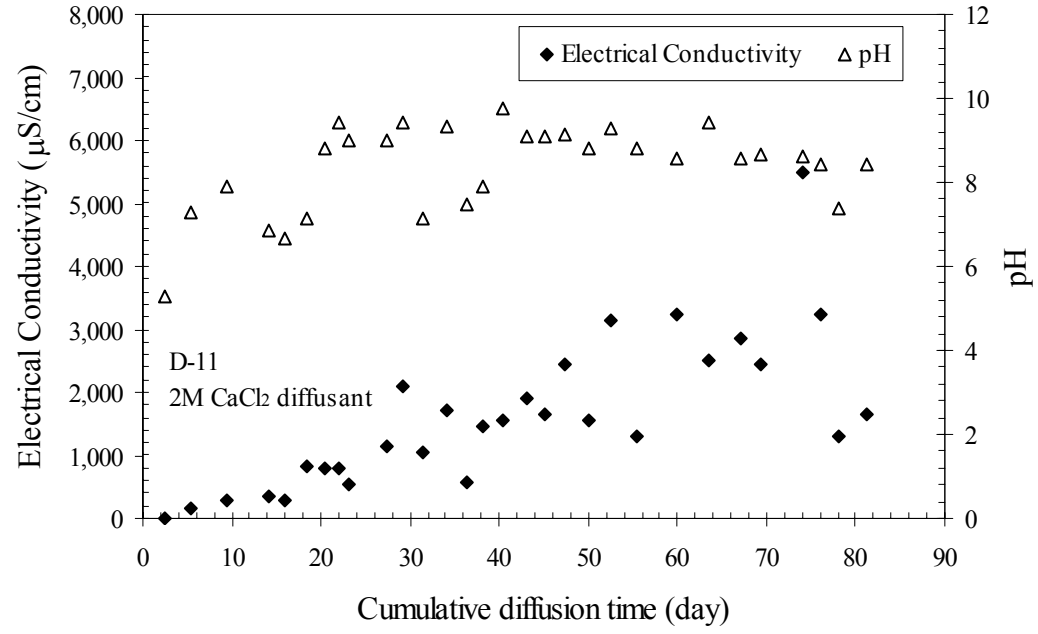

(a)

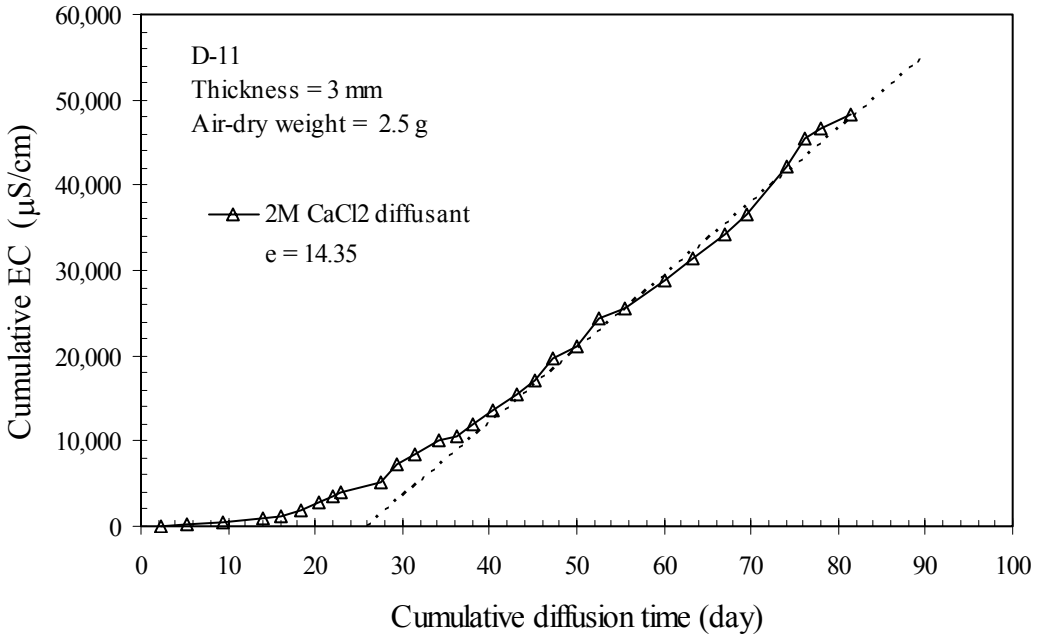

(b)

Figure B.6 Diffusion Test Results for D-11 (a) pH and Electrical Conductivity and (b) Cumulative EC versus Cumulative Diffusion Time

Appendix B: (Continued)

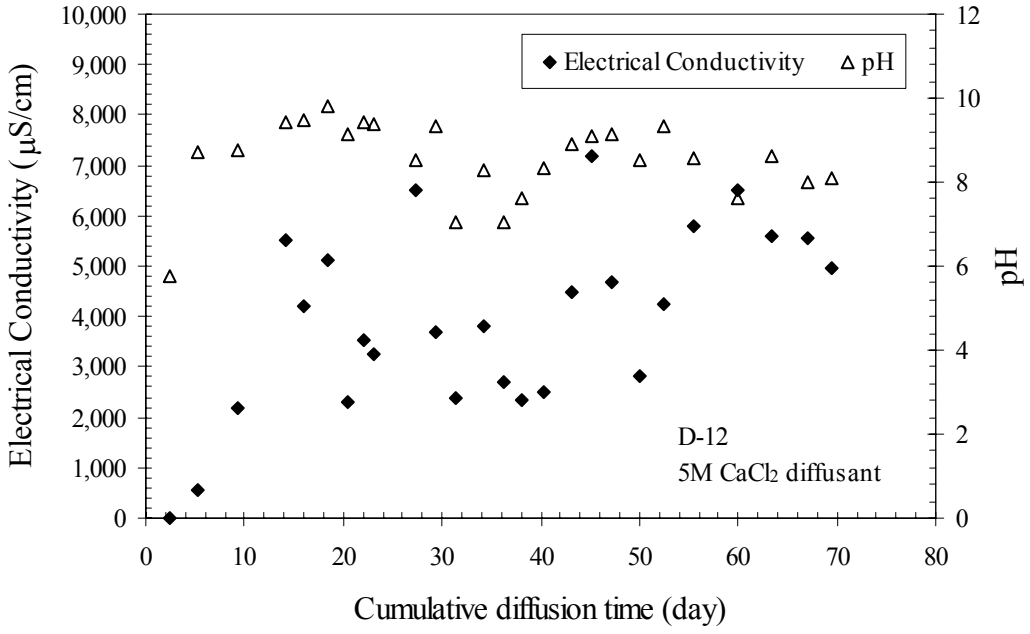

(a)

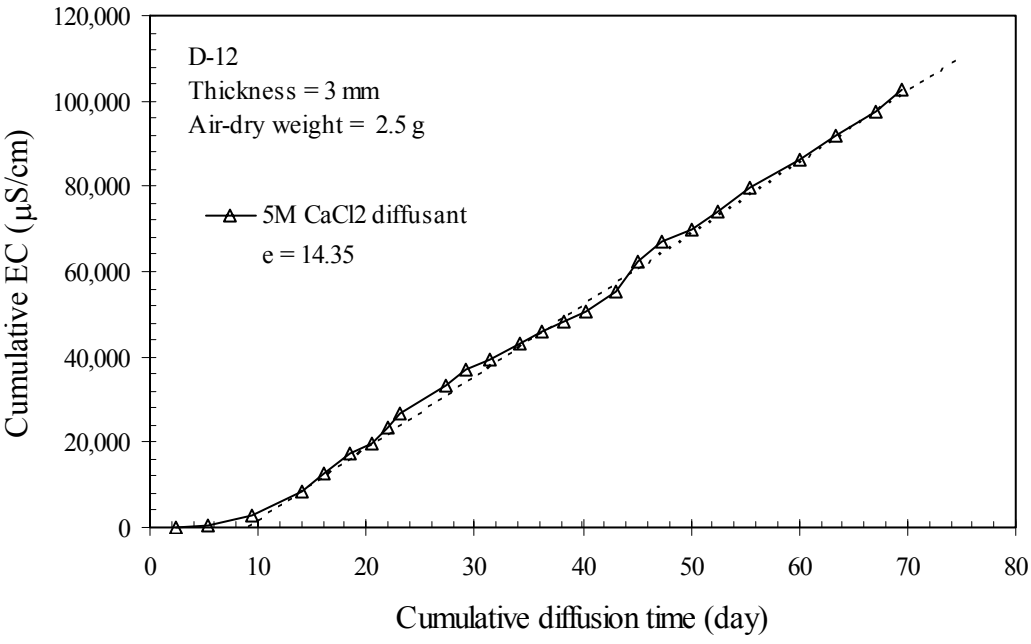

(b)

Figure B.7 Diffusion Test Results for D-12 (a) pH and Electrical Conductivity and (b) Cumulative EC versus Cumulative Diffusion Time

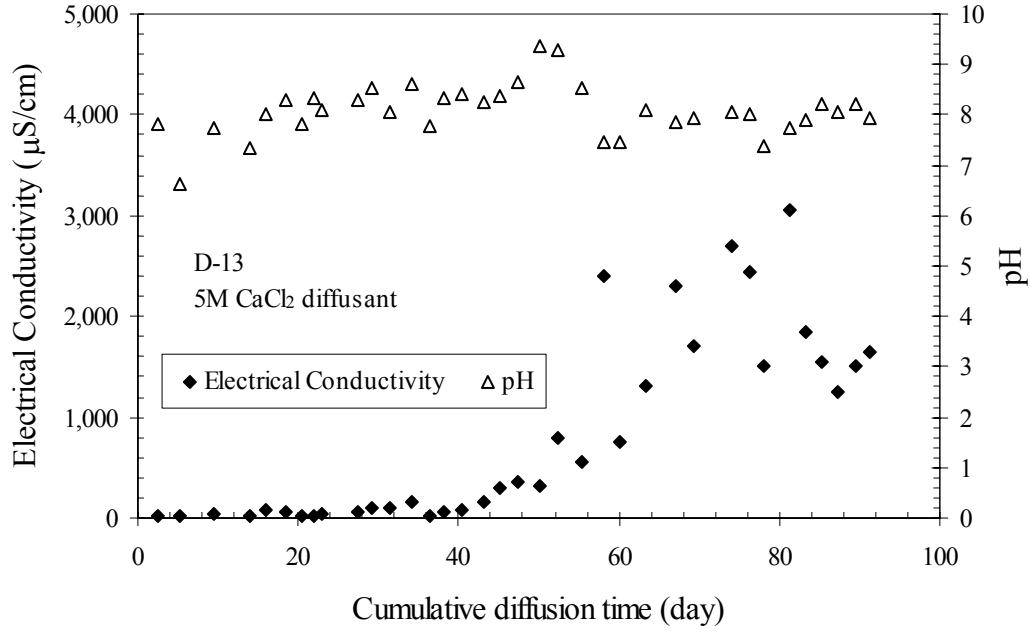

(a)

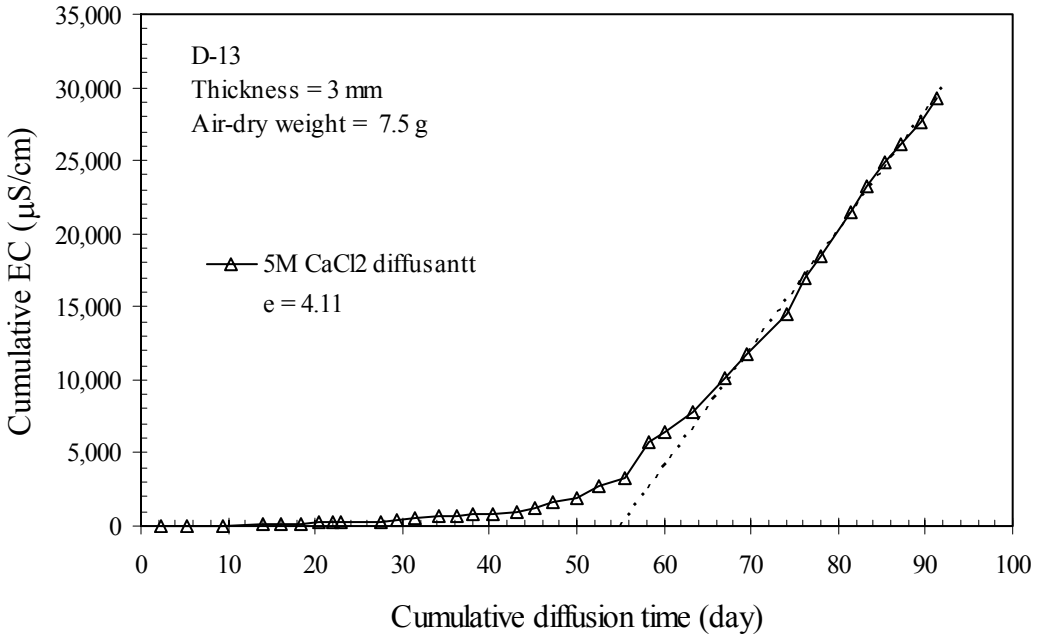

(b)

Figure B.8 Diffusion Test Results for D-13 (a) pH and Electrical Conductivity and (b) Cumulative EC versus Cumulative Diffusion Time

Appendix B: (Continued)

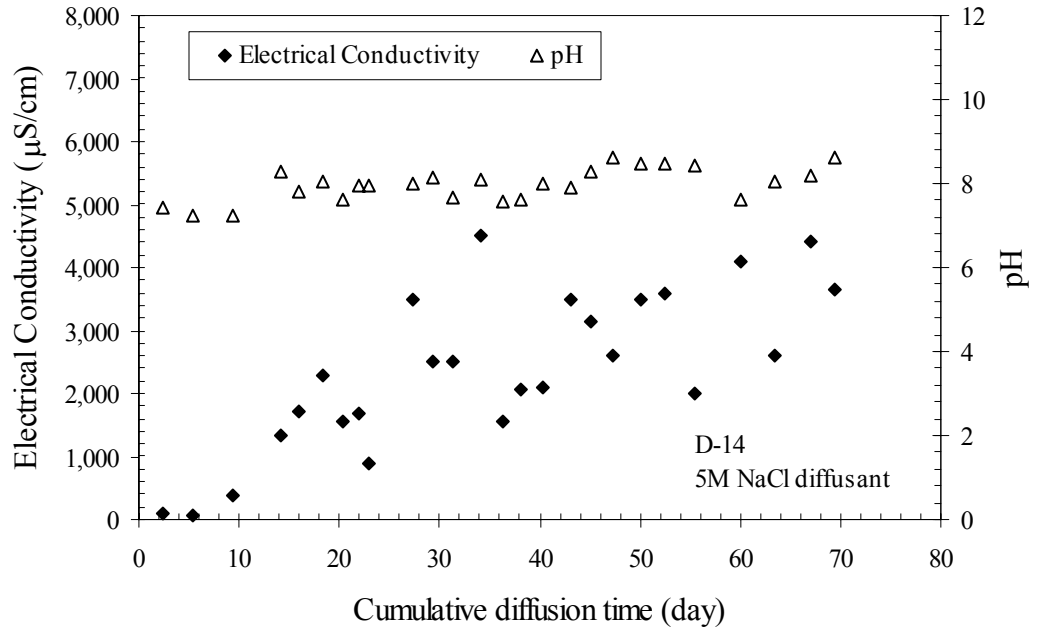

(a)

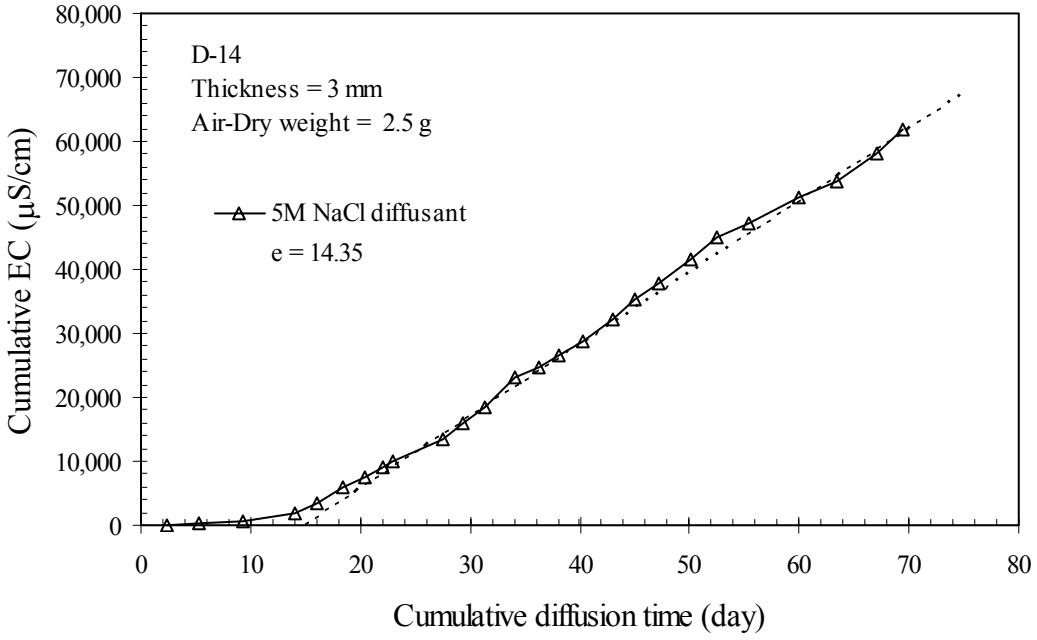

(b)

Figure B.9 Diffusion Test Results for D-14 (a) pH and Electrical Conductivity and (b) Cumulative EC versus Cumulative Diffusion Time

Appendix B: (Continued)

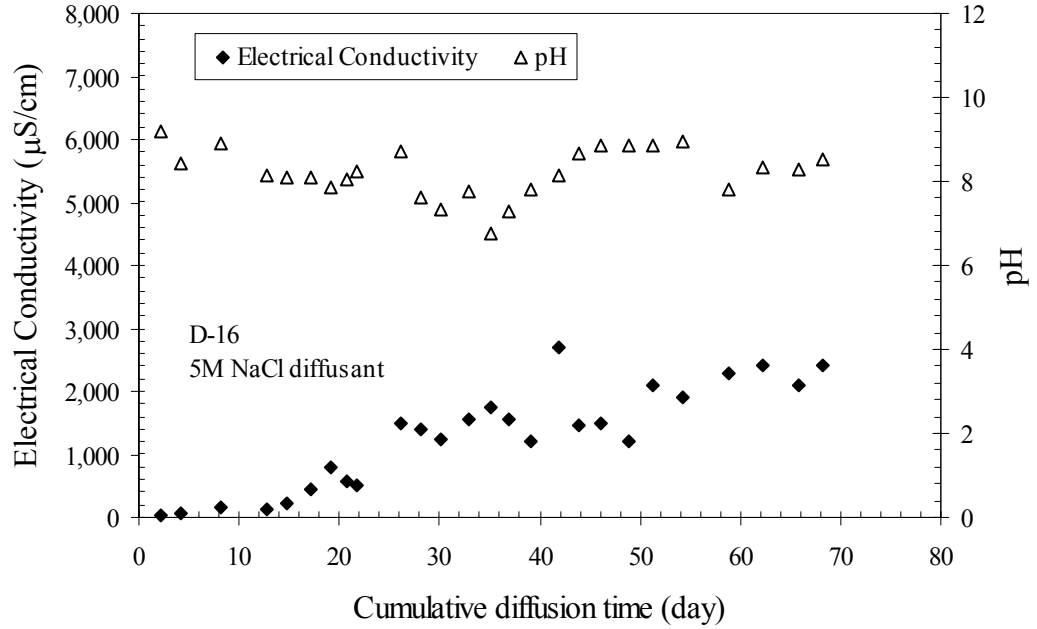

(a)

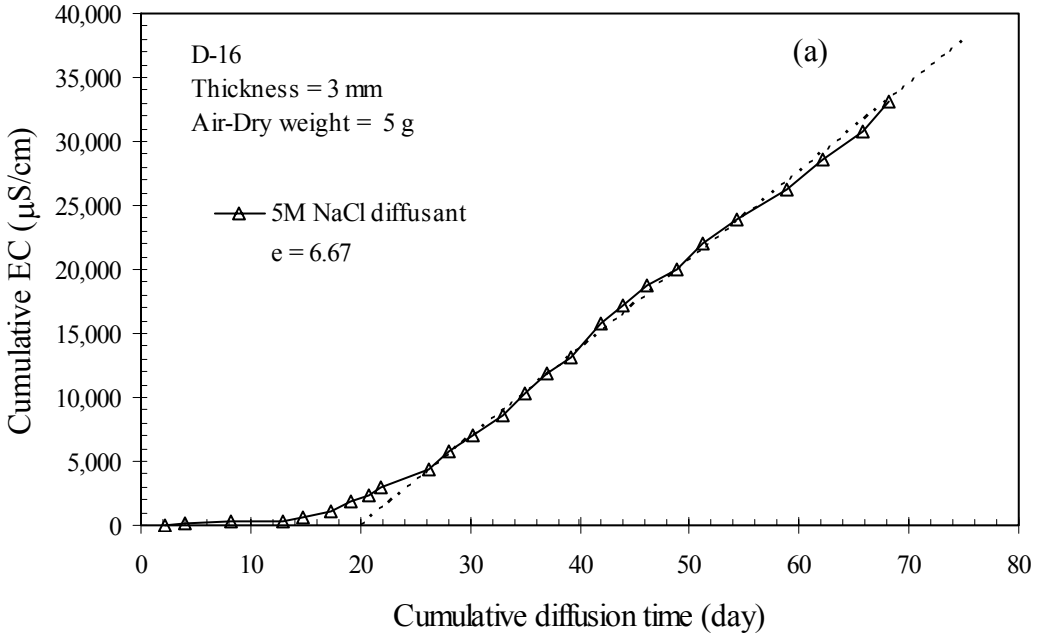

(b)

Figure B.10 Diffusion Test Results for D-16 (a) pH and Electrical Conductivity and (b) Cumulative EC versus Cumulative Diffusion Time

Appendix B: (Continued)

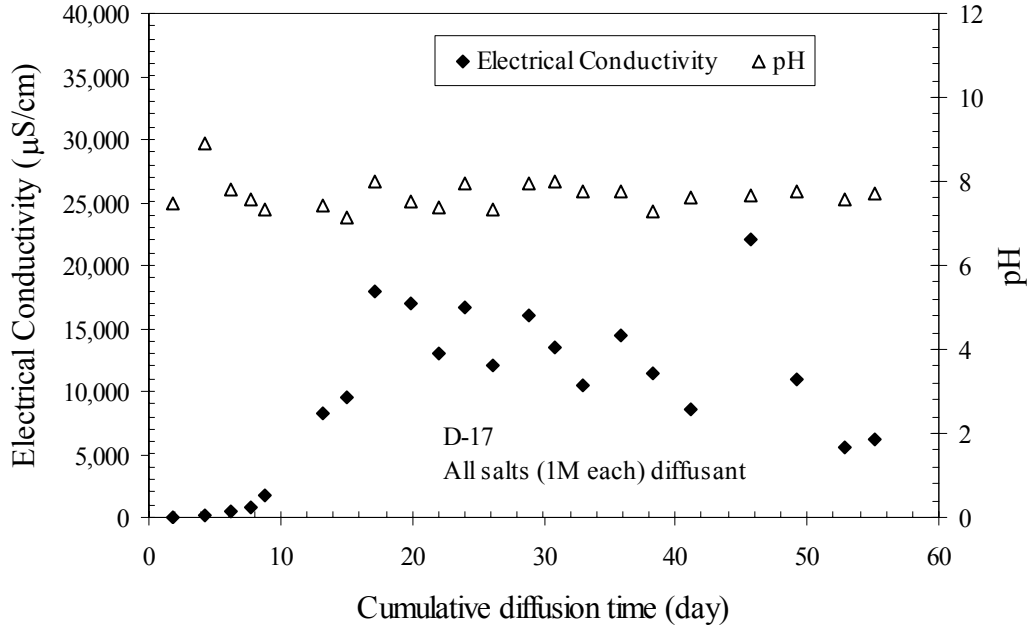

(a)

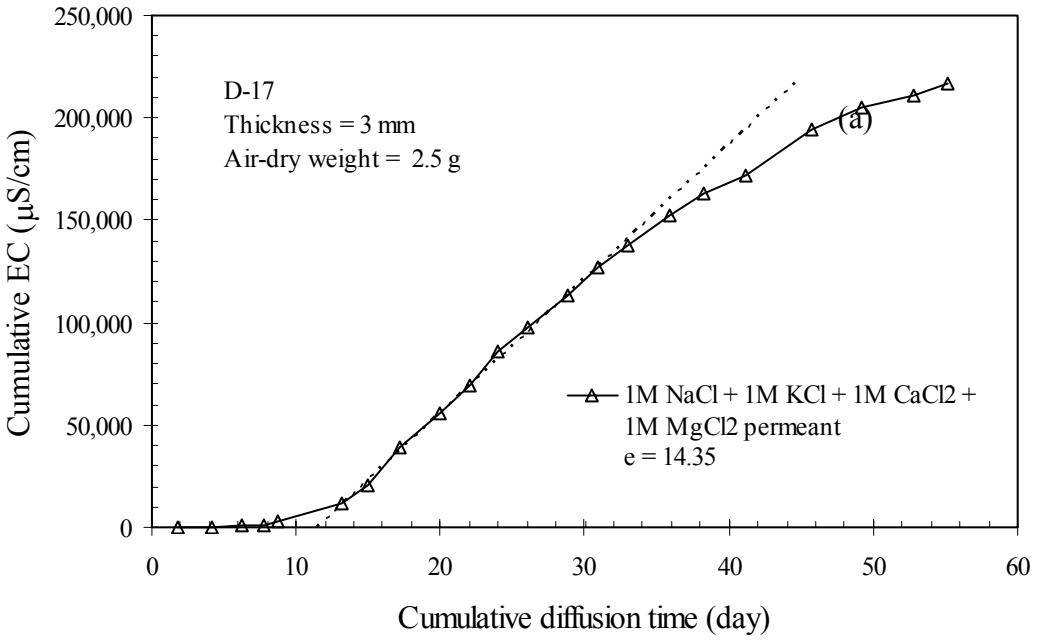

(b)

Figure B.11 Diffusion Test Results for D-17 (a) pH and Electrical Conductivity and (b) Cumulative EC versus Cumulative Diffusion Time

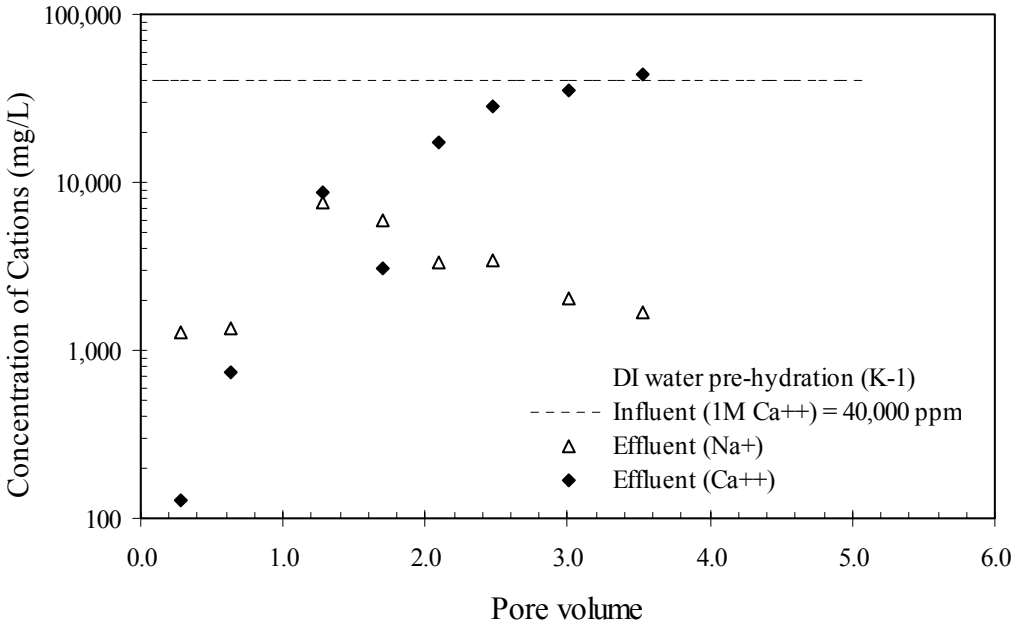

Figure C.1 Concentration of Various Cations in Effluent During Permeability (K-1)

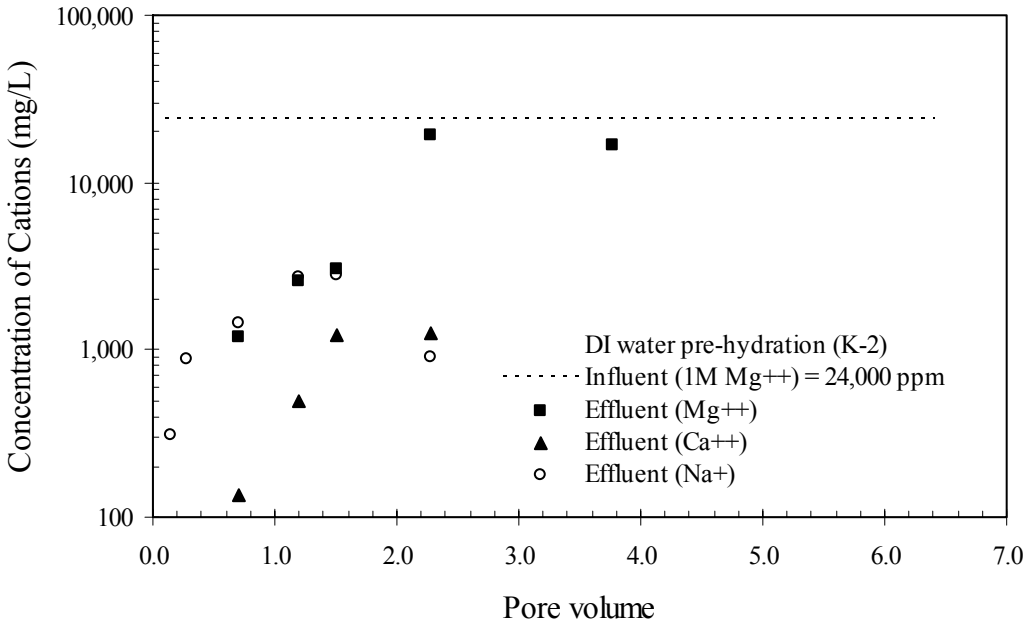

Figure C.2 Concentration of Various Cations in Effluent During Permeability (K-2)

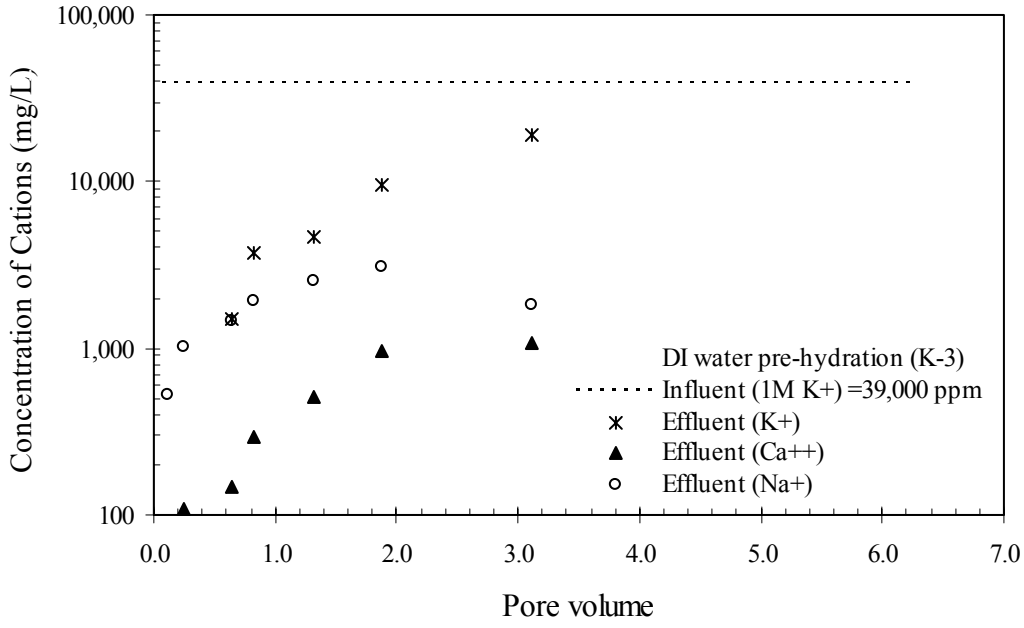

Figure C.3 Concentration of Various Cations in Effluent During Permeability (K-3)

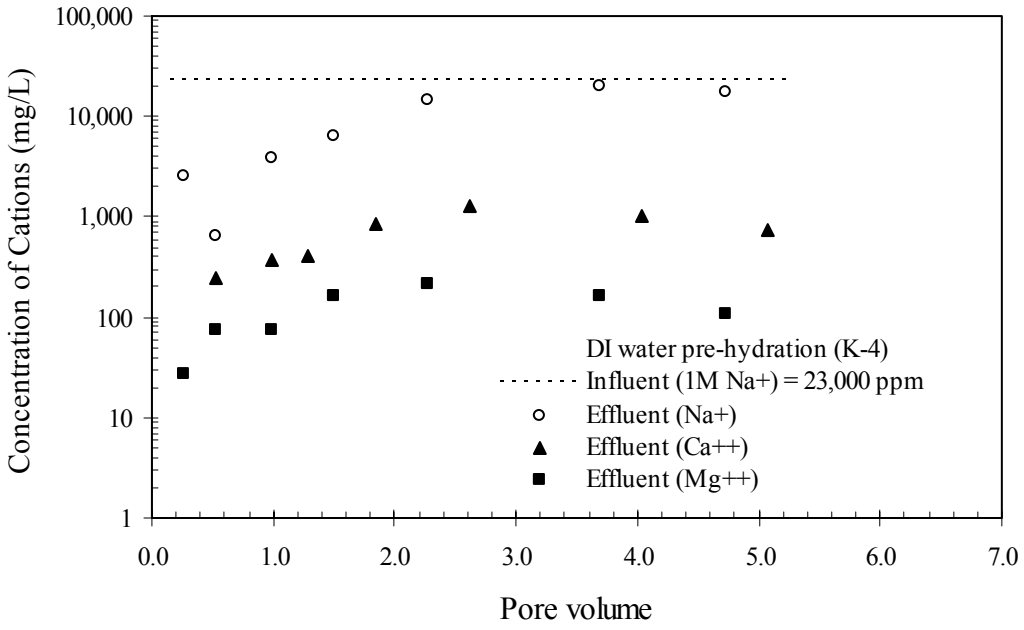

Figure C.4 Concentration of Various Cations in Effluent During Permeability (K-4)

ABOUT THE AUTHOR

Naim Muhammad received his Bachelor of Science in Civil Engineering (B.Sc. Engg.) in 1988 from the Bangladesh University of Engineering and Technology (BUET). He received his Master of Engineering (M.Eng.) in Civil Engineering specializing in Geotechnical Engineering in 1993 from the National University of Singapore (NUS). Following his Masters degree, Naim worked as a Geotechnical Engineer for four years in various consulting and construction companies in Singapore. Naim also worked as a Lecturer in Singapore Polytechnic for three years before heading to United States in 2000 for his Ph.D. program.

During his PhD program at University of South Florida (USF), Naim has carried out research works on landfill liner materials and bentonite clay. He has authored jointly with NUS faculty members a number of journal papers and international conference proceedings on land reclamation and marine clay slurry and is currently in the process of publishing a number of technical papers with USF faculty members on hydraulic, chemical, and diffusion characteristics of bentonite clay.